DOCTORAL DISSERTATION

PREPARATION OF ORGANOSILICA MEMBRANE AND APPLICATION TO USE IN GAS SEPARATION AND REVERSE OSMOSIS

（オルガノシリカ膜の開発と気体分離および逆浸透への応用）

SUHAINA MOHD IBRAHIM

DEPARTMENT OF CHEMICAL ENGINEERING
GRADUATE SCHOOL OF ENGINEERING, HIROSHIMA UNIVERSITY

（広島大学大学院工学研究科物質科学システム専攻）

SEPTEMBER, 2015

TABLE OF CONTENTS

Chapter 1

General Introduction

1.1.Membrane Separation

In today's competitive climate, separation processes play an essential role in the chemical process industries for purifying raw materials, recovering product streams of desired purity and preventing pollution through treatment of waste streams released to the environment. The major separation processes are based on absorption, adsorption, crystallization, distillation, extraction, evaporation, filtration, ion exchange and membrane permeation. Among this large scope of separation processes, membrane separation will be focused in this study.

Membrane can be used to satisfy many of the separation requirements in the process industries and can be applied over various industries such as metal industries (metal recovery, pollution control, air enriching for combustion), food and biotechnology industries (separation, purification, sterilization and by product recovery), leather and textile industries (sensible heat recovery, pollution control and chemicals recovery), pulp and paper industries (replacing evaporation process, pollution control, fiber and chemical recovery), chemical process industries (organic material separation, gas separation, recovery and recycle of chemicals), health pharmaceutical and medical industries (artificial organ, control release (pharmaceuticals), blood fractionation, sterilization and water purification) and waste treatment (separation of salt or other minerals and deionization). A general definition of membrane is that it is a selective barrier between two phases [1,2] as shown in Figure 1-1.

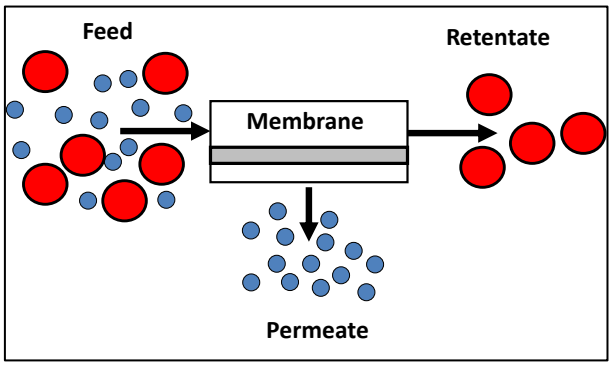

Figure 1-1 Schematic diagram of membrane separation process [1,2]

Membrane separation processes can be categorized based on the phases of the feed and permeate as well as pore sizes of the membrane as shown in Figure 1-2. For the case where both the feed and permeate streams are a liquid phase and the driving force is a pressure difference between the two phases, the separation process is referred to a filtration process such as microfiltration (MF) and ultrafiltration (UF) which pore sizes > 10 Å, nanofiltration (NF); pore sizes between 5 and 20 Å and lastly reverse osmosis (RO); pore sizes < 5 Å. On the other hand, pervaporation (PV) which membrane pore sizes are < 5 Å, the feed stream is a liquid phase, while permeate stream is a gas phase by evacuation. For gas separation (GS), the membrane pore sizes are also < 5 Å and both feed and permeate stream is in the gas phase. Most of these applications have been carried out using polymeric membranes and only limited applications involving inorganic and organosilica membranes.

Due to this matter, this study concentrates on the preparation of organosilica membrane and application in gas separation (GS) and reverse osmosis (RO) areas.

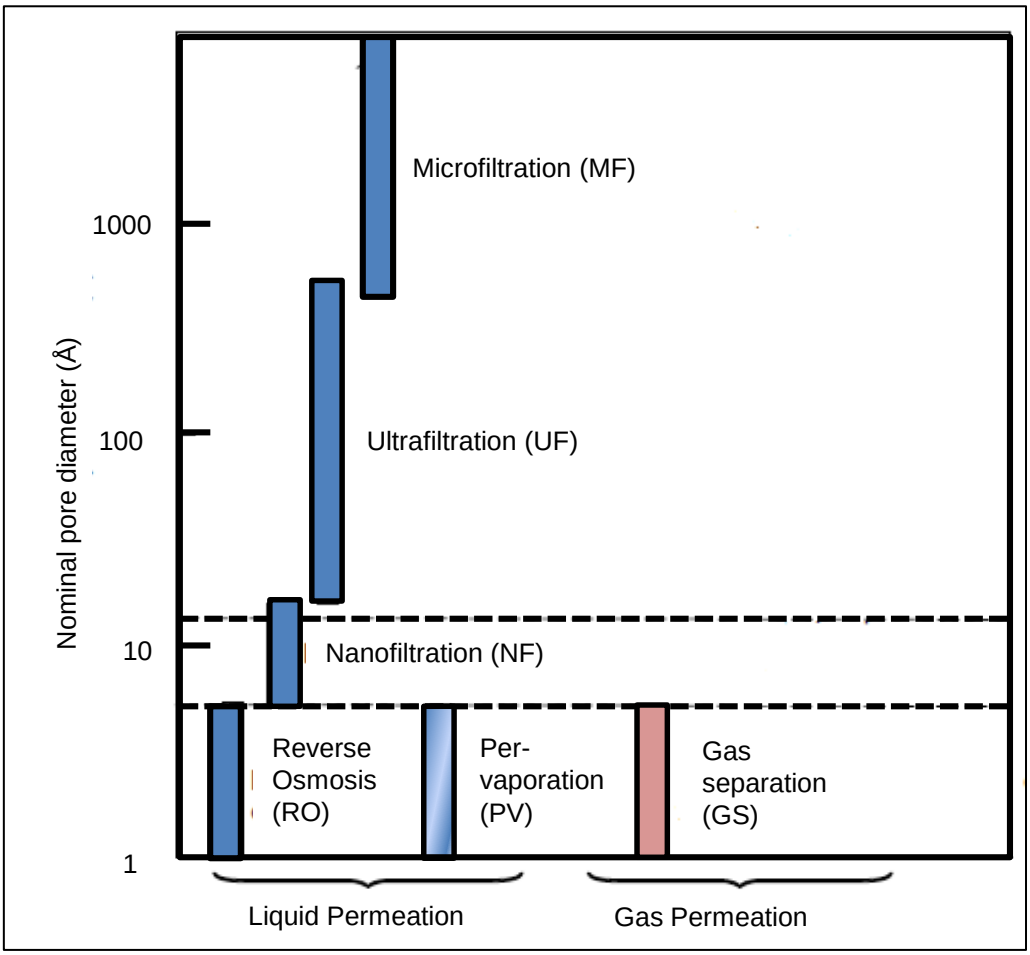

Figure 1-2 Schematic diagram of the membrane processes based on phase and pore sizes [2]

1.2. Inorganic membranes

The inorganic membranes as shown in Figure 1-3 can be described as an asymmetric porous material formed by a macroporous support with successive thin layers deposited on it. The support provides mechanical resistance to the medium [3]. Meanwhile, Table 1-1 shows some advantages and disadvantages of inorganic membranes [4-6].

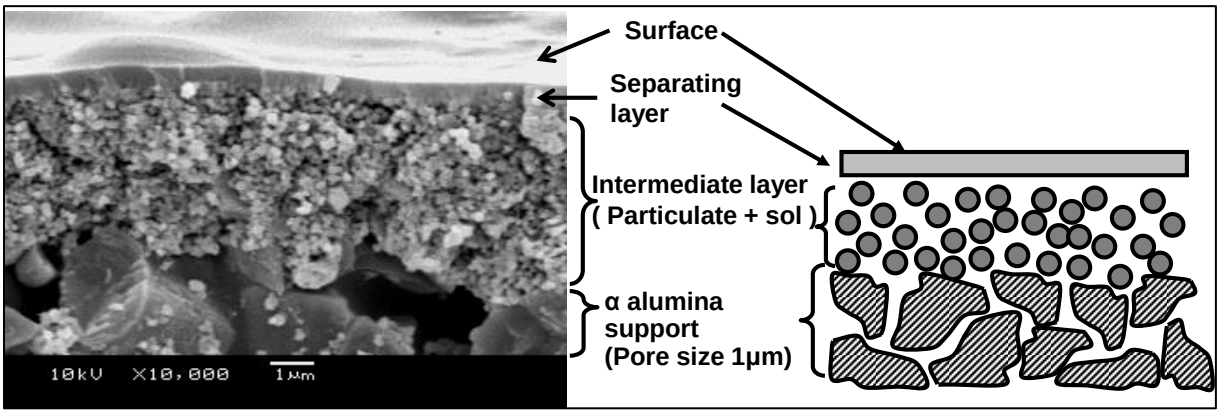

Figure 1-3 Typical structure of inorganic membrane [4]

Table 1-1 Advantages, disadvantages and applications of inorganic membranes [4-6]

Advantages/ Disadvantages	Applications
Advantages	
Thermal stability	Separation at high temperature, steam sterilization
Resistance to organic solvents	Separation of non-aqueous systems, separation of oil
Resistance to chemicals, acidic, alkali	Chemical cleaning, recovery of acid/basic
Resistance to peroxide	Chemical cleaning, application of textile processing
Mechanical strength	Back-washing
Long life time	
Uniform pore size	Depend on the preparation methods
Disadvantages	
Difficult sealing and module construction	

1.2.1. Brief history of inorganic membranes

Research on inorganic membranes was performed as early as the 1940's. The use of inorganic membranes started when the United States (U.S.) government utilizing porous alumina membranes for their uranium enrichment process for power generation and nuclear weapons [6]. This enrichment generates the highly corrosive by-products such as hydrogen fluoride (HF) and other harmful oxyfluorides [5] which made the use of polymeric membranes impossible. In the 1970's the oil crisis had spurred, hence more interest in nuclear power and the need for large capacity uranium enrichment [6]. In addition, inorganic materials could also catalyze reactions at their surface, which led to further investigations into catalysis applications [7]. Moreover, as stated in Table 1-1, inorganic membranes has also been found to have more chemical, temperature and structural stability than commercial polymeric membranes. Due to this matter, it leads the evolution of several materials to be used as a inorganic membrane, including metal oxides [8-10], zeolites [11-13] and silica [14,15].

1.2.2. Brief evolution of silica and organosilica membranes

Generally, silica membranes are prepared by using tetraethoxysilane (TEOS) as a precursor and exhibits micropores of ~0.3 nm that allow small molecules such as helium (He) (kinetic diameter 2.6 Å) and hydrogen (H_2) (kinetic diameter 2.89 Å) to permeate. So it is reasonable to expect a high selectivity for water (H_2O) (kinetic diameter 2.6 Å) to permeate in a RO process too. These membranes have been extensively investigated for hydrogen separation from gaseous mixtures such as H_2/CO_2, H_2/N_2, and H_2/CH_4. However, the sizes of the micropores for these silica membranes appeared to be too small to achieve an efficient separation of, for example, CO_2/N_2 and CO_2/CH_4, as well as hydrogen separation from light hydrocarbons such as C_2 to C_4 [16,17]. However, in the presence of water, SiO_2 has a low microstructural and hydrothermal stability [18, 19], even at temperatures as low as 60 °C [18-21]. Continuous exposure to water results in the release of silica moieties; as a result, dense particles or defects with large nonselective pores are formed [20]. Therefore, extensive efforts have been devoted in controlling the pore size of amorphous silica membranes as well as improving the hydrothermal stability of silica membranes. Due to this matter, indirectly, the research on organosilica membranes start blooming as discussed below.

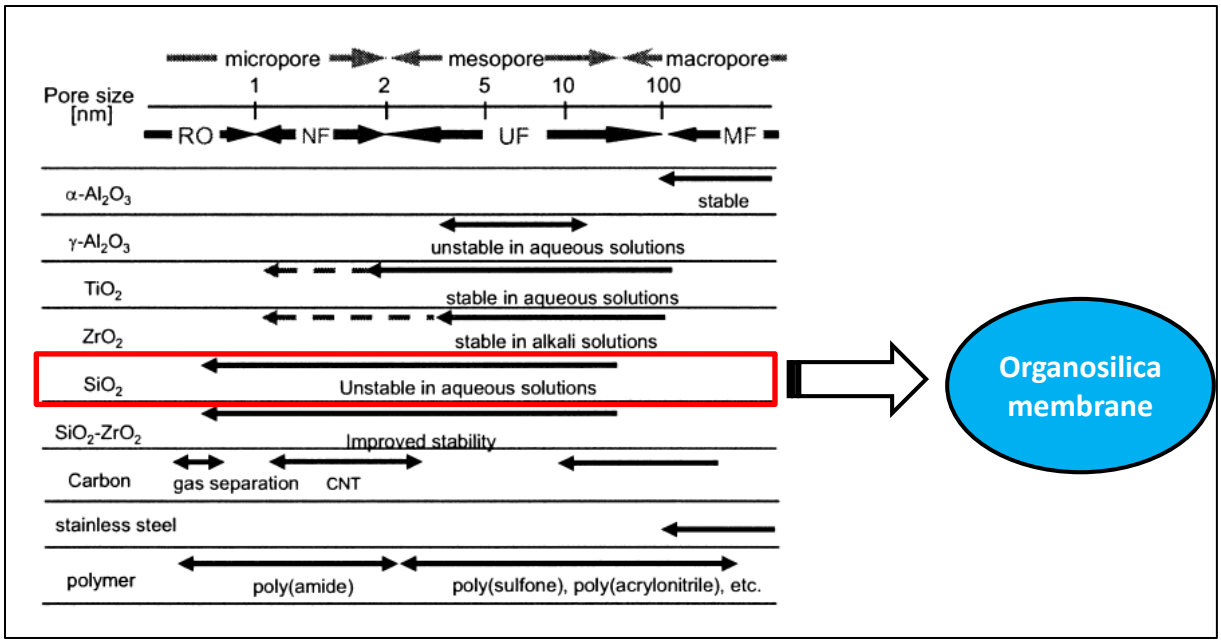

Figure 1-4 Inorganic materials and membrane pore sizes for use in membrane separation [4]

1.2.2.1.Tuning of silica pore network engineering

Currently, there are two types of techniques to control the pore sizes of the amorphous silica membranes known as template [22] and spacer [20; 23, 24] methods. Figure 1-5 (a-c) shows three types of pore tuning methods of silica membrane.

In the organic-template method as shown in Figure 1-5 (b), the pore sizes can be controlled by burning out the organic functional groups during the post synthesis treatment. Therefore, the size and shape of the micropores in the membranes will be determined by the size and shape of the organic functional groups. Kusakabe et al. [25] investigated the effect of the length of alkyl groups on pore structure, as well as the permeation properties for silica membranes, which were prepared by co-polymerization of TEOS and either octyl-, dodecyl- or octadecyltriethoxysilane. However, the inorganic networks prepared by pyrolysis of organic groups might be densified in a hydrothermal condition, since the amorphous silica structures created by the (–Si–O) unit after the organic groups burn out in air is not stable in the presence of water vapor, even at room temperature, due to the dissolution and rearrangement of silanol groups [26, 27].

Due to this matter, Castricum et al. 2008 [20], had developed a hydrothermally stable microporous network membrane using 1,2-bis(triethoxysilyl)ethane (BTESE) and methyltriethoxysilane (MTES) for pervaporation of alcohol mixtures application. On the other hand, Kanezashi et al. 2010 [24] proposed spacer method as to control the amorphous silica network. The spacer method as shown in Figure 1-5 (c) that consists of an amorphous network with both organic Si–C_n–Si bridges and inorganic Si–O–Si bonds are reported as a

promising method for the fabrication of microporous organosilica membranes. A great variety of organic bridges can be used for both methods, including aromatic, alkyne, alkene, alkane and functional moieties [18; 28, 29].

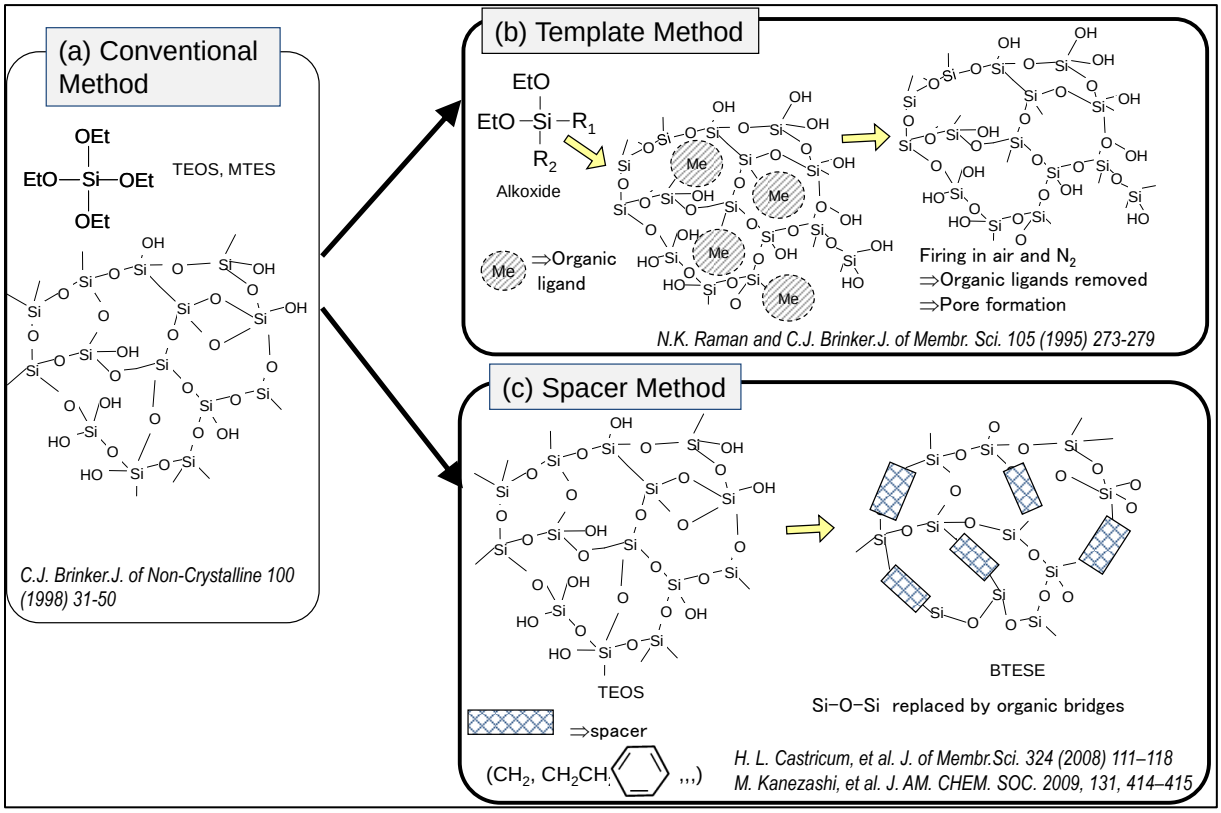

Figure 1-5 Methods of pore tuning of silica membranes (a) conventional method (b) template method (c) spacer method

In this study, we focused on the spacer method to study on the applicability of organosilica membranes by adjusting the size, flexibility, and shape of the organic bridging groups as a silica precursor. Thus, BTESE was chosen as a linear alkylene bridge with two silicon alkoxides while 2,4,6-tris[3(triethoxysilyl)-1-propyl]-1,3,5-triazine (TTESPT) was chosen as a triple silicon alkoxides with a 1,3,5-triazine as a core unit. Figure 1-6 shows the structures of different Si-precursors used in this work.

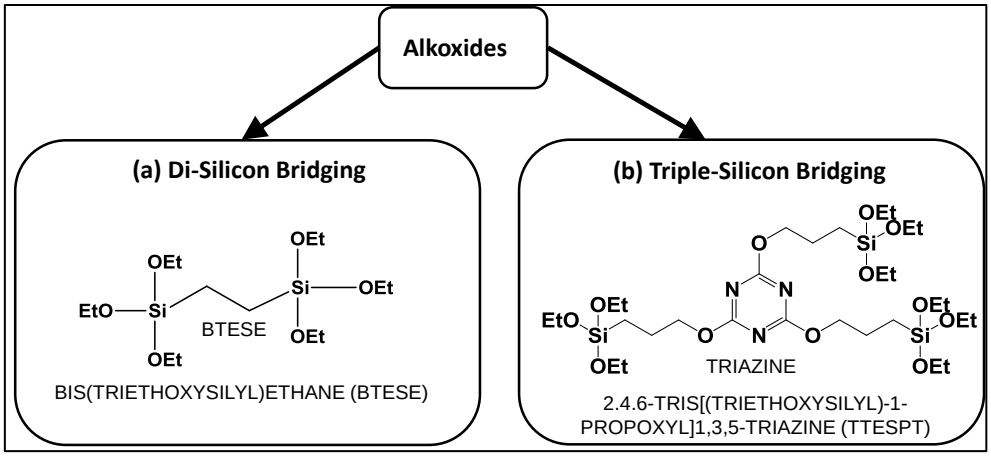

Figure 1-6 Structures of different Si-precursors

In this research work, sol-gel method was employed to prepare and tune the pore size of the organosilica membranes. The sol gel process is divided into two main routes: the colloidal and polymeric sol-gel routes as shown in Figure 1-7 [6; 31, 32]. In the colloidal sol-gel route, the hydrolysis and condensation steps cannot be distinguished, due to the faster kinetics thus formed packed colloidal particle, whereas in the case of the polymeric sol-gel route these two processes were believed to occur consecutively (low hydrolysis rate), which is achieved by adjusting sol process parameters (i.e. hydrolysis ratio, acid ratio, water ratio, precursor concentration and reaction time) thus resulting in a fully hydrolyzed alkoxide (highly branched polymer) [4,30]. Since, the size of the gel network is smaller than the size of the colloidal sols, the polymeric sol route is appropriate for the preparation of microporous materials [4,6].

Besides, in the sol–gel membrane fabrication process, coating is one of the most critical steps for the formation of the selective layer formation. Multi-step dip-coating, which is often used in literature, results in a multi-layered structure with thicker selective layers that can be more selective but will show lower permeances [33]. In addition, a high separation performance of molecular sieving membrane needs to be coupled with a good mechanical structure membranes as to achieve sufficient lifetime of the membrane coatings on the support as their functionalities can be lost if the coated membrane are deteriorated due to wear or environmental degradation. In many cases, the good morphology and mechanical integrity of the membranes can be designed by applying different types of thermal treatment or firing environments. According to Burggraaf, [34], the tensile stresses induced by drying and subsequent firing of the membrane module must be minized in order to produce high qualitity membrane layers. If water is expelled from the pores too quickly, pinholes and flaws will form. It was reported that higher temperatures result in a decrease of membrane surface area and a larger pore size due to the grain growth of ceramic particles [35]. However, limited number of study reported on the effect of different firing environments during membrane

preparation.

Here, the main focus of our study was put on the effect of water ratio, coating and firing environments during membrane preparation.

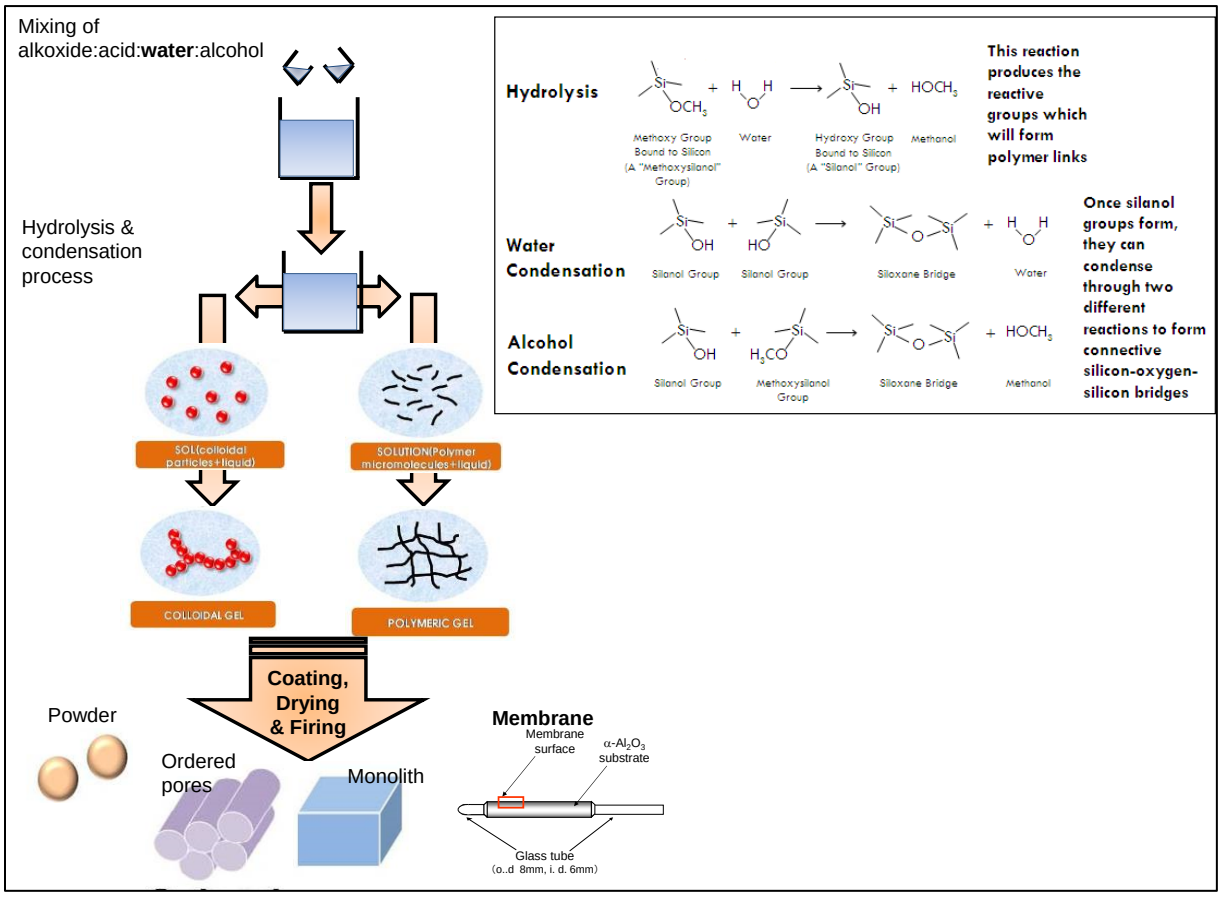

Figure 1-7 Schematic of sol gel routes [6; 31, 32]

1.3.Emerging applications of organosilica membranes

A new class of hybrid silica materials, known as periodic mesoporous organosilicas (PMOs), is highly promising for applications in various fields since they were first synthesized by three different research groups; Toyota Central R&D Laboratories Japan [36], Materials Chemistry Research Group, University of Toronto [37] and Department of Chemistry, University of Minnesota [38] in 1999 [36-38]. In PMOs, the functional organic groups are homogeneously incorporated in the three-dimensional silica networks as bridges. The versatility of organic bridges offers the ability to tune the bulk properties such as thermal stability, surface area, porosity, flexibility, chemical resistance and hydrophobicity [39]. A variety of complex functional groups have been introduced into PMOs, as described in specialized reviews [40-42]. However, pore size of mesoporous PMOs always larger than 2 nm and has no molecular sieving properties. Hence, as mentioned earlier, research on

organosilica membrane (pore size < 1 nm) was started to bloom, indirectly, from extensive efforts by several researchers [20; 22-24] in order to control the pore size of amorphous silica membranes as well as improving the hydrothermal stability of silica membranes. Nowadays, organosilica membranes have been used in many applications such as pervaporation (PV), gas separation (GS), and reverse osmosis (RO). In this study, our focus was on the applicability of organosilica membrane in gas and reverse osmosis (RO) separation areas with a major concern on the RO separation. Below are some explanations on the progress of organosilica membranes in these three areas.

1.3.1. Organosilica membrane in pervaporation (PV)

In 2004, Campaniello et al. [43] has modified the hydrophilic part of SiO_2 by incorporating methyl groups in the SiO_2 microstructure. The microporous silica membranes was proven to enhance the service time in the dehydration of a butanol–water mixture at 95 °C from a few weeks to more than 18 months with a water flux of about 4 kg m^{-2} h^{-1} and a selectivity between 500 and 20 000. Another approach had been made by Castricum et al. in 2008 [20, 23]. They reported the development of microporous organosilica membranes by co-condensation of 1,2-bis(triethoxysilyl)ethane (BTESE) and methyltriethoxysilane (MTES). The resulting organosilica membranes showed a quite stable performance of 2 years for the pervaporative dehydration of butanol at 150 °C with high separation 4000 and water flux 20 kg m^{-2} h^{-1} [20, 23]. On the other hand, Tsuru et. al. [44] had reported that BTESE-derived silica membranes could be applied in the dehydration of aqueous acetic acid (AcOH) solutions. It was found to show high permselectivity with excellent stability ~1800 h. The permeate flux for aqueous AcOH solutions (AcOH: 90wt%, 75°C) was 2.0–4.0 kg m^{-2} h^{-1} with water selectivity of 200–500. Table 1-1 shows summary of organosilica membranes in pervaporation (PV), area.

Table 1-1 Summary of organosilica membranes in pervaporation (PV), area.

	Pervaporation (PV)			
Organosilica membranes	Operating condition	Water flux [kg m^{-2} h^{-1}]	Separation factor [-]	Ref
MTES/TEOS	BuOH/H_2O mixture at 95°C	4	~500 and 20 000	[43]
BTESE/MTES	BuOH/H_2O mixture at 150°C	20	4000	[20,23]
BTESE	AcOH/H_2O mixtures at 75°C	~2.0–4.0	~200–500	[44]

1.3.2. Organosilica membrane in gas separation (GS)

Another utilization of organic inorganic hybrid alkoxides is in GS application. Brinker et al. [22] issued the first report on CO_2 separation membranes by controlling the silica network size created by the organic template method using methyltriethoxysilane (MTES)/TEOS derived silica. The CO_2 permeance showed ~10^{-7} mol m^{-2} s^{-1} Pa^{-1} with CO_2/CH_4 selectivity higher than 70.

After that more design on silica networks was reported by using bis(triethoxysilyl)ethane (BTESE, Si-C-C-Si unit structure) as a silica precursor in the development of a highly permeable hydrogen separation membranes with hydrothermal stability [24, 45]. BTESE-derived silica membrane showed extremely high H_2 permeance (as high as 10^{-5} mol m^{-2} s^{-1} Pa^{-1}) with separation factors moderate for H_2/N_2 (~20), and quite high for H_2/SF_6 (~20,000). It was reported that BTESE-derived silica membranes can also be used in membrane reactors for methylcyclohexane (MCH) dehydrogenation to toluene (TOL). The hydrogen permeance was reported higher than 1×10^{-6} mol m^{-2} s^{-1} Pa^{-1} with H_2/TOL selectivity increased from 100 to 10,000 by increasing the H_2O/BTESE molar ratio from 6 to 240, while in MCH dehydrogenation, a BTESE-derived silica membrane reactor with a Pt/γ-Al_2O_3/α-Al_2O_3 bimodal catalytic layer achieved MCH conversion of 75% that was higher than the equilibrium conversion of 60%, and a hydrogen purity in the permeate stream of more than 99.9% at 230 °C [46].

Since BTESE-derived silica membranes are suitable for the separation of hydrogen from organic gas mixtures, [24, 45] bis (triethoxysilyl) methane (BTESM, Si–C–Si unit) membranes with a silica network size that is between those of TEOS-derived and BTESE-derived membranes are supposed to be suitable for the separation of mixed gases of similar molecular sizes, such as olefin/paraffin, which is one of the most attractive applications of membrane separation. M. Kanezashi et al. [47] had reported that BTESM-derived silica membranes fired at 200 °C and 350 °C showed moderate C_3H_6/C_3H_8 permeance ratio ~6.83 and ~7.8–13.2 at permeation temperature 180-200 °C, respectively. However, by doping Al into BTESM membranes, the separation for C_3H_6/C_3H_8 was found high approximately 25-35 at the same permeation temperature [48].

Furthermore, the influences of size, flexibility, and shape of various alkyl and aryl bridges on the membrane pore size, nanostructure, and affinity was described to determine the relationship between the bridging group and the membrane properties in both GS and PV separation [28]. Table 1-2 shows summary of organosilica membranes in gas separation (GS) area.

Table 1-2 Summary of organosilica membranes in gas separation (GS) area

Gas separation (GS)				
Organosilica membranes	Operating condition [°C]	Permeance [mol $m^{-2}s^{-1}$ Pa^{-1}]	Separation factor [-]	Ref
(MTES)/TEOS	-	CO_2~1×10^{-7}	CO_2/CH_4~>70	[22]
BTESE	200	H_2~1×10^{-5}	H_2/N_2~20 ; H_2/SF_6~20,000	[24,45]
BTESE water ratio 6 to 240	200	H_2~1×10^{-6}	H_2/TOL~100 to 10,000	[46]
BTESM-200	180–200	C_3H_6~1.85×10^{-8}	C_3H_6/C_3H_8~6.83	[47]
BTESM-350	180–200	C_3H_6~$1.2–10.7\times 10^{-8}$	C_3H_6/C_3H_8~7.8–13.2	[47]
Al-BTESM-200 (Si : Al = 9 : 1)	180–200	C_3H_6~$0.63–0.71\times 10^{-8}$	C_3H_6/C_3H_8~25–35	[48]

1.3.3. Organosilica membrane in reverse osmosis (RO)

Organosilica materials also seem to be another promising candidate for RO desalination membranes due to their excellent molecular sieving ability. However, only limited paper published on the application of RO organosilica membranes. This motivates our group to examine the possibility of using organosilica membranes for RO desalination.

According to Xu et al. [49] BTESE-derived organosilica membranes have shown superior retention performance for mono and bivalent ions and neutral solutes of low-molecular weight, such as isopropyl alcohol and glucose. The BTESE-derived organosilica membranes exhibited excellent resistance to chlorine and exceptional hydrothermal stability, as well as superior salt rejection of >97%, showing great promise as robust RO membranes.

Compared with BTESE membranes, bis(triethoxysilyl)ethylene, BTESEthy membranes [50], with polarizable and rigid ethenylene bridges in the network structure have led to improved water permeability and high NaCl rejection (>98.5%). Bis(triethoxysilyl)acetylene, BTESA membranes [51] on the other hand, shows high water permeability and lower salt rejection due to enhanced H_2O-affinity both in the pore channels and on the membrane surface.

Owing to the limited literatures on organosilica materials applied in the RO area, Table 1-3 summarized all the materials that had been used in RO area including polymer and inorganic membranes for performance comparison. From the listed data in Table 1-3, by comparing organosilica membranes performance with inorganic zeolite membranes such as ZSM-5 and

silicalite, organosilica membranes showed higher water permeability. Although, the commercial polyamide RO membranes (seawater RO membrane, SW30HR; low-pressure RO membrane, ES10) had higher water permeability than organosilica membranes, these polyamide membranes suffered from poor resistance to chlorine, the concentration of which was normally recommended to be lower than 5000 ppm h and low thermal stability [52-56]. BTESE and BTESEthy membranes had already exhibited high chlorine tolerance and thermal stability [49,50].

Due to this versatile characteristic of organosilica membrane, it is a great importance to examine the technical capabilities of the BTESE membrane in term of fouling and cleaning processes.

Table 1-3 Summary of membranes in reverse osmosis (RO) area

Reverse osmosis (RO) for NaCl sols separation					
Organosilica membranes					
	Operating condition	L_p [m^3 m^{-2} s^{-1} Pa^{-1}]	R_{NaCl} [%]	Comments	Ref
BTESE	1.15 MPa;25°C;2000 ppm	1.0×10^{-13}	97	Cl~ 35,000 ppm h	[49]
	1.15MPa;90°C; 2000 ppm	9.0×10^{-13}	98	Thermal stability~90°C	
BTESEthy	1.15 MPa;25°C;2000 ppm	2.0×10^{-13}	99	Cl~ 22,500 ppm h	[50]
	1.15MPa;90°C; 2000 ppm	1.5×10^{-12}	98	Thermal stability~90°C	
BTESA	1.15 MPa;25°C;2000 ppm	7.0×10^{-13}	95		[51]
Other types of membrane materials					
SW30HR (Film Tec)	2.76 MPa, 21°C;2000 ppm	2.2×10^{-12}	98.5	Cl~ 5,000 ppm h	[52-55]
				Thermal stability~55°C	
ES10 (Nitto Denko)	1 MPa, 24°C;104 ppm	1.2×10^{-11}	99.2	Cl~ 5,000 ppm h	[53-56]
				Thermal stability~<55°C	
NaA-TFC polyamide	1.6 MPa; 25 °C; 2000 ppm	~5.6×10^{-12}	~96	High L_p and improved in	[35]
Silicate 1-TFC polyamide	1.6 MPa; 25 °C; 2000 ppm	~1.3×10^{-11}	~92	R_{NaCl} after coupled with	[35]
Graphene Oxide -TFC polyamide	1.5 Mpa; 25 °C; 2000 ppm	~5.6×10^{-12}	~96.4	polyamide	[36]
				No Cl test found	
Silicalite	2.7 MPa; 25 °C; 0.1 M	~4.3×10^{-14}	~99	Low L_p and R_{NaCl}	[38]
ZSM-5, Si/Al = 50	2.7 MPa; 25 °C; 0.1 M	~1.4×10^{-13}	~92	No Cl test found	[39]
MFI- Zeolite	7 MPa; 21 °C; 3000 ppm	~2.9×10^{-13}	~80		[40]
	7 MPa; 90 °C; 3000 ppm	~5.9×10^{-13}	~75		
Ultrathin graphene Nano-filtration	0.5 MPa; 25 °C; 1168 ppm	~6.1×10^{-11}	~41		[41]

1.4. Fouling and cleaning of membrane

Membrane fouling can be reversible or irreversible. The original permeate flux of a membrane fouled from reversible fouling can be recovered after system pressure is released and the necessary cleaning protocol (such as backwashing or chemical cleaning) has been performed. Irreversible fouling causes a permanent decrease in membrane productivity through decreased permeate flux even after cleaning has been performed. Irreversible fouling will decrease the integrity of the membrane by reducing its lifetime and productivity.

1.4.1. RO membrane fouling

RO membrane fouling is one of the pressing issue the industry need to solve. In the literature, Potts et al. [57] provided a range of definitions for membrane fouling varying from a simple to complex definitions. The simplest of all definitions is "the phenomenon where foulants accumulate on RO membranes leading to performance deterioration [57] as shown in Figure 1-8 (a).

In order to predict membrane permeate flux decline, a thorough out understanding of all contributing fouling mechanisms is required. As mentioned earlier, membrane fouling occurs as a result of foulants being brought to and accumulating on the membrane surface. Mechanisms leading to flux decline for loose membranes, such as MF and UF, include pore blocking (when foulants cover membrane pore surfaces] and pore constriction (when foulants reduce pore size by clogging pores). Concentration polarization and cake/gel layer formation are fouling mechanisms of all types of membranes. Fouling during NF and RO is often assumed to occur only on the membrane surface or form cake layer due to the tightness of NF and RO membranes and relative size of the foulants compared to membrane pore size [58]. Figure 1-8 (b to d) shows the three mechanisms of membrane: external pore blocking, internal pore blocking, and cake filtration while Table 1-4 shows the cause and effect of these 3 types of fouling [59].

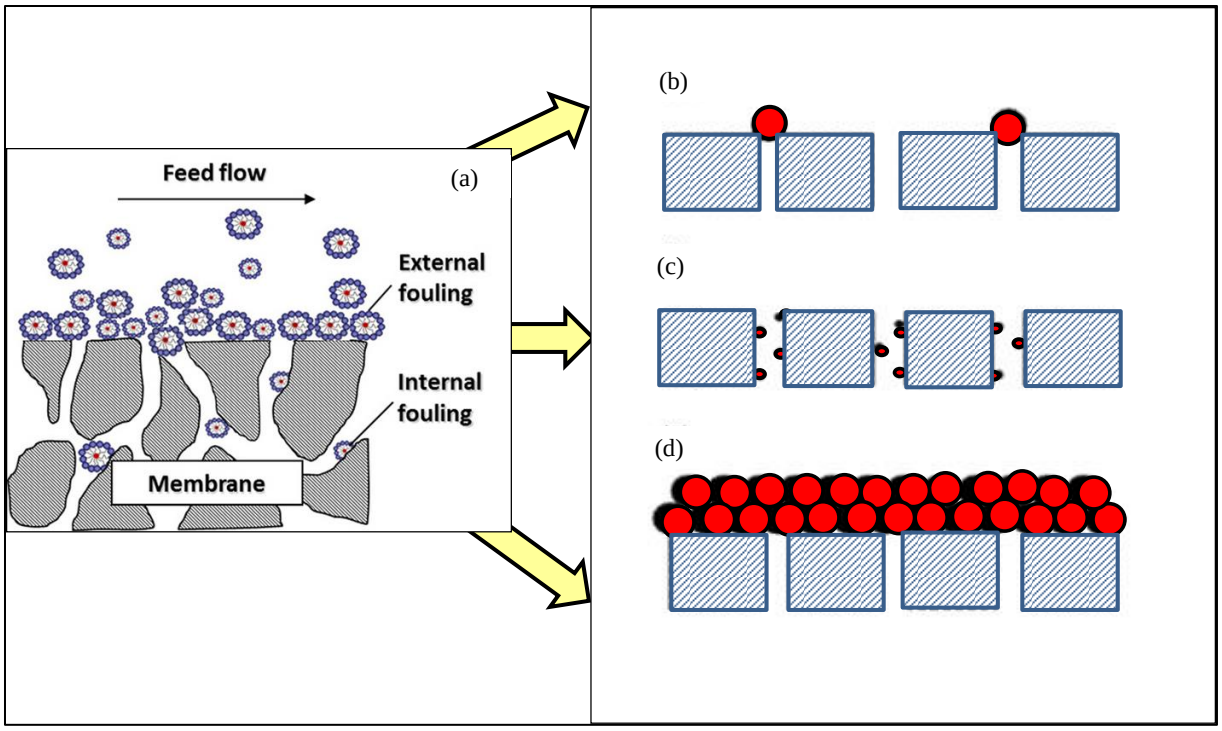

Figure 1-8 (a) Membrane fouling and three types of fouling mechanisms: (b) External pore blocking (c) Internal pore blocking (d) Cake filtration.

Table 1-4 Fouling mechanisms, cause and effect on mass transportation

Fouling mechanisms	Cause of fouling	Effect on mass transportation
(a) External pore blocking	Particles larger than the pore size block pores	Reduction of the active membrane area. Depends on feed velocity.
(b) Internal pore blocking	Particles smaller than pore size enter the pores and get either adsorbed or deposited onto the pore walls	Increase in membrane resistance due to pore size reduction. Internal pore blocking is independent of feed velocity.
(c) Cake filtration	Formation of a cake on the membrane surface by particles	The overall resistance becomes the resistance of the cake plus the resistance of the membrane

1.4.1.1. Factors affecting membrane fouling

Fouling behavior is mainly influenced by three factors; (a) Filter configuration, (b) membrane properties and (c) foulants and solution properties as shown in Figure 1-9.

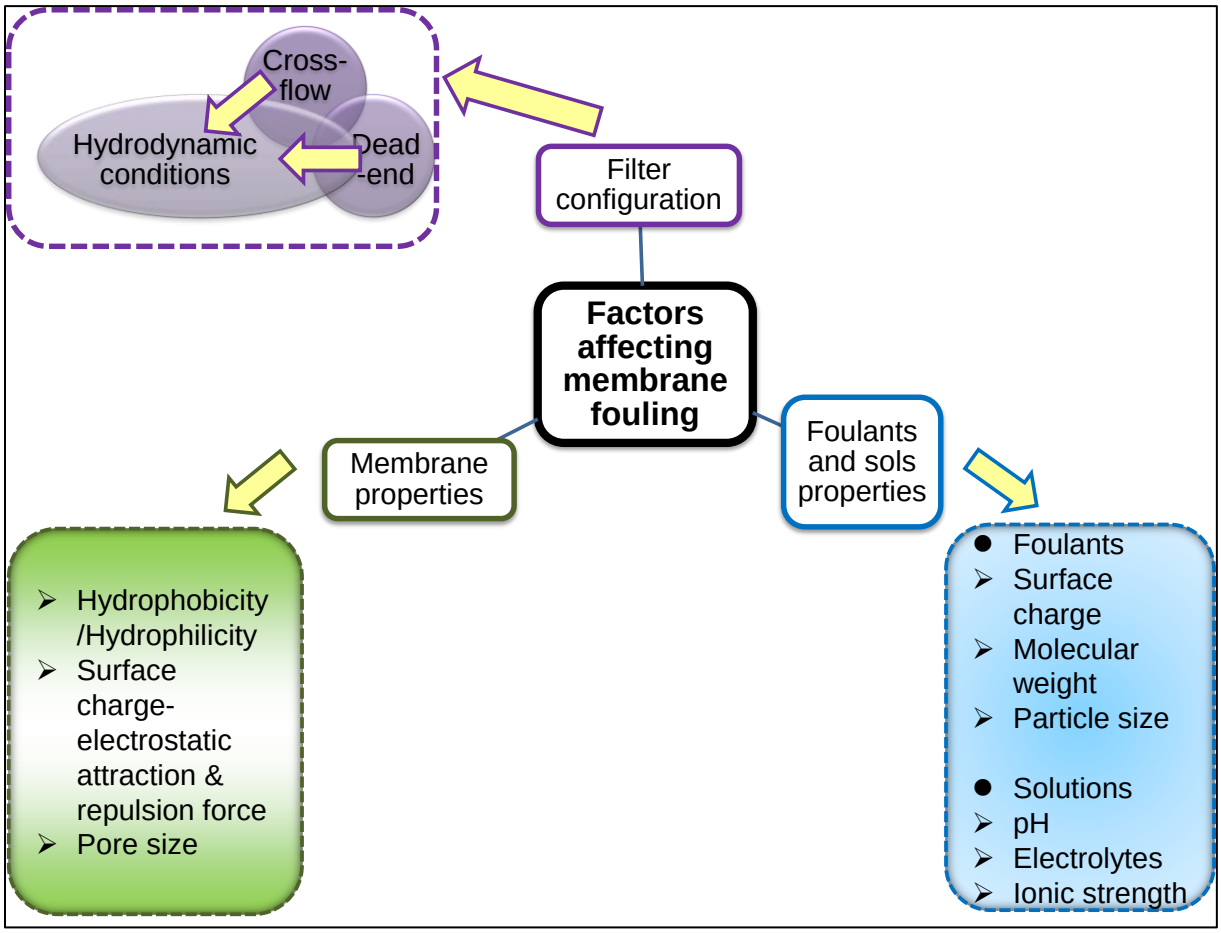

Figure 1-9 Charts of factors affecting membrane fouling

Filter geometry is very important during membrane processes, as hydrodynamic conditions determine particle accumulation and fouling layer formation on the membrane surface, which in turn affects resistance and flux decline. Generally, spiral wound, hollow fiber, plate and frame set-ups are all used in industrial applications incorporating with two configurations such as a “cross-flow” and “dead-end” configurations. “Cross-flow” configuration utilizes tangential dynamics along the surface of the membrane, while a "dead-end" configuration only allows for flow through the membrane (perpendicular to the membrane) (Figure 1-10). In this study, cross-flow configuration was chosen. The advantage of cross-flow filtration over dead-end filtration is that accumulation of particles on the membrane surface is reduced [60]. Cross-flow filtration creates shear effects on the surface of the membrane that can help alleviate the formation of thick fouling layers. In cross-flow

configurations, the retentate (concentrated water retained by the membrane) can also be recycled back to the beginning to be filtered again, whereas in dead-end filtration the fluid exposed to filtration is limited by permeate flux.

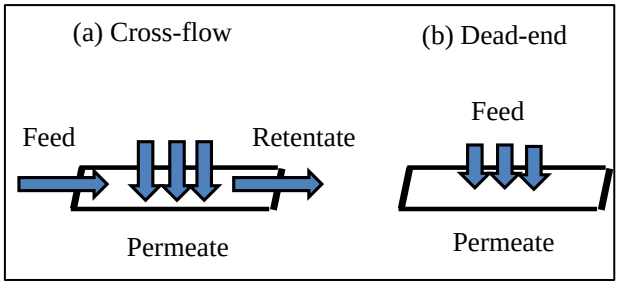

Figure 1-10 Schematic image of (a) cross-flow and (b) dead-end

In term of membrane properties, RO membranes are usually characterized by hydrophobicity/hydrophilicity, and surface charge of the thin outermost layer [58, 61,62]. The hydrophobicity of RO membranes is considered one of the most influential factors in membrane fouling [62]. A large portion of fouling is thought to be caused by organic compounds that adsorb on the membrane surface via hydrophobic interactions. Meanwhile, hydrophilic non-interacting membranes are thought to decrease protein adsorption, even though hydrophobic interaction is not the only interaction involved in adsorption [63]. If the membrane surface is charged, electrostatic attraction or repulsion forces between charged foulant components and the membrane surface can also influence the degree of fouling [64].

Generally, type of foulant being filtered was characterized by its surface charge, molecular weight or particle size, or hydrophobicity. Solution conditions (i.e. pH, salt ion type, and ionic strength) can affect foulant characteristics, membrane surface properties, and how foulants interact with each other and the membrane surface. Fouling is the greatest during filtration of solutions that have conditions in which foulant molecules are the least stable and exhibit the weakest attractive interactions [65, 66]. For example, hydrophilic uncharged dissolved foulants exhibited the least fouling at neutral pH, while negatively charged components perform better at high pH [62]. As an example bovine serum albumin [BSA] shows that fouling of solutions with a pH close to BSA's iso-electric point (IEP) created the greatest fouling flux decline due to aggregation caused by weakened electrostatic repulsion of the BSA molecules [66]. High ionic strength solutions enhance double layer compression and charge-shielding effects, leading to weaker electrostatic repulsion, also creating more rapid fouling conditions [66]. Calcium ions have been shown to significantly enhance fouling in the presence of natural organic matter (NOM) by forming complexes which result in highly compacted fouling layers and thus more severe flux decline [65, 67, 68]. The strength of the intermolecular adhesion forces between bulk foulants and the membrane surface has been shown to control the rate of fouling [69]. Furthermore, the strength of the foulant-foulant

interactions also plays a key role in determining the rate and extent of organic fouling [69]. Another type of foulants is a surfactant. Surfactants are a class of industrially very important amphiphilic substances which consist of a hydrophilic head group to which a hydrocarbon chain is connected. One of the characteristic properties of amphiphilic substances is that they tend to assemble at interfaces. They are therefore often referred to as surface-active agents. Another characteristic property of amphiphilic substances is the formation of large aggregates (micelles). In these micelles, the hydrophilic heads are directed towards the aqueous solution, while the hydrophobic tails are turned inside. Surfactants are categorized into four groups depending on the charge on the head group: nonionic, anionic, cationic and zwitterionic surfactants [70].

In this study, our fouling module is a cross flow unit and BTESE membrane. Four types of foulants were chosen for this study such as bovine serum albumin (BSA), sodium alginate (SA), sodium dodecyl sulfate (SDS), and dodecyltrimethyl ammonium bromide (DTAB).

1.4.2. Membrane Cleaning

A common method of recovering water flux caused by membrane fouling is through membrane cleaning. Backwashing is one method of cleaning ultrafiltration and microfiltration membranes that involves reversing the water flow [71]. In water treatment plants, one membrane module or treatment train will be periodically shut-down for a short amount of time anywhere from 15 min. to 1 hour [72, 73] during cleaning while the other trains continue to operate. Foulant is removed through turbulent hydrodynamic forces at the membrane surface that loosens the fouling layer.

Chemical cleaning is a common method of cleaning nanofiltration and reverse osmosis membranes, where backwashing is not physically possible due to membrane asymmetry and tighter pore structures. Cleaning with chemicals works by creating solution conditions favorable for foulant dissolution as opposed to deposition on the membrane surface [74]. Generally, increased temperatures will increase dissolution, however most membrane materials are sensitive to degradation at high temperatures [75]. Cleaning agents accomplish this by changing the morphology of the foulants, the relative activity of the foulant in solution or the interaction between foulants within the fouling layer [69]. Typical cleaning agents include surfactants such as sodium dodecyl sulfate (SDS) and Tween 20, alkaline agents such as sodium hydroxide (NaOH), acidic agents such as hydrochloric acid (HCl), sulphuric acid, citric acid, and oxalic acid, chelating agents such as ethylenediaminetetraacetic acid (EDTA], and enzymes [69, 73, 76-79].

Choosing the most effective chemical cleaning agent is dependent upon a combination of the foulants present in the water and the membrane material. Surfactants are effective at cleaning protein adsorption if the concentration is above a critical micelle concentration [65].

Alkaline chelating agents are efficient at chemical cleaning nanofiltration membranes when fouled by a combination of NOMmetal complexes, however, they can also permanently reduce membrane ion rejection [77]. EDTA is particularly effective at cleaning Ca-organic complexed fouling layers when used at a high enough concentration [69, 70] Inorganic foulants, however, may not be removed by alkaline agents and may require periodic acidic cleaning [77]. Table 1-5 summarized all these types of chemical cleaning agents and its usage.

Table 1-5 Summary of chemical cleaning agents and its usage

Types of chemical cleaning agents	Example	Usage in cleaning	Ref
Surfactants	Sodium dodecyl sulfate (SDS) and Tween 20	Protein adsorption	[65]
Alkaline	Sodium hydroxide (NaOH)	A combination of NOMmetal complexes	[77]
Acidic	Hydrochloric acid, Sulphuric acid, Citric acid, and Oxalic acid	Inorganic foulants	[77]
Chelating agents	Ethylenediaminetetraacetic acid (EDTA) and enzymes	Ca-organic complexed	[69,70]

In this study, it is worthwhile to point out that inorganic membranes have inherently versatile characteristics; high thermal stability and chemical resistance. Thus, these advantages make them suitable candidates for hot water cleaning conditions.

1.5.Objectives and organization of this research

The overall of this dissertation research is focus on the preparation of organosilica membrane and application to use in gas separation (GS) and reverse osmosis (RO) applications. Two types of organosilica materials; TTESPT and BTESE were chosen for this study. Since, TTESPT is a new existence organosilica; hence we emphasized more extra study on its potential in gas and RO separation areas (Chapter 2 and 3). However, due to much coating times of top layer (6 times) needed to prepare a good separation performance of TTESPT membranes, thus we decided to study more detail on the optimization part of the BTESE membranes involving a more comparative study for the temperature dependency permeation properties of NaCl as well alcohols (ethanol and isopropanol) via different water ratio (WR) of BTESE membranes (Chapter 4). In Chapter 5, the morphology, structural properties and separation performance of BTESE membranes in gas and reverse osmosis

(RO) applications were investigated with respect to WR and different firing environments. Furthermore, we tried to correlate the relationship between gas and water permeance as well permeance ratio of gases with the rejection of solute. In Chapter 6 we examined the technical capabilities of the BTESE membrane in term of fouling and cleaning processes. Finally, conclusions and recommendation were presented in Chapter 7. Figure 1-11 shows the simplified of the flow of this dissertation

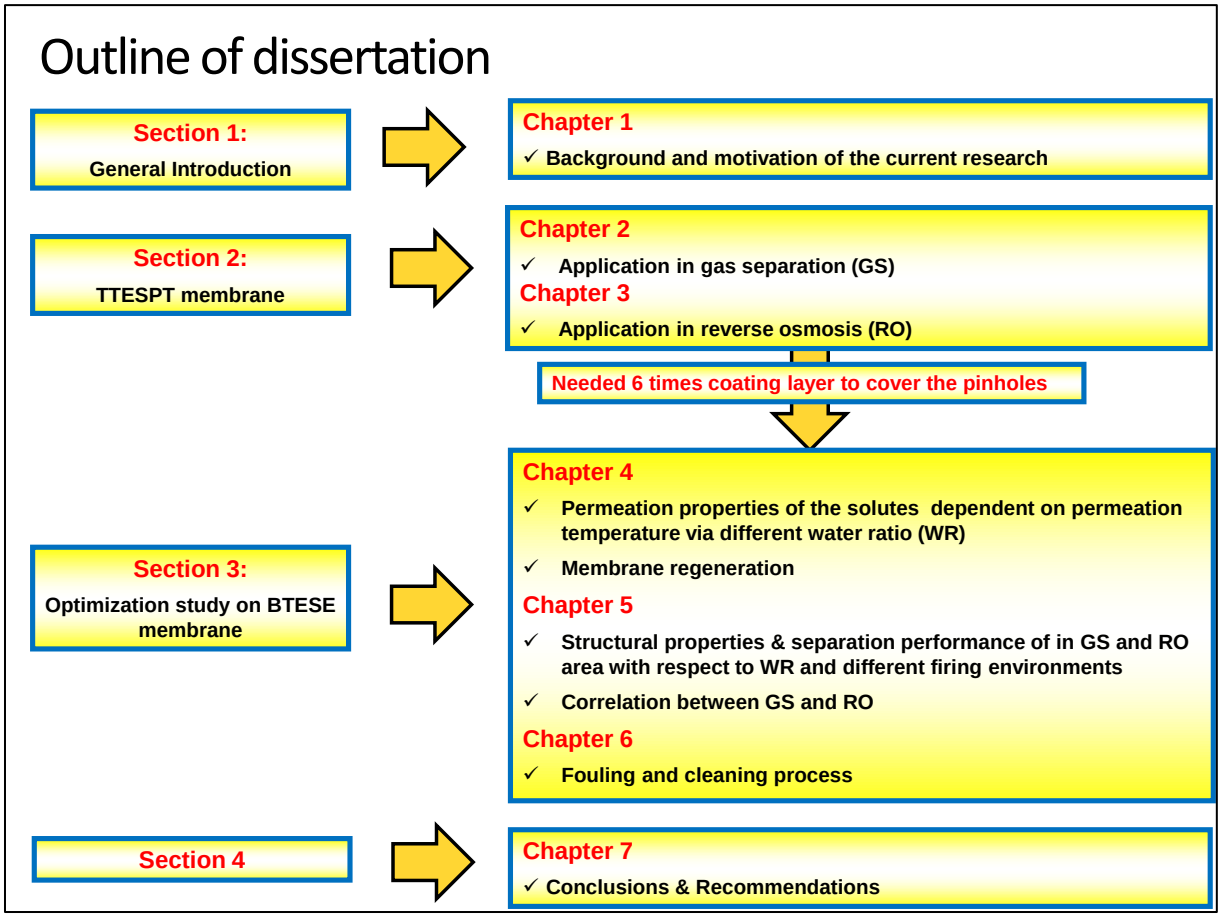

Figure 1-11 shows the simplified of the flow of this dissertation

The brief descriptions of each chapter in this dissertation are shown below:

Chapter 1 is **"General introduction"** which provides the background and motivation of the current research.

Chapter 2 is **"Effect of firing temperature on the structural and gas separation performance of 2,4,6-tris- [3(triethoxysilyl)- 1-propoxyl]-1,3,5-triazine (TTESPT)"** which describes a development on the 2,4,6-Tris[3(triethoxysilyl)-1-propoxy]-1,3,5-triazine (TTESPT) membrane. Since, TTESPT is a new existence organosilica; hence we emphasized more extra study on its potential in gas separation area. The TTESPT-derived silica membrane exhibits a significant degree of selectivity for C_3H_6–C_3H_8 ~37 at a permeation

temperature of 50 °C, which greatly surpasses the upper-bounds of selectivity and permeance trade-off of carbon membranes. This indicates the potential for further development toward C_3H_6–C_3H_8 separation applications.

Chapter 3 is **"Effect of water ratio on the structural and performance evaluation; gas separation and reverse osmosis of 2,4,6-tris- [3(triethoxysilyl)- 1-propoxyl]-1,3,5-triazine (TTESPT)".** In this research, TTESPT membrane has been developed for molecular separation processes in gas (gas separation) and liquid phases (reverse osmosis (RO)). By adjusting the H_2O/TTESPT molar ratio, we found a promising technique for tuning the pore network of TTESPT membranes. A TTESPT membrane with a high H_2O/TTESPT molar ratio exhibited a high degree of selectivity for H_2/SF_6 (greater than 4000) at a permeation temperature of 200 °C and demonstrated high sodium chloride (NaCl) rejection (>98.5%) with water permeability of $>1 \times 10^{-12}$ m^3 m^{-2} s^{-1} Pa^{-1} under operating conditions of 1 MPa and 60 °C during a RO experiment.

Chapter 4 is **"Robust BTESE membranes for high temperature reverse osmosis (RO) application: Membrane preparation, separation characteristics of solutes and membrane regeneration."** In this study, a pore network of bis(triethoxysilyl)ethane (BTESE) organosilica membranes was controlled by adjusting the molar ratios of BTESE/H_2O/acid=1/*x*/0.2 (*x*=3 and 240). The mechanisms for solute transport in the BTESE RO membrane were investigated using three different aqueous solutions of sodium chloride (NaCl), ethanol (EtOH) and isopropanol (IPA). It was noteworthy that the rejection of alcohols decreased with an increase in the RO operating temperature, while the electrolyte rejection remained almost constant. The BTESE membranes exhibited high thermal robustness under the long-term testing conditions, delivering salt rejections >98% until the end of the testing period (50 h). The BTESE membranes could also be regenerated after use in the gas and RO experiments, thus demonstrating robust properties.

Chapter 5 is **"Favorable of BTESE membranes for gas and reverse osmosis (RO) applications: Effect of preparation conditions on the structural and the correlation between gas and liquid permeation properties."** The aim of this work was to study the simultaneous effects of H_2O/BTESE molar ratio (WR) = (3, 60, 120, 240) in different firing environments on the structural and permeation properties of BTESE membranes. We found that most of organic peaks for sample fired in N_2 environment were more intense as compared with the samples fired in air environment. Thus, the samples fired in N_2 environment are more hydrophobic compared with the sample fired in air environment and can be proven by contact angle and H_2O adsorption results. In term of separation performance, the permeance of gases and H_2O were clearly dependent on WR. Increasing WR decreased the permeance of both gases and H_2O via the pore network of BTESE membrane. On the other hand, changing the firing environments also affected the permeance of gases and H_2O. Samples fired in air environment exhibited higher permeance of gases and H_2O due to more open pore networks.

In addition, the relationship between gas and liquid permeances was correlated by assuming He gas as a predictor of water permeance, N_2 gas as a predictor for IPA and SF_6 gas as a predictor for NaCl permeance. Increasing in He and permeance ratio resulted in increasing in water permeance and rejection of solutes.

Chapter 6 is **"New insights on fouling and cleaning properties of reverse osmosis (RO) BTESE membrane."**Initially, our attention is restricted to BTESE membranes and to understand the fundamentals of fouling phenomenon as well as its cleaning process. Four types of foulants such as bovine serum albumin (BSA), sodium alginate (SA), sodium dodecyl sulfate (SDS) and dodecyltrimethyl ammonium bromide (DTAB) were chosen. More pronounced fouling was seen for DTAB foulant compared with other foulants. It is worthwhile to point out that inorganic membranes have inherently versatile characteristics; high thermal stability and chemical resistance. Thus, these advantages make them suitable candidates for hot water cleaning conditions. Our main concern is to avoid any types of chemical cleaning agents in order to cleaning BTESE membranes. It was found out the optimize cleaning condition of fouled BTESE membrane by DTAB was by using hot water at 80 °C for 30 minutes.

Chapter 7 is **"Conclusions and Recommendations"**. Main conclusions and recommendations were presented here.

References

[1] M. Mulder, Basic Principles of Membrane Technology, Kluwer Academic Publishers, Dordrecht, (1996)

[2] R. W. Baker, Membrane Technology and Application, Second Edition, John Wiley and Son, Ltd

[3] L. Cot, A. Ayral, J. Durand, C. Guizard, N. Hovnanian, A. Julbe, A. Larbot, Inorganic membranes and solid state sciences, Solid State Sciences 2 (2000) 313–334.

[4] T. Tsuru, Inorganic porous membranes for liquid phase separation, Sep. and Purif. Methods, 30 (2001), 191-220.

[5] H. P. Hsieh, Inorganic membranes for separation and reaction. Amsterdam: Elsevier (1996).

[6] R.R. Bhave, Inorganic membrane synthesis, characteristics, and applications, New York: Van Nostrand Reinhold.(1991)

[7] A. C. Pierre, Introduction to sol gel processing. Boston: Kluwer Academic Publishers (1998).

[8] J. Sekulić, J. E. ten Elshof , D. H. A. Blank, A microporous titania membrane for nanofiltration and pervaporation, Adv. Mater. 16 (2004) 1546-1550

[9] T. Tsuru, K. Ogawa, M. Kanezashi, T. Yoshioka, Permeation characteristics of electrolytes and neutral solutes through titania nanofiltration membranes at high temperatures, Langmuir 26 (2010) 10897–10905.

[10] T. Tsuru, S. Izumi, T. Yoshioka, M. Asaeda, Temperature effect on transport performance by inorganic nanofiltration membranes. AIChE J. 46 (2000) 565–574.

[11] B. Zhu, J.H. Kim, Y.H. Na, I.S. Moon, G. Connor, S. Maeda, G. Morris, S. Gray and M. Duke, Temperature and Pressure Effects of Desalination Using a MFI-Type Zeolite Membrane, Membranes 3 (2013) 155-168.

[12] N. Liu, L. Li, B. McPherson, and R. Lee, Removal of organics from produced water by reverse osmosis using MFI-type zeolite membranes, J Membr. Sci. 325 (2008) 357–361

[13] L. Li, N. Liu, B. McPherson, and R. Lee, Enhanced Water Permeation of Reverse Osmosis through MFI-Type Zeolite Membranes with High Aluminum Contents, Ind. Eng. Chem. Res. 46 (2007) 1584-1589

[14] R. de Vos, H. Verweij, High-selectivity, high flux silica membranes for gas separation. Science. 279 (1998) 1710–1711.

[15] G. Lu, J. da Costa, M. Duke, S. Giessler, R. Socolow, R. Wiliams, T. Kreutz. Inorganic membranes for hydrogen production and purification: a critical review and perspective. J Colloid Interface Sci. 314 (2007) 589–603.

[16] H. R. Lee, M. Kanezashi, Y. Shimomura, T. Yoshioka, and T. Tsuru Evaluation and Fabrication of Pore-Size-Tuned Silica Membranes with Tetraethoxydimethyl Disiloxane

for Gas Separation AIChE Journal 57 (2011) 2755-2765

[17] H. Nagasawa, T. Niimi, M. Kanezashi, T. Yoshioka, and T. Tsuru, Modified Gas-Translation Model for Prediction of Gas Permeation Through Microporous Organosilica Membranes, AIChE Journal 60 (2014) 4199-4210

[18] I. Agirre, P. L. Arias, H. L. Castricum, M. Creatore, J. E. ten Elshof, G. G. Paradis, P. H. T. Ngamou, H. M. van Veen, J. F. Vente, Hybrid organosilica membranes and processes: Status and outlook, Sep. Purif. Technol. 121 (2014) 2–12.

[19] M. Asaeda, J. Yang, Y. Sakou, Porous silica–zirconia (50%) membranes for pervaporation of iso-propyl alcohol (IPA)/water mixtures, J. Chem. Eng. Jpn. 35 (2002) 365-371.

[20] H. L. Castricum, A. Sah, R. Kreiter, D. H. A. Blank, J. F. Vente and J.E. ten Elshof, Hydrothermally stable molecular separation membranes from organically linked silica, J. Mater. Chem. 18 (2008) 2150–2158.

[21] H. Imai, H. Morimoto, A. Tominaga, H. Hirashima, Structural Changes in Sol-Gel Derived SiO_2 and TiO_2 Films by Exposure to Water Vapor, J. Sol–Gel Sci. Technol. 10 (1997) 45-54.

[22] N. K. Raman, C. J. Brinker. Organic “template” approach to molecular sieving silica membrane. J Membr Sci. 105 (1995) 273–279.

[23] H. L. Castricum, A. Sah, R. Kreiter, D. Blank, J. F. Vente, J. E. Ten Elshof. Hybrid ceramic nanosieves: stabilizing nanopores with organic links. Chem Commun. (2008)1103–1105.

[24] M. Kanezashi, K. Yada, T. Yoshioka, T. Tsuru. Organic-inorganic hybrid silica membranes with controlled silica network size: preparation and gas permeation characteristics. J Membr Sci. 348 (2010) 310–318.

[25] K. Kusakabe, S. Sakamoto, T. Saie, S. Morooka, Pore structure of silica membranes formed by a sol–gel technique using tetraethoxysilane and alkyltriethoxysilanes, Sep. Purif. Technol. 16 (1999) 139.

[26] M. Asaeda, S. Yamasaki, Separation of inorganic/organic gas mixtures by porous silica membranes, Sep. Purif. Technol. 25 (2001) 151.

[27] T. Tsuru, Nano/subnano-tuning of porous ceramic membranes for molecular separation, J. Sol–Gel Technol. 46 (2008) 349.

[28] H. L. Castricum, G. G. Paradis, M. C. Mittelmeijer-Hazeleger, R. Kreiter , J. F. Vente, and J. E. ten Elshof, Tailoring the Separation Behavior of Hybrid Organosilica Membranes by Adjusting the Structure of the Organic Bridging Group Adv. Funct. Mater. 21 (2011) 2319–2329

[29] K.J. Shea, D.A. Loy, Bridged polysilsesquioxanes. Molecular-engineered hybrid

organic–inorganic materials, Chem. Mater. 13 (2001) 3306–3319.
[30] B. C. Bonekamp, R. Kreiter, J. F. Vente. Sol gel approaches in the synthesis of membrane materials for nanofiltration and pervaporation, Sol-Gel Methods for Materials Processing, P. Innocenzi, Y.L. Zub and V.G Kessler (eds) (2008) 47-65.
[31] A.J. Burggraaf, K.. Keizer and B.A. van Hassel, Nanophase ceramics, membranes and ion implanted layers, (1989a) Paper read at S.I.C. Mat. 88-Nato ASI, Surfaces and interfaces of ceramic materials, 4-16 September 1988, Ile d' Oléron
[32] A.J. Burggraaf, K.. Keizer and B.A. van Hassel, Ceramix nanostructure materials, membrane and composite layers, Solid States Ionics 32/33 (1989b) Part 2: 71-82
[33] B.C. Bonekamp, Preparation of asymmetric ceramic membrane supports by dip-coating, in: A.J. Burggraaf (Ed), Fundamentals of Inorganic Membrane Science and Technology, Elsevier Science, Amsterdam (1996).
[34] A.J. Burggraaf, Fundamentals of membrane top-layer synthesis and processing. Fundamentals of inorganic membrane science and technology, Amsterdam: Elsevier (1996) 259-329.
[35] Q. Xu and M.A. Anderson, Synthesis of porosity controlled ceramic membranes, J. of Mater. Reseacrh, 6 (5), (1991) 1073-1081
[36] S. Inagaki, S. Guan, Y. Fukushima, T. Ohsuna, O. Terasaki, Novel Mesoporous Materials with a Uniform Distribution of Organic Groups and Inorganic Oxide in Their Frameworks, J. Am. Chem. Soc. 121 (1999) 9611-9614.
[37] T. Asefa, M.J. MacLachlan, N. Coombs, G.A. Ozin, Periodic mesoporous organosilicas with organic groups inside the channel walls, Nature 402 (1999) 867-871.
[38] B.J. Melde, B.T. Holland, C.F. Blanford, A. Stein, Mesoporous Sieves with Unified Hybrid Inorganic/Organic Frameworks, Chem. Mater. 11 (1999) 3302-3308.
[39] K.J. Shea, D.A. Loy, Bridged Polysilsesquioxanes. Molecular-Engineered Hybrid Organic-Inorganic Materials, Chem. Mater. 13 (2001) 3306-3319.
[40] P. Van Der Voort, D. Esquivel, E. De Canck, F. Goethals, I. Van Driessche, F.J. Romero-Salguero, Periodic Mesoporous Organosilicas: from simple to complex bridges; a comprehensive overview of functions, morphologies and applications, Chem. Soc. Rev. 42 (2013) 3913-3955.
[41] F. Hoffmann, M. Cornelius, J. Morell, M. Froeba, Silica-based mesoporous organicinorganic hybrid materials, Angew. Chem., Int. Ed. 45 (2006) 3216-3251.
[42] B. Hatton, K. Landskron, W. Whitnall, D. Perovic, G.A. Ozin, Past, Present, and Future of Periodic Mesoporous Organosilicas—The PMOs, Acc. Chem. Res. 38 (2005) 305-312
[43] J. Campaniello, C. W. R. Engelen, W. G. Haije, P. P. A. C. Pex and J. F. Vente, Long-term pervaporation performance of microporous methylated silica membranes, C hem. Commun., 2004 , 834 – 835
[44] T. Tsuru, T. Shibata, J. Wang, H. R. Lee, M. Kanezashi, T. Yoshioka, Pervaporation of

acetic acid aqueous solutions by organosilica membranes, J. of Membr. Sci. 421–422 (2012) 25–31

[45] M. Kanezashi, K. Yada K, T. Yoshioka, T. Tsuru, Design of silica networks for development of highly permeable hydrogen separation membranes with hydrothermal stability. J Am Chem Soc. 131 (2009) 414–415.

[46] T. Niimi, H. Nagasawa, M. Kanezashi, T. Yoshioka, K. Ito, T. Tsuru, Preparation of BTESE-derived organosilica membranes for catalytic membrane reactors of methylcyclohexane dehydrogenation, J of Membr Sci 455 (2014) 375–383

[47] M. Kanezashi, W. N. Shazwani,T. Yoshioka,T. Tsuru Separation of propylene/propane binary mixtures by bis(triethoxysilyl) methane (BTESM)-derived silica membranes fabricated at different calcination temperatures J of Membr. Sci. 415–416 (2012) 478–485

[48] M. Kanezashi, S. Miyauchi, H. Nagasawa, T. Yoshioka and T. Tsuru, Pore size control of Al-doping into bis (triethoxysilyl) methane (BTESM)-derived membranes for improved gas permeation properties,RSC Adv., 3 (2013) 12080–12083

[49] R. Xu, J. Wang, M. Kanezashi, T. Yoshioka and T. Tsuru, Development of Robust Organosilica Membranes for Reverse Osmosis, Langmuir, 27 (2011) 13996–13999.

[50] R. Xu, M. Kanezashi, T. Yoshioka, T. Okuda, J. Ohshita and T. Tsuru, Tailoring the Affinity of Organosilica Membranes by Introducing Polarizable Ethenylene Bridges and Aqueous Ozone Modification, ACS Appl. Mater. Interfaces, 5 (2013) 6147–6154.

[51] R. Xu, S. Ibrahim, M. Kanezashi, T. Yoshioka, K. Ito, J. Ohshita, and T. Tsuru, New insights into the microstructure-separation properties of organosilica membranes with ethane, ethylene and acetylene bridges, ACS Appl. Mater. & *Interfaces*, 6 (12) (2014) 9357–9364.

[52] E. S. Hatakeyama, C. J. Gabriel, B. R. Wiesenauer, J. L. Lohr, M. J. Zhou, R. D. Noble, D. L. Gin, Water filtration performance of a lyotropic liquid crystal polymer membrane with uniform, sub-1-nm pores, J Membr Sci. 366 (2011) 62–72.

[53] M. Manttari, A. Pihlajamaki, E. Kaipainen, M. Nystrom, Effect of temperature and membrane pretreatment by pressure on the filtration properties of nanofiltration membranes, Desalination, 145 (2002) 81–86.

[54] H. Saidani, N. B. Amar, J. Palmeri, A. Deratani, Interplay between the transport of solutes across nanofiltration membranes and the thermal properties of the thin active layer, Langmuir, 26 (2010) 2574–2583.

[55] Y. Kiso, K. Muroshige, T. Oguchi, M. Hirose, T. Ohara, T. Shintani, Pore radius estimation based on organic solute molecular shape and effects of pressure on pore radius for a reverse osmosis membrane, J Membr Sci. 369 (2011) 290–298.

[56] S.P. Nunes, K. V. Peinemann, Membrane materials and membrane preparation. In: Nunes SP, Peinemann KV, eds. Membrane Technology in the Chemical Industry. Weinheim:

Wiley-VCH; 2001;1–68.

[57] D.E. Potts, R.C. Ahlert, S.S. Wang. A critical review of fouling or reverse osmosis membranes, Desalination, 36, (1981) 235-264.

[58] K. Boussu, A. Belpaire, A. Volodin, C. Van Haesendonck, P. Van der Meeren, C. Vandecasteele, B. Van der Bruggen, Influence of membrane and colloid characteristics on fouling of nanofiltration membranes. J of Membr. Sci., 289 (2007) 220-230.

[59] L. Giorno, et al., Study of fouling phenomena in apple juice clarification by enzyme membrane reactor. Sep. Sci. and Tech., 1998. 33(5): p. 739-756.

[60] S. Chellam and M.R. Wiesner, Evaluation of crossflow filtration models based on shear-induced diffusion and particle adhesion: Complications induced by feed suspension polydispersivity. J of Membr. Sci., 138(1998) 83-97.

[61] W. Peng, I. C. Escobar, and D.B. White, Effects of water chemistries and properties of membrane on the performance and fouling--a model development study. J of Membr. Sci., 238 (1-2) (2004) 33-46.

[62] K. Boussu, C. Vandecasteele, and B. Van der Bruggen, Relation between membrane characteristics and performance in nanofiltration. J of Membr. Sci., 310 (1-2) (2008) 51-65.

[63] L. Gourley, M. Britten, S.F. Gauthier, Y. Pouliot, Characterization of adsorptive fouling on ultrafiltration membranes by peptides mixtures using contact angle measurements. J of Membr. Sci., 97 (1994) 283-289.

[64] M. Mänttäri, L. Puro, J. Nuortila-Jokinen, M. Nyström, Fouling effects of polysaccharides and humic acid in nanofiltration. J of Membr. Sci., 165 (2000) 1-17.

[65] C.Y. Tang, Y. N. Kwon, and J.O. Leckie, Fouling of reverse osmosis and nanofiltration membranes by humic acid—Effects of solution composition and hydrodynamic conditions. J of Membr. Sci., 290 (2007) 86-94.

[66] H. Mo, K.G. Tay, and H.Y. Ng, Fouling of reverse osmosis membrane by protein (BSA): Effects of pH, calcium, magnesium, ionic strength and temperature. J of Membr. Sci., 315 (2008) 28-35.

[67] S. Hong and M. Elimelech, Chemical and physical aspects of natural organic matter (NOM) fouling of nano filtration membranes. J of Membr. Sci., 132 (1997) 159-181.

[68] S. Lee, J.W. Cho, and M. Elimelech, Combined influence of natural organic matter (NOM) and colloidal particles on nanofiltration membrane fouling. J of Membr. Sci., 262 (2005) 27-41.

[69] Q.L. Li and M. Elimelech, Organic fouling and chemical cleaning of nanofiltration membranes: Measurements and mechanisms. Environmental Science & Technology, 38 (2004) 4683-4693.

[70] K. Boussu, C. Kindts, C. Vandecasteele, and B. Van der Bruggen, Surfactant Fouling of Nanofiltration Membranes: Measurements and Mechanisms, ChemPhysChem 8 (2007)

1836 – 1845

[71] K. Katsoufidou, S.G. Yiantsios, and A.J. Karabelas, Experimental study of ultrafiltration membrane fouling by sodium alginate and flux recovery by backwashing. J of Membr. Sci., 300 (1-2) (2007) 137-146

[72] S. K. Sayed Razavi, J.L. Harris, and F. Sherkat, Fouling and cleaning of membranes in the ultrafiltration of the aqueous extract of soy flour. J of Membr. Sci., 114 (1) (1996) 93-104.

[73] M.J. Munoz-Aguado, D.E. Wiley, and A.G. Fane, Enzymatic and detergent cleaning of a polysulfone ultrafiltration membrane fouled with BSA and whey. J of Membr. Sci., 117 (1-2) 1996 175-187.

[74] I. Koyuncu, A. Liittge, and M.R. Wiesner, Interferometric observations and kinetic modeling of the chemical cleaning ofhumic materials deposited on membranes. J of Membr. Sci., 313 (1-2) (2008) 127-134.

[75] M. Bartlett, M.R. Bird, and J.A. Howell, An experimental study for the development of a qualitative membrane cleaning model. J of Membr. Sci., 105 (1-2) (1995) 147-157.

[76] W. S. Ang, S. Lee, and M. Elimelech, Chemical and physical aspects of cleaning of organic-fouled reverse osmosis membranes. J of Membr. Sci., 272 (1-2) (2006) 198-210.

[77] R. Liikanen, J. Yli-Kuivila, and R. Laukkanen, Efficiency of various chemical cleanings for nanoflltration membrane fouled by conventionally-treated surface water. J of Membr. Sci., 195 (2) (2002) 265-276.

[78] E. Zondervan, and B. Roffel, Evaluation of different cleaning agents used for cleaning ultrafiltration membranes fouled by surface water. J of Membr. Sci. 304 (1-2) (2007) 40-49.

[79] E. Arkhangelsky, E, D. Kuzmenko, and V. Gitis, Impact of chemical cleaning on properties and functioning of poly ethersulfone membranes. J of Membr. Sci., 305 (1-2) (2007) 176-184.

Chapter 2

Effect of firing temperature on the structural and gas separation performance of 2,4,6-tris- [3(triethoxysilyl)- 1-propoxyl]-1,3,5-triazine (TTESPT)

2.1. Introduction

A new membrane-based gas separation offers the greatest potential in the chemical industry because of its low-energy requirement and simple system features compared with conventional technologies such as cryogenic distillation that require phase change, which adds a significant amount of energy cost to the price of separation [1]. In order to substitute this new technology, membrane materials with better separation performance must be developed. Inorganic membranes such as sol–gel derived silica [2], zeolites [3] and carbon [4] were chosen for this purpose because of their high permeability and excellent permselectivity in gas separations such as H_2–N_2, CO_2–CH_4, CO_2–N_2 and C_3H_6–C_3H_8.

Tetraethoxysilane (TEOS) is a highly versatile and traditionally has been the most commonly used Si precursor for the fabrication of a silica membrane via the sol– gel method. However, the pore networks usually consist of micropores of approximately 0.3 nm in size; which only allows small molecules such as helium and hydrogen to permeate, which makes it impractical for separating large gas molecules such as propane and propene [5]. In order to overcome this obstacle, a great deal of effort has been devoted to the design and synthesis of an organic–inorganic hybrid of organoalkoxysilane membranes, because they are recognized as one of a new class of advanced materials. The advantages of this hybridization process is that the material possess the network stability of inorganic silica and the flexibility of organic polymer thus improving the thermal, mechanical and gas transport properties [6-8].

Therefore, numerous generations of organoalkoxysilanes with double silicon alkoxides have emerged and been used as Si precursors to prepare membranes via sol–gel processes such as alkanebridged precursors, which include bis(triethoxysilyl)methane (BTESM), bis(triethoxysilyl)ethane (BTESE), 1,3-bis(triethoxysilyl) propane (BTESP), and the aromatic bridging groups; benzene and biphenyl [9, 10]. To the best of our knowledge, organoalkoxysilanes with triple silicon alkoxides with a triazine unit for membrane preparation have not been tried, although 1,3,5-triazine derivatives have been acknowledged for quite some time. Previous reports have found that the CO_2 uptake was significantly enhanced by 70 to 90% for microporous polymers based on 1,3,5-triazine units carbonized at

400 °C for 1 h and at 800 °C for an additional 1 h under nitrogen. Hence, it is suggested that it could be used as a precursor for the synthesis of advanced porous carbon materials without an activation process [11]. Herein, we present the first report on the synthesis of a new triazine-based nitrogen rich organoalkoxysilane, 2,4,6-tris- [3(triethoxysilyl)-1-propyl] -1,3,5-triazine. Figure 2-1 shows the schematic images of amorphous silica networks, as derived by TTESPT. This new material is believed to serve as both a rigid and flexible material as it consists of one unit of a heterocyclic ring of 1,3,5-triazine and three arms of propene groups that are connected to silicon alkoxides. The functionality of the N-hetero building unit linkages, imine (–C=N–), may facilitate the surface basic sites to improve the affinity and uptake capacity of some gases. Thus, we are attempting to implement this new material into a gas-separation membrane.

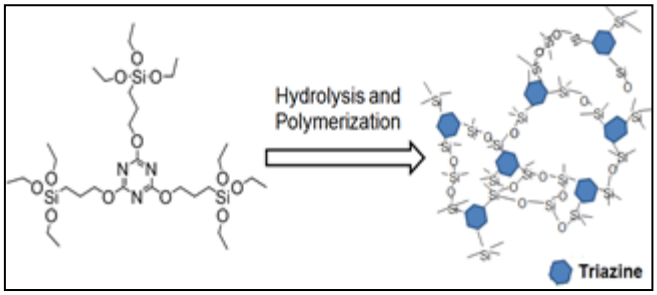

Figure 2-1 Schematic images of amorphous silica networks derived by TTESPT

2.2. Experimental

2.2.1. Synthesis of 2,4,6-tris[3(triethoxysilyl)-1-propoxyl]-1,3,5-triazine (TTESPT)

TTESPT was synthesized in a (30 mL) two-necked flask equipped with a stirrer and a reflux condenser, into which was placed (4.40 g, 17.7 mmol) of 2,4,6-tris(allyloxy)-1,3,5-triazine and (10.40 g, 63.3 mmol) of triethoxysilane in (10 mL) of toluene. Two drops of (0.1 M) H_2PtCl_6 in *i*PrOH were added, and the mixture was heated to reflux for 4 hours. Excess reactant and the solvent were removed under vacuum to give a colorless liquid (12.08 g). All reactions were performed under an atmosphere of dry nitrogen. Figure 2-2 is a schematic diagram of the synthesis of 2,4,6-tris[3(triethoxysilyl) -1-propoxyl]-1,3,5-triazine (TTESPT)

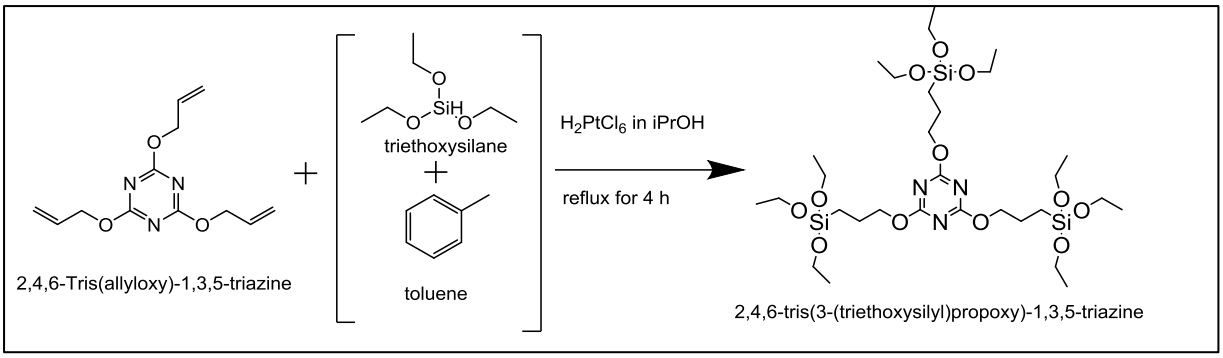

Figure 2-2 Schematic diagram of the synthesis of 2,4,6-tris[3(triethoxysilyl) -1-propoxyl] -1,3,5-triazine (TTESPT)

Anal. Calcd and NMR spectra for $C_{30}H_{63}N_3O_{12}Si_3$ (TTESPT) [1a,b] are shown as below (Figure 2-3):

^{1}H NMR (δ $CDCl_3$) 0.69 (m, 6H, CH_2Si) 1.18 (t, 27H, CH_3, J = 7.0 Hz), 1.82-1.92 (m, 6H, CH_2), 3.78 (q, 18H, CH_2O, J = 7.0 Hz), 4.28-4.36 (m, 6H, CH_2O);

^{13}C NMR (δ$CDCl_3$) 6.40 (CH_2Si), 18.20 (CH_3), 22.18 (CH_2), 58.34 (OCH_2), 70.26 (OCH_2), 173.02 (triazine carbon).

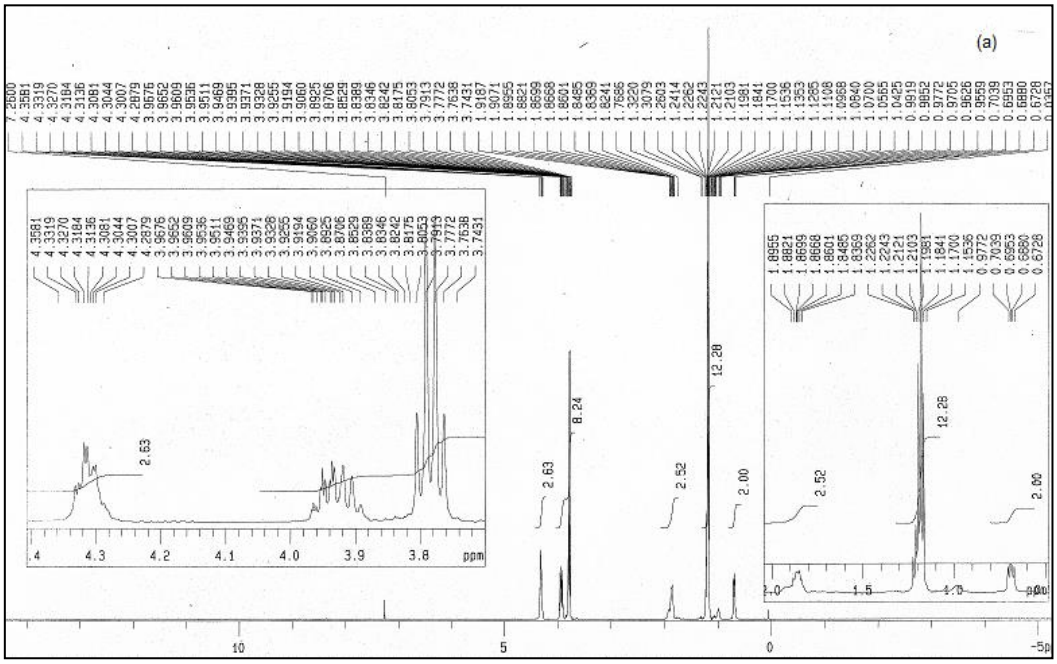

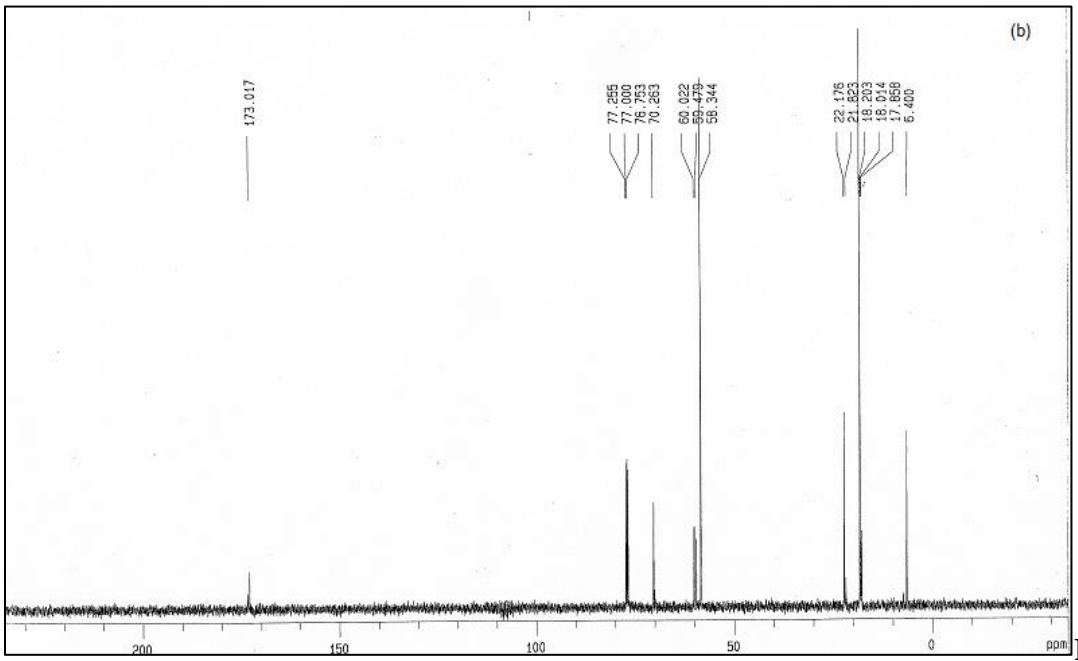

Figure 2-3 NMR spectra of 2,4,6-tris[3(triethoxysilyl)-1-propyl]-1,3,5-triazine $C_{30}H_{63}N_3O_{12}Si_3$ (TTESPT) solution (a)^{1}H NMR and (b) ^{13}C NMR

2.2.2. Preparation of a TTESPT-silica derived membrane

A TTESPT-derived silica solution was prepared using hydrochloric acid as a catalyst. First, TTESPT as a silica precursor was homogeneously dissolved in an ethanol solution. A mixture of water and hydrochloric acid were then added dropwise to the solution under vigorous stirring, resulting in a final solution with molar ratios of TTESPT/H_2O/acid = (1/240/0.2). Then, the solution was kept in a closed system under continuous stirring at 25 °C for 6 h to form silica sols. TEOS, and BTESE-derived silica solutions were prepared for comparison, and the details of the preparation procedure can be found elsewhere [2-4].

Porous α-alumina tubes (porosity: 50%, average pore size: 1 μm, outside diameter: 10 mm) were used as the supports for TTESPT-derived silica membranes. α-Alumina particles (average particle diameter: 0.2, 1.9 μm) were coated on the outer surface of a porous support using silica-zirconia colloidal sol as the binder, and the support was fired at 550 °C for 30 min to make the surface smooth. These procedures were repeated several times to cover large pores that might have resulted in pinholes in the final membrane. Then, a SiO_2–ZrO_2 (Si/Zr = 1/1) solution diluted to about (0.5 wt%) was coated on the substrate to form an intermediate layer with pore sizes of several nm, followed by calcination at 550 °C for about 30 min. Finally, the TTESPT-derived silica layer was fabricated by coating a TTESPT solution, followed by drying and calcination at 200, 300 and 400 °C under nitrogen for 30 min.

2.2.3. Characterization of TTESPT-silica derived membrane

^{1}H NMR and ^{13}C NMR spectra were recorded using a JNM–LA500 spectrometer. Thermogravimetric analysis (TG) was performed to investigate the decomposition behavior of the organic groups in the silica matrix at temperatures ranging from 100 to 800 °C with a heating rate of 10 °C min^{-1} in a Helium flow of 300 ml min^{-1} using a Thermogravimetric Mass Spectrometer (TGA-DTA-PIMS 410/S, Rigaku, Japan). The TTESPT-derived film coated on the KBr plate was fired between 200 and 550 °C under an N_2 atmosphere, and was characterized by in situ Fourier transform infrared (FTIR) spectroscopy (FTIR-JASCO, Japan). The morphology of TTESPT membranes were examined by using a Hitachi S-48000 scanning electron microscopy (SEM). A N_2 adsorption isotherm was carried out at 77 K to study the micropore structures of the silica gels. Prior to the measurement, all the silica gel samples were evacuated at 150 °C for 12 h. The measurements were carried out using BELMAX (BEL JAPAN INC., Japan).

2.2.4. Single gas permeation measurement

Gas permeation tests were performed at temperatures ranging from 200 to 50 °C using a single component of He, H_2, CO_2, N_2, CH_4, C_3H_8, and SF_6 before and after the coating process as shown in Figure 2-4. The permeation stream was maintained at atmospheric pressure, and the pressure drop through the membranes was maintained at 1 bar. Prior to the measurement, all membranes were outgassed in a He flow of 50 ml min^{-1} at 200 °C for 8 to 12 h to remove any water that possibly absorbed through the membranes.

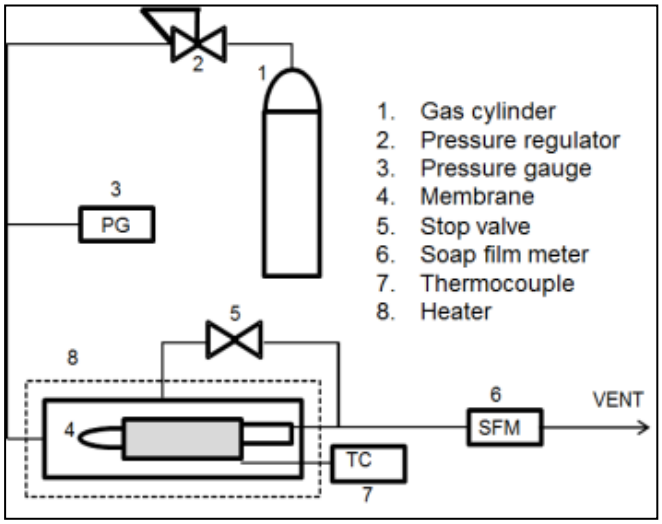

Figure 2-4 Schematic diagram of the experimental apparatus for single gas permeation measurement

2.3. Results and discussion

2.3.1. Characterization of TTESPT

2.3.1.1. Thermogravimetric mass spectrometer (TGMS) analysis

Fig. 2(a) shows a TG/DTG curve recorded for the TTESPT derived silica gel powders for the water ratio (H2O = 240) in a helium flow; the corresponding mass spectra (MS) is shown in Fig. 2(b). Analysis of the TG/DTG curve indicated that thermal decomposition occurred in two steps. The first degradation stage indicated a weight loss of ~18% in a temperature range of ~140 to 320 °C. The corresponding mass spectra showed only the mass spectra number (m/z = 44) for carbon dioxide (CO_2), which showed a peak at 306 °C. This was probably due to the decomposition of unreacted ethoxy groups and to the partial decomposition of some branching bonds of triazine units in the powder. In fact, the evaporation of adsorbed water, ethanol and acid is believed to have occurred [5, 11]. The second degradation stage that occurred between ~310 and 640 °C caused a weight loss of ~26%. This may correspond to the pyrolysis for the cleavage of the C–H, C–C, C–O, C–N and C=N branching bonds of the TTESPT unit, showing that CH_4 (m/z = 15), CO_2 (m/z = 44), CH_3CN (m/z = 41), and H_2 (m/z = 2) were generated. The same observation was seen by Chang et al. [11] for another new class of 1,3,5-triazine-based microporous polymer sample that was flowed under a N_2 atmosphere.

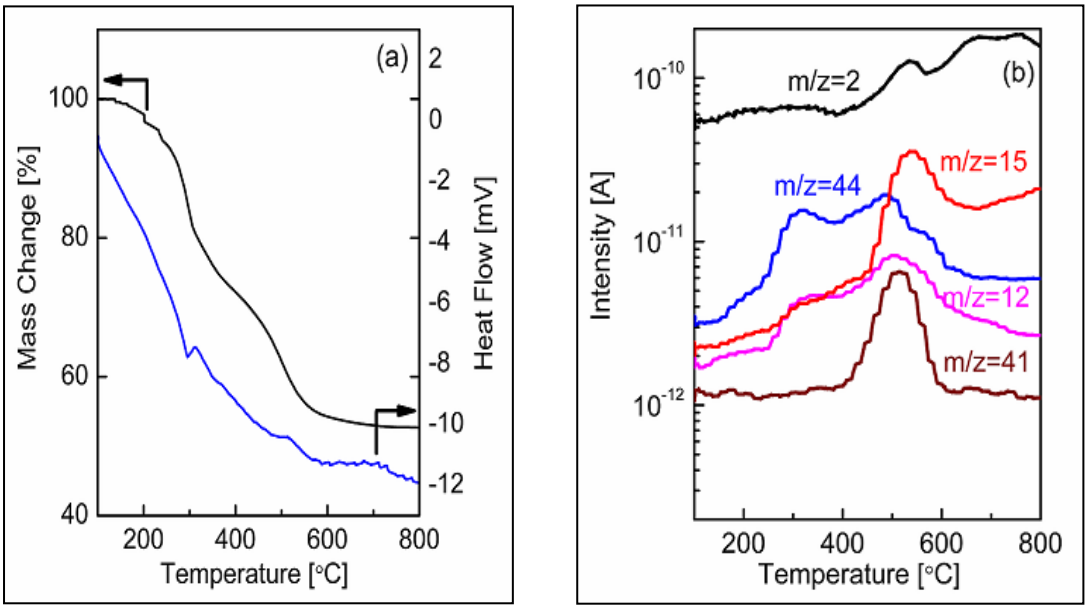

Figure 2-5 Material characterizations of TTESPT-derived silica powder (a) TG/DTG and (b) MS curves of TTESPT-derived silica gel powder (water ratio H_2O=240), ramping rate, 10 °C min^{-1}; He flow rate, 300 ml min^{-1}

2.3.1.2. Fourier transform infrared (FTIR) analysis

Analysis by in situ FTIR (Figure 2-6) did reveal a good agreement with the TGMS result. TTESPT started to degrade partially at 300 °C and as the calcination temperature was further raised to 550 °C, nearly all functional groups disappeared and only the skeleton of Si–O–Si remained. This implies that triazine structures such as C=N and C–N were less thermally stable compared with methyl and phenyl groups, which could still be observed at temperatures as high as 600 °C [12].

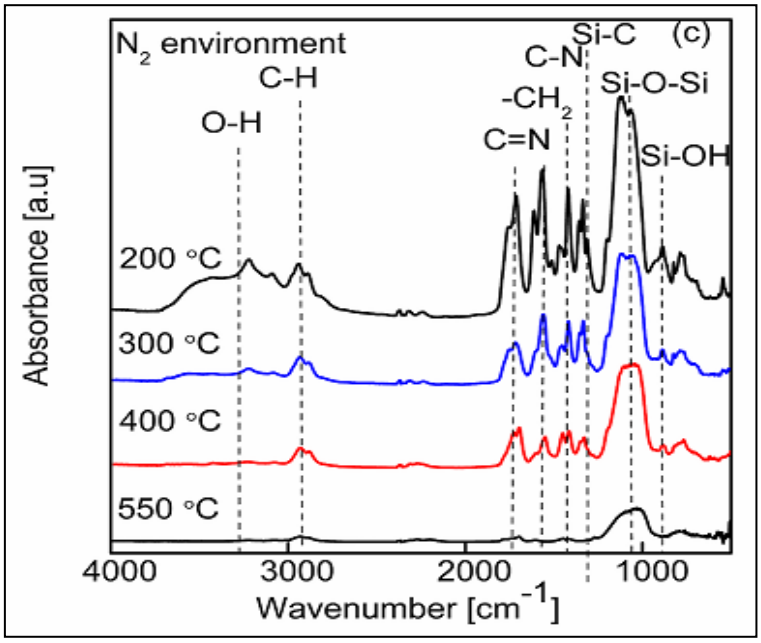

Figure 2-6 FTIR spectra of TTESPT-derived silica membrane (water ratio H_2O=240) at different calcination temperatures (200, 300, 400, and 550 °C) under a N_2 environment

2.3.1.3. Scanning electron microscopy (SEM) analysis

Figure 2-7 shows the SEM images of the surfaces, (a) and (c), and cross-sections, (b) and (d), of TTESPT membranes calcined at 200 and 400 °C under N_2 environment at magnification of 10,000 and 2,000, respectively. As shown in Figures 2-7 (a) and (c), almost no change occurred to the membrane top surface areas. On the other hand, a very thin layer of TTESPT was successfully coated on the top of SiO_2-ZrO_2 intermediate–alumina particle layer from the cross section shown in Figures 2-7 (b) and (d).

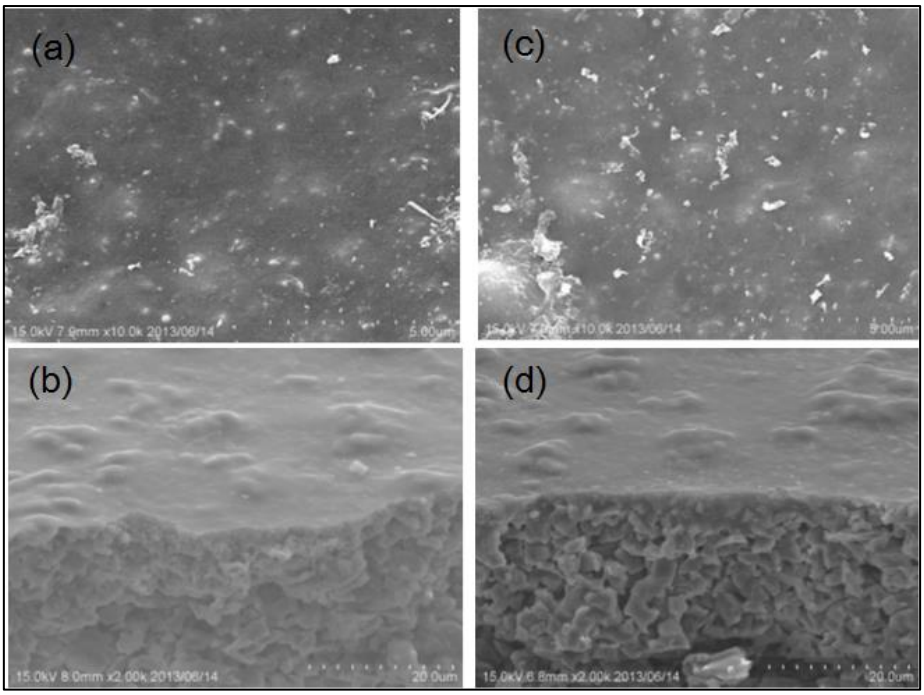

Figure 2-7 SEM images of the surface and cross sections of TTESPT membranes calcined at 200 °C (a and b); 400 °C (c and d) under N_2 environment

2.3.1. 4. N_2 adsorption analysis

As shown in the SEM images of the surface and cross-section of TTESPT-derived silica membranes calcined at 200 and 400 °C under an N_2 environment, it was difficult to observe the change in the surface morphology of both membranes. Thus, we applied N_2 adsorption/desorption analysis to these TTESPT derived silica gels powders to provide a clear view of the transformation of the pore size of these materials during the calcination process.

As shown in Figure 2-8 (a), the TTESPT-derived silica gel powders calcined at 200 °C probably exhibited the characteristics of a type IV isotherm with a hysteresis loop H4. The adsorption and desorption branches remained almost horizontal and parallel over a wide range of P/P_0. According to Sing [13], the H4 loop sometime appeared to be associated with narrow slit-like pores. The sample indicated that very limited pores were available in the silica for N_2 adsorption. However, as the calcination temperatures were increased from 200 to 300 and 400 °C, the N_2 adsorption isotherm changed to that of a type I pattern, and the S_{BET} of these samples increased from 16 to 80 and 178, respectively (Table 2-1). The effect of calcination temperature could possibly be explained as follows. The TTESPT-derived silica gel powders calcined at 200 °C under a N_2 atmosphere showed a lower value for S_{BET}, suggesting that the flexible arms of the organic branching bonds of a rigid triazine unit were successfully incorporated within the silica matrix. Triazine units may have acted as “building blocks” between the silica pores, and occupied some space in the silica network, resulting in only a

limited number of open pores and a lower S_{BET}. This can be proven by the shifting of the pore diameter from a large to a small size with increases in the calcination temperature, as shown in Figure 2-8 (b) and Table 2-1. As the calcination temperature was increased, some of the organic bonds of these rigid triazine units were partially degraded, suggesting that micropores were generated through the thermal treatment process thereby remarkably increasing the amount of N2 adsorption via the template technique.

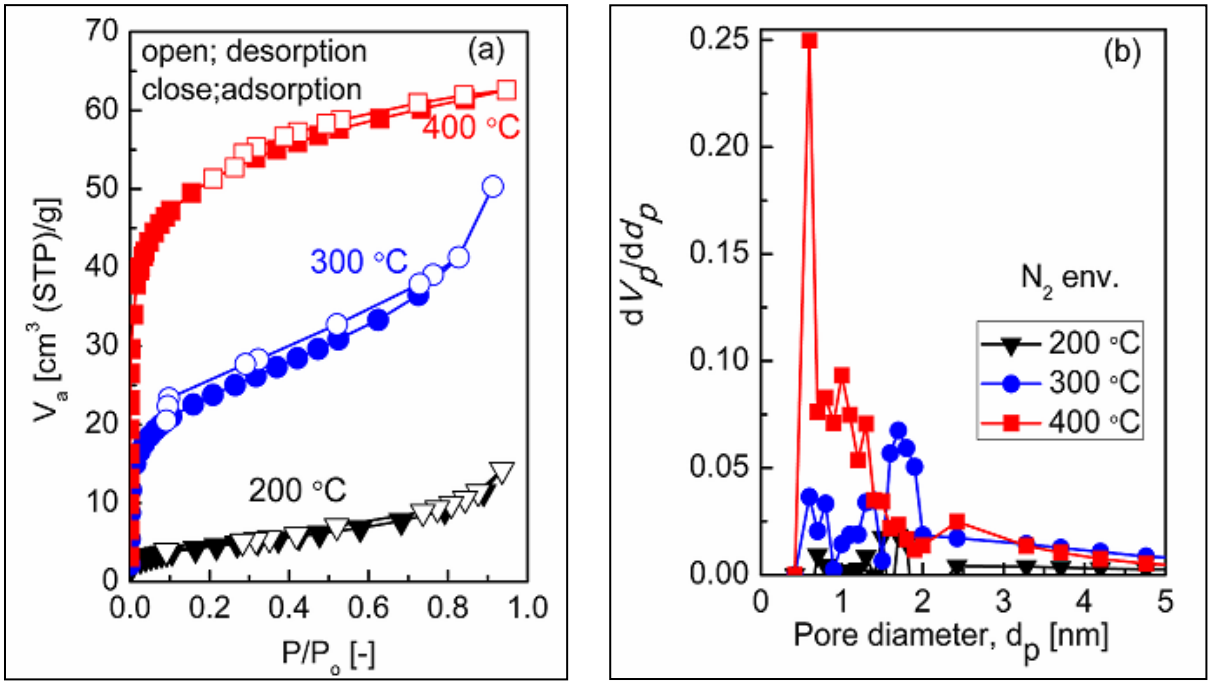

Figure 2-8 N_2 adsorption/desorption (a) and pore size distribution (b) of TTESPT membranes calcined at 200, 300 and 400 °C under N_2 environment

Table 2-1 Summary of surface area for TTESPT membranes calcined at different calcination temperatures

TTESPT membranes	Surface Area, S_{BET} (m^2/g)
Calcined at 200 °C	16
Calcined at 300 °C	80
Calcined at 400 °C	178

2.3.2. Gas separation performance of TTESPT

Membrane performance was assessed by evaluating the gas permeance properties and selectivities at different permeation temperatures of 200 and 50 °C for TTESPT derived silica membrane calcined at 200 and 400 °C (Table 2-2). High selectivity of CO_2/N_2 is expected for this membrane as there is much documentation by other researchers [11, 14, 15]. Interestingly,

this membrane also exhibited an outstanding selectivity of C_3H_6/C_3H_8~37 with C_3H_6 a permeance of 2.95 $\times 10^{-9}$ mol m^{-2} s^{-1} Pa^{-1} at a permeation temperature of 50 °C for a membrane calcined at 200 °C. To the best of our knowledge, C_3H_6/C_3H_8 separation properties using organoalkoxysilanes with triple silicon alkoxides with a triazine unit have not been reported yet.

Table 2-2 Permeance and Selectivity of TTESPT-derived Silica Calcined at 200 °C for Single Gas

Calcination temperature: 200 °C				
Permeation Temperature [°C]	Permeance [mol/(m^2.s.Pa)]		Selectivity [-]	
	CO_2 x 10^{-7}	C_3H_6 x 10^{-9}	CO_2/ N_2	C_3H_6/ C_3H_8
200	3.11	26.9	6.80	6
50	0.94	2.95	20.59	37
Calcination temperature: 400 °C				
200	14.1	471	4.32	4.12
50	11.2	305	11.2	6.62

Hence, the permeation properties of this membrane will be discussed in detail using an Arrhenius plot (Figure 2-9). The gas permeances for both membranes increased with the permeation temperature, revealing that the activated diffusion transport mechanism was dominant. The activation energies of both gases for the TTESPT membrane calcined at 400 °C were much smaller compared with the membrane calcined at 200 °C due to the larger pore size, as discussed earlier. It is understandable that the critical temperatures (T_c) for C_3H_6 and C_3H_8 were around 91.8 °C and 96.8 °C, respectively.

Above the T_c, it is believed that gas-state permeation through the microporous structure of a membrane might occur. However, the opposite phenomenon was seen for gas permeation below the T_c, where the gas permeation properties were affected by a 'micropore- filling' phase. Even if the bulk pressure is lower than the saturation pressure of the permeating vapor, a potential field in a micropore would effectively work to compress the permeant and change the vapor to a liquid-like high-density phase, leading to the formation of a so-called micropore-filling phase in a pore. Therefore, the mobility of the permeating gas will be decreased as the permeating molecules move into a micropore-filling phase against the attractive intermolecular interactions [16]. Moreover, the pore size of this membrane was smaller compared to the membrane calcined at 400 °C. Consequently, this also contributed to the lower permeance of both gases.

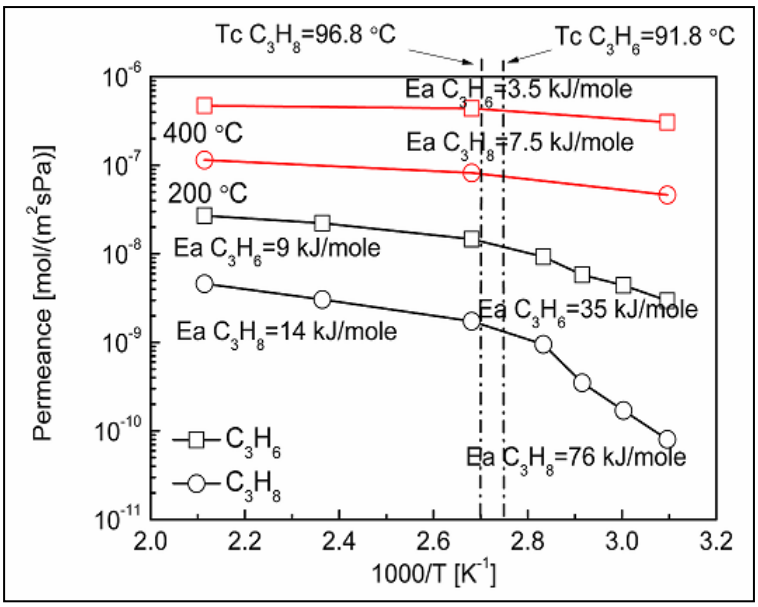

Figure 2-9 Arrhenius plot of the permeances observed for C_3H_6 and C_3H_8 of the TTESPT-derived silica membrane calcined at temperatures of 200 and 400 °C.

Figure 2-10 shows the C_3H_6–C_3H_8 selectivity as a function of C_3H_6 permeance for themembranes reported in the literature [10, 17–21], as well as for the membranes reported in the present study. The solid line shows the upper-bound trade-offs between permeance and selectivity for the reported carbon membranes. In general, the C_3H_6/C_3H_8 selectivity decreases with increasing C_3H_6 permeance as a result of defect or variation in pore size distribution. Interestingly, the separation performances of TTESPT-derived silica membranes calcined at 200 °C showed similar properties to carbonized membranes, 3,3',4,4'-biphenyltetracarboxylic dianhydride (BPDA), 4,4'-oxidianiline(4,4'-ODA), and 2,4-diaminotoluene (2,4-DAT), which were tested from 35 to 100 °C. On the other hand, the separation performance of TTESPT-derived silica membranes calcined at temperatures of 300 and 400 °C showed similar or better separation properties than BTESM and Titanosilicate membranes at the permeation temperature range of 50-200 °C. This could be attributed to the presence of the π-bond (C=C double bond) in propene, which can have an affinity for the hydroxyl groups of silica and –C=N-triazine units. It is noteworthy that all TTESPT-derived silica membranes calcined at different temperatures exhibited a significant selectivity of C_3H_6/C_3H_8 and well surpassed the "upper-bound-trade-off" line of carbon membranes.

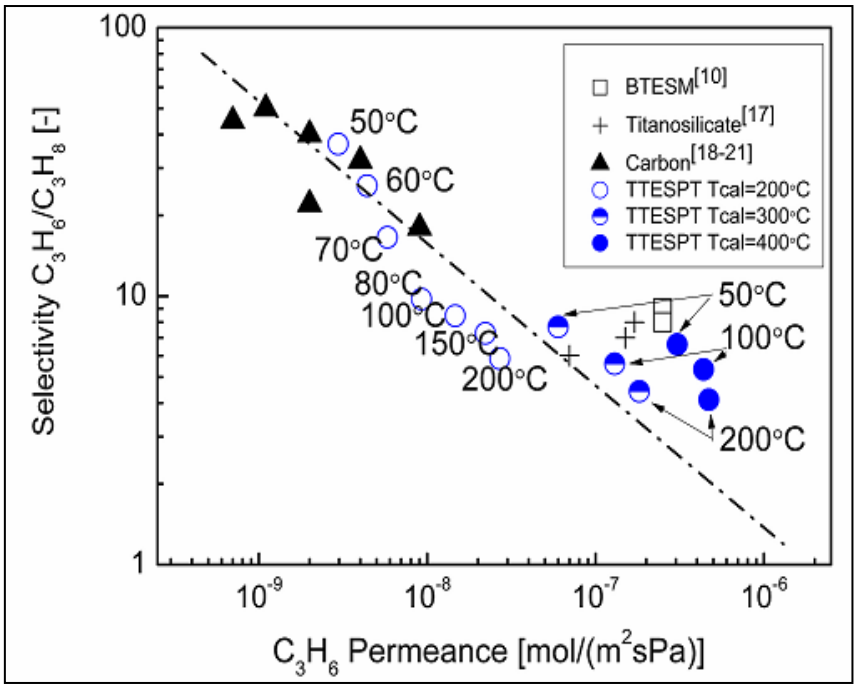

Figure 2-10 Trade-off curve of separation factor and C_3H_6 permeance of a TTESPT-derived silica membrane (calcination temperature=200 °C)

2.4. Conclusions

In conclusion, the present study marks the first successful preparation of a TTESPT membrane that exhibits dual characteristics as organic (the flexibility via high chain mobility) and inorganic (Si–O–Si backbone that provides structural stability). By adjusting the calcination temperatures, the permeation properties of this membrane were enhanced. Lastly, TTESPT membrane therefore show the potential to be further developed toward C_3H_6/C_3H_8 separation applications.

References

[1] M. Freemantle, Advanced organic and inorganic materials being developed for separations offer cost benefits for environmental and energy-related processes, Chem. and Eng. News, 83 (2005) 49-57.

[2] R.M. de Vos, H. Verweij, Science, High-Selectivity, High-Flux Silica Membranes for Gas Separation, 279 (1998) 1710-1711.

[3] M. L. Carreon, S. Li and M. A. Carreon, AlPO-18 Membranes for CO2/CH4 Separation, Chem. Commun., 45 (2012) 2310-2312.

[4] X. Ma, B.K. Lin, X. Wei, J. Kniep, and Y. S. Lin, Gamma-alumina supported carbon molecular sieve membrane for propylene/propane separation, Ind. Eng. Chem. Res. 52 (2013) 4297- 4305

[5] H. R. Lee, M. Kanezashi, Y. Shimomura, T. Yoshioka, T. Tsuru, Evaluation and Fabrication of Pore-Size-Tuned Silica Membranes with Tetraethoxydimethyl Disiloxane for Gas Separation AIChE J. 57 (2011) 2755- 2765.

[6] R.M. de Vos, W.F. Maier, H. Verweij, Hydrophobic silica membranes for gas separationJ. Membr. Sci. 158 (1999) 277-288.

[7] M. Kanezashi, K. Yada, T. Yoshioka, T. Tsuru, Design of silica networks for development of highly permeable hydrogen separation membranes with hydrothermal stability.J. Am. Chem. Soc. 131 (2009) 414-415.

[8] H.L. Castricum, A. Sah, R. Kreiter, D.H.A. Blank, J.F. Vente, J.E. ten Elshof, Hydrothermally stable molecular separation membranes from organically linked silica J. Mater. Chem. 18 (2008) 2150- 2158.

[9] H. L. Castricum, G. G. Paradis , M. C. Mittelmeijer-Hazeleger, R. Kreiter , J. F. Vente , and J.E. ten Elshof, Tailoring the Separation Behavior of Hybrid Organosilica Membranes by Adjusting the Structure of the Organic Bridging GroupAdv. Funct. Mater. 21 (2011) 2319- 2329

[10] M. Kanezashi, M. Kawano, T. Yoshioka, T. Tsuru, Organic_Inorganic Hybrid Silica Membranes with Controlled Silica Network Size for Propylene/Propane Separation, Ind. Eng. Chem. Res. 51 (2012) 944- 953

[11] H. Lim, M. C. Cha, J. Y. Chang, Preparation of Microporous Polymers Based on 1,3,5-Triazine Units Showing High CO_2 Adsorption Capacity,Macromol. Chem. Phys. 213 (2012) 1385- 1390.

[12] G. Li, M. Kanezashi, T. Tsuru, Preparation of organic–inorganic hybrid silica membranes using organoalkoxysilanes: The effect of pendant groups, J. Membr. Sci. 379 (2011) 287-295.

[13] K. S. W. Sing, Reporting physisorption data for gas/solid systems with Special Reference to the Determination of Surface Area and Porosity, Pure & Appl.Chem.54 (1982)

2201-2218.

[14] W.C. Song, X.K. Xu, Q.Chen, Z.Z. Zhuang, X.H.Bu, Nitrogen-rich diaminotriazine-based porous organic polymers for small gas storage and selective uptake, Polym. Chem. 4 (2013) 4690–4696

[15] T.Suzuki, Y. Yamada, J. Appl. Polym. Sci. Synthesis and Gas Transport Properties of Novel Hyperbranched Polyimide–Silica Hybrid Membranes (2013) 316-322 DOI:10.1002/APP.37893

[16] T. Yoshioka, J. Tanaka, S. Furutani, T. Tsuru, M. Aseda, Transport properties of condensable gases through microporous silica membranes, Trans. Mater. Resear. Soc. Japan. 29 (2004) 3247-3250.

[17] I. Tiscornia, S. Irusta, C. T´ellez, J. Coronas, J. Santamaria, Separation of propylene/propane mixtures by titanosilicate ETS-10 membranes prepared in one-step seeded hydrothermal synthesis.J. Membr. Sci. 311 (2008) 326-335.

[18] J. Hayashi, H. Mizuta, M. Yamamoto, K. Kusakabe, S. Morooka, S.H. Suh, Separation of ethane/ethylene and propane/propylene systems with a carbonized BPDA-pp‘ODA polyimide membrane Ind. Eng.Chem. Res. 35 (1996) 4176-4181.

[19] J. Hayashi, M. Yamamoto, K. Kusakabe, S. Morooka, Effect of oxidation on gas permeation of carbon molecular sieving membranes based on BPDA-pp‘ODA polyimide. Ind. Eng. Chem. Res. 36 (1997) 2134-2140.

[20] M. Yamamoto, K. Kusakabe, J. Hayashi, S. Morooka, Carbon molecular sieve membrane formed by oxidative carbonization of a copolyimide film coated on a porous support tube. J. Membr. Sci. 133 (1997) 195-205.

[21] M. Yoshino, S. Nakamura, H. Kita, K. Okamoto, N. Tanihara, Y. Kusuki, Olefin/paraffin separation performance of carbonized membranes derived from an asymmetric hollow fiber membrane of 6FDA/ BPDA-DDBT copolyimide. J. Membr. Sci. 215 (2003) 169-183.

Chapter 3

Effect of water ratio on the structural and performance evaluation; gas separation and reverse osmosis of 2,4,6-tris- [3(triethoxysilyl)-1-propoxyl]-1,3,5-triazine (TTESPT)

3.1. Introduction

The desalination of seawater and brackish water has been practiced regularly for more than 50 years and is a well-established source of water supply in many countries. It is now feasible, technically and economically, to produce large quantities of water of excellent quality from these desalination processes [1]. The major desalination technologies currently in use are based on membrane separation via RO and thermal distillation, with RO accounting for more than 50% of the installed capacity [2-4]. Because of its relatively lower energy cost and simplicity, RO is expected to see robust growth in the near future, though new technologies such as membrane distillation (MD), [5,6] electrodialysis, [5,7] capacitive deionization, [5,8] and forward osmosis [5,9] have been proposed.

At present, water desalination is accomplished using many types of membrane materials such as polymers and ceramics. Polymeric membranes such as polyamide and cellulose-based membranes for RO and polytetrafluoroethylene membranes for MD are commonly used due to their low cost, and ease of fabrication. However, the polyamide thin-film composite membranes are the most leading materials in the desalination industry due to their superior water fux, and a high degree of salt and organic rejection [10-12]. However, these membranes have some drawbacks. They often suffer from the swelling effect, have a short life-time due to bio fouling, have a narrow operating temperature (0 to 45 °C) and pH range, and are prone to chlorine attack [12-14]. Emerging materials made up of inorganic membranes such as zeolite and amorphous silica, on the other hand, are more resistant to harsh conditions [10]. Zeolites silicabased membranes have been studied extensively and because of their very specific pore structure and narrow pore size distribution, they have shown potential advantages for desalination.

Li et al. [15] reported on high chemical-stability silicalite membrane-based desalination. For a 0.1 M NaCl solution, a silicalite membrane of 1 nm pore diameter showed transient (time dependent) water flux and Na^+ rejections at 2.07 MPa. After a RO time of 50 h, the water flux and Na^+ rejections were stabilized at 0.112 kg m^{-2} h^{-1} and 76.7%. For a

multiple-salt solution of 0.1M NaCl, KCl, NH_4Cl, $CaCl_2$, and $MgCl_2$, the water flux was 0.058 kg m^{-2} h^{-1}, and the rejections of Na^+, K^+, NH_4^+, Ca^{2+}, and Mg^{2+} reached 58.1, 62.6, 79.9, 80.7, and 88.4%, respectively, at a RO pressure of 2.4 MPa. These results show that the filtration mechanism is not only dependent on size exclusion, but also on Donnan exclusion due to the charged double layer induced by ions adsorbed onto the pores or on the inter crystalline walls. Although the first RO test with a zeolite membrane was unsuccessful, i.e., both salt rejection and water flux were too low to be of practical use, subsequent work has been conducted to improve both by modifying the zeolite structure. The same research group also reported that defects in the crystal structure can be improved by incorporating aluminum ions into the zeolite framework; hence, both water flux and ion rejection was increased from 0.112 to 1.129 kg m^{-2} h^{-1} and ion rejection was improved from 90.6 to 92.9% [16]. Another recent study on MFI membranes showed that desalination performance of the prepared silicalite membrane was carried out with a seawater solution (0.3 wt% TDS (total dissolved solids)) for as long as 180 days at a constant pressure of 700 kPa and at various temperatures. The prepared silicalite membrane achieved a high rate of rejection (>93%) for allmajor seawater ions, including Na^+ (except for K^+, 83%) at an applied pressure of 700 kPa and at room temperature (22 °C), but showed a continuous decrease in ion rejection when the temperature was increased from 22 to 90 °C. However, the permeation flux was significantly increased with an increase in temperature [17].

Another promising candidate for use in RO desalination is an amorphous silica-based membrane. These materials are gaining in demand because of their simple fabrication techniques, low-cost and excellent molecular sieving properties. These membranes have shown superior performances in gas separation [18-20]. However, these membranes have a weakness due to structural instability when exposed to water, and probably undergo dissolution or densification [21,22]. Thus, the overall separation performance is decreased as a consequence, and the quality of the desalinated water drops. Therefore, alternative effort has been devoted to improving the hydrothermal stability of these silica membranes. Recently, a significant hydrothermal improvement was achieved when the siloxane bridges (Si–O–Si) were partially replaced by organic bridges (Si–CH_2–CH_2–Si) such as bis(triethoxysilyl)ethane (BTESE). These promising organosilica membranes had been studied in liquid and vapor separation (pervaporation) [23–25] and gas separation [26,27] and were then extended to desalination (reverse osmosis) [28]. Numerous generations of organoalkoxysilanes have emerged and been prepared as membranes via sol–gel processes such as bis(triethoxysilyl)-methane (BTESM), 1,3-bis(triethoxysilyl)propane (BTESP), and the aromatic bridging groups: benzene and biphenyl [29, 30]. Thus far, however, only BTESE and bis(triethoxysilyl)ethylene (BTESEthy) have been used in the preparation of RO membranes.

According to Tsuru et al. [31] BTESE-derived organosilica membranes have shown

superior retention performance for mono and bivalent ions and neutral solutes of low-molecular weight, such as isopropyl alcohol and glucose. Compared with BTESE membranes, BTESEthy membranes [32], with polarizable and rigid ethenylene bridges in the network structure have led to improved water permeability and high NaCl rejection (>98.5%). Both membranes have shown a tolerance of high temperatures [31, 32].

Therefore, the purpose of the present study was to introduce a new organoalkoxysilane – 2,4,6-tris[3-(triethoxysilyl)-1-propoxy]-1,3,5-triazine(TTESPT) – with triple silicon alkoxides and a triazine unit structure to determine its performance in an RO application. This material was chosen because we believed that the TTESPT membrane is more polarizable and attractive to water molecules compared with the BTESE and BTESEthy membranes. Recently, high CO_2 uptakes (~38–51 cm^3 g^{-1}) were obtained at ambient pressure and temperature using a new class of 1,3,5-triazine-based microporous polymers. The CO_2 uptake was enhanced by 70–90% when the polymers were carbonized at 400 °C for 1 h and at 800 °C for an additional 1 h under nitrogen [33]. Rabbani and El-Kaderi [34] also demonstrated that microporous polybenzimidazole containing nitrogen atoms had high CO_2 uptake capacity and selectivity over N_2 based on the interaction between N_2 atoms and CO_2 molecules. Thus, we expected TTESPT membranes to have similar adsorption properties towards selected gases and water molecules. In addition, we adjusted the H_2O/TTESPT molar ratio during the preparation of the TTESPT sols to tune the pore size of TTESPT membranes to achieve optimal desalination performance. To the best of our knowledge, we are the first to test the performance of TTESPT membranes in gas separation [35] and RO.

3.2. Experimental

3.2.1. Synthesis of 2,4,6-tris[3-(triethoxysilyl) -1-propoxy]-1,3,5-triazine (TTESPT)

TTESPT was synthesized in a (30 mL) two-necked flask equipped with a stirrer and a reflux condenser, into which was placed (4.40 g, 17.7 mmol) of 2,4,6-tris(allyloxy)-1,3,5-triazine and (10.40 g, 63.3 mmol) of triethoxysilane in (10 mL) of toluene. Two drops of (0.1 M) H_2PtCl_6 in *i*PrOH were added, and the mixture was heated to reflux for 4 hours. Excess reactant and the solvent were removed under vacuum to give a colorless liquid (12.08 g). All reactions were performed under an atmosphere of dry nitrogen. Figure 3-1 is a schematic diagram of the synthesis of 2,4,6-tris[3(triethoxysilyl) -1-propoxyl]-1,3,5-triazine (TTESPT)

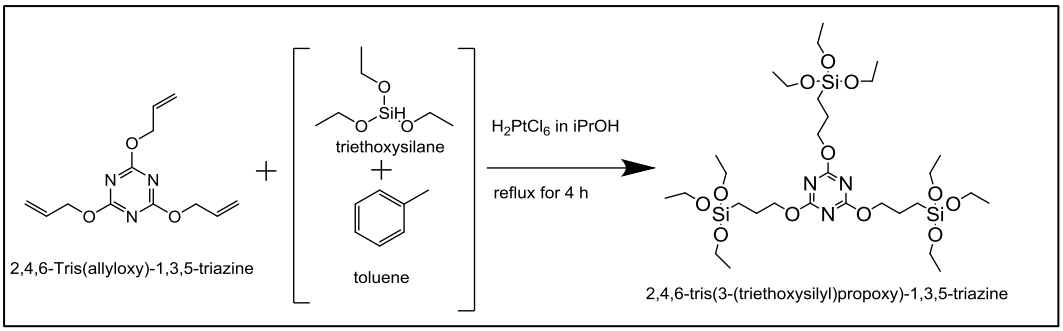

Figure 3-1 Schematic diagram of the synthesis of 2,4,6-tris[3(triethoxysilyl) -1-propoxyl] -1,3,5-triazine (TTESPT)

3.2.2. Preparation of TTESPT organosilica sols and membranes

TTESPT as a silica precursor was homogeneously dissolved in an ethanol solution. A mixture of water and hydrochloric acid were then added dropwise to the solution under vigorous stirring, resulting in a final solution with molar ratios of TTESPT/H_2O/acid = 1/60/0.2 and 1/240/0.2. Then, the solution was kept in a closed system under continuous stirring at 25 °C for 6 h to allow the formation of silica sols. Porous a-alumina tubes (porosity: 50%, average pore size: 1 mm, outside diameter: 10 mm) were used as the supports for TTESPT-derived silica membranes. a-Alumina particles (average particle diameter: 0.2, 1.9 mm) were coated onto the outer surface of a porous support using a silica–zirconia colloidal sol as the binder, and the support was fired at 550 °C for 30 min to smooth the surface. These procedures were repeated several times to cover large pores that might have resulted in pinholes in the final membrane. Then, a SiO_2–ZrO_2 (Si/Zr = 1/1) solution (diluted to about 0.5 wt%) was coated onto the substrate to form an intermediate layer with pore sizes of several nm, followed by calcination at 550 °C for approximately 30 min. Finally, the TTESPT-derived silica layer was fabricated by coating a TTESPT solution, followed by drying and calcination at 300 °C under nitrogen for 30 min.

3.2.3. Characterization of TTESPT organosilica sols and membranes

The sizes of freshly prepared TTESPT sols in a 10% dilution in ethanol were measured by dynamic light scattering (DLS) Zetasizer Nano (Malvern, ZEN3600) at 25 °C. Thermogravimetric analysis (TG) was performed to investigate the decomposition behavior of the organic groups in the silica matrix at temperatures ranging from 100 to 1000 °C with a heating rate of 10 °C min^{-1} in a helium flow of 300 mL min^{-1} using a thermogravimetric analyzer (TGA-DTA-PIMS 410/S, Rigaku, Japan). A N_2 adsorption isotherm was obtained at 77 K to study the micropore structures of the silica gels. Prior to the measurement, all the silica gel samples were evacuated at 150 °C for 12 h. The measurements were carried out

using BELMAX software (BEL JAPAN INC., Japan). The morphologies of the TTESPT membranes were examined using a Hitachi S-48000 field emission scanning electron microscope (FESEM).

3.2.4. Performance evaluation of the TTESPT membranes

3.2.4.1. Single-gas permeation.

Figure 3-2 shows a schematic diagram of the experimental apparatus for the single-gas permeation measurement. Gas permeation tests were performed at 200 °C using single components of He, H_2, CO_2, N_2, CH_4, C_3H_6, C_3H_8, and SF_6. The permeation stream was maintained at atmospheric pressure, and the pressure drop through the membranes was maintained at 1 bar. Prior to the measurement, all membranes were outgassed in a He flow of 50 mL min^{-1} at 200 °C for 8 to 12 h to remove any water that had possibly adsorbed on the membranes.

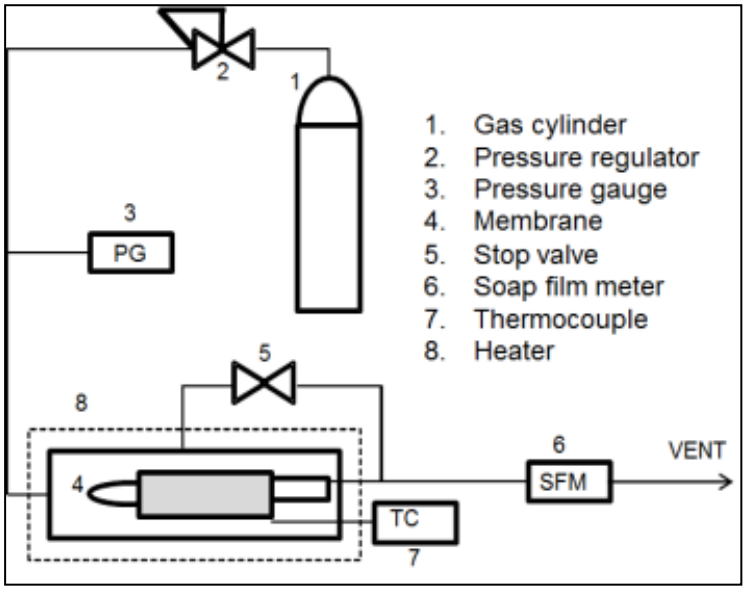

Figure 3-2 Schematic diagram of the experimental apparatus for single gas permeation measurement.

3.2.4.2. Reverse osmosis performance test.

The RO experiment was conducted in a cross-flow filtration system, as shown in Figure 3-3. The feed solution was pressurized with a plunger pump at a pressure of 1 MPa, and a temperature of 25 °C was maintained unless otherwise specified. The retentate was recycled back to the feed container while the permeate stream was maintained at atmospheric pressure and collected using a microtube pump. The concentrations of feed solutions were 2,000 ppm

of NaCl, and 500 ppm of ethanol, isopropanol, and glucose. The concentrations of feed and permeate were measured with a conductivity meter (HORIBA, ES-51) for electrolytes and a total organic carbon analyzer (Shimadzu, TOC-VE) for neutral solutes. Performance evaluation of the RO membrane was conducted via the calculation of water permeability, L_p, and observed rejection, R. Water permeability, L_p, was calculated from the volume flux J_v divided by the effective transmembrane pressure, $\Delta P - \Delta\pi$.

$$L_p = J_v/(\Delta P - \Delta\pi) \quad (3\text{-}1)$$

For sufficiently dilute solutions, the osmotic pressure difference, $\Delta\pi$, for NaCl was determined using the van′t Hoff equation:[36]

$$\Delta\pi \cong 2RT(C_f - C_p) \quad (3\text{-}2)$$

where R is the gas constant, T is the absolute temperature, C_p is the permeate concentration, and C_f is the feed concentration. The effect of concentration polarization was rationally ignored in this work due to low permeate flux. An observed rejection, R, was expressed as follows:

$$R\ (\%) = (1-C_p/C_f) \times 100 \quad (3\text{-}3)$$

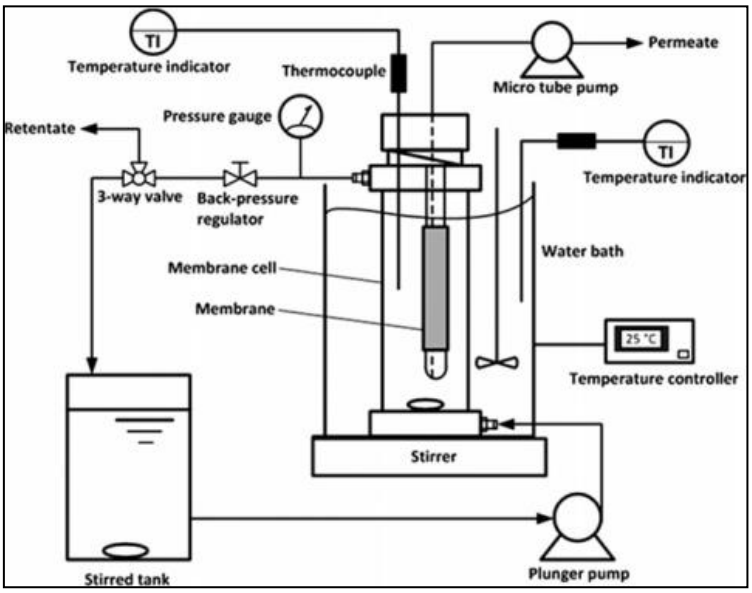

Figure 3-3 Schematic diagram of the experimental apparatus for reverse osmosis measurement.

3.3. Results and discussion

3.3.1. Characterization of TTESPT sols, powders and membranes

3.3.1.1. Dynamic light scattering (DLS)

To study the effect of the H_2O/TTESPT molar ratio, two different molar ratios, 60 and 240, were prepared. Theoretically, increasing the amount of water content can encourage bond formation and create an open fractal polymer, which is needed to attain molecular sieving ability [23, 37]. Figure 3-4 shows the size distributions of the TTESPT sols determined by dynamic light scattering at 25 °C. The TTESPT-60 and TTESPT-240 were used to denote TTESPT sols prepared at H_2O/TTESPT molar ratios of 60 and 240, respectively. In this work, the TTESPT-60 sol produced a small sol size of 0.8 nm. On the contrary, the TTESPT-240 sol exhibited a sol size of approximately 2.3 nm, which was slightly larger than the former sol. This phenomenon can be related to a faster rate of the hydrolysis reaction. The increment of the sol size distribution was probably dominated by the polymerization reaction of monomer species, instead of the aggregation reaction. If an aggregation of nanoparticles occurred, it would result in a dramatic increment of sol size distribution compared with the sizes that are shown in Figure 3-4 [38-40].

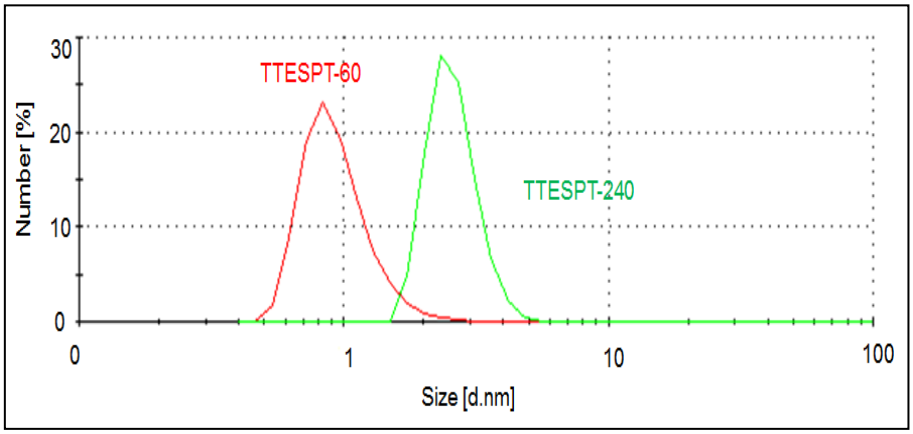

Figure 3-4 Colloidal size distribution of the TTESPT sols at 25° C.

3.3.1.2. Thermogravimetric analysis (TG)

Figure 3-5 shows the TG curves of TTESPT-60 and TTESPT-240 powders as a function of temperature. As shown in Figure 3-5, analysis of the TG curves for both samples indicated that thermal decomposition occurred in two steps. The same observation was reported by other researchers for a new class of 1,3,5-triazine-based microporous polymer sample that was conducted under an N_2 atmosphere [33]. Two degradation steps occurred during the TG analysis: the first degradation stage occurred in temperatures that ranged from 100 to 310 °C, while the second stage was observed in temperatures that ranged from 310 to 650 °C. The

firstdegradation stage can be ascribed to the evaporation of adsorbed water, solvent, acid and the decomposition of unreacted ethoxy groups, and also to the partial decomposition of some branching bonds of triazine units in the powder [41]. The second degradation stage for TTESPT-60 and TTESPT-240 occurred at temperatures that ranged from ～310 to 650 °C; this may correspond to the pyrolysis of cleavage of the C-C, C-O, C-N and C=N branching bonds of the TTESPT units induced by thermal treatment. The decomposition of these bonds signifies that CH_4, CO_2, CH_3CN, and H_2 were generated [33, 41, 42].

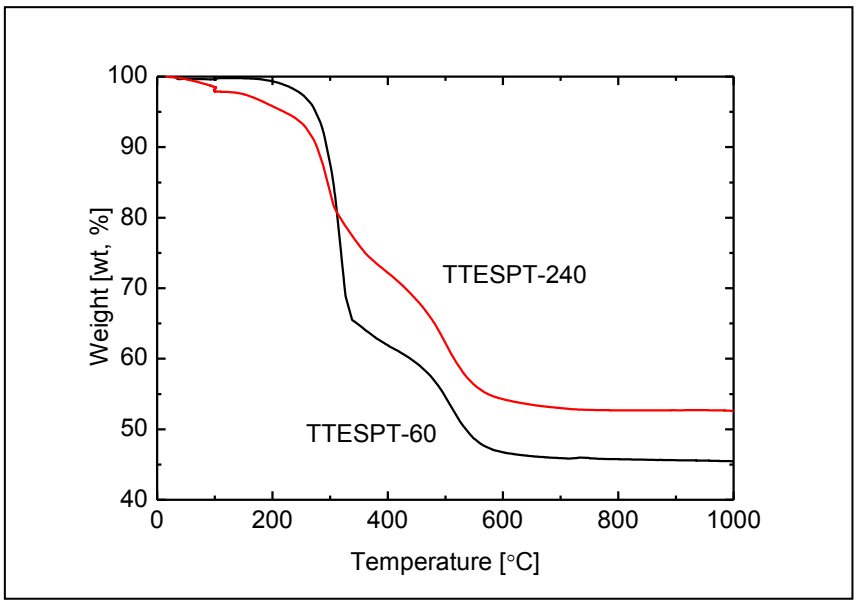

Figure 3-5 TG curves of TTESPT-derived silica gel powder (Ramping rate: 10 °C min^{-1}; He flow rate: 300 ml min^{-1}).

3.3.1.3. N_2 adsorption isotherm

The N_2 adsorption isotherms and pore size distribution of TTESPT powders after calcination at 300 °C, are shown in Figure 3-6. In accordance, Table 1 summarizes the specific surface area for both powders. It is possible that different amounts of water content exhibited significant changes within the isotherm patterns and pore size distributions. TTESPT-60 powder displayed a non-porous isotherm forming pores with an average size that ranged from 1.9 to 20 nm, or larger. This may have been due to the unreacted ethoxide groups that blocked the pore mouth of the silica network. Moreover, triazine units may have acted as “building blocks” between the silica pores, and occupied some space in the silica network, resulting in a limited number of open pores and a lower surface area. On the contrary, the adsorption branch of TTESPT-240 powder seems to have been a combination of Type I and IV isotherms. Therefore, as the water content increased, some micropores were created by the hydrolysis and condensation reaction. The pore diameters for TTESPT-240 powder ranged

from 0.6 to 1.7 nm, and, hence, the surface area was increased, showing that the TTESPT-240 was more porous than the TTESPT-60. A schematic diagram of TTESPT pore networks with a different H_2O/TTESPT molar ratio appears in Figure 3-7. Obviously, increasing the H_2O/TTESPT molar ratio can stimulate the formation of a network of smaller pores in a TTESPT membrane due to a higher degree of cross-linking.

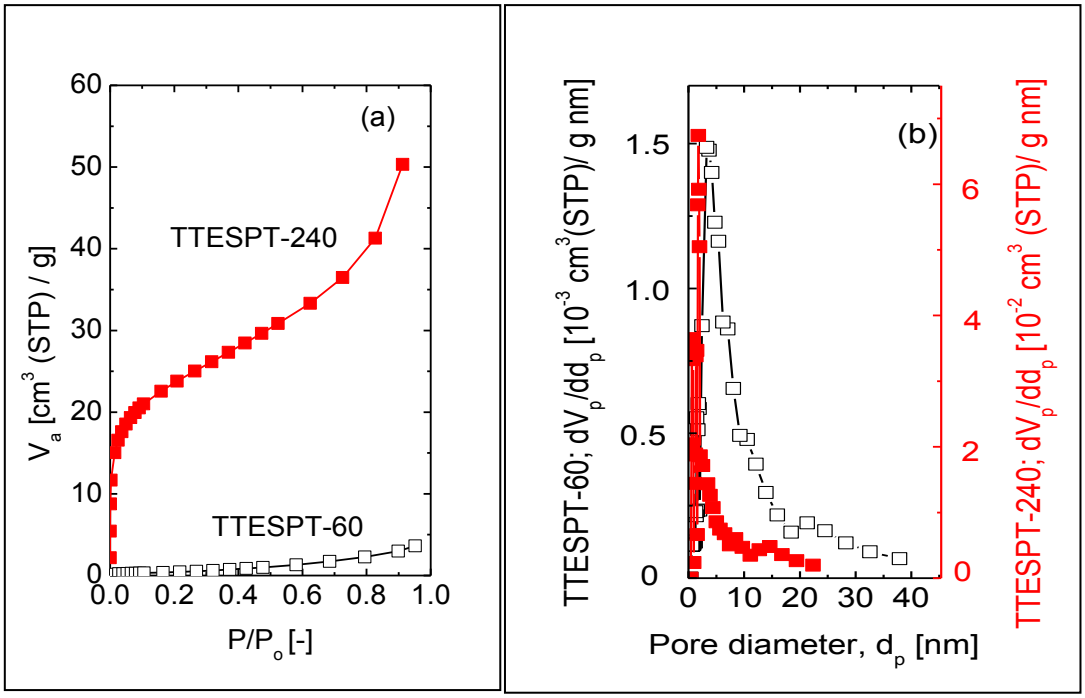

Figure 3-6 (a) N_2 Adsorption and (b) Pore size distribution of TTESPT-silica gel powders.TTESPT-60 (open keys) and TTESPT-240 (closed keys).

Table 3-1 Summary of the surface area for TTESPT membranes calcined at 300 °C.

Membranes	Surface Area [m^2/g]
TTESPT-60	2
TTESPT-240	80

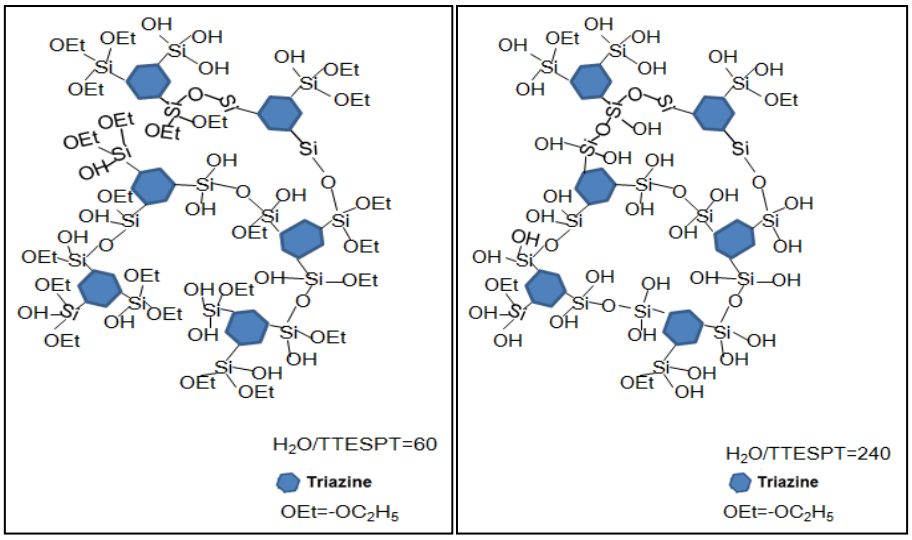

Figure 3-7 Schematic diagram of the effect of the H_2O/TTESPT molar ratio on a TTESPT pore network.

3.3.1.4. Scanning electron microscope (FESEM)

Figure 3-8 shows the cross-section of a SEM image of a TTESPT membrane. This clearly shows that a crack-free, continuous separation layer was formed on the top of the SiO_2-ZrO_2 and alumina layers after the calcination process at 300 °C.

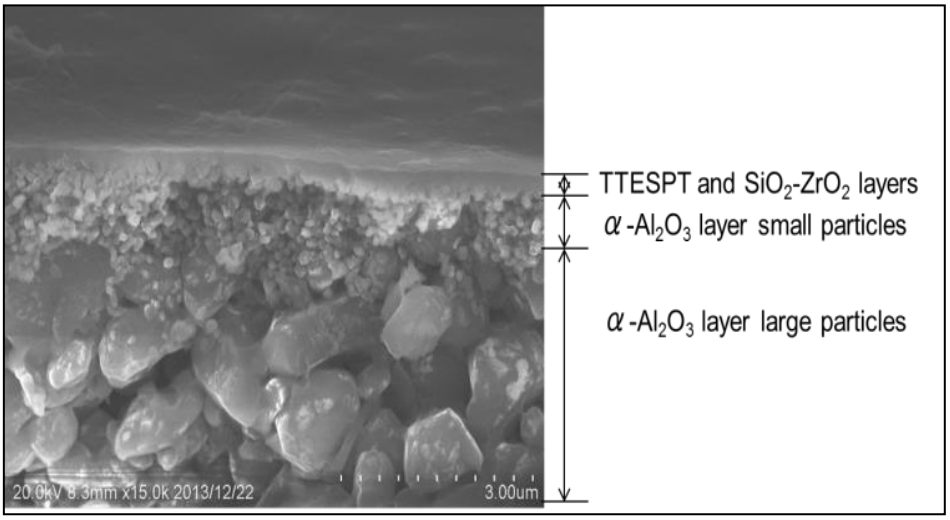

Figure 3-8 Cross-sectional SEM image of a TTESPT membrane calcined at 300 °C.

3.3.2. Gas permeation properties of TTESPT membranes

To investigate the separation efficiency of a TTESPT membrane calcined at 300 °C, gas permeation was conducted at a permeation temperature of 200 °C using He, H_2, CO_2, N_2, C_3H_6, C_3H_8, and SF_6, as shown in Figure 3-9 (a). It is noteworthy that both TTESPT

membranes exhibited a H_2 permeance of higher than 10^{-6} mol m^{-2} s^{-1} Pa^{-1}, but a moderate H_2/N_2 selectivity of approximately 9 to 14, as shown in Table 3-2. On the other hand, the H_2/SF_6 selectivity for the TTESPT-60 membrane was approximately 720 and was increased drastically (to 4700) by increasing the H_2O/ TTESPT molar ratio to 240.

In order to quantitatively evaluate the pore size of these membranes, a normalized Knudsen-based permeance (NKP) method was applied [41]. This NKP method was based on a modified gas translation (GT) model that was derived by modifying the original GT model proposed by Xiao and Wei [43] and by Shelekhin et al. [44] for the determination of membrane pore sizes of less than 1 nm. A more detailed explanation of this model can be found elsewhere [41]. NKP is the ratio of the permeance of the *i-th* component to that predicted with He, which is the smallest molecule, under the Knudsen diffusion mechanism. The expression for normalized Knudsen-based permeance can be obtained as follows.

$$NKP = \frac{P_i \sqrt{M_i}}{P_{He}\sqrt{M_{He}}} = \frac{\left(d_p - d_{k,i}\right)^3}{\left(d_p - d_{k,He}\right)^3} exp\left(-\frac{E_{p,i} - E_{p,He}}{RT}\right) \quad (3\text{-}4)$$

where $d_{k,i}$ is the molecular size of the *i*-th component and d_p is the average pore size of the membrane. The activation energy of the *i-th* and He components, the gas constant, and the temperature are denoted as $E_{p,i}$, $E_{p,He}$, R and T, respectively. In the present study, for simplicity, the assumption of a negligible difference in the activation energy of permeation was made, in order to easily evaluate the pore sizes of microporous membranes, leading to the following expression for NKP (eq 3-5).

$$NKP = \frac{\left(d_p - d_{k,i}\right)^3}{\left(d_p - d_{k,He}\right)^3} \quad (3\text{-}5)$$

Figure 3-9 (b) shows the NKP plot at 200 °C where the effect of surface flow can be negligible. It seems the pore size of TTESPT-derived silica membranes obtained via the NKP method shifted from a large to a small size, i.e., from 8 to 5 Å, when the H_2O/TTESPT molar ratio was increased from 60 to 240. This was because the TTESPT-240 membrane structure consisted of a smaller pore network compared with the TTESPT-60 membrane. One possible reason was due to the high degree of cross-linking that occurred in the TTESPT-240 membrane. As the H_2O/TTESPT molar ratio increased, the 9 ethoxy groups in TTESPT-240 should have been fully hydrolyzed and formed silanol groups. These silanol groups were then condensed with one another to form siloxane bonds that created a network of progressively smaller pores, as shown in Figure 3-7.

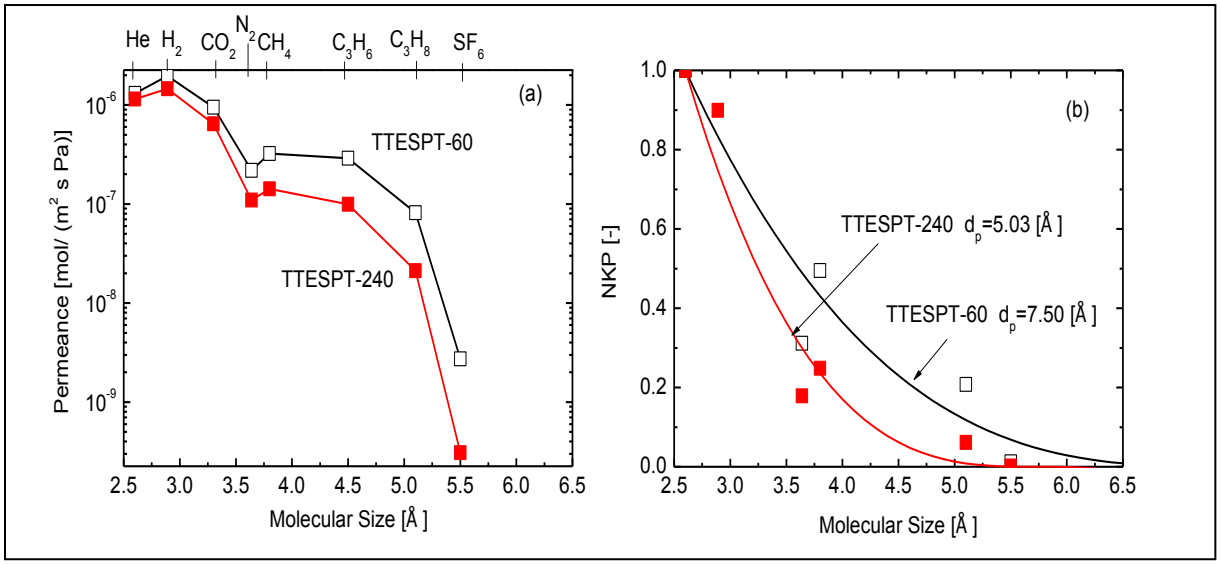

Figure 3-9 (a) Gas permeation properties **(b)** Normalized Knudsen-based permeance (NKP) of TTESPT-derived silica membranes calcined at 300 °C at a permeation temperature of 200 °C as a function of molecular size: TTESPT-60 (open keys) and TTESPT-240 (closed keys).

Table 3-2 Summary of Gas Permeance and Selectivity at 200 °C for TTESPT membranes.

Membranes	Permeance [10^{-9} mol/(m^2 s Pa)]			Selectivity [-]	
	H_2	N_2	SF_6	H_2/N_2	H_2/SF_6
TTESPT-60	1970	218	2.72	9.0	722
TTESPT-240	1460	109	0.30	13.3	4725

In our previous manuscript [35], we reported that TTESPT-derived silica membranes calcined at different calcination temperatures (200, 300 and 400 °C) exhibited an outstanding degree of selectivity for adsorptive molecules such as C_3H_6 and C_3H_8 at permeation temperatures of 50 °C, as shown in Table 3-3. In general, the C_3H_6/C_3H_8 selectivity decreases with increasing C_3H_6 and C_3H_8 permeance as a result of defects or variations in the pore size distribution. Interestingly, the separation performances of TTESPT-derived silica membranes calcined at 200 °C showed similar properties to carbonized membranes. Meanwhile, the separation performance of TTESPT-derived silica membranes calcined at temperatures of 300 and 400 °C showed similar or better separation properties than BTESM and Titanosilicate membranes at permeation temperatures that ranged from 50-200 °C. This tendency could be attributed to the presence of the π-bond (C=C double bond) in propene, which can have an affinity for the hydroxyl groups of silica and –C=N- triazine units. The superior sieving ability and adsorption affinity of TTESPT membranes motivated us to study its desalination performance.

Table 3-3 Summary of C_3H_6 permeance and selectivity for C_3H_6/C_3H_8 at a permeation temperature of 50 °C for TTESPT-derived silica membranes H_2O/TTESPT=240.

Calcination temperatures [°C]	C_3H_6 Permeance [10^{-9} mol/(m^2 s Pa)]	C_3H_6/C_3H_8 Selectivity [-]
200	2.95	37
300	59.8	8
400	305	7

3.3.3. Reverse osmosis properties of TTESPT membranes

Figure 3-10 shows the molecular weight cut-off (MWCO) curves of the TTESPT membranes determined by RO experimentation using neutral solutes with different molecular weights (MW) at 1 MPa and 25 °C. As shown in Figure 3-10, rejection increased in an ascending order of the molecular weight of solutes. Both membranes showed a quite high degree of rejection for neutral solutes of low molecular weight. Rejections for all the neutral solutes are as follows: ethanol, 38% (TTESPT-60) and 43% (TTESPT-240); isopropanol, 80% (TTESPT-60) and 90% (TTESPT-240); and, glucose, >98% (both TTESPT-60 and TTESPT-240). The values for MWCO, determined at a 90% rejection for TTESPT-60 and TTESPT-240 membranes, were estimated to be approximately 110 and 60, respectively. Stokes diameters for ethanol, isopropanol and glucose were 0.4, 0.48 and 0.73 nm, respectively.[45] Therefore, it was suggested that the rejection of the solutes had occurred mainly based on the molecular sieving effect. Table 3-4 compares the pore sizes of TTESPT membranes estimated by the different methods. Apparently, small pore sizes exhibited smaller MWCO values, indirectly, suggesting that the separation performance was strongly induced by molecular sieving.

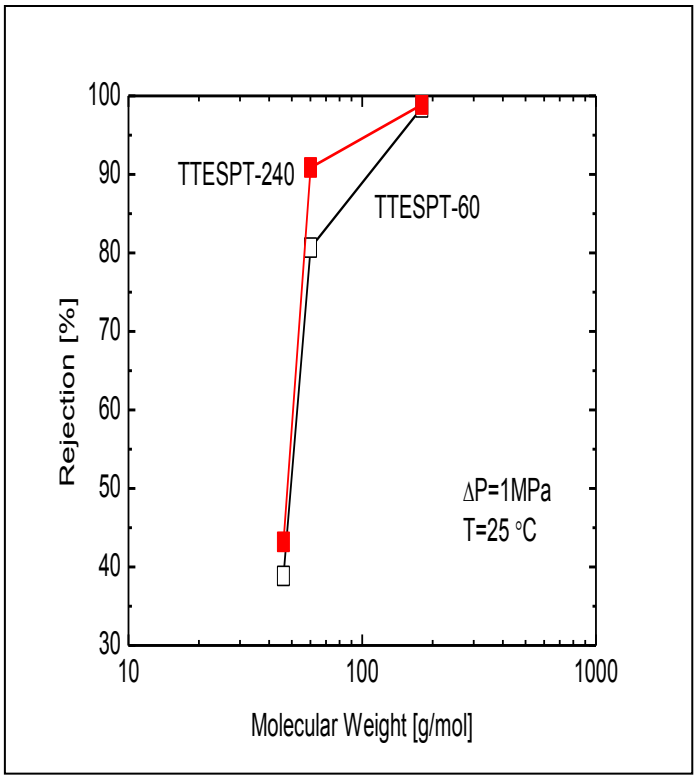

Figure 3-10 MWCO curves of TTESPT membranes.

Table 3-4 Comparison of the pore sizes of TTESPT membranes.

	TTESPT-60	TTESPT-240
N_2 Adsorption (nm)	>1.9 to 20	0.6 to 1.7
NKP calculation (Å)	8	5
MWCO (g/mol)	110	60

Water permeability and NaCl rejection capability was used to assess the desalination performance of TTESPT membranes. The RO desalination performance was evaluated using a 2,000 ppm NaCl solution at pressures that ranged from 0.4 to 1 MPa at 25 °C. Figure 3-11 shows the effect of feed pressure on the permeation of water and salt rejection using TTESPT membranes. The water flux (J_v) of both membranes increased simultaneously as operating pressure increased, whereas the water permeability (L_p) was almost constant, confirming that the pressure difference was the only driving force of water permeation. As the pressure increased, the enhanced water permeation led to an increase in salt rejection in TTESPT-60 and TTESPT-240 membranes that ranged from 93 to 96% and 95 to 98%, respectively. This can be easily explained by a solution-diffusion (SD) model that can be found elsewhere.[31] According to this model, the water permeation was influenced by the operating pressure, but the ion permeation was not. The TTESPT-240 membrane exhibited a higher rejection but a lower water flux than the TTESPT-60 membrane due to the small-sized pore networks that were formed in this membrane.

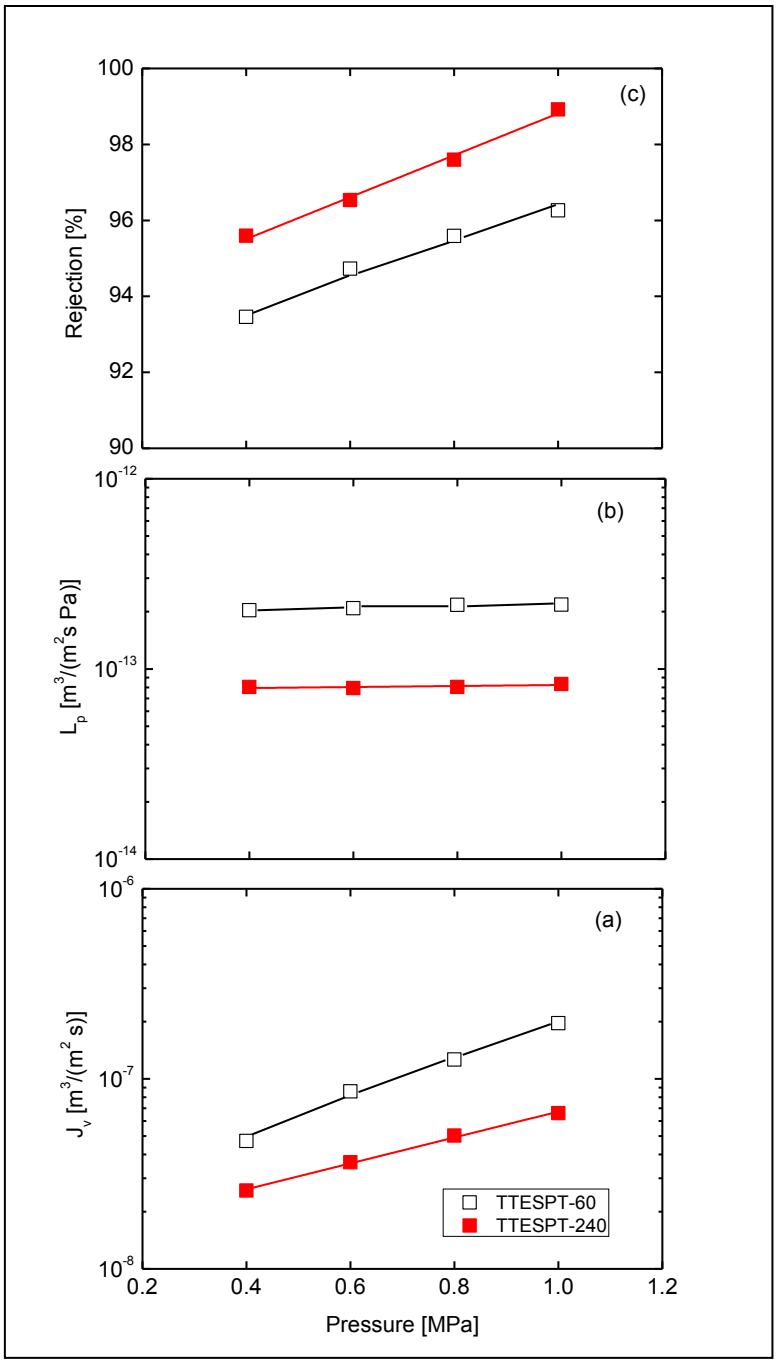

Figure 3-11 (a) Water flux, J_v, (b) Water permeability, L_p, and (c) Rejection, R, as a function of pressure at 25 °C and 2,000 ppm NaCl: TTESPT-60 (open keys) and TTESPT-240 (closed keys).

Figure 3-12 illustrates the schematic image of water transport through the amorphous silica networks of a TTESPT membrane. It is acknowledged that the transport mechanism of water and NaCl during RO is influenced by a molecular sieving phenomenon, which is the same as that of single-gas permeation. Hence, a TTESPT membrane must possess a pore size that falls between that of ions and water in order to increase its suitability for molecular sieving (ion

rejection). The hydrated sizes of $Na^{+}_{(aq)}$, $Cl^{-}_{(aq)}$ and H_2O are 0.72, 0.66 and 0.276 nm, respectively [17]. On the other hand, the molecular sizes of helium, hydrogen and SF6 gases are 0.26, 0.289 and 0.55 nm, respectively. Therefore, it is reasonable to use helium or hydrogen gases as a predictor of water permeance and SF6 gas as a predictor for NaCl permeance. The H_2/SF_6 selectivity for the TTESPT-60 membrane was approximately 720 and was increased drastically (to 4700) by increasing the H_2O/TTESPT molar ratio to 240, resulting in smaller MWCO and higher NaCl rejection. The TTESPT-240 membrane was believed to consist of dense silica networks and small pores compared to the TTESPT-60 membrane. Thus, it should be possible to estimate the rejection of NaCl molecules by comparing the selectivities of either He/SF_6 or H_2/SF_6. As mentioned earlier, the application of a variation in the H_2O/TTESPTmolar ratio, succeeded in tuning the pore size of TTESPT membranes. A rough estimation of the pore sizes of these TTESPT membranes via NKP demonstrated that high water content produced a smaller pore size. This enhancement of water permeability for the TTESPT-60 can be fully explained by this phenomenon. Larger pore size may accommodate more water molecules being transported continuously through the membrane, but the rejection status will be lowered. On the other hand, a smaller pore size will exert a strong blocking effect that will reject NaCl ions, thus inhibiting water molecules from entering the membrane pores and lowering the water flux.

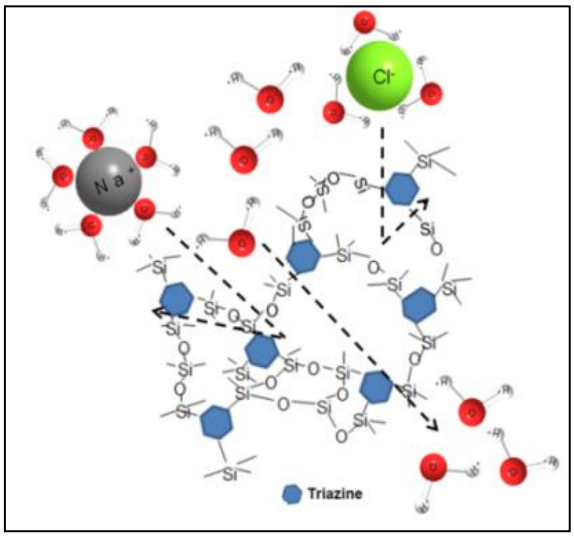

Figure 3-12 Schematic images of water transport through the amorphous silica networks of a TTESPT membrane.

The water permeation performance of the membranes as a function of temperature is shown in Figure 3-13 (a)–(d). The water permeability increased approximately 10-fold as the operating temperature increased from 25 to 60 °C, as shown in Figure 3-13 (a). The Hagen-Poiseuille equation (3-6) below was employed to theoretically estimate the

permeability through porous membranes.

$$L_p\mu = r_p^2 A_k / 8\Delta x \quad (3\text{-}6)$$

where r_p is the effective pore size, Δx is the effective membrane thickness, and A_k is the porosity.

If the transport mechanism obeys the viscous flow mechanism, the viscosity-corrected water permeability, $L_p\mu$, should remain constant with the origin, despite the permeation temperature. As shown in Figure 3-13 (b), the values for the $L_p\mu$ of both TTESPT membranes were not constant and clearly increased with temperature. Therefore, the transport mechanism through TTESPT membranes was confirmed to deviate from the viscous flow mechanism. The transport mechanism through the TTESPT membranes may be attributed to an activated transport mechanism, which is typical for microporous materials. Hence, for further investigation into the effect of temperature on permeability, the $L_p\mu$, was normalized at 25 °C for the TTESPT membranes and at 30 °C for the TiO_2 membrane [46], as shown in Figure 3-13 (c). Obviously, the normalized $L_p\mu$ for the membranes was increased as temperature increased. However, the steepness of the line increases in corresponding to the order of TTESPT-240>TTESPT-60>TiO_2. From Figure 3-13 (a) and (b), the observed activation energies of $\Delta E(L_p)$ and $\Delta E(L_p\mu)$ can be obtained using the Arrhenius equations below.

$$L_p = (L_p)_o \exp(-\Delta E(L_p)/RT) \quad (3\text{-}7)$$

$$L_p\mu = (L_p\mu)_o \exp(-\Delta E(L_p\mu)/RT) \quad (3\text{-}8)$$

where ΔE, R and T, are the the activation energy of the membrane, the gas constant, and the temperature, respectively.

Table 3-5 summarizes the values of the observed activation energies of L_p and $L_p\mu$ for each membranes. The observed activation energies of each membrane increased with decreasing pore size and MWCO values, which is in agreement with an activated transport mechanism. Since the average pore size of the TTESPT membranes was smaller than that of the TiO_2 membranes, water molecules were expected to exert strong friction against the pore walls. As the temperature increased, the water molecules with sufficient energy could break through the energy barrier to be transported through the TTESPT micropore networks. Another possible reason could have been the adsorption of water on the membrane pore wall. It is believed water adsorption to the hydrophilic portions of the TTESPT pore wall were governed by the bonds of Si-OH, C=N, and C-N groups. On the other hand, the rejection of TTESPT membranes seemed to have been constant or even increased (Figure 13 (d)), which confirmed that the pore sizes of these membranes were not influenced by the thermal

expansion in the present operating temperature range. Although similar temperature dependence for water permeability was reported for polymeric membranes [47, 48], this had been attributed to the enlargement of the pore size due to thermal expansion during the high-temperature conditions, which lowered the rate of rejection.

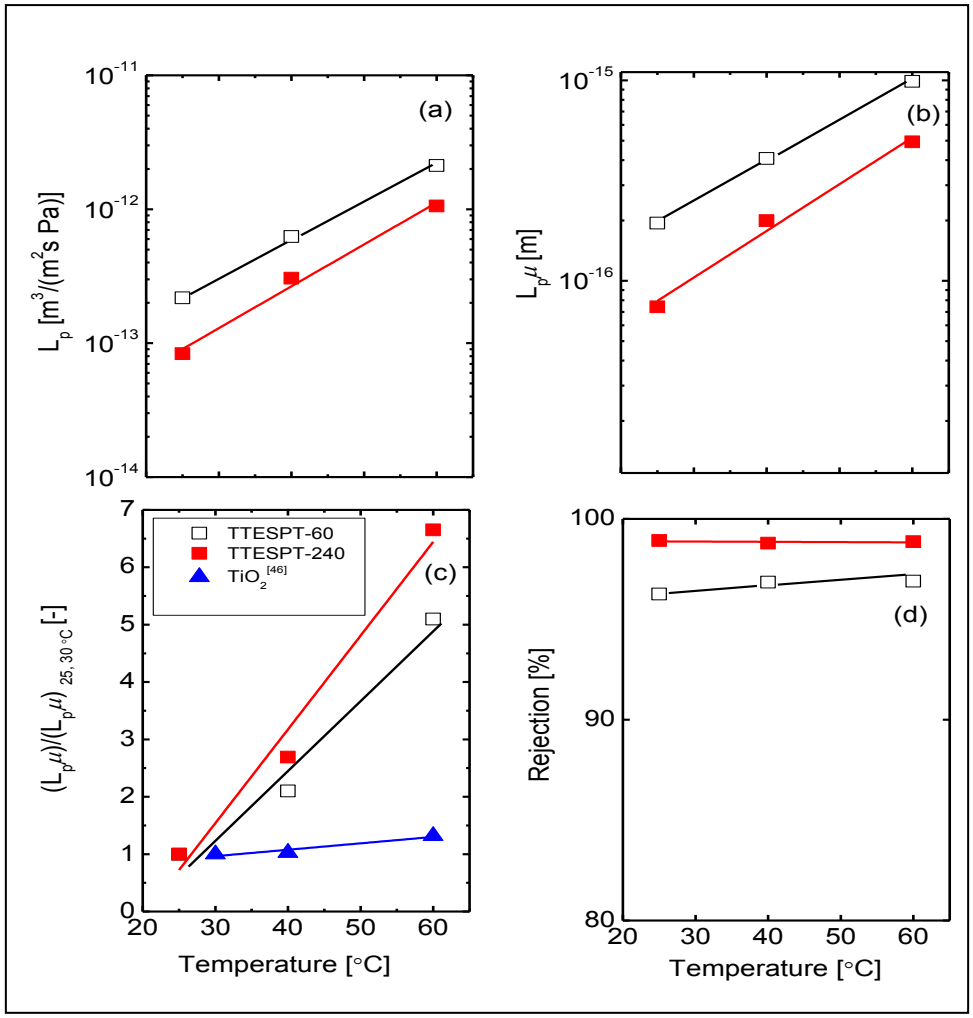

Figure 3-13 (a) Water permeability, L_p, (b) Viscosity-corrected water permeability, $L_p\mu$, (c) Normalized viscosity-corrected water permeability, $L_p\mu$, and (d) Rejection, R, as a function of temperature at 1 MPa and 2,000 ppm NaCl: TTESPT-60 (open keys), TTESPT-240 (closed keys) and TiO_2 (triangle closed keys).

Table 3-5 Activation Energies of L_p and $L_p\mu$ for TTESPT and TiO_2 membranes.

Membranes	TTESPT-60	TTESPT-240	TiO_2-1000 [46]
MWCO	110	60	1000
ΔE (L_p) (kJ/mol)	53.6	59.7	19.7
ΔE ($L_p\mu$) (kJ/mol)	38.4	44.5	5.1

In order to investigate the membrane hydrothermal durability, both TTESPT membranes were evaluated for 30 hours at temperatures that ranged from 25 to 60 °C at 1 MPa with 2,000 ppm NaCl. As shown in Figure 3-14 (a) and (b), the water permeabilities for TTESPT-60 and TTESPT-240 membranes were more than 1 x 10^{-12} $m^3/(m^2$ s Pa) and showed excellent salt rejection of >96 and 98%, respectively, at operating conditions of 1 MPa and 60 °C. The water permeabilities increased as the operating temperature increased. It was noteworthy that the rejection remained unchanged over time and temperature. This result fully supported the idea mentioned above that the increment of water permeability was due to activated diffusion whereas passage through the membrane of the NaCl ions was still hindered due to the small sizes of the pores in the TTESPT membrane network. These results also suggest that no alteration of the effective pore diameters and structures occurred. The excellent thermal stability can be attributed to the main body of the TTESPT structure that consisted of chemically strong bonds such as Si-C and Si-O-Si. To substantiate this fact, FTIR analysis was done to investigate the TTESPT structure after the RO thermal experiment.

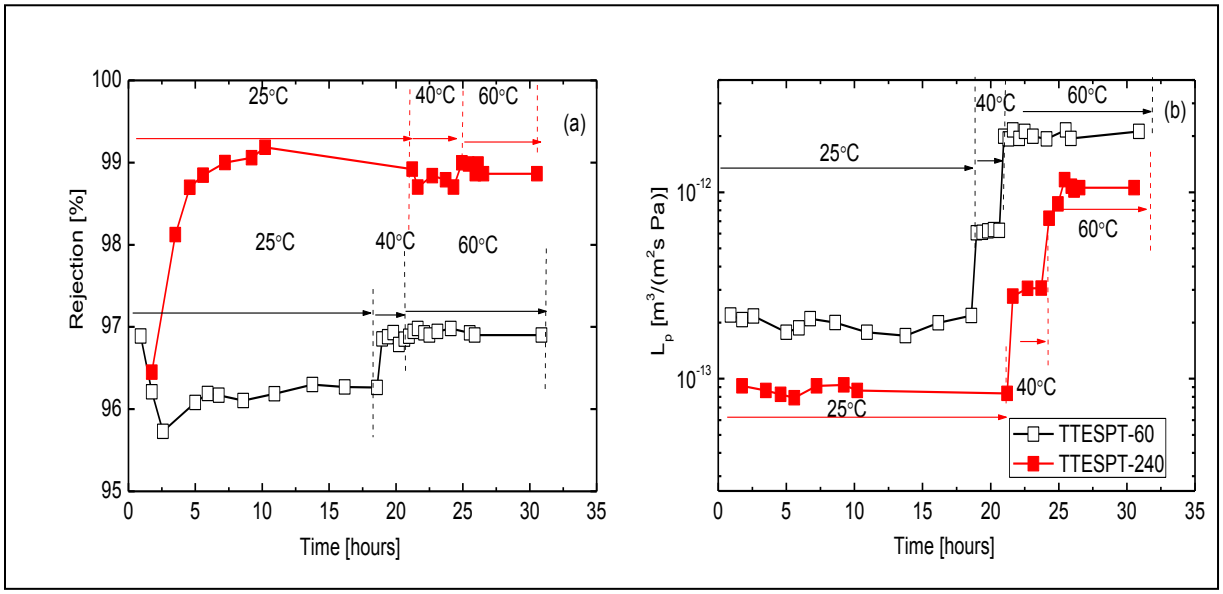

Figure 3-14 (a) Salt rejection, *R*, and (b) Water permeability, L_p, for TTESPT membranes as a function of temperature at 1 MPa and 2,000 ppm NaCl.

Figure 3-15 shows that most of the peaks of the TTESPT membrane remained nearly the same with no significant changes or structural deterioration before and after the RO thermal experiment. Therefore, it was confirmed that the TTESPT membrane had an inherently stable organosilica network and structure. Table 3-6 summarizes the comparisons of the desalination performances of different types of membranes. Currently, interfacial polymerized polyamide membranes are the industry standard in this area as they exhibit superior water flux and salt rejection.[49] However, organosilica membranes shows only a moderate degree of water

permeance with a high degree of rejection. Generally speaking, as we compared the performance of organosilica membranes with other zeolite membranes such as ZSM-5 [16], silicalite [50] and graphene [51] membranes, organosilica membranes can still be considered a high performance membrane, as shown in Table 3-6. If we narrow the comparison to the temperature dependency of organosilica membranes, the water permeability and salt rejection of TTESPT membranes displayed exactly the same characteristic as BTESE and BTESEthy membranes [28, 32]. Obviously, TTESPT membranes can be considered one of the choices for water desalination.

Table 3-7 summarizes the observed activation energies of L_p and $L_p\mu$ for all organosilica membranes. It is notable that smaller pore sizes exhibit larger activation energies. TTESPT membranes showed a larger degree of activation energies compared with the other two membranes even though the MWCO value was nearly the same. This was because the TTESPT membrane exhibited dual characteristics ascribable to organic (the flexibility via high chain mobility) and inorganic (Si-O-Si backbone that provides structural stability) groups. However, both BTESE and BTESEthy represent a rigid structure.

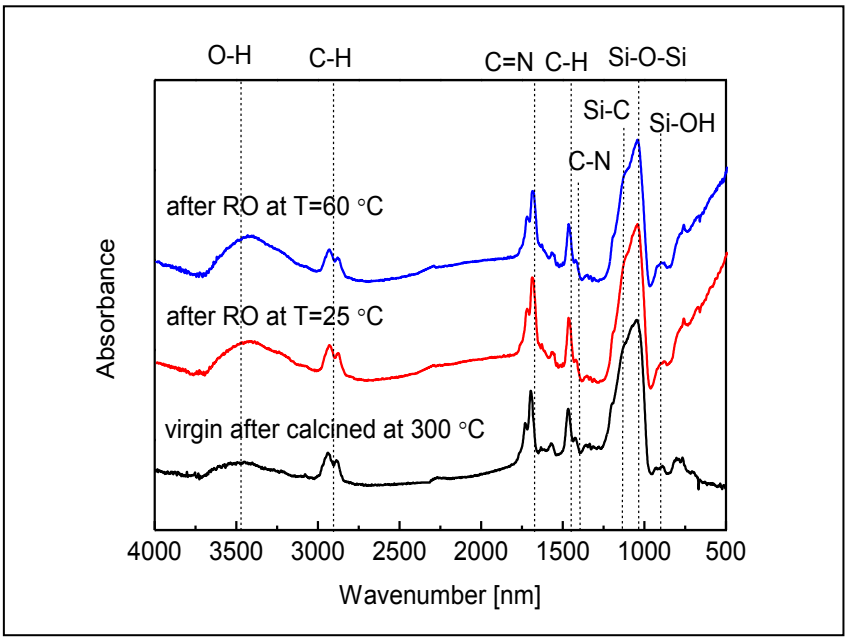

Figure 3-15 FTIR spectra of the TTESPT membranes: virgin and after the RO thermal experiment at 25 and 60 °C.

Table 3-6 Comparisons of the desalination performance of different types of membranes.

Membranes	Operating Condition	Water Permeability [$m^3/(m^2 s\ Pa)$]	Rejection [%]	Ref.
NaA-TFC Polyamide	1.6 MPa; 25 °C; 2000 ppm NaCl	5.6×10^{-12}	98	[49]
Silicate 1-TFC Polyamide	1.6 MPa; 25 °C; 2000 ppm NaCl	1.3×10^{-11}	96	[49]
ZSM-5, Si/Al=50	2.7 MPa; 25 °C; 0.1 M NaCl	1.4×10^{-13}	92	[16]
Silicalite	2.7 MPa; 25 °C; 0.1 M NaCl	4.3×10^{-14}	99	[50]
Ultrathin Graphene Nano-filtration	0.5 MPa; 0.02 M NaCl	None	40	[51]
BTESE	1.15 MPa; 25 °C; 2000 ppm NaCl	1.0×10^{-13}	97	[28]
	1.15 MPa; 60 °C; 2000 ppm NaCl	2.2×10^{-13}	98	[28]
BTESEthy	1.15 MPa; 25 °C; 2000 ppm NaCl	2.0×10^{-13}	98	[32]
	1.15 MPa; 60 °C; 2000 ppm NaCl	1.0×10^{-12}	98	[32]
TTESPT-60	1 MPa; 25 °C; 2000 ppm NaCl	2.2×10^{-13}	96	This work
	1 MPa; 60 °C; 2000 ppm NaCl	2.2×10^{-12}	96	
TTESPT-240	1 MPa; 25 °C; 2000 ppm NaCl	8.3×10^{-14}	98	This work
	1 MPa; 60 °C; 2000 ppm NaCl	1.0×10^{-12}	98	

Table 3-7 Summary of MWCO and Activation Energy of L_p and $L_p\mu$ for TTESPT, BTESE and BTESEthy membranes.

Membranes	TTESPT-240	BTESE [28]	BTESEthy [32]
MWCO	60	50	50
ΔE (L_p) (kJ/mol)	59.7	30.8	30.7
ΔE ($L_p\mu$) (kJ/mol)	44.5	15.3	15.7

Figure 3-16 shows the schematic images of the BTESE and TTESPT membranes. According to Castrium et al. [29] polymer material usually exhibits an increased diffusivity at higher temperatures, and this is related to an increased mobility of the organic chains. The TTESPT material consists of three long arms of propene groups that are connected to silicon alkoxides. The permeance through this material may have a similarity to the temperature-dependent chain mobility. This is in agreement with the findings in our previous manuscript [35] revealing that an activated diffusion transport mechanism was dominant for this material.

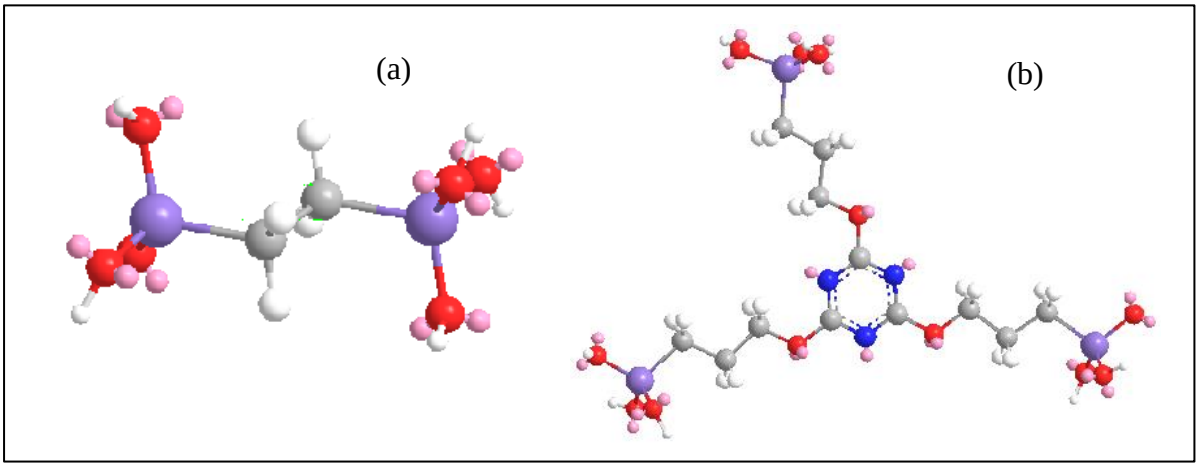

Figure 3-16 Schematic images of (a) BTESE (b) TTESPT membranes.

In addition, the high water permeability, L_p, for a TTESPT membrane was likely due to high water affinity for the hydrophilic portions of the TTESPT pore wall that consisted of polar Si-OH, C-O, C=N and C-N groups. This was proven by quantum chemical calculations at the level of B3LYP/6-31G (d) using a Gaussian09 program. Figure 3-17 shows the optimized geometry and electrostatic potentials of the TTESPT model simplified by replacing the ethoxy units on the silicon atoms with methoxy groups. The electrostatic potentials (ESPs) derived from the calculations also are depicted in Figure 3-17, and these closely relate the electron density distribution. The colors ranged from -0.04 to +0.01 with red and blue denoting extremely electron rich and deficient regions, respectively. Clearly, the ESPs of this monomer model show that negative potentials are mainly localized on the C-O, C=N and C-N groups, while the non-polar C-H groups bear relatively positive potentials.

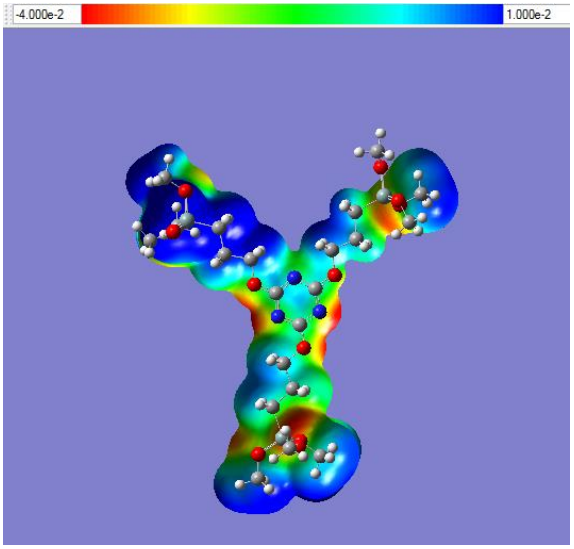

Figure 3-17 Optimized geometry and electrostatic potentials of the TTESPT model, derived from DFT-calculations at B3LYP/6-31G(d).

3.4. Conclusions

In conclusion, the present study marks the first successful preparation of a TTESPT membrane that exhibits dual characteristics that are both organic (the flexibility via high chain mobility) and inorganic (Si-O-Si backbone that provides structural stability). By adjusting the H_2O/TTESPT molar ratio, the permeation properties of this membrane were enhanced. A higher H_2O/TTESPT molar ratio seemed to exhibit a smaller pore network membrane with high separation factors for H_2/SF_6 (>4,000) and salt rejection almost constant (>98%) with increases in the operating temperature that ranged from 25–60 °C at 1 MPa. It was evident that the variation of sol–gel parameters such as the water ratio played an important role in the separation properties of the TTESPT membranes. Thus, further study on long-term stability under robust conditions (temperature, pH, etc.) and variations in salt rejection for the TTESPT membrane would be important.

References

[1] S. Otles and S. Otles, Desalination Techniques, Electron. J. Environ., Agric. Food Chem., 4 (2004) 963–969.

[2] M. A. Shannon, P. W. Bohn, M. Elimelech, J. G. Georgiadis, B. J. Marin and A. M. Mayes, Science and technology for water purification in the coming decades, Nature, 452 (2008) 301–310.

[3] Y. Zhou and R. S. J. Tol, Evaluating the costs of desalination and water transport, Water Resour. Res., 41 (2005) 1–10.

[4]S. Veerapaneni, B. Long, S. Freeman and R. Bond, Reducing energy consumption for seawater desalination, J.–Am. Water Works Assoc., 99 (2007) 95–106.

[5] K. P. Lee, T. C. Arnot and D. Mattia, A review of reverse osmosis membrane materials for desalination—Development to date and future potential, J. Membr. Sci., 370 (2011) 1–22.

[6] S. T. Hsu, K. T. Cheng and J. S. Chiou, Seawater desalination by direct contact membrane distillation, Desalination, 143 (2002) 279–287.

[7] M. Sadrzadeh and T. Mohammadi, Sea water desalination using electrodialysis, Desalination, 221 (2008) 440–447.

[8] Y. Oren, Capacitive deionization (CDI) for desalination and water treatment — past, present and future (a review), Desalination, 228 (2008) 10–29.

[9] R. L. McGinnis and M. Elimelech, Energy requirements of ammonia–carbon dioxide forward osmosis desalination, Desalination, 207 (2007) 370–382.

[10] M. Elma, C. Yacou, D. K. Wang, S. Smart and J. C. D. da Costa, Microporous silica based membranes for desalination, Water, 4 (2012) 629–649.

[11] L. F. Greenlee, D. F. Lawler, B. D. Freeman, B. Marrot and P. Moulin, Reverse osmosis desalination: water sources, technology, and today's challenges, Water Res., 43 (2009) 2317–2348.

[12] D. Li and H. Wang, Recent developments in reverse osmosis desalination membranes J. Mater. Chem., 20 (2010) 4551–4566.

[13] H. B. Park, B. D. Freeman, Z. B. Zhang, M. Sankir and J. E. McGrath, Highly Chlorine‐Tolerant Polymers for Desalination, Angew. Chem., Int. Ed., 120 (2008), 6108–6113.

[14] R. J. Petersen, Composite reverse osmosis and nanofiltration membranes, J. Membr. Sci., (83) 1993 81–150.

[15] L. Li, J. Dong, T. M. Nenoff and R. Lee, Desalination by reverse osmosis using MFI zeolite membranes, J. Membr. Sci., 243 (2004) 401–404.

[16] L. Li, N. Liu, B. McPherson and R. Lee, Enhanced Water Permeation of Reverse Osmosis through MFI-Type Zeolite Membranes with High Aluminum Contents, Ind.

Eng. Chem. Res., 46 (2007) 1584–1589.
[17] B. Zhu, Z. Hong, N. Milne, C. M. Doherty, L. Zhou, Y. S. Lin, A. J. Hill, X. Gu and M. Duke, Desalination of seawater ion complexes by MFI-type zeolite membranes: Temperature and long term stability, J. Membr. Sci., 453 (2014) 126–135.
[18] R. Igi, T. Yoshioka, Y. H. Ikuhara, Y. Iwamoto and T. Tsuru, Characterization of Co-Doped Silica for Improved Hydrothermal Stability and Application to Hydrogen Separation Membranes at High Temperatures, J.Am. Ceram. Soc., 91 (2008) 2975–2981.
[19] T. Tsuru, R. Igi, M. Kanezashi, T. Yoshioka, S. Fujisaki and Y. Iwamoto, Permeation properties of hydrogen and water vapor through porous silica membranes at high temperatures AIChE J., 57 (2011) 618–629.
[20] C. Yacou, S. Smart and J. C. D. da Costa, Long term performance cobalt oxide silica membrane module for high temperature H_2 separation, Energy Environ. Sci., 5 (2012) 5820–5832.
[21] R. Leboda and E. Mendyk, Hydrothermal modification of porous structure of silica adsorbents, Mater. Chem. Phys., 27 (1991) 189–212.
[22] M. C. Duke, J. C. D. da Costa, D. D. Do, P. G. Gray and G. Q. Lu, Hydrothermally robust molecular sieve silica for wet gas separation, Adv. Funct. Mater., 16 (2006) 1215–1220.
[23] H. L. Castricum, A. Sah, R. Kreiter, D. H. A. Blank,J. F. Vente and J. E. tenElshof, Hydrothermally stable molecular separation membranes from organically linked silica, J. Mater. Chem., 18 (2008) 2150–2158.
[24] H. L. Castricum, R. Kreiter, H. M. vanVeen, D. H. A. Blank,J. F. Vente and J. E. ten Elshof, High-performance hybrid pervaporation membranes with superior hydrothermal and acid stability, J. Membr. Sci., 324 (2008) 111–118.
[25] H. M. van Veen, M. D. A. Rietkerk, D. P. Shanahan,M. M. A. vanTuel, R. Kreiter, H. L. Castricum, J. E. tenElshof and J. F. Vente, Pushing membrane stability boundaries with HybSi® pervaporation membranes, J. Membr. Sci., 2011, 380,124–131.
[26] M. Kanezashi, K. Yada K, T. Yoshioka, T. Tsuru, Design of silica networks for development of highly permeable hydrogen separation membranes with hydrothermal stability. J Am Chem Soc. 131 (2009) 414–415
[27] M. Kanezashi, K. Yada, T. Yoshioka and T. Tsuru, Organic–inorganic hybrid silica membranes with controlled silica network size: Preparation and gas permeation characteristics, J. Membr. Sci., 348 (2010) 310–318.
[28] R. Xu, J. Wang, M. Kanezashi, T. Yoshioka and T. Tsuru, Development of Robust Organosilica Membranes for Reverse Osmosis, Langmuir, 27 (2011) 13996–13999.
[29] H. L. Castricum, G. G. Paradis, M. C. Mittelmeijer-Hazeleger, R. Kreiter , J. F. Vente, and J. E. ten Elshof, Tailoring the Separation Behavior of Hybrid Organosilica Membranes by Adjusting the Structure of the Organic Bridging Group Adv. Funct.

Mater. 21 (2011) 2319–2329

[30] M. Kanezashi, M. Kawano, T. Yoshioka and T. Tsuru, Organic_Inorganic Hybrid Silica Membranes with Controlled Silica Network Size for Propylene/Propane Separation, Ind. Eng. Chem. Res., 51 (2012) 944–953.

[31] R. Xu, J. Wang, M. Kanezashi, T. Yoshioka, T. Tsuru, Reverse osmosis performance of organosilica membranes and comparison with the pervaporation and gas permeation properties, AIChE J. 59 (2013) 1298–1307

[32] R. Xu, M. Kanezashi, T. Yoshioka, T. Okuda, J. Ohshita and T. Tsuru, Tailoring the Affinity of Organosilica Membranes by Introducing Polarizable Ethenylene Bridges and Aqueous Ozone Modification, ACS Appl. Mater. Interfaces, 5 (2013) 6147–6154.

[33] H. Lim, M. C. Cha, J. Y. Chang, Preparation of Microporous Polymers Based on 1,3,5-Triazine Units Showing High CO_2 Adsorption Capacity,Macromol. Chem. Phys. 213 (2012) 1385- 1390.

[34] M. G. Rabbani and H. M. El-Kaderi, Synthesis and Characterization of Porous Benzimidazole-Linked Polymers and Their Performance in Small Gas Storage and Selective Uptake, Chem. Mater., 23 (2011) 1650–1653.

[35] S. M. Ibrahim, R. Xu, H. Nagasawa, A. Naka, J. Ohshita, T. Yoshioka, M. Kanezashi and T. Tsuru, A closer look at the development and performance of organic–inorganic membranes using 2,4,6-tris-[3(triethoxysilyl)-1-propoxyl] -1,3,5-triazine (TTESPT), RSC Adv., 4 (2014) 12404–12407.

[36] M. L. Lind, D. E. Suk, T. V. Nguyen and E. M. V. Hoek, Tailoring the structure of thin film nanocomposite membranes to achieve seawater RO membrane performance, Environ. Sci. Technol., 44 (2010) 8230–8235.

[37] O. Lev, K. Tsionsky, L. Rabinovich, V. Glezer, S. Sampath, I. Pankratov and J. Gun, Organically modified sol-gel sensors,Anal. Chem., 67 (1995) 22A–31A.

[38] R. S. A. Delange, J. H. A. Hekkink, K. Keizer and A. J. Burggraaf, Polymeric silica based sols for membrane modification applications: sol gel synthesis and characterization with SAXS, J. Non-Cryst. Solids, 191 (1995)1–16.

[39] D. R. Azolin, C. C. Moro, T. M. H. Costa and E. V. Benvenutti, Effects of organic content and H2O/TEOS molar ratio on the porosity and pore size distribution of hybrid naphthaleneamine propylsilica xerogel, J. Non-Cryst. Solids, 337 (2004) 201–206.

[40] Y. Ma, M. Kanezashi and T. Tsuru, Preparation of organic/ inorganic hybrid silica using methyltriethoxysilane and tetraethoxysilane as co-precursors, J. Sol–Gel Sci. Technol., 53 (2010) 93–99.

[41] H. R. Lee, M. Kanezashi, Y. Shimomura, T. Yoshioka and T. Tsuru, Evaluation and Fabrication of Pore-Size-Tuned Silica Membranes with Tetraethoxydimethyl Disiloxane for Gas Separation AIChE J., 57 (2011) 2755–2765.

[42] M. Kanezashi, M. Kawano, T. Yoshioka and T. Tsuru, Organic_Inorganic Hybrid Silica

Membranes with Controlled Silica Network Size for Propylene/Propane Separation, Ind.Eng. Chem. Res., 51 (2012) 944–953.

[43] J. Xiao and J. Wei, Diffusion mechanism of hydrocarbons in zeolites—I. Theory.Chem. Eng. Sci., 47 (1992) 1123–1142.

[44] A. B. Shelekhin, A. G. Dixon and Y. H. Ma, Theory of gas diffusion and permeation in inorganic molecular-sieve membranes. AIChE J., 41 (1995) 58–67.

[45] X. L. Wang, T. Tsuru, S. Nakao and S. Kimura, The electrostatic and steric-hindrance model for the transport of charged solutes through nanofiltration membranes J. Membr. Sci., 135 (1997) 19–32.

[46] T. Tsuru, K. Ogawa, M. Kanezashi and T. Yoshioka, Permeation characteristics of electrolytes and neutral solutes through titania nanofiltration membranes at high temperatures, Langmuir, 26 (2010) 10897–10905.

[47] N. B. Amar, H. Saidani, J. Palmeri and A. Deratani, Effect of temperature on the rejection of neutral and charged solutes by Desal 5 DK nanofiltration membrane, Desalination, 246 (2009) 294–303.

[48] H. Saidani, N. B. Amar, J. Palmeri and A. Deratani, Interplay between the transport of solutes across nanofiltration membranes and the thermal properties of the thin active layer, Langmuir, 26 (2010) 2574–2583.

[49] H. Huang, X. Qu, X. Ji, X. Gao, L. Zhang, H. Chena and L. Hou, Acid and multivalent ion resistance of thin film nanocomposite RO membranes loaded with silicalite-1 nanozeolites J. Mater. Chem. A, 1 (2013) 11343–11349.

[50] N. Liu, L. X. Li, B. McPherson and R. Lee, Removal of organics from produced water by reverse osmosis using MFI-type zeolite membranes, J. Membr. Sci., 325 (2008) 357–361.

[51] Y. Han, Z. Xu and C. Gao, Ultrathin Graphene Nanofi ltration Membrane for Water Purifi cation, Adv. Funct. Mater., 23 (2013) 3693–3700.

Chapter 4

Robust BTESE membranes for high temperature reverse osmosis (RO) application: Membrane preparation, separation characteristics of solutes and membrane regeneration

4.1. Introduction

State-of-the-art silica membranes consist of a nanoporous SiO_2 top layer (SiO_4 tetrahedra) coated onto a ceramic support and normally exhibit molecular sieve-like properties. The potential application of this nanoporous SiO_2 is mainly dependent on material properties, such as pore size and pore size distribution, as well as on the surface chemistry of the pores, and the defects that are formed. Generally, silica membranes show a high permeability for small molecules and a low permeability for larger molecules. So it is reasonable to expect a high selectivity for He (2.6 Å) and H_2 (2.9 Å) in gas separation and for H_2O (2.6 Å) in a RO process. In gas separation, silica membranes have exhibited relatively high permeances and good stability in temperatures as high as 600 °C and in corrosive atmospheres [1, 2]. In the presence of water, however, SiO_2 has a low microstructural and hydrothermal stability [3, 4], even at temperatures as low as 60 °C [2-5]. Continuous exposure to water results in the release of silica moieties; as a result, dense particles or defects with large nonselective pores are formed [2]. Therefore, research on alternative materials to improve hydrothermal stability is needed to address these material-based limitations in water application.

Reverse osmosis (RO) membranes typically are pressure-driven membranes that are classified according to the characteristic pore size (0.3-0.6 nm) [6] and are used mostly for desalination, water reuse, and ultrapure water production. Besides important uses in desalination, RO membranes have also shown great potential for use in many industrial applications when operating temperatures reach > 60 °C [7-9]. For example, in the sugar industry temperatures in the range of 70-80 °C are needed to prevent biological contamination; in the textile industry, the operating temperatures sometimes reach 90 °C [8], which most commercially available polymeric RO membranes cannot withstand [9-11]. In addition to that, RO membranes have the potential to be applied in the Steam Assisted Gravity Drainage (SAGD) industry due to the capability of withstanding high temperatures. These can be used to purify and reuse high-temperature boiler feed water.

Polymer membranes have been used to evaluate permeation performance, such as

permeate flux and the rejection of neutral and electrolyte solutes at temperatures that typically range from 5 to 65 °C [8]. To date, polyamide thin film composites (PA TFC) are widely used in commercial single-pass seawater desalination plants around the world [9, 12] due to a high water flux, the level of salt and organic matter rejection, and a wide pH range (1 to 11) [11]. However, PA TFC membranes have some drawbacks such as chlorine, fouling and limitations to the operating temperature (0-45 °C) [12].

Hence, the effect of temperatures higher than 60 °C has been investigated using ceramic and organosilica membranes, because these show thermal stability and chemical resistance, as mentioned above. Irrespective of the huge potential for high temperature applications, however, only a limited number of papers have focused on the development of inorganic-organic membranes. To date, nanoporous inorganic membranes such as zeolites [13-16] and organically bridged silica [17, 18] have been studied both theoretically and experimentally to reject ions in RO for the separation of salt from aqueous solutions. Organically bridged silica membranes that consist of an amorphous network with both organic Si–C_n–Si bridges and inorganic Si–O–Si bonds have attracted a considerable amount of recent attention because of their high performance in a variety of applications. In our previous study, we demonstrated that a bis(triethoxysilyl)ethane (BTESE) membrane could withstand temperatures as high as 90 °C in desalination applications with no obvious changes in filtration performance. We found that BTESE membranes also demonstrate excellent chlorine resistance during RO [17]. We also studied the performance of nanoporous titania membranes [19] and silica-zirconia (Si-Zr) membranes [20]. We found that the rejection of neutral solutes and alcohols decreased with temperature, whereas the rejection for electrolytes and alkanes remained approximately constant. In addition to these ceramic membranes, our group extended the RO research using varieties of organosilica membranes with ethane, ethylene and acetylene bridges [17, 21, 22] and triazine-based nitrogen-rich structures [18] on NaCl separation. All of these membranes exhibited the same trend whereby the salt rejection was almost constant (>98%) with increases in the operating temperature that ranged from 25 to 80 °C. However, when using organic solutes, the influence of temperature on these RO membranes has not yet been studied.

Mastering the practical application of BTESE membranes for RO requires a detailed understanding of the pressure-temperature influence on permeate volume flux and solute rejection for electrolyte and alcohol solutions. In addition, we also adjusted the molar ratios of BTESE/H_2O/acid= 1/x/0.2 (x=3 and 240) during the preparation of the BTESE sols to tune the pore sizes of the BTESE membranes. Furthermore, the membrane long-term stability and regeneration experiments of the BTESE membranes were carried out to further clarify the robustness of a BTESE membrane.

4.2.Experimental

4.2.1. Preparation of BTESE-derived sols and membranes

Bis(triethoxysilyl)ethane (BTESE) as a silica precursor was homogeneously dissolved in an ethanol (EtOH) solution. A mixture of water (H_2O) and hydrochloric acid (HCl) were then added dropwise to the solution under vigorous stirring, resulting in a final solution with molar ratios of BTESE/H_2O/HCl = 1/x/0.2 (x=3 and 240). The concentration of BTESE was kept at 5 wt% by adjusting the amount of EtOH added into the solutions. Then, the solution was kept in a closed system under continuous stirring at 25 °C for 6 h to allow the formation of silica sols.

4.2.2. Preparation of BTESE-derived sols and membranes

For membrane preparation, the same procedure was reported in our previous studies [17, 18]. Porous α-alumina tubes (porosity: 50%, average pore size: 1 μm, outside diameter: 10 mm) were used as the supports for BTESE-derived silica membranes. At first, α-alumina particles (average particle diameter: 1.9 μm) were coated onto the outer surface of a porous support using a silica-zirconia colloidal sol as the binder. Then the support was directly inserted in a furnace at a temperature 550 °C for 30 min to smooth the surface. After that, the membranes were coated with α-alumina particles (average particle diameter: 0.2 μm) under the same firing conditions. These procedures were repeated several times to cover large pores that might have resulted in pinholes in the final membrane. Then, a SiO_2–ZrO_2 (Si/Zr = 1/1) solution (diluted to about 0.5 wt%) was coated onto the substrate to form an intermediate layer with pore sizes of several nm, followed by firing at 550 °C for approximately 30 min [17, 18]. Finally, the BTESE-derived silica layer was fabricated by the coating of a BTESE solution 2 times, followed by drying and firing at 300 °C in air for 30 min. In the regeneration process, the membrane was washed with water, dried overnight in an oven at 200 °C, and then fired again at 300 °C in air for 15 minutes.

4.2.3. Reverse osmosis performance test

By using experimental data, membrane performances such as solutes rejection, $R_{solutes}$, water flux, J_v, and solute flux, J_s, were calculated directly. Solutes rejection, $R_{solutes}$, was expressed as follows:

$$R_{solutes}\,(\%) = (1-C_p/C_f) \times 100 \qquad (4\text{-}1)$$

where C_p and C_f are the concentration of permeate and feed, respectively. Meanwhile, the water flux, J_v, was calculated as follows:

$$J_v = W_p/\rho_p tA \quad (4\text{-}2)$$

where W_p is the mass of the permeate solutions (kg), ρ_p is the density of the permeate (kg/m^3), t is the time for collecting the permeate (s), and A is the membrane area (m^2). Solute flux, J_s, was obtained as follows:

$$J_s = C_p J_v \quad (4\text{-}3)$$

Membrane intrinsic parameters such as water permeability, L_p, and solute permeability, P, can be calculated using RO performance. The water permeability, L_p, was calculated using equation 4:

$$J_v = L_p (\Delta p - \Delta \pi) \quad (4\text{-}4)$$

where Δp and $\Delta \pi$ are the differences in applied pressure and osmotic pressure, respectively.

The osmotic pressure was calculated using equation 5: $\pi = \phi C_s R T$ (4-5)

where ϕ is the osmotic coefficient known as the van't Hoff equation. For dilute neutral solutions such as EtOH, IPA and glucose, ϕ was assumed to be unity. Meanwhile, for NaCl, ϕ is equal to 1.8 due to the ion pairing concept [23, 24]. C_s is the molar concentration of solutes, R is the gas constant and T is the absolute temperature. The solute permeability, P, through the membrane was calculated using equation 6:

$$J_s = P (C_f - C_p) \quad (4\text{-}6)$$

where $(C_f - C_p)$ is the concentration difference between the feed and the permeate.

The effect of concentration polarization was rationally ignored in this study due to the low permeate flux. The feed solution was vigorously agitated using a magnetic stirrer at 600 rpm to minimize the effect of concentration polarization [19, 25, 26]. Each of the feed and permeate solutions were sampled at a predetermined time interval for at least 5 hours to confirm a steady flux and rejection. Each of the experimental data points reported in this manuscript is the average value of 3 samples. The experimental error in water flux and observed rejection during each measurement was less than 5 and 1%, respectively.

4.3.Results and Discussion

4.3.1. BTESE RO Membranes

The molecular weight cut-offs (MWCOs) of BTESE membranes were determined using neutral solutes, as shown in Figure 4-1 (a) and (b). B-3 and B-240 denote BTESE membranes prepared at H_2O/BTESE molar ratios of 3 and 240, respectively. As shown, L_p was approximately the same for all types of solutes because of low feed concentration. Rejection for all neutral solutes was increased with an increase in the molecular weight of the solutes. The molecular size was based on the Stokes diameters of EtOH, IPA and glucose and were reported to be 0.39, 0.48 and 0.76 nm [20], respectively, which confirmed that the separation mechanism was primarily the molecular sieving. The MWCOs were determined as a molecular weight, the rejection of which was 90%. The MWCO for the B-3 membrane was approximately 160 g/mol, while the MWCO for the B-240 membrane was smaller than 50 g/mol, which was due to the smaller pore size. The rejection curves, or molecular weight cut-off (MWCO) curves, can also be reflected by the effective pore size of a membrane, which can be controlled by varying the BTESE/H_2O molar ratio.

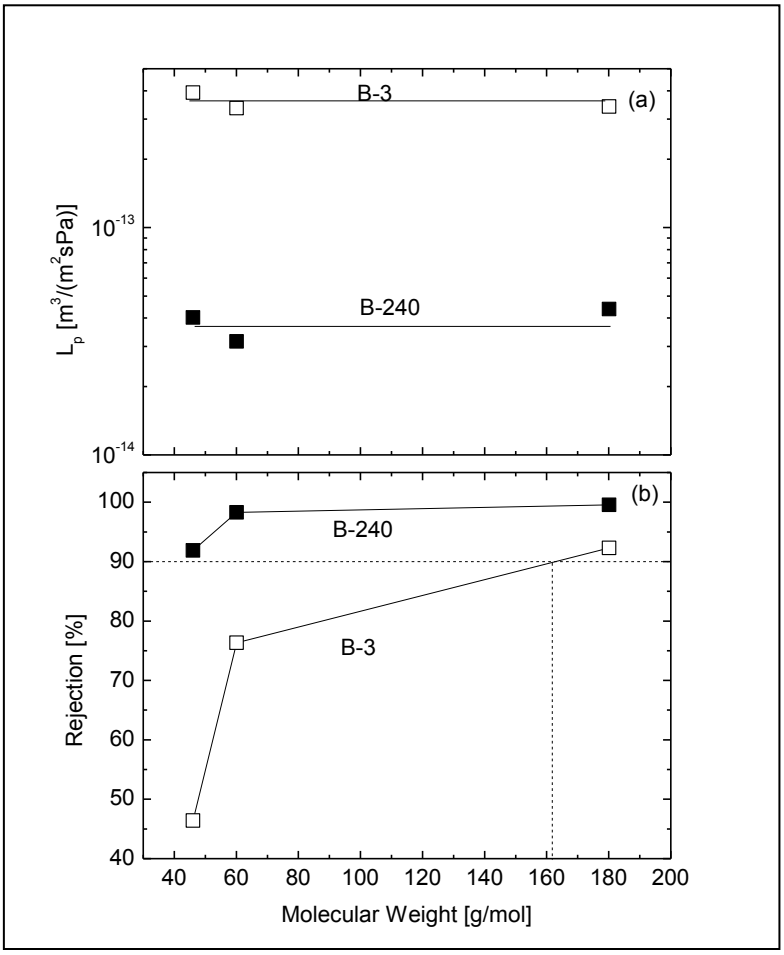

Figure 4-1 (a) Water permeability, L_p, and (b) rejection neutral solutes, $R_{\text{neutral solutes}}$, as a function of the molecular weight were measured at 1 MPa, 25 °C

In order to estimate the pore size of the membrane, a hindered transport model by Deen [27-29] was applied. According to Deen et al. [27-29], a sieving effect occurs within the nanopores, particularly when molecules are transported via diffusion in the nanopores. In this study, we used the rejection values of ethanol (EtOH), isopropanol (IPA) and glucose measured at 1 MPa and 25 °C. Pore size was best fitted to the Deen model as a function of the Stokes diameter of the solutes. Based on this model, the effective pore size for these membranes was estimated to be 0.53 nm for B-240 and 0.85 nm for B-3, as shown in Figure 4-2 (a). Obviously, increasing the BTESE/H_2O molar ratio can stimulate the formation of a network of smaller pores in a BTESE membrane due to a higher degree of cross-linking [19, 30] as shown in Figure 4-2 (b). When the BTESE/H_2O molar ratio increases, large numbers of BTESE ethoxide groups are fully hydrolyzed, and the density of silanol groups increases. Hence, Si-OH groups are condensed either with another silanol group or with an unreacted ethoxide group to form siloxane bonds [30]. The same phenomenon was presented and confirmed by all the characterizations including that from Fourier transform infrared spectroscopy (FTIR), Thermogravimetry - Mass Spectrometry (TG MASS), and Positron annihilation spectroscopy (PALS), all of which were basically similar to those in a previously published paper [17, 30].

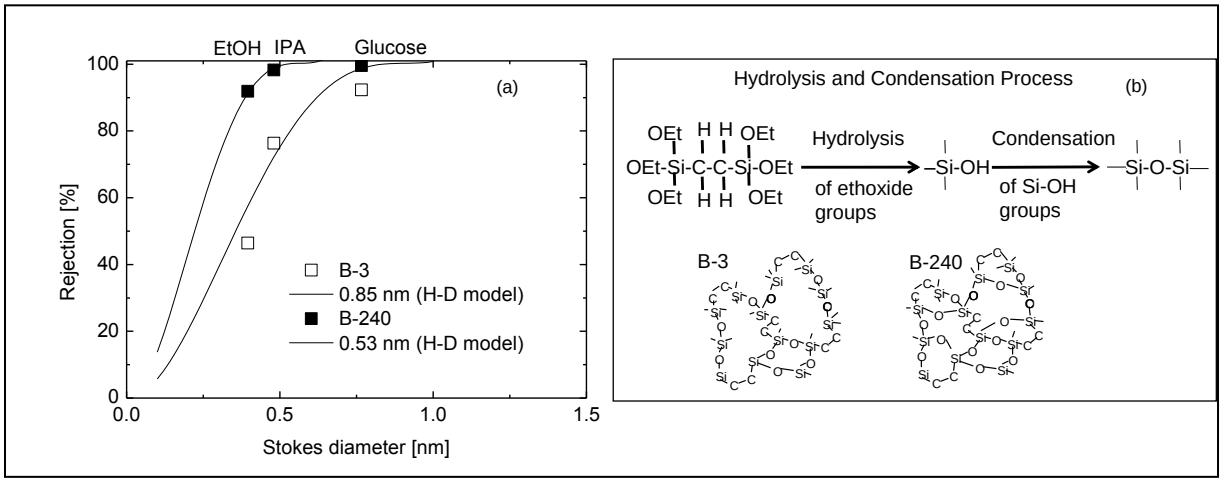

Figure 4-2 (a) Rejection of neutral solutes, $R_{\text{neutral solutes}}$ measured at 1 MPa, 25 °C, as a function of the Stokes diameter (curves in the figure are calculated using best-fitted pore sizes (0.85 nm (B-3) and 0.53 nm (B-240) to the Deen model); and (b) Schematic images of the pore networks of B-3 and B-240 of the BTESE membranes.

4.3.2. Pressure dependency of the BTESE reverse osmosis membranes

B-3 and B-240 membranes were used in order to study the effect of pressure on the permeation properties of alcohols and NaCl solutions, as shown in Figure 4-3. The rejection of NaCl for both membranes increased with increasing operating pressure. The increased

rejection with increased operating pressure is a typical tendency of polymeric reverse osmosis membranes [18]. As expected, rejection was higher for the tighter membrane, B-240. The rejection of the solutes for both membranes occurred in the following sequence order: NaCl>IPA>EtOH. J_v for all the solutions for both membranes increased proportionately with applied pressure, while the water permeability, L_p, remained constant. This can be explained according to Equation (4-4) as the (Δp-$\Delta \pi$) was the driving force for the water transport across the membrane, and, hence, J_v increased linearly while L_p remained constant. Generally, the state of water molecules is unclear if they are permeating through a pore size that is less than 1 nm in diameter. If the water evaporates at the inlet of the pores and permeates as a vapor through a nanoporous membrane, the permeability is dependent on the vapor pressure of the water and not on the applied pressure. In this case, however, the constant L_p indicates that Δp is the single driving force for water permeation through BTESE membranes, confirming that water permeated through BTESE membranes in the liquid state.

Again, the B-240 membrane showed a lower J_v than that of the B-3 membrane due to the smaller pore sizes, as mentioned in section (4.3.1). The high J_v of the alcohol solutions compared with that of the electrolyte solution—irrespective of the same L_p—was due to the differences in their osmotic pressure values (equation (4-4)). Meanwhile, the solute permeabilities, P, were almost constant with pressure at 25 °C, as obtained by equations (4-3), (4-4) and (4-6). Therefore, the permeation of water and solutes could be described by equations (4-4) and (4-6), which showed a similarity with the principles of the solution-diffusion (SD) model [31]. According to equation (4-6), the driving force for solute permeation, P, is dependent on differences in the concentration gradient and not on the operating pressure. Thus, NaCl exhibited the lowest solute permeability, which was consistent with its high rate of rejection. $R_{solutes}$ and J_v increased with an increase in the applied pressure, which was also observed in our previous studies on titania [19], triazine [18] and silica zirconia [20] and also MFI zeolite membranes [13-16,23]. The rejection behavior of the solutes in NF and RO is sometimes caused by both the charge effect and the sieving effect. If the charge effect plays a major role, an increase in the ion concentrations should result in a significant drop in salt rejection, which is often observed for many NF membranes. In our previous studies [25], the NaCl permeability, P_{NaCl}, remained approximately constant, which indicates that the influence of the charge effect between ions and the pores of a silica network has only a minor effect on the electrolyte rejection through BTESE membranes. This is evidence that the transport mechanism for this membrane is based on molecular sieving.

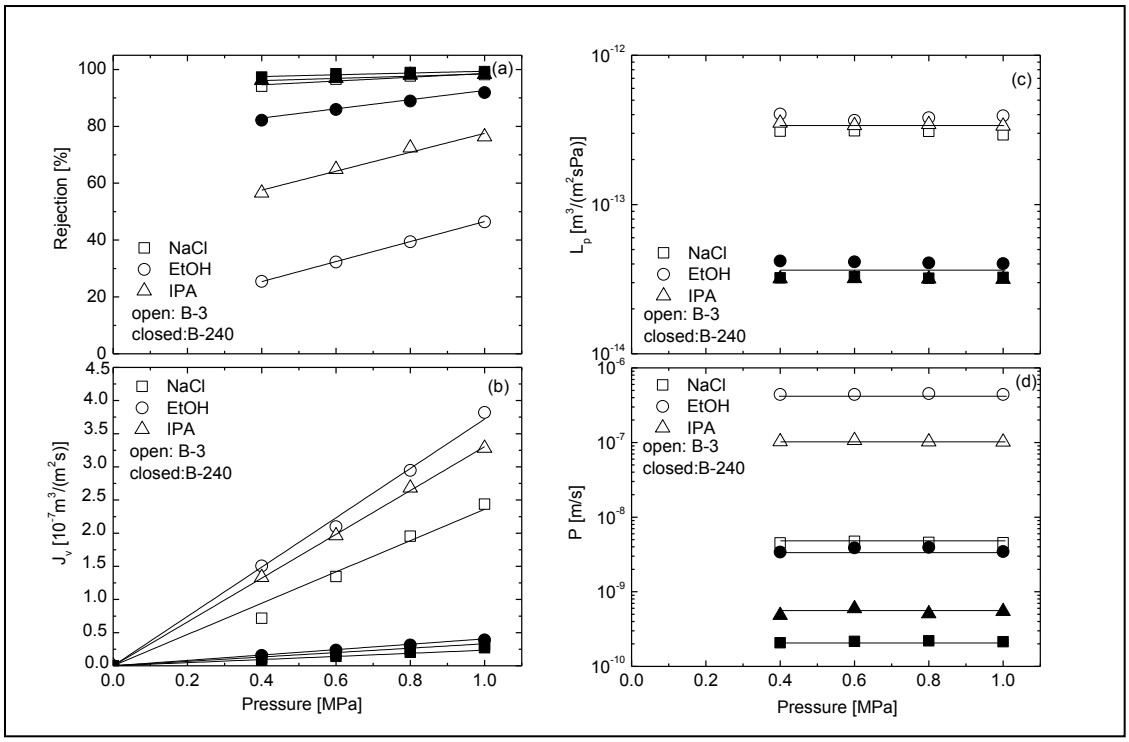

Figure 4-3 (a) Rejection, R, (b) water flux, J_v, (c) water permeability, L_p, and (d) solute permeability, P, as a function of pressure for RO experiments at 25 °C with 2,000 ppm NaCl, and 500 ppm EtOH and IPA.

4.3.3. Temperature dependency of the BTESE reverse osmosis membranes

The influence of the temperature-induced RO performance of BTESE membranes is shown in Figure 4-4. It should be noted that in Figure 4-4 (a), the rejection of alcohols decreased with increasing temperature, while NaCl showed a slightly increased rejection. Decreases in rejection for polymeric RO membranes were attributed mostly to an enlargement in the pore size due to thermal expansion at high-temperatures [12, 32-34]. However, in the present study an increase in pore size was not considered to be one of the reasons for the decreased rejection of alcohols, since the BTESE membranes were organic/inorganic hybrids prepared by firing at 300 °C, which makes them more thermally stable than polymeric membranes. In addition, the R_{NaCl} was constant, or even increased, which confirmed that the pore sizes of these membranes were not influenced by the thermal expansion in the present operating temperature range. A similar trend was observed in our previous studies [18-20].

It is well accepted that the interaction between solutes and membranes plays an important role in determining the temperature dependency of rejection. As shown in Figure 4-4 (b). 4b to 4d, the J_v, L_p and P for both membranes increased as the operating temperature increased from 25 to 80 °C, which is characteristic of an activated process. It is noteworthy that L_p for both membranes increased approximately 10-fold without diminishing the rejection value of

NaCl (R_{NaCl}). As the operating temperature increased from 25 to 80 °C, L_p and R_{NaCl} values of the B-3 membrane increased from 2 x 10^{-13} to 2 x 10^{-12} $m^3/(m^2 s Pa)$ and from 98.1 to 98.1%, respectively. Likewise, the L_p and R_{NaCl} for B-240 membrane increased from 3 x 10^{-14} to 2 x 10^{-13} $m^3/(m^2 s Pa)$ and 99.2 to 99.4%, respectively. It should be noted that the performance of the B-3 membrane at operating conditions of 1 MPa and 80 °C approximated that of the L_p and R_{NaCl} of a commercially polyamide RO membrane, SW30HR, (FilmTec) at an operating temperature of 25 °C with L_p and R_{NaCl} values of around 2.2 x 10^{-12} $m^3/(m^2 s Pa)$ and 98.5%, respectively [35] which confirmed the robustness of the hybrid organic/inorganic membrane when used in a high-temperature RO desalination process or to purify and reuse high-temperature production water.

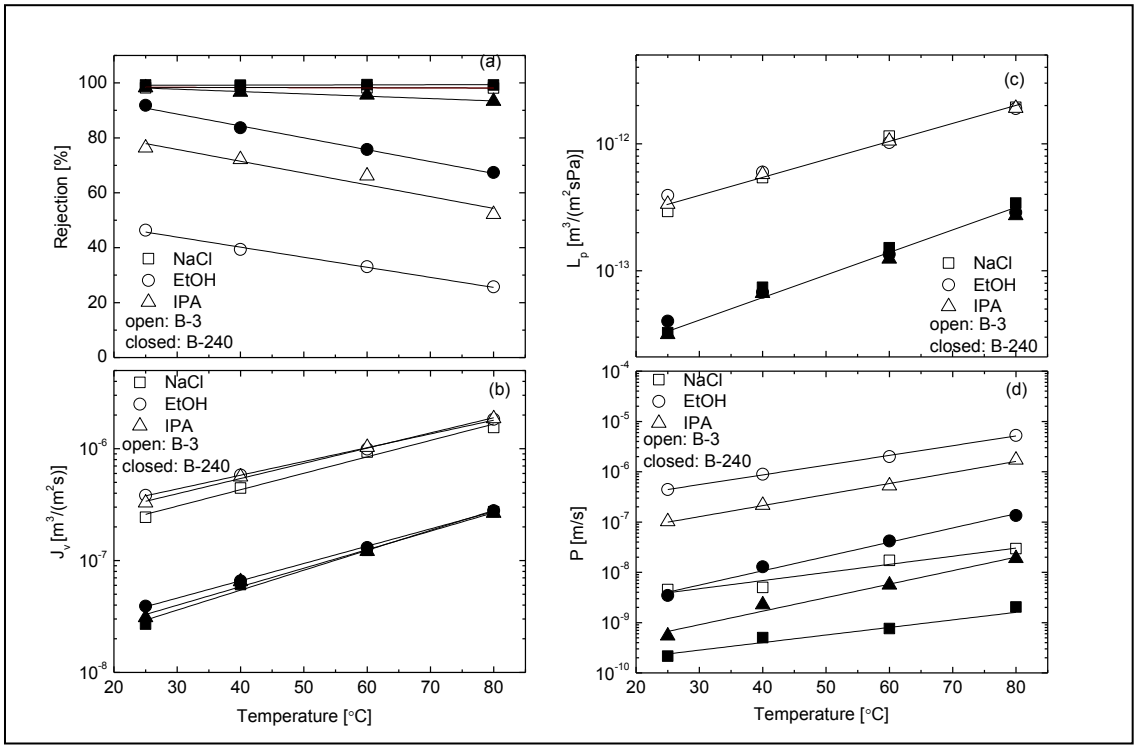

Figure 4-4 (a) Rejection, $R_{solutes}$, (b) water flux, J_v, (c) water permeability, L_p, and (d) solute permeability, P, as a function of temperature at 1 MPa, 500 ppm EtOH, IPA and 2,000 ppm NaCl.

4.3.4. Effect of temperature on the transport mechanism and activation energies of electrolyte and alcohol solutions

Figure 4-5 shows the relationship between (a) viscosity-corrected water permeability, $L_p\mu$, and (b) solute permeabilities, P, as a function of temperature for both membranes. In order to determine the transport of a solvent (water) through the BTESE membrane, the Hagen-Poiseuille [26] (equation 7) value was conventionally employed to theoretically

estimate the water permeability through porous membranes.

$$L_p\mu = \frac{{r_p}^2 A_k}{8\Delta x} = \text{constant} \quad (7)$$

where r_p is the effective pore size, Δx is the effective membrane thickness, A_k is the porosity, and μ is the viscosity of the solution in the pores.

When the transport mechanism obeys the viscous flow mechanism, $L_p\mu$ should be constant irrespective of the permeation temperature and the types of solutions. As shown in Fig. 5a, the values for the $L_p\mu$ of both BTESE membranes were not constant and clearly increased with temperature, which confirmed that the transport mechanism through BTESE membranes deviates from the viscous flow mechanism. This is consistent with previous reports on the permeation mechanism of both aqueous [19] and nonaqueous solutions [20, 36, 37] via nanoporous membranes at high temperature. This is because the viscosity of water in small pores shows a temperature dependence that differs from that in bulk [26].

In terms of surface chemistry, Cohen-Tanugi and Grossman [38] reported that from their simulation study, OH-groups could hydrogen-bond with water and offer water molecules to traverse, thus allowing faster overall water flow. In fact, in our previous studies [18, 22], we also calculated the electrostatic potentials (ESPs), using a Gaussian09 program, which is related to the electron density distribution where negative potential represents electron rich-polar groups, and vice versa, for positive potentials. For BTESE, the ESPs showed that the negative potentials were mainly localized near oxygen atoms [22]. Indirectly, it provides additional evidence that the interaction between the membrane surface and the permeating molecules is thought to be responsible for the difference in the temperature dependence compared with that in the bulk.

$L_p\mu$ values (Figure 4-5 (a)) for the B-3 membrane that are larger than those for the B-240 membrane can be fully explained due to the larger pore size, which should continuously accommodate the transport of a greater volume of water molecules and solutes through the membrane. On the other hand, a smaller pore size should exert a strong blocking effect that would inhibit water molecules and solutes from entering the membrane pores and would lower both the L_p and $L_p\mu$. The solute permeabilities, P, (Figure 4-5 (b)) for three different solutes also increased with temperature, which is characteristic of an activated process and can be explained as an increase in diffusion coupled with a decrease in viscosity. This is consistent with previous reports regarding the temperature dependence of electrolytes [19, 34, 39] and neutral solutes [19, 26, 32, 33, 40]. They have remarkably different permeances and sensitivities to temperature.

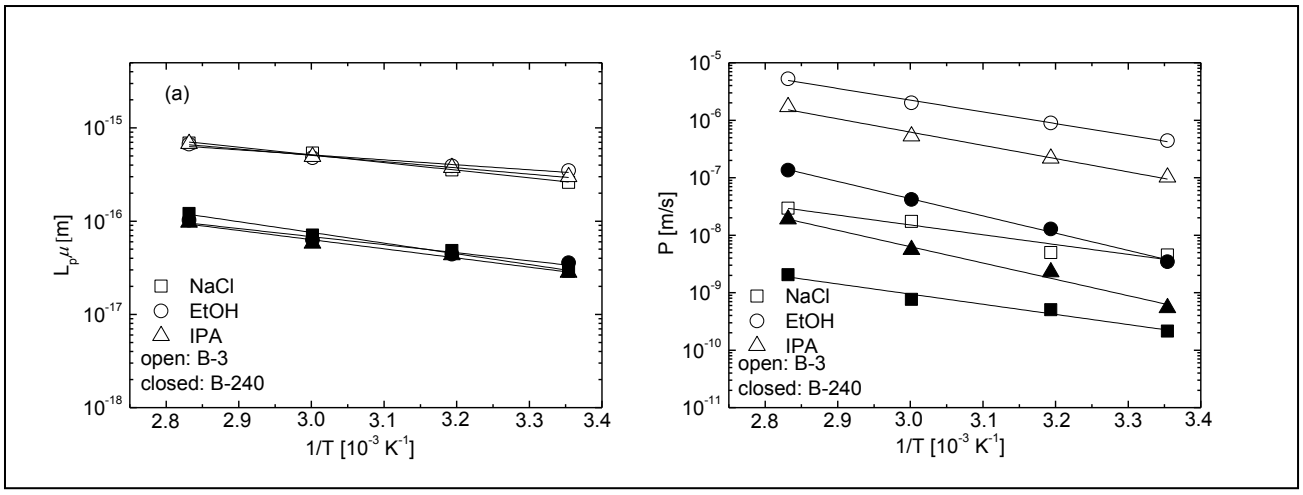

Figure 4-5 (a) Viscosity-corrected water permeability, $L_p\mu$, and (b) Solute permeabilities, P, as a function of temperature at 1 MPa, 500 ppm EtOH, IPA and 2,000 ppm NaCl.

The linearity of $L_p\mu$ and P in Figure 4-5 (a) and (b) reveals a linear relationship with reciprocal temperature that validates the applicability of the Arrhenius relationship. As summarized in Table 4-1, the observed values for $\Delta E(L_p)$ and $\Delta E(L_p\mu)$ were larger for membranes with smaller MWCOs and pore sizes. The $\Delta E(L_p)$ and $\Delta E(L_p\mu)$ terms describe the interaction between permeating water molecules and the membrane pores. These interactions are formed and then broken during the process whereby water makes permeation "jumps" through the pore of the membrane. Since the average pore size of the B-240 membrane was smaller than that of the B-3 membrane, water molecules were expected to exert stronger friction against the pore walls of the B-240 membrane than against those of the B-3 membrane. As the temperature increased, a greater number of water molecules with sufficient energy can break through the energy barrier to be transported through the membrane micropores, which leads to an increased L_p and $L_p\mu$ with temperature. In addition to the interpretation based on the activation energy above, the temperature dependency could be explained as follows. The thickness of adsorbed water on the pore wall decreases as temperature increases, which creates larger spaces for water molecules to permeate. Moreover, the viscosity of the water in these nanoporous networks might be higher than that of the bulk solution [26].

The observed $\Delta E(P)$ for the B-3 membrane ranged from 32 to 44 kJ /mol and from 34 to 57 kJ /mol for the B-240 membrane. For both membranes, the energies increased on the order $\Delta E(P_{NaCl}) < \Delta E(P_{alcohols})$. Although NaCl exhibited a smaller ΔE value, it has a higher rejection compared with other solutes for both membranes. The values for ΔE of NaCl permeation through both membranes ranged from 32 to 34 kJ /mol, which was much smaller than the hydration energy values of 371 and 374 kJ /mol that was reported for Na^+ and Cl^- ions, respectively [41]. The very large hydration energies of Na^+ and Cl^- ions meant that a

large amount of energy was needed to remove the water molecules from the hydration shells of the Na^+ and Cl^- ions, thus lowering, or making less favorable, the permeation of Na^+ and Cl^- ions as a hydrated sphere. In general, ions permeate confined channels in either a hydrated, dehydrated or partially hydrated state. The crystal ($d_{crystal}$) and hydrated ($d_{hydrated}$) diameters are for Na^+ ion ($d_{crystal\ Na^+}$ = 0.19 nm and $d_{hydrated\ Na^+}$ = 0.71 nm) and Cl^- ion ($d_{crystal\ Cl^-}$ = 0.36 nm and $d_{hydrated\ Cl^-}$ = 0.66 nm) [41, 42], respectively. Based on MWCOs and NaCl rejection (Figure 4-1 (b) and Figure 4-3 (a)), almost 99.9% of glucose and NaCl was rejected by the B-240 membrane, whereas the B-3 membrane rejected only 92% of the glucose and 98% of the NaCl. Hence, it is reasonable to suggest that the size of the hydrated sphere of NaCl is at least similar to and possible larger than 0.76 nm, which is the Stokes diameter of glucose. NaCl permeated through only a limited number of large pores for both membranes, thus exhibiting a lower ΔE value due to a weak interaction between the ions and the membrane pore wall. On the other hand, we assumed EtOH and IPA would permeate through pore sizes that were smaller than their own Stokes diameters (Stokes diameter for EtOH = 0.39 nm and IPA = 0.48 nm, respectively) hence contributing larger ΔE values for both membranes (Please refer ESI-2; Fig. S2). In our previous paper [43], we reported that the activation energies of He and H_2 were below 10 kJ/mol for BTESE membranes with variations in water ratio (6, 120 and 240). This was due to the smaller kinetic diameter and lighter weight; hence, these gases easily diffused through the pore network. On the other hand, the activation energy for water depends on the viscosity of water. It should be noted that even macroporous membranes such as microfiltration (MF) and ultrafiltration (UF) follow the viscous flow, and the activation energy of water permeation is 15 kJ/mol.

Table 4-1 Summary of the pore sizes and activation energies of L_p, $L_p\mu$, and P for B-3 and B-240 membranes

	Membranes	
	B-3	B-240
MWCO	160	<50
Average pore size, H-D model (nm)	0.85	0.53
ΔE (L_p) (kJ/mol)[a]	30.3	36.6
ΔE ($L_p\mu$) (kJ/mol)[b]	15.7	22.0
ΔE (P_{NaCl}) (kJ/mol)[c]	32	34
ΔE (P_{EtOH}) (kJ/mol)[c]	39	57
ΔE (P_{IPA}) (kJ/mol)[c]	44	54

[a] Activation energies ΔE (L_p) were calculated using $L_p=(L_p)_o\exp(-\Delta E(L_p)/RT)$

[b] Activation energies ΔE ($L_p\mu$) were calculated using viscosity in bulk $L_p\mu=(L_p\mu)_o\exp(-\Delta E(L_p\mu)/RT)$

[c] Activation energies ΔE (P_{solute}) (solute = NaCl, EtOH and IPA) were obtained using $P_{solute}=(P_{solute})_o \exp(-\Delta E(P_{solute})/RT)$

Note (1): The experimental error in activation energies of water and solutes during each measurement was less than 5%.

Note (2): The activation energies of viscous flow were calculated based on the temperature dependence of the water viscosity, μ, in the bulk assuming a constant $L_p\mu$; ΔE (L_p)=15.4 and ΔE ($L_p\mu$)=0 kJ/mol.

Hence, in order to distinguish the mechanisms governing the transport between NaCl and alcohols through the BTESE membrane in terms of diffusivity, two of the main transport parameters (P and L_p) from our experimental analysis, were plotted as normalized P/L_p over an operating temperature at 1 MPa, as shown in Figure 4-6. P can be expressed as the effective diffusivity of solutes divided by the membrane thickness, as shown by equation 4-8 [19]:

$$P = \frac{D_m A_k}{\Delta x_m} \tag{4-8}$$

where D_m is the diffusivity, A_k is the surface porosity, and Δx_m is the membrane thickness. According to the Wilke-Chang equation [20] shown below, the diffusivity, D_{bulk}, of the dilute concentration of a solute in liquid is expressed as the inverse of the solvent viscosity in equation 4-9:

$$D_{bulk} = 7.4 \times 10^{-12} \frac{(\varphi M_B)^{1/2} T}{\mu_B V_A^{0.6}} \tag{4-9}$$

where φ is the association factor of a solvent (2.6 for water), M_B is the molecular weight of a solvent B (kg/mol), T is the absolute temperature in K, μ_B is the solvent viscosity in (Pa s), and V_A is the molar volume of solute A in (m^3/mol) at its normal boiling temperature. Under the assumption that the diffusivity inside the nanopores shows a dependency on viscosity that is similar to that in bulk, then by dividing the solute permeability, P, by the water permeability, L_p (equation 4-7), it is possible to discuss the temperature dependence of the solute permeability in nanosized pores by eliminating the effect of the viscosity of the solvents. As shown in Figure 4-6, $P/L_{p(alcohols)}$ increased by a larger rate, indicating that the solute flux increased with temperature more rapidly than it did with water flux, compared with $P/L_{p(NaCl)}$. Indirectly, this supports a decrease in the rejection of EtOH and IPA when temperatures and rejection values are high for NaCl. Water permeability increased faster than the diffusion of NaCl, leading to a $(P/L_p)/(P/L_p)_{25°C}$ that was either ≅1 or <1. The normalized value for the P/L_p of NaCl solutes was either approximately 1 or less than 1, which indicates that NaCl permeability in membrane pores was increased with an increase in temperature in the same manner as with the inverse of water viscosity in membrane pores. This suggests that there was no activated process in the NaCl diffusion through either of these BTESE membranes.

Rejection, therefore, was independent of permeation temperatures or could possibly have even increased due to the activated permeation of water. On the other hand, the normalized P/L_p of EtOH and IPA solutes increased with temperature for both membranes, indicating that permeability of EtOH and IPA increased with temperature more rapidly than the inverse of viscosity through the membranes, hence exhibiting a molecular sieving mechanism.

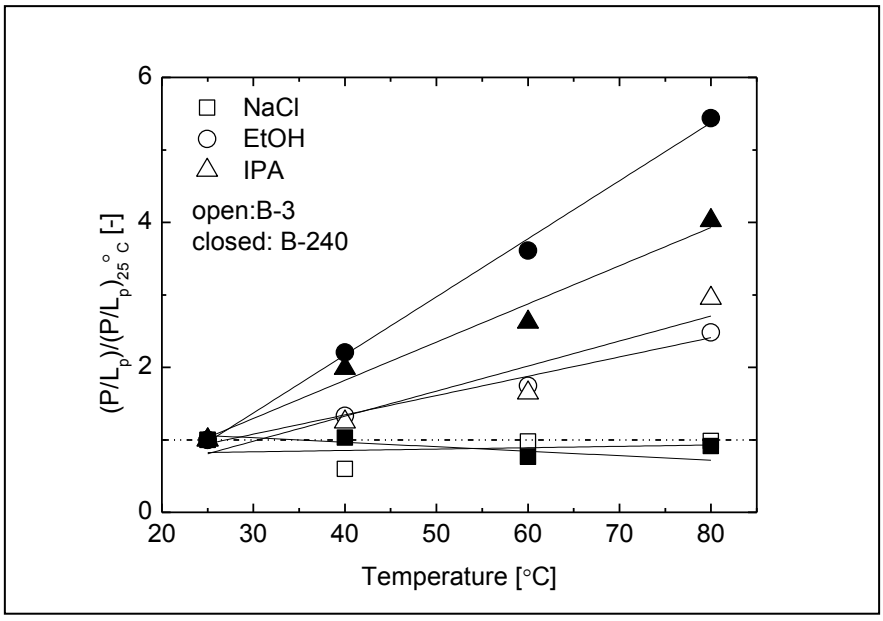

Figure 4-6 Normalized P/L_p as a function of temperature at 1 MPa, 500 ppm EtOH, IPA and 2,000 ppm NaCl.

4.3.5. Thermal stability and regeneration of BTESE reverse osmosis membranes

Figure 4-7 demonstrates the stability of the B-3 membrane at temperatures that were elevated from 25 to 80 °C at 1 MPa with 2,000 ppm NaCl. No flux decrease was observed. It should be noted that the water permeabilities for the B-3 membrane were more than 1 x 10^{-12} $m^3/(m^2$ s Pa) and showed an excellent salt rejection of >98% at 60 and 80 °C. The water permeabilities increased as the operating temperature increased. It was noteworthy that the rejection remained unchanged for as long as 50 hours at temperatures as high as 80 °C. When the feed temperature was decreased gradually back to the starting temperature (25 °C), the water permeability returned to approximately the initial value, while the rejection remained the same. These results also show that no alteration of the effective pore diameters and structures had occurred.

The excellent hydrothermal stability can be attributed to the main body of the BTESE structure that consists of chemically strong bonds such as Si-C and Si-O-Si. This contrasts with other silica membranes. According to Yazawa et al. [44], after reflux for 48 hours in water, a porous glass membrane (pure silica) showed about 60% of SiO_2 elution by dissolving

into water. It is clear that the porous glass (pure silica) membranes used in that study exhibited no thermal stability in aqueous solutions. Another study [45] found that a pure silica membrane with ordered pores was tested for desalination via membrane distillation at an operating temperature of 60 °C for 30 minutes. The water flux dropped approximately 50% after 30 minutes and salt rejection decreased from 96.4 to 70.3%. The decrease in rejection was ascribed to the hydrophilic surface of the pure silica membrane while the drop in flux was probably because of the build-up of salt within the membrane pores due to pore wetting and subsequent evaporation [44].

However, only a limited number of papers have reported on the hydrothermal stability of zeolite during RO. Li et al. [13] found that for a 0.1 M NaCl solution, a silicalite membrane showed transient (time dependent) water flux and Na^+ rejections at 2.07 MPa, 25 °C. After a RO time of 50 h, the water flux and Na^+ rejections were stabilized at 0.112 kg/m^2 h and 76.7%. By incorporating aluminum ions into the zeolite framework, both water flux and ion rejection was increased from 0.112 to 1.129 kg/ m^2 h and from 90.6 to 92.9%, respectively [14]. Another recent study on MFI membranes reported desalination performance of the prepared silicalite membrane of a seawater solution (0.3 wt% TDS (total dissolved solids)) for as long as 180 days at a constant pressure of 700 kPa and at various temperatures. The prepared silicalite membrane achieved a high rate of rejection (>93%) for all major seawater ions, including Na^+ (except for K^+, 83%) at an applied pressure of 700 kPa and at room temperature (22 °C), but showed a continuous decrease in ion rejection when the temperature was increased from 22 to 90 °C. However, the permeation flux was significantly increased with an increase in temperature [15]. Therefore, these results suggest that BTESE membranes can provide a unique solution for hot water desalination. In addition, these membranes provide a feasible way to improve water flux by increasing the operating temperature with no drop in salt rejection.

Another challenge was to demonstrate the possibility for the regeneration of a BTESE membrane after its use under conditions of temperature-variation (25-80 °C) in a hot-water desalination RO experiment with alcohols and electrolytes. A B-3 membrane was chosen for thermal stability and regeneration study since B-3 membranes have shown a higher water permeability than the B-240 and a similar R_{NaCl}. Following the regeneration process, the regenerated membrane was used for the gas permeation experiment at a permeation temperature of 200 °C using He, H_2, N_2, CH_4, and SF_6 (Please refer ESI-3 Fig.S3). Fig. 8a shows the gas permeation performance for the B-3 membrane just after membrane fabrication (before the RO experiment) and after the regeneration process. These results show that the gas performances before the RO experiment and after the regeneration process were approximately the same. In order to verify the robust properties, we also conducted a RO experiment with the B-3 membrane using neutral solutes at 1 MPa and 25 °C and a NaCl solution at 1 MPa and 25 and 80 °C, as shown in Fig. 8b. The L_p and $R_{\text{neutral solutes}}$ for the B-3

membrane before RO and after the regeneration process were confirmed to be approximately the same, which showed that the MWCOs for B-3 membranes before RO and after the regeneration process remained unchanged at approximately 160. The capability to regenerate the membrane would depend on the decomposition of foulants such as proteins in order to prevent biofouling. Generally speaking, based on all the experimentation such as the hydrothermal stability studies, regeneration studies, and chlorine-resistant testing [17], we concluded that the robust properties of BTESE membranes make them a good choice for innovative water desalination.

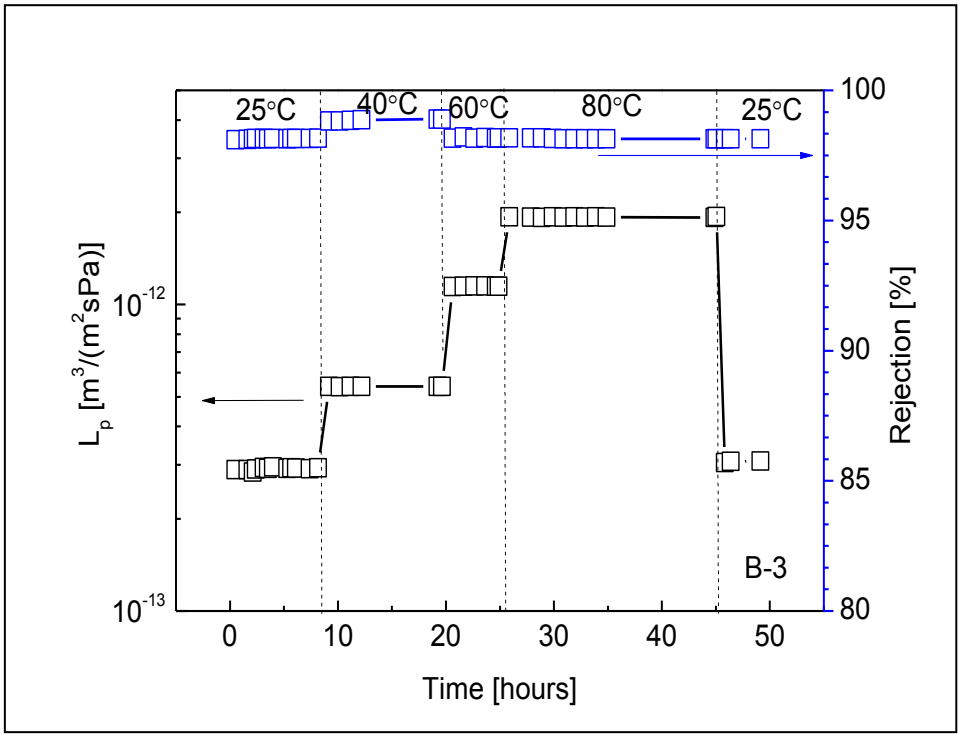

Figure 4-7 Salt rejection, *R*, and water permeability, L_p, for a B-3 membrane as a function of temperature and time at 1 MPa and 2,000 ppm NaCl.

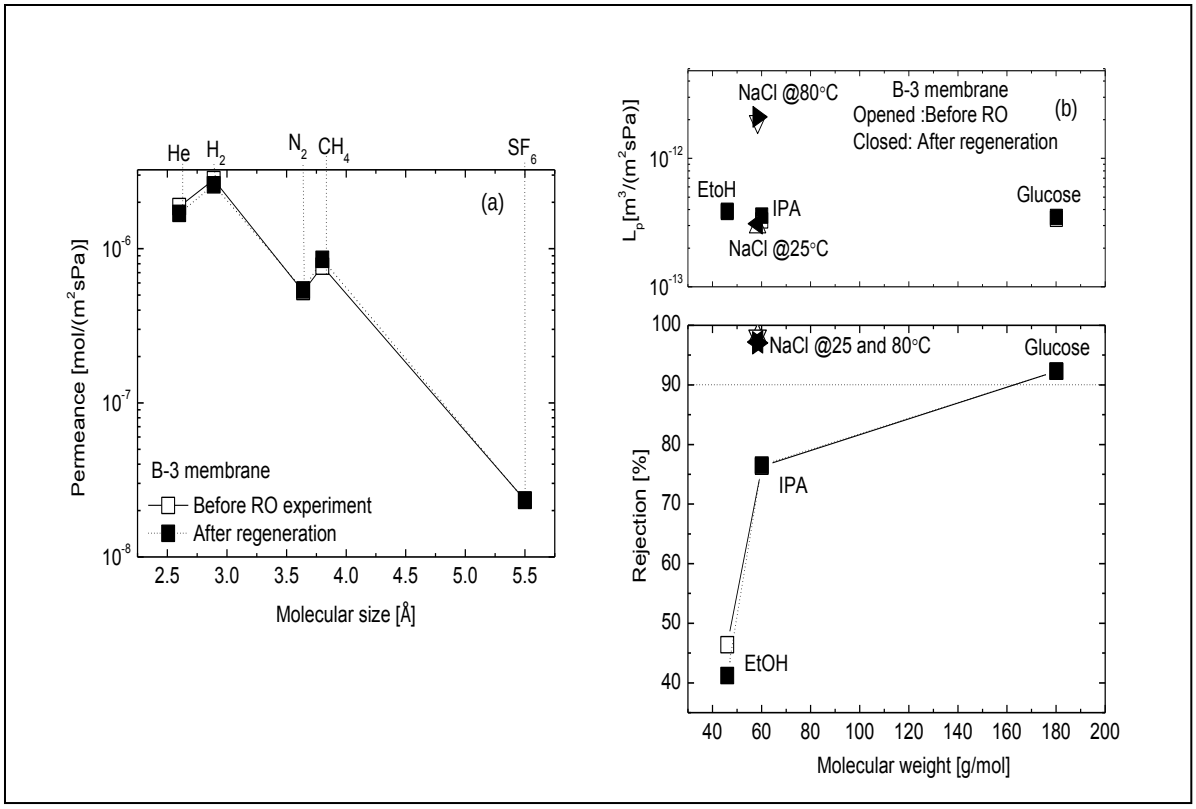

Figure 4-8 (a) Gas permeation properties at a permeation temperature of 200 °C as a function of molecular size and (b) Water permeability, L_p, and rejection, R, as a function of the molecular weights of 500 ppm neutral solutes (EtOH, IPA and Glucose) and 2,000 ppm NaCl at 1 MPa and 25 and 80 °C for B-3 membranes calcined at 300 °C

4.4.Conclusions

In the present study, we demonstrated that as the BTESE/H_2O molar ratio was increased from 3 to 240, the pore sizes decreased from 0.85 to 0.53 nm. Both membranes exhibited high degrees of water flux and rejection for both alcohols and an electrolyte with an increase in the applied pressure. As the operating temperature increased from 25 to 80 °C, L_p and R_{NaCl} values of B-3 membrane increased from 2 x 10^{-13} to 2 x 10^{-12} $m^3/(m^2$ s Pa) and from 98.1 to 98.1%, respectively. Likewise, the L_p and R_{NaCl} for a B-240 membrane increased from 3 x 10^{-14} to 2 x 10^{-13} $m^3/(m^2$ s Pa) and 99.2 to 99.4%, respectively. The transport mechanisms for water and alcohols were predominantly influenced by activated diffusion. In the case of NaCl, which showed the highest rejection, we concluded that only a limited number of large pores were available for NaCl permeation. As compared with other silica membranes such as pure silica and zeolites, BTESE membrane also showed a thermal stability in a hot desalination experiment with improved water flux by increasing the operating temperature with no drop in salt rejection, as well as exhibiting the capability to be regenerated after being used in a hot desalination experiment.

References

[1] R.M. de Vos and H. Verweij, Improved performance of silica membranes for gas separation, J. Membr. Sci. 143 (1998) 37-51.

[2] H.L. Castricum, A. Sah, R. Kreiter, D.H.A. Blank, J.F. Ventec and J.E. ten Elshof, Hydrothermally stable molecular separation membranes from organically linked silica, J. Mater. Chem. 18 (2008) 2150–2158.

[3] I. Agirre, P.L. Arias, H.L. Castricum, M. Creatore, J.E. ten Elshof, G.G. Paradis, P.H.T. Ngamou, H.M. van Veen, J.F. Vente, Hybrid organosilica membranes and processes: Status and outlook, Sep. Purif. Technol. 121 (2014) 2–12.

[4] M. Asaeda, J. Yang, Y. Sakou, Porous silica–zirconia (50%) membranes for pervaporation of iso-propyl alcohol (IPA)/water mixtures, J. Chem. Eng. Jpn. 35 (2002) 365-371.

[5] H. Imai, H. Morimoto, A. Tominaga, H. Hirashima, Structural Changes in Sol-Gel Derived SiO_2 and TiO_2 Films by Exposure to Water Vapor, J. Sol–Gel Sci. Technol. 10 (1997) 45-54.

[6] M.T.M. Pendergast and E.M.V. Hoek, A review of water treatment membrane nanotechnologies, Energy Environ. Sci. 4 (2011) 1946-1971.

[7] J.H.M. Snow, D.D. Winter, R. Buckingham, J. Campbell, J. Wagner, New techniques for extreme conditions: high temperature reverse osmosis and nanofiltration, Desalination 105 (1996) 57–61.

[8] M. Manttari, A. Pihlajamaki, E. Kaipainen, M. Nystrom, Effect of temperature and membrane pre-treatment by pressure on the filtration properties of nanofiltration membranes, Desalination 145 (2002) 81–86.

[9] D. Li, H. Wang, Recent developments in reverse osmosis desalination membranes. J. Mater.Chem. 20 (2010) 4551–4566.

[10] H.B. Park, B.D. Freeman, Z.B. Zhang, M. Sankir, J.E. McGrath, Highly chlorine-tolerant polymers for desalination, Angew. Chem. Int. Ed. 47 (2008) 6019–6024.

[11] R.J. Petersen, Composite reverse osmosis and nanofiltration membranes, J. Membr. Sci. 83 (1993) 81–150.

[12] M.H. Liu, S.C. Yu, J. Tao and C.J. Gao, Preparation, structure characteristics and separation properties of thin-film composite polyamide-urethane seawater reverse osmosis membrane, J. Membr. Sci. 325 (2008) 947–956.

[13] L. Li, J. Dong, T.M. Nenoff, R. Lee, Desalination by reverse osmosis using MFI zeolite membranes, J. Membr. Sci. 243 (2004) 401–404.

[14] L. Li, N. Liu, B. McPherson, R. Lee, Enhanced Water Permeation of Reverse Osmosis through MFI-Type Zeolite Membranes with High Aluminum Contents, Ind. Eng. Chem. Res. 46 (2007) 1584-1589.

[15] B. Zhu, Z. Hong, N. Milne, C.M. Doherty, L. Zou, Y.S. Lin, A.J. Hill, X. Gu, M. Duke,

Desalination of seawater ion complexes by MFI-type zeolite membranes: Temperature and long term stability, J. Membr. Sci. 453 (2014) 126–135.

[16] M. Kazemimoghadam, T. Mohammadi, Synthesis of MFI zeolite membranes for water desalination, Desalination 206 (2007) 547–553.

[17] R. Xu, J. Wang, M. Kanezashi, T. Yoshioka, T. Tsuru, Development of robust organosilica membranes for reverse osmosis, Langmuir 27 (2011) 13996–13999.

[18] S.M. Ibrahim, R. Xu, H. Nagasawa, A. Naka, J. Ohshita, T. Yoshioka, M. Kanezashi, T. Tsuru, Insight into the pore tuning of triazine-based nitrogen-rich organoalkoxysilane membranes for use in water desalination, RSC Adv. 4 (2014) 23759-23769.

[19] T. Tsuru, K. Ogawa, M. Kanezashi, T. Yoshioka, Permeation characteristics of electrolytes and neutral solutes through titania nanofiltration membranes at high temperatures, Langmuir 26 (2010) 10897–10905.

[20] T. Tsuru, M. Miyawaki, T. Yoshioka, M. Asaeda, Reverse osmosis of nonaqueous solutions through porous silica-zirconia membranes, AIChE J. 52 (2006) 522-531.

[21] R. Xu, M. Kanezashi, T. Yoshioka, O. Tetsuji, O. Joji, T. Tsuru, Tailoring the affinity of organosilica membranes by introducing polarizable ethenylene bridges and aqueous ozone modification, ACS Appl. Mater. Interfaces. 5 (2013) 6147-6154.

[22] R. Xu, M.I. Suhaina, M. Kanezashi, T. Yoshioka, I. Kenji, O. Joji, T. Tsuru, New insights into the microstructure-separation properties of organosilica membranes with ethane, ethylene and acetylene bridges, ACS Appl. Mater. Interfaces. 6 (2014) 9357-9364.

[23] B. Zhu, J.H. Kim, Y.H. Na, I.S. Moon, G. Connor, S. Maeda, G. Morris, S. Gray and M. Duke, Temperature and Pressure Effects of Desalination Using a MFI-Type Zeolite Membrane, Membranes 3 (2013) 155-168.

[24] Osmosis equation: http://www.chemteam.info/Solutions/Osmosis-Equation.html

[25] R. Xu, J. Wang, M. Kanezashi, T. Yoshioka, T. Tsuru, Reverse osmosis performance of organosilica membranes and comparison with the pervaporation and gas permeation properties, AIChE J. 59 (2013) 1298–1307.

[26] T. Tsuru, S. Izumi, T. Yoshioka, M. Asaeda, Temperature effect on transport performance by inorganic nanofiltration membranes. AIChE J. 46 (2000) 565–574.

[27] W.M. Deen, Hindered transport of large molecules in liquid-filled pores, AIChE J. 33 (1987) 1409–1425.

[28] P. Dechadilok and W.M. Deen, Hindrance Factors for Diffusion and Convection in Pores, Ind. Eng. Chem. Res. 45 (2006) 6953-6959.

[29] H. Jongyoon, F. Jianping, B.S. Reto, Molecular sieving using nanofilters: Past, present and future, Lab Chip. 1 (2008) 23–33.

[30] T. Niimi, H. Nagasawa, M. Kanezashi, T. Yoshioka, K. Ito, T. Tsuru, Preparation of BTESE-derived organosilica membranes for catalytic membrane reactors of

methylcyclohexane dehydrogenation. J. Membr. Sci. 455 (2014) 375–383.
[31] J.G. Wijmans, R.W. Baker, The solution-diffusion model: A review, J Membr. Sci. 107 (1995) 1–21.
[32] R.R. Sharma, R. Agrawal, S. Chellam, Temperature effects on sieving characteristics of thin-film composite nanofiltration membranes: pore size distributions and transport parameters, J. Membr. Sci. 223 (2003) 69–87
[33] N. Ben Amar, H. Saidani, A. Deratani, J. Palmeri, Effect of Temperature on the Transport of Water and Neutral Solutes across Nanofiltration Membranes, Langmuir 23 (2007) 2937–2952.
[34] L.A. Richards, B.S. Richards, B. Corry, A.I. Schäfer, Experimental Energy Barriers to Anions Transporting through Nanofiltration Membranes, Environ. Sci. Technol. 47 (2013) 1968−1976.
[35] E.S. Hatakeyama, C.J. Gabriel, B.R.Wiesenauer, J.L. Lohr, M.J. Zhou, R.D. Noble, D.L. Gin, Water filtration performance of a lyotropic liquid crystal polymer membrane with uniform, sub-1-nm pores, J. Membr. Sci. 366 (2011) 62–72.
[36] T. Tsuru, T. Sudoh, S. Kawahara, T. Yoshioka, M. Asaeda, Nanofiltration in non-aqueous solutions by porous silica–zirconia membranes, J. Membr. Sci. 185 (2001) 253-261
[37] T. Tsuru, H. Kondo, T. Yoshioka, and M. Asaeda, Permeation of Nonaqueous Solution through Organic/Inorganic Hybrid Nanoporous Membranes, AIChE J. 50 (2004) 1080-1087.
[38] D. Cohen-Tanugi and J.C. Grossman, Water Desalination across Nanoporous Graphene, Nano Lett. 12 (2012) 3602−3608.
[39] R.R. Sharma, S. Chellam, Temperature and concentration effects on electrolyte transport across porous thin-film composite nanofiltration membranes: Pore transport mechanisms and energetics of permeation, J. Colloid Interface Sci. 298 (2006) 327–340.
[40] R.R. Sharma, S. Chellam, Temperature Effects on the Morphology of Porous Thin Film Composite Nanofiltration Membranes, Environ. Sci. Technol. 39 (2005) 5022–5030.
[41] I.S. Joung, T.E. Cheatham, Determination of Alkali and Halide Monovalent Ion Parameters for Use in Explicitly Solvated Biomolecular Simulations, J. Phys. Chem. B 112 (2008) 9020–9041.
[42] E.R. Nightingale Jr., Phenomenological theory of ion solvation. Effective radii of hydrated ions, J.Phys.Chem. 63 (1959) 1381–1387.
[43] H. Nagasawa, T. Niimi, M. Kanezashi, T. Yoshioka, and T. Tsuru. Modified Gas-Translation Model for Prediction of Gas Permeation Through Microporous Organosilica Membranes. AIChE J. 60 (2014) 4199- 4210.
[44] T. Yazawa, H. Tanaka, H. Nakamichi, T. Yokoyama, Preparation of water and alkali durable porous glass membrane coated on porous alumina tubing by sol gel method. J.

Membr. Sci. 60 (1991) 307-317.
[45] Y.T. Chua, C.X.C. Lin, F. Kleitz, X.S. Zhao, S. Smart, Nanoporous organosilica membrane for water desalination, Chem. Commun. 49 (2013) 4534-4536.

Chapter 5

Favorable of BTESE membranes for gas and reverse osmosis (RO) applications: Effect of preparation conditions on the structural and the correlation between gas and liquid permeation properties

5.1. Introduction

Nowadays, molecular separation by inorganic membranes is widely considered as an energy-efficient alternative for conventional industrial separation techniques [1]. They received a great deal of attention owing to their versatile characteristics such as high thermal stability that can be operated at elevated temperatures, with many ceramic membranes usable over 1000 ºC. They are also much more resistant to chemical attack such as corrosive liquids and gases [2]. In many of the harsh operational environments listed above, organic membranes will not perform well, or will not survive at all. For these environments, only inorganic membranes offer needed solutions.

Generally molecular separation via inorganic membranes is based on their pore size either by molecular sieving or on the basis of affinity. In particular, amorphous silica based membranes are attractive candidates for gas separation and water desalination due to the advantages of their tunable pore sizes and morphology thereby offering higher selectivity and solutes rejection. Hence, increasing interest in inorganic membranes has led to an expanded knowledge base of fabrication technology, with the result that membranes have been designed with larger throughput, improved selectivity and longer stability. Several methods have been reported for the preparation of inorganic membranes via sol–gel [3-5] and chemical vapor deposition [6, 7].

For the preparation of such membranes (pore sizes < 1 nm) sol-gel technology [8] is highly suitable. The main reactions of the sol–gel process are the hydrolysis and polycondensation of silicon alkoxides that result in a crosslinked silica network [8]. This method allows us to prepare materials with morphological characteristics as mentioned above by varying the type and amount of the precursor and solvent used [9-11], concentration of water [3-5, 9, 10, 12] and acid [10, 12, 13] added in the synthesis. To date, organically bridged silica membranes that consist of an amorphous network with both organic Si–C_n–Si bridges and inorganic Si–O–Si bonds have attracted a considerable amount of recent attention because of their high performance in a variety of applications. In our previous study, we had proven that the

strategy by changing water ratio (WR) to design pore network of BTESE membrane in gas separation application was succeeded [4, 14] where BTESE membranes achieved methylcyclohexane (MCH) conversion ~75 % with a hydrogen purity in the permeate stream of more than 99.9 % at 230 °C [4] and exhibited a superior performance in gas separation applications such as a very high H_2 permeance with high H_2-to-SF_6 selectivity [14]. We also demonstrated that a bis(triethoxysilyl)ethane (BTESE) membrane could withstand temperatures as high as 90 °C in desalination applications with no obvious changes in filtration performance with excellent chlorine resistance during reverse osmosis (RO) [15]. However, the influence of WR on these BTESE membranes in RO applications has not yet been studied. In addition, a high separation performance of molecular sieving membrane needs to be coupled with a good mechanical structure membranes as to achieve sufficient lifetime of the membrane coatings on the support as their functionalities can be lost if the coated membrane is deteriorated due to wear or environmental degradation. In many cases, the good morphology and mechanical integrity of the membranes can be designed by applying different types of thermal treatment or firing environments. However, there are limited studies reported on the effect of thermal treatment or firing environments during membrane preparation.

Hence, in the present study, the morphology, structural properties and separation performance of BTESE membranes in gas and reverse osmosis (RO) applications were investigated with respect to WR and different firing environments. Furthermore, we tried to correlate the relationship between gas and water permeance as well permeance ratio of gases with the rejection of solute.

5.2. Experimental

5.2.1. Preparation of BTESE-derived sols

Bis(triethoxysilyl)ethane (BTESE) as a organosilica precursor was homogeneously dissolved in an ethanol (EtOH) solution. A mixture of water (H_2O) and hydrochloric acid (HCl) were then added dropwise to the solution under vigorous stirring, resulting in a final solution with molar ratios of BTESE/H_2O/HCl = 1/x/0.2 (x=3 and 240). The concentration of BTESE was kept at 5 wt% by adjusting the amount of EtOH added into the solutions. Then, the solution was kept in a closed system under continuous stirring at 25 °C for 6 h to allow the formation of silica sols.

5.2.2. Preparation of BTESE-derived membranes

For membrane preparation, the same procedure was reported in our previous studies [15, 16]. Porous α-alumina tubes (porosity: 50%, average pore size: 1 μm, outside diameter: 10

mm) were used as the supports for BTESE-derived silica membranes. At first, α-alumina particles (average particle diameter: 1.9 μm) were coated onto the outer surface of a porous support using a silica-zirconia colloidal sol as the binder. Then the support was fired at 550 °C for 30 min to smooth the surface. After that, the membrane were coated with α-alumina particles (average particle diameter: 0.2 μm) with the same firing condition. These procedures were repeated several times to cover large pores that might have resulted in pinholes in the final membrane. Then, a SiO_2–ZrO_2 (Si/Zr = 1/1) solution (diluted to about 0.5 wt%) was coated onto the substrate to form an intermediate layer with pore sizes of several nm, followed by firing at 550 °C for approximately 30 min [15, 16]. Finally, the BTESE-derived organosilica layer was fabricated by the coating of a BTESE solution, followed by drying and firing at 300 °C in air or N_2 for 30 mins.

5.2.3. Characterization of BTESE thin films and powders

Fourier transform infrared (FTIR) spectroscopy was performed for the samples prepared by coating the sols onto a Si wafer (thickness: 280 μm), followed by drying at 100 °C under air and firing at 300 °C in air or N_2 environments. The same thin films were used for contact angle measurement using Kyowa instrument. The microstructures and surface properties of the organosilica networks were studied by nitrogen (77 K) and water sorption (298 K), respectively, using a Belsorp-Max (Bel-Japan, Inc) instrument. Before analysis, the samples were outgassed at 200 °C overnight under vacuum.

5.2.4. Performance Evaluation

5.2.4.1. Gas separation

Figure 5-1 shows a schematic diagram of the experimental apparatus for the single-gas permeation measurement. Gas permeation tests were performed at 200 °C using single components of He, N_2, and SF_6. The permeate stream was maintained at atmospheric pressure, and the pressure drop through the membranes was maintained at 1 bar. Prior to the measurement, all membranes were outgassed in a He flow of 50 mL min^{-1} at 200°C for 8 to 12 h to remove any water that had possibly adsorbed on the membranes.

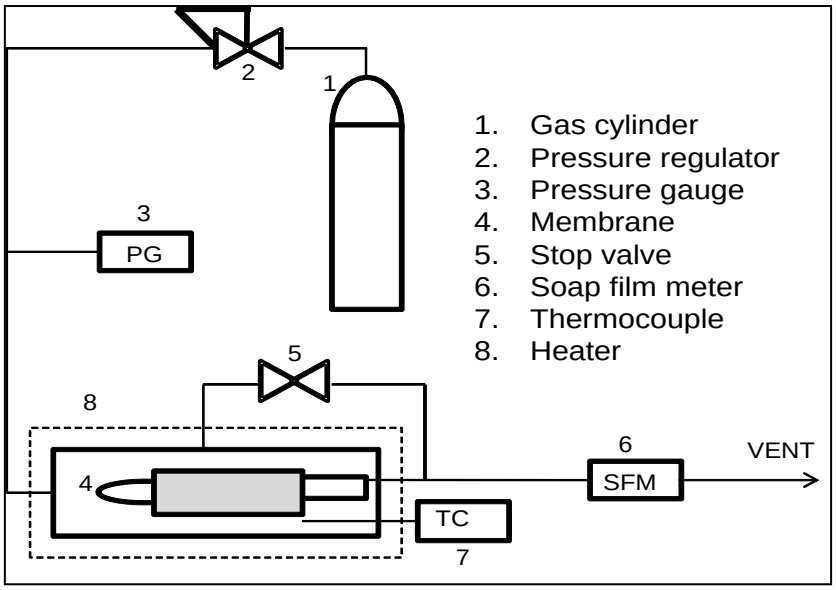

Figure 5-1 Schematic diagram of the experimental apparatus for single gas permeation measurement

5.2.4.2. Reverse osmosis

The RO experiment was conducted in a cross-flow filtration system, as shown in Figure 5-2. The feed solution was pressurized with a plunger pump at a pressure difference of 1 MPa. The feed solution was vigorously agitated using a magnetic stirrer at 600 rpm to minimize the effect of concentration polarization [19-21]. The water bath was maintained at a temperature of 25 °C unless otherwise specified. The retentate was recycled back to the feed container, and the permeate stream was maintained at an atmospheric pressure and collected using a peristaltic tube pump. The permeate was then transported, at ambient pressure, to a sample-collecting vial via silicone tubing. The concentrations of feed solutions were 2000 ppm (0.2 %) of sodium chloride (NaCl) and 500 ppm (0.05 %) of ethanol (EtOH), isopropanol (IPA), and glucose. The concentrations of feed and permeate were measured using a conductivity meter (HORIBA, ES-51) for NaCl and a total organic carbon analyzer (Shimadzu, TOC-VE) for neutral solutes.

By using experimental data, membrane performances such as solutes rejection, $R_{solutes}$, water flux, J_v, and solute flux, J_s, were calculated directly. Solutes rejection, $R_{solutes}$, was expressed as follows:

$$R_{solutes}\,(\%) = (1-C_p/C_f) \times 100 \qquad (5\text{-}1)$$

where C_p and C_f are the concentration of permeate and feed, respectively. Meanwhile the water flux, J_v was calculated as follows:

$$J_v = W_p/\rho_p tA \qquad (5\text{-}2)$$

where W_p is the mass of the permeate solutions (kg), ρ_p is the density of the permeate (kg/m^3),

t is the time for collecting the permeate (s), and A is the membrane area (m^2).

Membrane intrinsic parameters such as water permeability, L_p, can be calculated using RO performance equations. The water permeability, L_p, was calculated using equation 5-3:

$$J_v = L_p (\Delta p - \Delta \pi) \quad (5\text{-}3)$$

where Δp and $\Delta \pi$ are the differences in applied pressure and osmotic pressure, respectively.

The osmotic pressure was calculated using equation 5-4:

$$\pi = \phi C_s R T \quad (5\text{-}4)$$

where ϕ is the osmotic coefficient known as van't Hoff equation. For dilute neutral solutions such as EtOH, IPA and glucose, ϕ was assumed to be unity. Meanwhile, for NaCl, ϕ is equal to 1.8 due to ion pairing concept [17, 18]. C_s is the molar concentration of solutes, R is the gas constant and T is the absolute temperature.

The effect of concentration polarization was rationally ignored in this study due to the low permeate flux. Each feed and permeate solutions were sampled at a predetermined time interval for at least 5 hours to confirm a steady flux and rejection. Each experimental data points reported in this manuscript was the average value of 3 samplings.

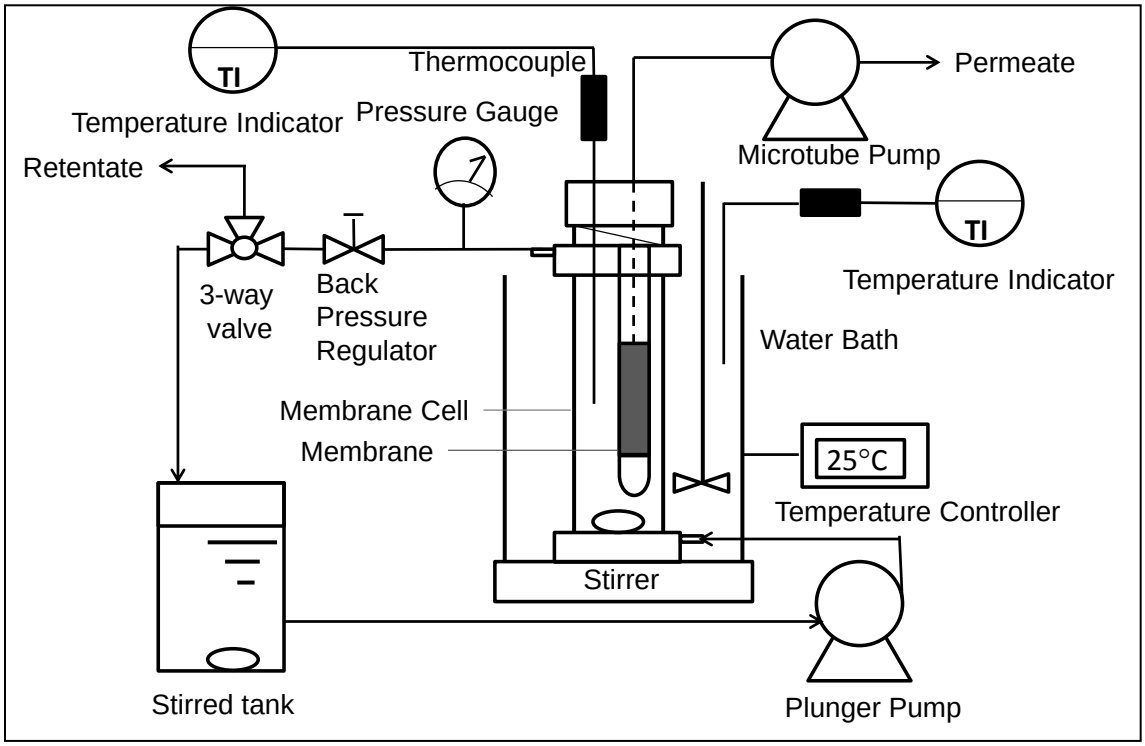

Figure 5-2 Schematic diagram of the experimental apparatus for reverse osmosis measurement.

5.3. Results and discussions

5.3.1. Characterization of BTESE films and powders

5.3.1.1. FTIR analysis

Figure 5-3 shows the FTIR spectras of thin films coated with BTESE sols of different WR and fired at 300 °C in air and N_2. All samples show typical pure BTESE infrared spectrum, with the main Si-O bonding band which can be assigned at about 1070 cm^{-1} due to the asymmetric stretching of symetric strecthing of the oxygen atoms [22]. Absorption at 950 and 3750 cm^{-1} can be assigned to the silanol bonds (Si-OH), while at 3000-4000 cm^{-1} can be assigned to the OH strecthing and adsorbed water [23]. Meanwhile the peaks at 2974 and 2929 cm^{-1} were attributed to the -CH_3- groups from the ethoxide groups and to the –CH_2- groups from the Si-$(CH_2)_2$-Si bonds [24, 25]. As can be seen, major peaks of organic bonds such as -CH_3, -CH_2, -CH and Si-C for samples fired in N_2 environment were more intense as compared with the samples fired in air environment. Hence, firing the films in the N_2 environment are shown to be more prominent way to slow down the decomposition of these organic bonds thus preserved higher rigid structures within the networks.

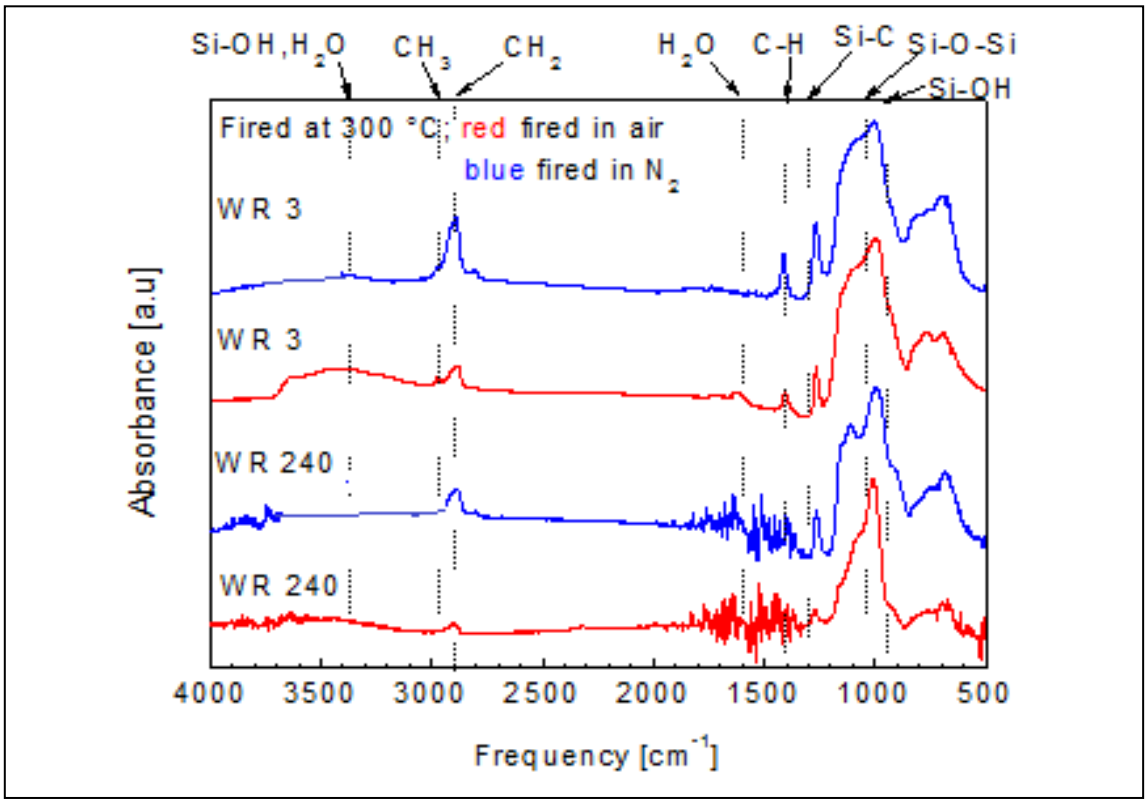

Figure 5-3 FTIR of BTESE-derived silica gel powder H_2O/BTESE molar ratio (WR) = (3 and 240) fired in air and N_2 at 300°C.

5.3.1.2. N_2 and H_2O adsorption

Figure 5-4 shows the N_2 adsorption-desorption isotherms of the BTESE-derived silica powders prepared at different WR and fired at 300 °C in different firing environments. N_2 adsorption-desorption isotherms for all samples exhibited Type I isotherm with a significant uptake of N_2 at low relative pressure which is normally characteristic of microporous materials. In addition, no hysteresis was observed, hence indicating the absence of the mesopores. Details of physochemical of these samples are summarized in Table 5-1. As can be seen, WR=240 samples fired in air and N_2 environment had a larger surface area and pore volume than the WR=3 samples. Obviously, this result explains that increasing the WR can stimulate high quantities of the formation of small pores network in a BTESE membrane hence increased the surface areas. In addition, it is proven that firing the powders in the N_2 environment can preserve higher rigidity of the network structures, which prevented the collapse of pores and the formation of dead-end pores during the firing process, thus creating a more open and accessible pore structure. The pore size for these membranes fired in both environments were estimated to be around 1 nm for WR 3 and 0.6 nm for WR 240, as shown in Table 5-1.

Figure 5-5 (a) and (b) show the water sorption isotherms of the all the samples measured at 298 K. As predicted the same trend of H_2O sorption was obtained for high WR samples due to its larger surface area. Adsorption at low pressure usually occurs by attractive forces of water vapor and pore wall, while adsorption at high pressure mainly depends on the pore structure such as capillary condensation. Hence, adsorption at low pressure is more reliable to compare the intrinsic affinity of water with BTESE powders. Figure 5-5 (b) shows the H_2O sorption capacities normalized by their specific surface area at low water vapor pressure up to 0.1 atm. A more rapid water- uptake was observed for samples fired in air environment compared with samples fired in N_2 environment. This indicates a stronger water affinity of the internal network of samples fired in air. The results were consistent with the contact angles of the thin films (Table 5-1), which also showed a higher surface hydrophilicity of the thin film BTESE fired in air.

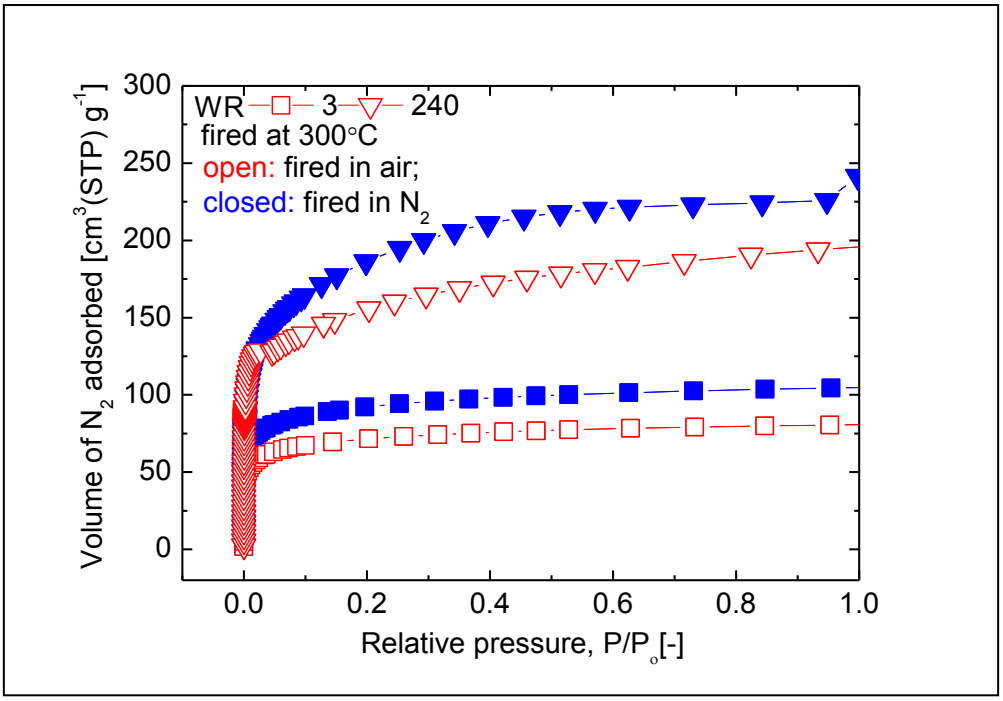

Figure 5-4 Nitrogen adsorption-desorption isotherms (77 K), for BTESE-derived silica gel powder H_2O/BTESE molar ratio (WR) = (3 and 240) fired at 300 °C in air and N_2

Table 5-1 Physicochemical Properties of BTESE films and powders

BTESE/H_2O and firing environments; fired at 300 °C	Contact Angle[a] [°]	Pore diameter[b], d_p [nm]	BET surface area[c], A_{BET} [m^2 g^{-1}]	Pore volume[d], V_p [cm^3 g^{-1}]	N_2 adsorbed, V_a N_2 [cm^3 (STP) g^{-1}]	H_2O adsorbed, V_a H_2O [cm^3 (STP) g^{-1}]
3-Air	45	1.1	~238	0.12	~81.1	~149
3-N_2	73	1.0	~322	0.16	~105.4	~153
240-Air	58	0.6	~533	0.30	~198.0	~465
240-N_2	83	0.6	~652	0.37	~241.5	~409

[a]Contact angle were evaluated by using thin film BTESE membrane coated on glass slide

[b] Pore size distribution was obtained through the analysis of the adsorption branch of nitrogen isotherms using the MP method

[c]Specific surface area was evaluated by using the Brunauer-Emmet-Teller (BET) method in the relative pressure range of P/P_0=0.01-0.25

[d]Pore volume was estimated using the t-plot method

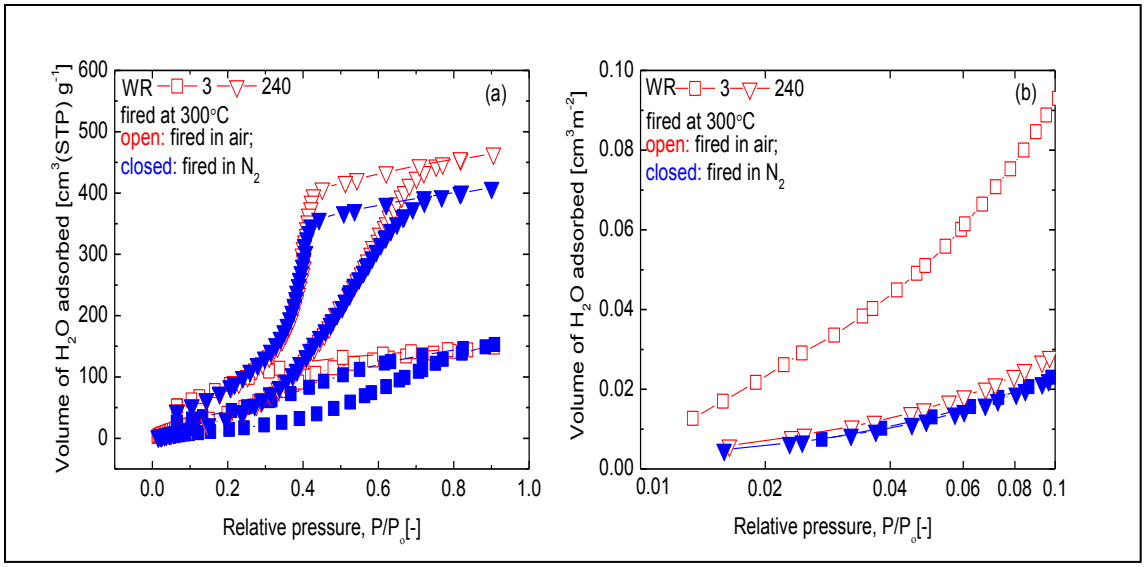

Figure 5-5 (a) Water sorption isotherms of samples (298 K) and (b) plot water sorption normalized by their specific surface area at low pressure for BTESE-derived silica gel powder H_2O/BTESE molar ratio (WR) = (3 and 240) fired at 300 °C in air and N_2

5.3.2. Performance of BTESE-derived silica membranes

5.3.2.1. Gas permeation characteristics of BTESE-derived membranes

Figure 5-6 (a) and (b) show the single gas permeance and the selectivity of BTESE membranes fired in air and N_2 environment as a function of WR. BTESE membranes fired in air environment and prepared with low WR sols showed a high permeance for all gases compared to those fired in N_2 environment. As mentioned earlier, by firing in air, some of the organic linking bonds and ethoxide groups were easily decomposed and removed via a template method compared to the sample fired in N_2 environment, thus making more loose pore networks. The permeances of gases were clearly dependent on WR, and types of permeating molecules. The permeance of He was only slightly affected by changing WR from 3 to 240 for both membranes fired in air and N_2. The permeance of He seems to be approximately constant around ~$1x10^{-6}$ and ~$9\ x10^{-7}$ mol m^{-2} s^{-1} Pa^{-1}, respectively. On the other hand, the effect of WR was more pronounced for larger gas molecules such as N_2 and SF_6 when WR increased from 60 to 240. The most significant decrease in permeance was observed for SF_6 molecule. The permeance of SF_6 for BTESE membranes fired in in air and N_2 was decreased from 2.34 x 10^{-8} to 8.06 x 10^{-11} and 2.25 x 10^{-9} to 1.21 x 10^{-10} mol m^{-2} s^{-1} Pa^{-1} when the WR increased from 3 to 240, respectively. As a result, the selectivity He/SF_6 was much large compared to selectivity He/N_2 as shown in Figure 5-6 (b). This is because larger WR induced high degree of condensation, followed by formation of silica-networks of smaller pore size, resulting in higher selectivities.

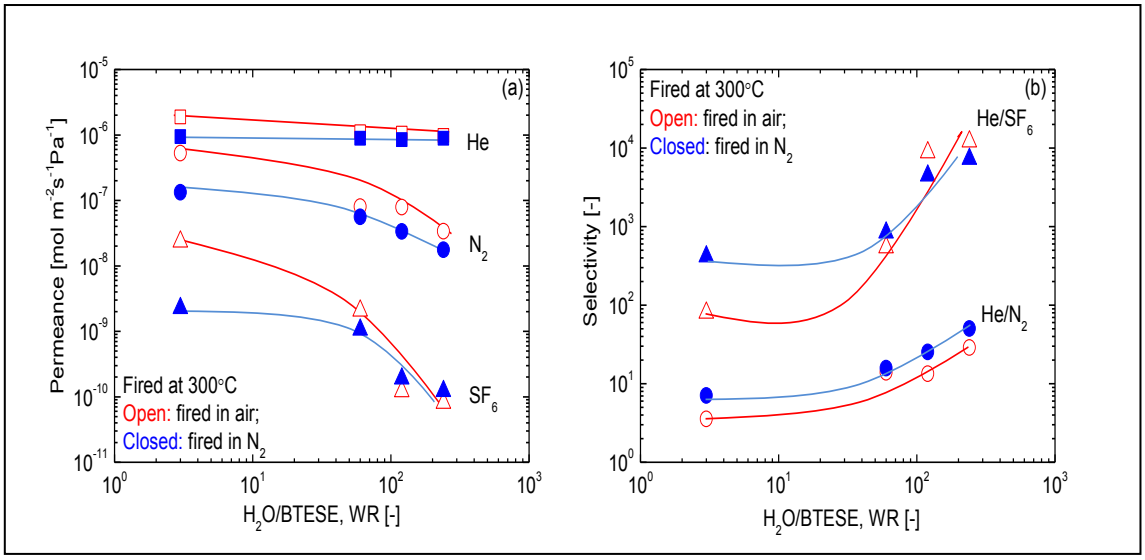

Figure 5-6 (a) Single gas permeances and the (b) selectivity of He/N_2 and He/SF_6 of BTESE-derived silica membranes fired at 300 °C in air and N_2 at a permeation temperature of 200 °C as function of H_2O/BTESE molar ratio (WR) = (3, 60, 120, 240)

5.3.2.2. RO characteristics of BTESE-derived membranes

The RO desalination performance was evaluated by using a 2000 ppm sodium chloride (NaCl) and 500 ppm neutral organic solutes (ethanol (EtOH) and propanol (IPA)) solutions at 1 MPa and 25 °C. The same membranes used for gas permeation experiment was used for reverse osmosis experiment. Figure 5-7 (a) to (d) show the water permeability, L_p and rejection, R of BTESE membranes fired in air and N_2 environment as a function of WR. As can be seen, L_p for WR 3 membrane fired in air environment showed a high water permeance (L_p~ 3.5×10^{-13} m^3 m^{-2} s^{-1} Pa^{-1}) compared to the WR 3 membranes fired in N_2 environment (L_p~0.7×10^{-13} m^3 m^{-2} s^{-1} Pa^{-1}). This can be explained as follows; as observed by gas permeation, BTESE membranes fired in air showed loose pore networks compared with those fired in N_2, so L_p increased. In addition, sample fired in air environment was more hydrophilic, thus producing a stronger water affinity on the surface and internal network of the samples fired in air due to removal of some organic bonds via template method. This result is in agreement with the water adsorption (Figure 5-5) and contact angle (Table 5-1). In particular, significant decrease in L_p for WR 3 membranes fired in N_2 environment is due to the existence of ethoxide groups that may have acted as "building blocks" between the silica pores, and occupied some space in the silica network, resulting a hydrophobic properties thus lowering the water permeance via the membrane pore networks. Similarly to gas permeances, L_p for all the membranes fired in both environments decreased with an increase in WR. On the other hand, WR 240 membranes fired in air and N_2 environments exhibited similar L_p values

around 2.5~3.5x10^{-14} m^3 m^{-2} s^{-1} Pa^{-1}. These results might suggest that, at higher WR, the pore sizes were more or less the same for both membranes.

In term of solutes rejection, it is acknowledged that the transport mechanism of water and solutes during RO is influenced by the molecular sieving, which is the same as that of single-gas permeation. Hence, a BTESE membrane must possess a pore size that falls between that of solutes and water in order to increase its suitability for molecular sieving. In addition, the rejection of the solutes in both firing environments occurred in the following sequence order: NaCl > IPA > EtOH. The hydrated sizes of $Na^{+}_{(aq)}$, $Cl^{-}_{(aq)}$, Stokes diameter of IPA and EtOH are 0.72, 0.66 0.48 and 0.39 nm, respectively [26]. The larger the molecular size, the rejection increased, confirming the primary separation mechanism is the molecular sieving. As can be seen the rejection for all solutes increased with an increase in the WR for membranes fired in both environments. The rejection of the solutes for all membranes fired in N_2 environment was slightly higher compared with membranes fired in air environment. This result supports the idea that firing in N_2 enviroment at the same WR can stimulate the formation of smaller pores network in a BTESE membrane.

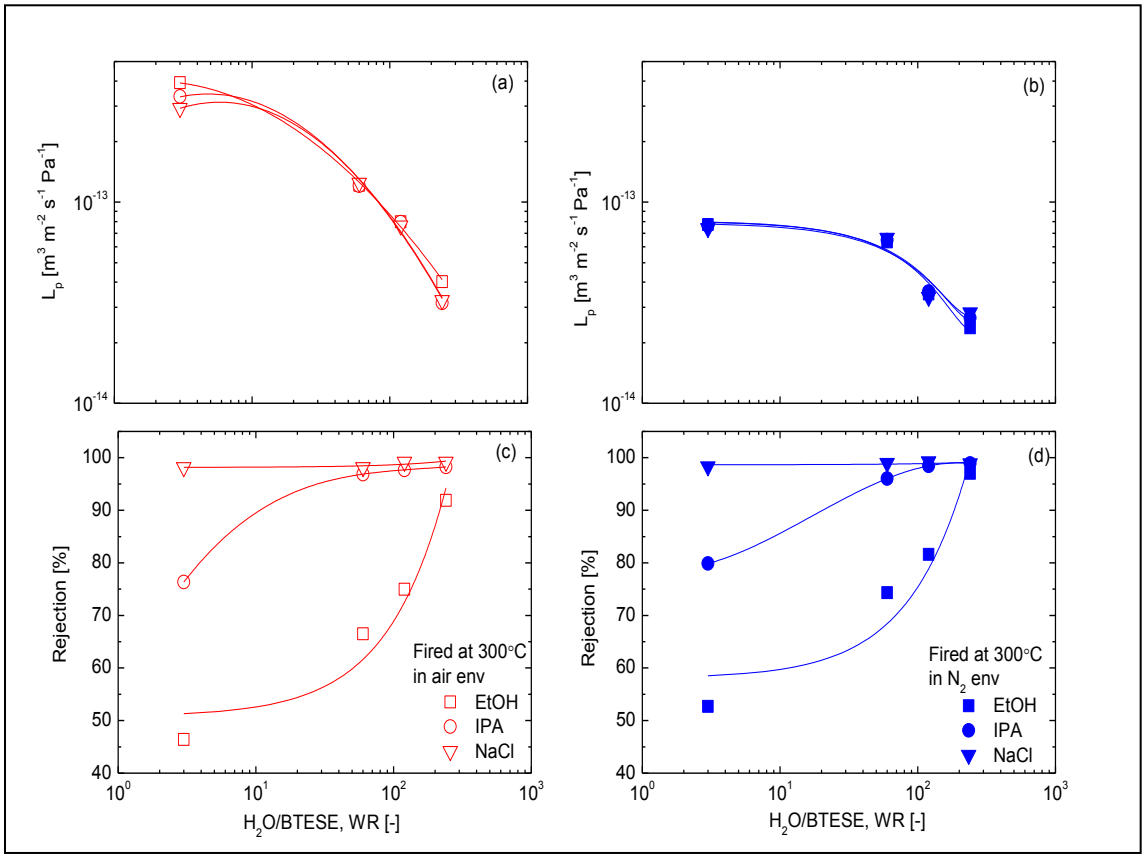

Figure 5-7 Water permeability, L_p and rejection, R as a function of the H_2O/BTESE molar ratio (WR) = (3, 60, 120, 240) measured at at 1 MPa and 25°C for BTESE membranes calcined at 300°C in air (a, c) and N_2 environments (b, d)

5.3.3. Pore size determination by NKP and H-D models

Pore size of nano-subnanometers is crucial in determining separation performance in gas phase as well as liquid phase. Traditionally, pore sizes, $d_{p,}$ in gas phase can be calculated by using gas translation model that was reported in our previous studies [27] meanwhile, pore sizes, $d_{p,}$ in liquid phase can be evaluated by Ferry or hindered diffusion (HD) models [28,29].

In the NKP method, the gas permeance data at 200 °C shown in Figure 5-6 was converted into NKP plot (Figure 5-8 (a) and (b)). The pore sizes for the BTESE membranes fired in air and N_2, with an increase in WR from 3 to 240, decreased from 10 to 4 Å and 7 to 4 Å, respectively. On the other hand, a hindered transport model [28,29] can be applied to estimate the pore size, $d_{p,}$ of the membrane by using neutral organic solutes solutions. According to Deen et al. [28,29], a sieving effect occurs within the nanopores, particularly when molecules are transported via diffusion in the nanopores. In this study, we used the rejection values of ethanol (EtOH), isopropanol (IPA) and glucose measured at 1 MPa and 25 °C. Pore size was best fitted to the Deen model as a function of the Stokes diameter of the solutes. Based on this model, the effective pore size for the BTESE membranes fired in air and N_2 with a WR increase from 3 to 240 were estimated from 0.95 to 0.52 nm and 0.77 to 0.47 nm, respectively as shown in Figure 5-8 (c) and (d).

The effect of WR on the pore size calculated by NKP and hindered-diffusion models can be seen more clearly by plotting the pore diameter as a function of WR for BTESE membranes fired in air and N_2 environment (Figure 5-9). Since pore size diameter calculated by using both models were based on the gas and solutes diffusion datas, only those pores effective (active pores) for gas and solutes diffusion are taken into account and the dead end pores, which have no contribution to the gas and solutes diffusion, are not measured [30]. Although, the pore sizes evaluated by H-D model seem to be slightly larger than the NKP model, these two models showed a reasonable agreement in pore sizes with each other. This suggests that pore sizes determined by both models can be accepted as a rough pore sizes indicator. Moreover, it is proven that by adjustment of WR and firing environments can tune the pore sizes of the membranes, and hence influence the separation properties.

As far as the authors know, no paper compared pore sizes determined in gas phase with those determining in liquid phase. Surprisingly, the pores were approximately consistent with each other. This direct comparison has been made possibly by using BTESE membranes

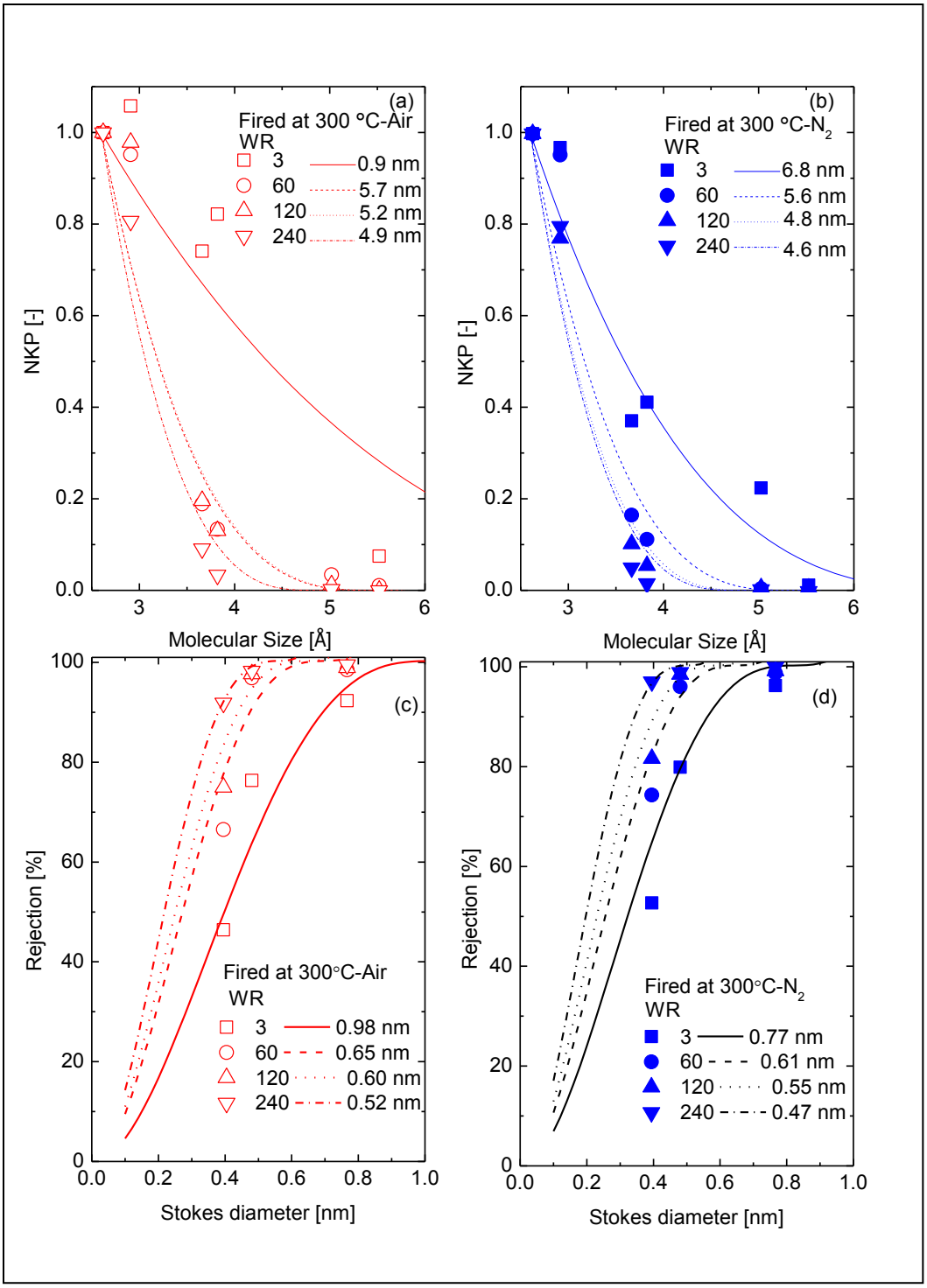

Figure 5-8 Pore size estimation for H_2O/BTESE molar ratio (WR) = (3, 60, 120, 240) fired in (a) air (b) N_2 by using NKP models at permeation temperature 200 °C; (c) air (d) N_2 by using H-D model at permeation temperature 1 MPa 25 °C

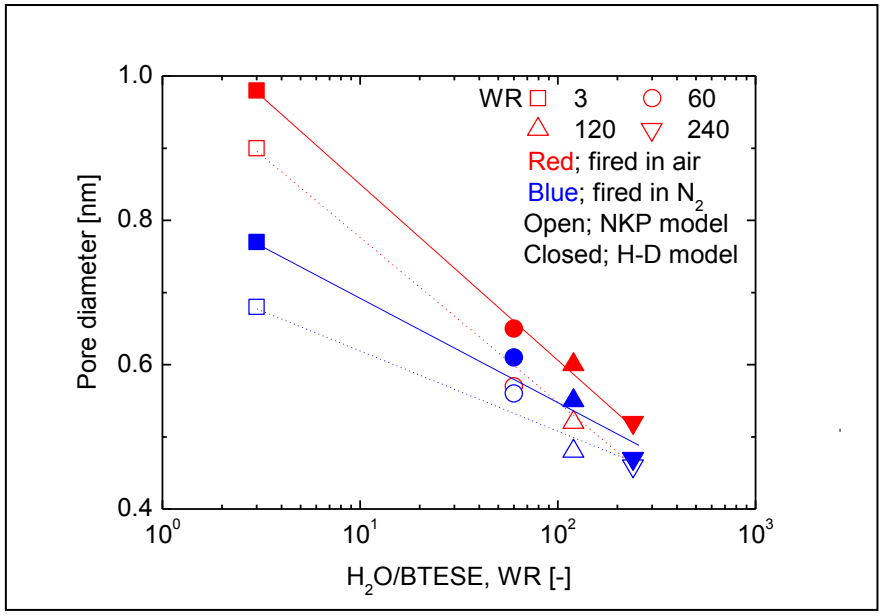

Figure 5-9 Relationship of pore diameter as a function of H_2O/BTESE molar ratio (WR) = (3, 60, 120, 240) membranes fired at 300 °C in air and N_2 . (NKP calculation at a permeation temperature of 200 °C and H-D calculation at a permeation temperature of 25 °C).

For better understanding, we illustrated the schematic images of the pore networks of different WR membranes fired in air and N_2 environment in Figure 5-10. In case of WR of 3 (low H_2O/BTESE), large number of ethoxide groups (OEt=-OC_2H_5) were un-hydrolyzed and removed by firing in air [4]. However, in N_2 environment, more ethoxide groups were believed to remain on the structure. This is due to the decomposition rate of organic bond fired in air was more pronounced than fired in N_2 (refer FTIR Figure 5-3), thus contributing the large pore network and hydrophilic properties for BTESE sample fired in air that will be discussed in the next section. On the other hand, for WR 240 membranes fired in both environments, large numbers of ethoxide groups are believed to hydrolyzed and this had be proven by the FTIR result as the dissappearance of -CH_3 peak (2,974 cm^{-1}). The density of silanol groups increased to form siloxane bonds due to high degree of cross-linking, hence smaller pore sizes were formed for both membranes fired in N_2 and air evironments.

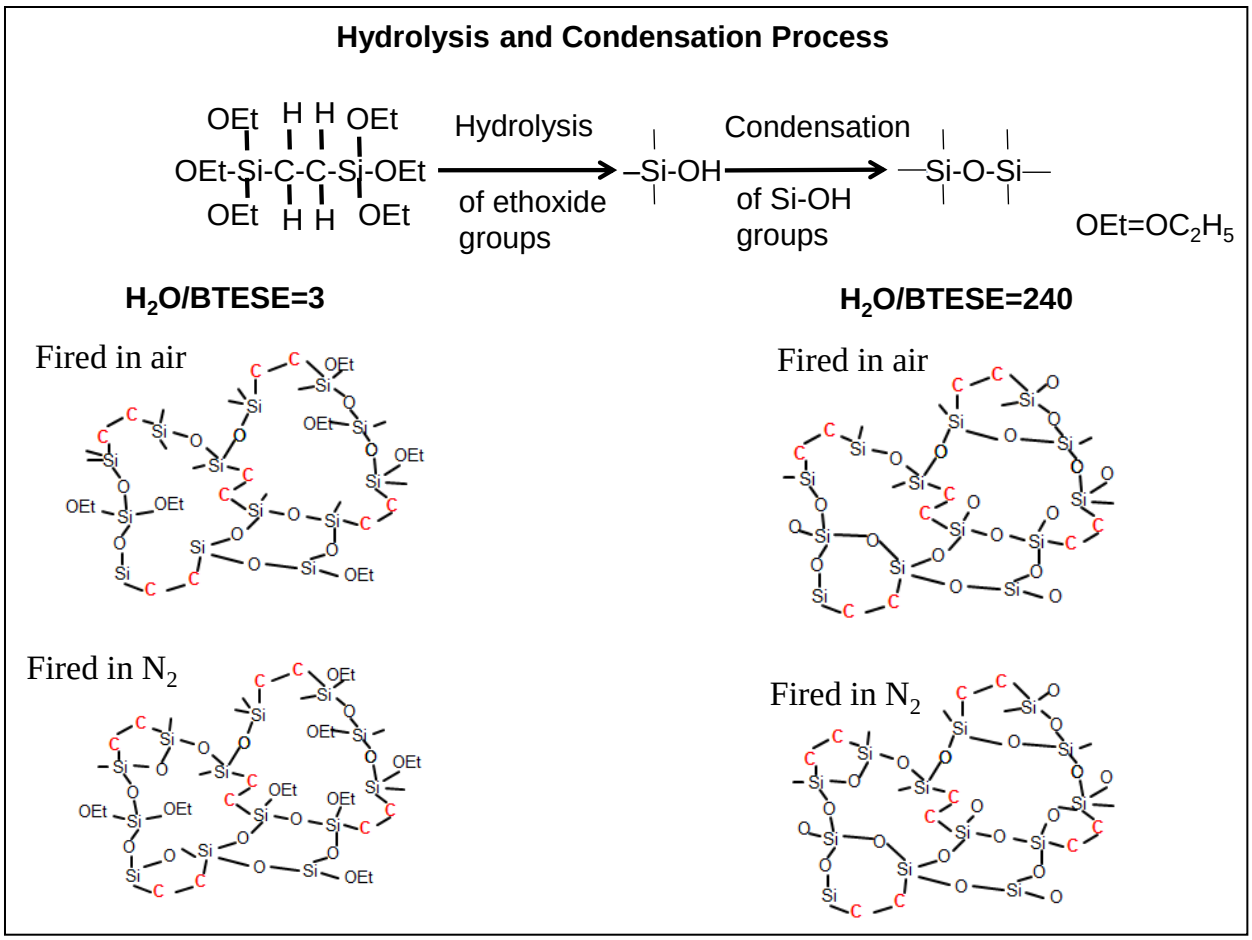

Figure 5-10 Schematic images of the pore networks of H_2O/BTESE molar ratio (WR) = (3 and 240) membranes.

5.3.4. Correlation between reverse osmosis and gas permeation performance

As explained in the previous section, the transport mechanism of water and NaCl during RO is mostly influenced by the molecular sieving phenomenon, which is the same as that of single gas permeation. Hence, a BTESE membrane must possess a pore size that falls between that of solutes and water in order to increase its suitability for molecular sieving (ion rejection). As mentioned earlier, the hydrated sizes of $Na^{+}_{(aq)}$, $Cl^{-}_{(aq)}$, Stokes diameter of EtOH, IPA and H_2O are 0.72, 0.66, 0.39, 0.48 and 0.276 nm, respectively [26]. On the other hand, the molecular sizes of helium (He), nitrogen (N_2) and SF_6 gases are 0.26, 0.36 and 0.55 nm, respectively. Figure 5-11 shows schematic of the sequence order of these all solutes, liquid and gases sizes.

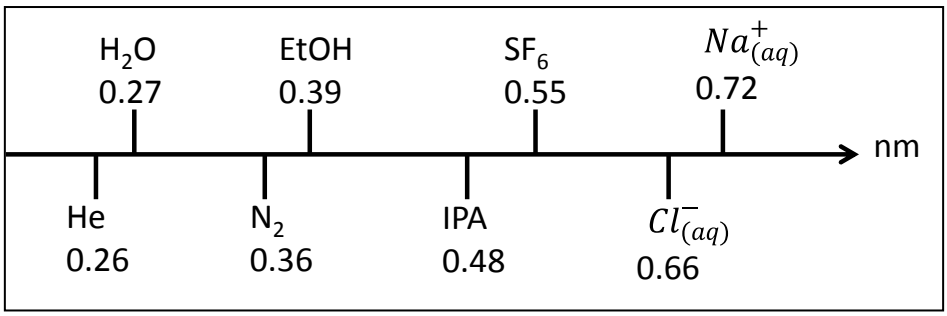

Figure 5-11 Schematic of the sequence order of these all solutes, liquid and gases sizes.

The molecular size of He is smaller than the molecular size of H_2O, so H_2O molecules are assumed to permeate through the same pores as He could permeate [31]. Water permeability, L_p was plotted against He permeance as shown in Figure 5-12. It should be noted that each point indicates the performances of a different membrane. L_p increased with increasing He permeance for BTESE membranes calcined in air environments. This phenomenon can be seen clearly for membranes WR 3 fired in air that exhibited high L_p values as well as He permeance due to larger pore size as well as it hydrophilic properties.

On the other hand, for BTESE membranes calcined in N_2 environment, the L_p and gas permeance values were just slightly affected due to the existence of ethoxide groups that may have acted as "building blocks" between the silica pores, and occupied some space in the silica network thus making a hindrance for gases to permeate via the pore networks hence resulting a hydrophobic properties hence lowering the water permeance.

For WR 240 membranes fired in air and N_2 environments were believed to have dense and more or less the same pore size thus exhibited approximately the same L_p and He permeance values around ~3.5×10^{-14} and ~9×10^{-7} mol m^{-2} s^{-1} Pa^{-1}, respectively. Although some points in the Figure 5-12 are scattered, it can still be concluded that the water permeability, L_p during reverse osmosis correlates with He permeance for BTESE membranes. The same observation can be seen for aromatic polyamide RO membranes, SWC4 regardless different membrane treatments [32], where in their result also indicates that increased in N_2 permeance indirectly increased the water permeance.

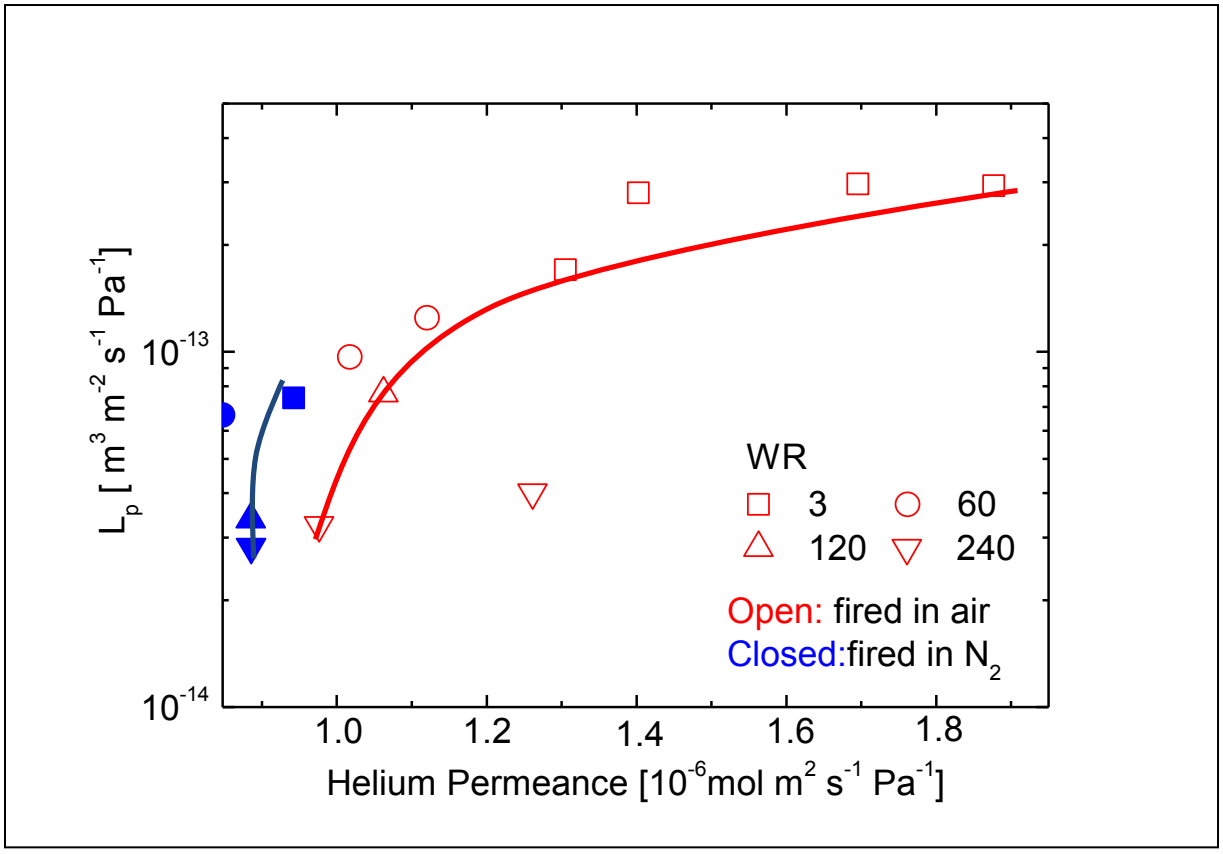

Figure 5-12 Water permeability, L_p (measured at Δp = 1 MPa; T=25°C) versus Helium permeance (measured at Δp = 33 kPa T=200°C) for variation range of WR =3-240 fired in air (blue) and nitrogen (red) environments

The rejection of EtOH, IPA and NaCl were plotted against permeance ratio of He/N_2 and He/SF_6 in order to see any possible correlation between solutes and gases. The rejection for all solutes were measured at 25 °C meanwhile permeance ratio He/N_2 and He/SF_6 were measured at 200 °C. Permeance ratio He/N_2 and He/SF_6 can be considered as a measurement of pore size distribution of BTESE membrane where He, N_2, SF_6 can permeate [14,26].

As can be seen in the Figure 5-13, with an increase in the permeance ratio of He/N_2 and He/SF_6 in both firing environment, the rejection of each solutes also increased. The membrane with high WR, which had small pore size, are plotted at the top right of the figures as these membranes possed high separation performance and vice versa for low WR membranes were plotted at bottom left of the figures due to low separation performance by large pore. Therefore, these results revealed it is a reasonable to use He gas as a predictor of water permeance, N_2 and SF_6 as a predictor for EtOH, IPA and NaCl permeance.

The rejection of EtOH and IPA seemed to be in the broad range around (40-97%) and (75-98 %), respectively compared to the rejection of NaCl more in the narrow range (97-99.5%) in both firing environments. In case of alcohols, despite the the similar concentration of the feed solutions, they have remarkable different permeances and

sensitivities to membrane surface and pores. EtOH which consist of 2 carbon and has smaller size than propanol is more permeable via BTESE membrane. On the other hand, NaCl showed much higher rejection compared with other solutes for BTESE membranes of all ranges of WR. NaCl have very large hydration energy values of 371 and 374 kJ mol^{-1} for Na^+ and Cl^- ions, respectively [33]. The very large hydration energies of Na^+ and Cl^- ions meants that a large amount of energy is needed to remove the water molecules from the hydration shells of the Na^+ and Cl^- ions, thus lowering, or making less favorable, the permeation of Na^+ and Cl^- ions as a hydrated sphere. In general, ions permeate confined channels in either a hydrated, dehydrated or partially hydrated state. The crystal ($d_{crystal}$) and hydrated ($d_{hydrated}$) diameters are for Na^+ ion ($d_{crystal\ Na^+}$ = 0.19 nm and $d_{hydrated\ Na^+}$ = 0.71 nm) and Cl^- ion ($d_{crystal\ Cl^-}$ = 0.36 nm and $d_{hydrated\ Cl^-}$ = 0.66 nm) **[**30,33], respectively. NaCl permeated through only a limited number of large pores for both membranes, thus exhibiting a lower ΔE value due to a weak interaction between the ions and the membrane pore wall.

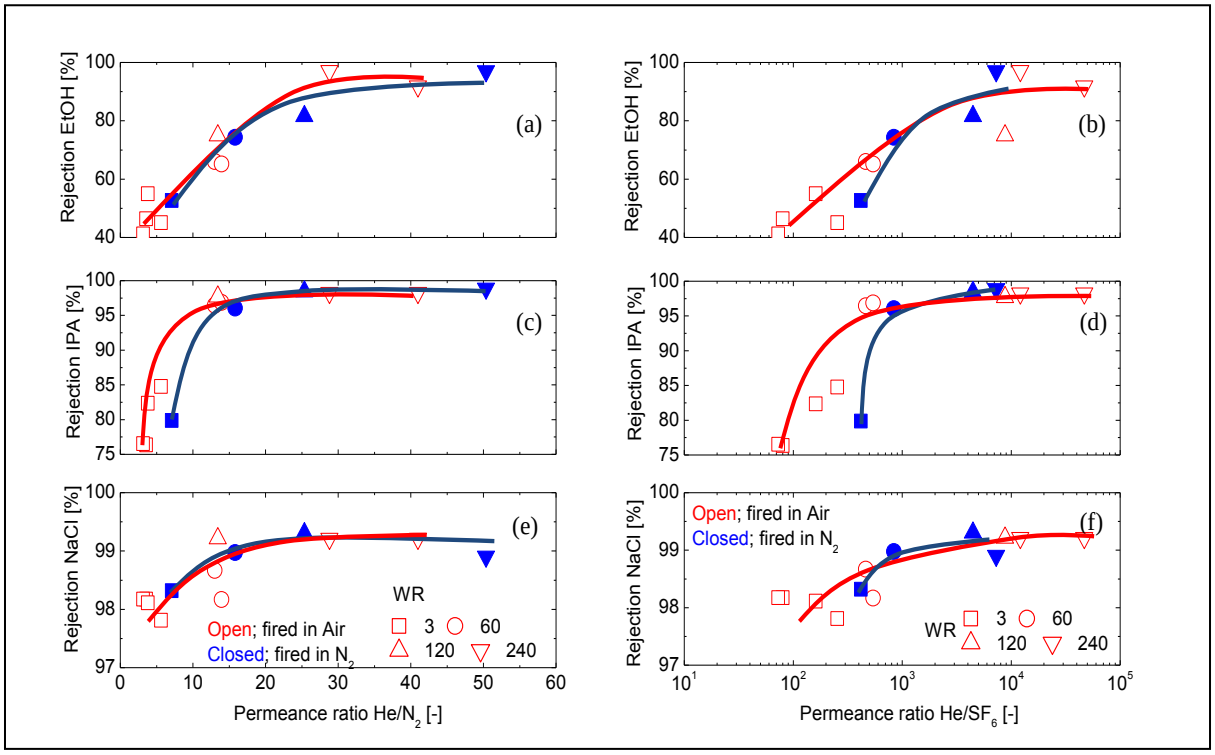

Figure 5-13 Rejection of IPA and NaCl (measured at Δp = 1 MPa; T=25 °C) versus permeance ration of He/N_2 and He/SF_6 (measured at 200 °C) for variation range of WR =3-240 calcined in air and nitrogen environments

Figure 5-14 shows the relationship between IPA and NaCl rejection for polyamide [33] and BTESE membranes. Both membranes exhibited scattered performance data according to the membrane properties. All these data can be plotted on one straight line with different degree of slope with rejection of NaCl always higher than IPA rejection, confirming IPA size smaller

than the NaCl size. In case of PA membrane, Kamada et al [33] reported that this one straight line with larger slope value suggests that the size of free volume effective for water permeation of PA membrane is a primary factor controlling the rejection of either type of solutes. BTESE membranes on the other hand show a moderate slope value despite the difference in membrane WR and firing environments. As we discussed in Figure 5-11, rejection of each solute depend on the solute size and pore size. So, the comparison of both rejections gives an insight of pore size distribution. We suggest that WR plays a primary factor in controlling the pore size during BTESE fabrication and more pronounced to IPA rejection. As can be seen, at WR 3 looser pore network are formed hence less IPA can be rejected. Increasing the WR from 60 to 240, tighter pore network was formed and more IPA can be rejected.

By comparison, it is clear that for both membranes in A region, both membranes consist have a large pore size thus exhibit low rejection for both solutes. As moved to B region, the pore size of PA membrane became smaller as NaCl rejection almost ~99.5% with IPA rejection ~95 to 96 %. On the other hand, BTESE membranes show slightly increased in rejection for solutes. NaCl and IPA rejection were found to be at the same level around ~99%. This support our idea that BTESE pore size distribution is more broad and consist large pinholes.

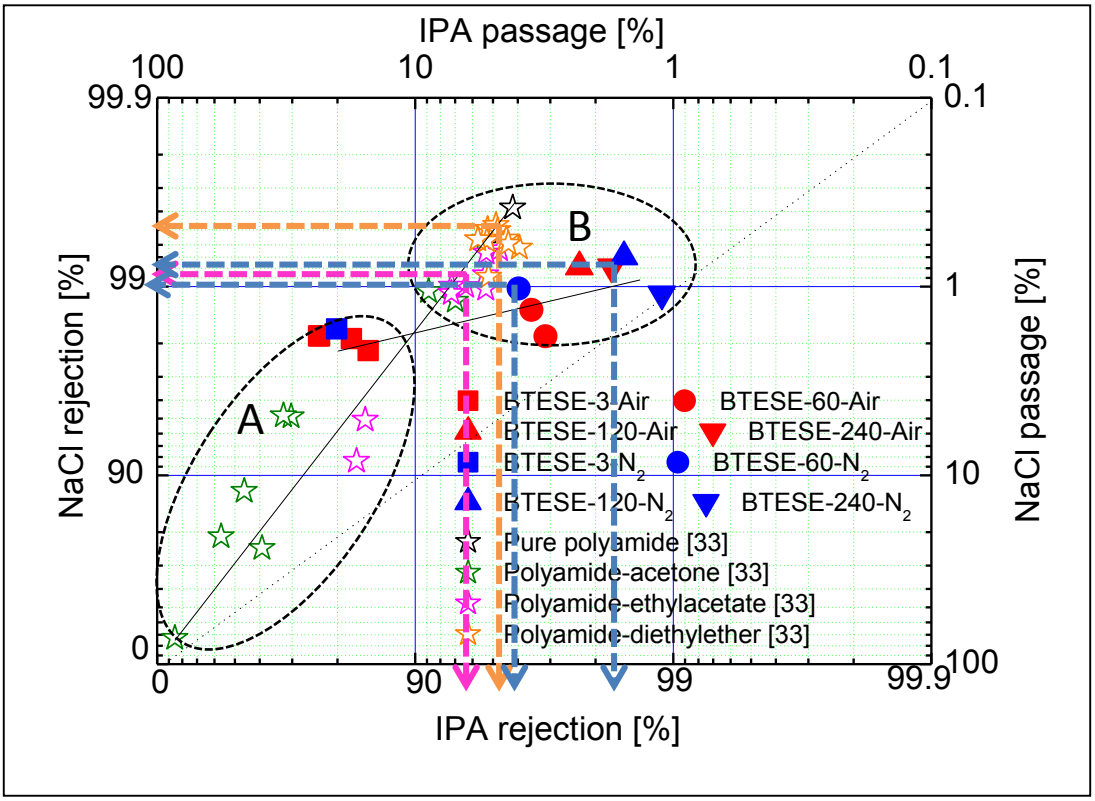

Figure 5-14 Comparison of the relationship between IPA rejection and NaCl rejection for polyamide and BTESE membranes. (500 ppm IPA and 2000 ppm NaCl, 1 MPa, 25 °C)

The L_p is a very important property for the RO membranes. Here we compare the L_p and R_{NaCl} of the present RO membrane with other reported materials as shown in Figure 5-15 and the detailed operating conditions were shown in Table 5-2. Interfacial polymerized and modified polyamide membranes [34-36] exhibited superior water flux and salt rejection at permeation temperature 25 °C. On the other hand, it can be seen that L_p value of organosilica membranes shows only a moderate degree of water permeance with a high degree of rejection at the same permeation temperature. However, as we compared the performance of our organosilica membranes including BTESE membranes and TTESPT [16] and BTESEthy [37] with other inorganic membranes such as zeolite and silicalite [38-40] and graphene [41] membranes, our organosilica membranes BTESE membranes can still be considered as high performance membrane in L_p and R_{NaCl}. As an example, the L_p of BTESE WR 3 membranes at operating condition 1 MPa, 80°C, around ~2 x10^{-12} m^3 m^{-2} s^{-1} Pa^{-1} was much large compared to the L_p of MFI-zeolite membrane [40] at operating condition 7 MPa, 90°C~, 5.9 x10^{-13} m^3 m^{-2} s^{-1} Pa^{-1}. It should also be noted that the water permeabilities for the BTESE WR 3 membranes (red open keys) were more than 1 x 10^{-12} m^3 m^{-2} s^{-1} Pa^{-1} and showed an excellent salt rejection of >98% at 60 and 80 °C approximated that of the L_p and R_{NaCl} of a commercially polyamide RO membrane, SW30HR, (FilmTec) at an operating temperature of 25 °C with L_p and R_{NaCl} values of around 2.2 x 10^{-12} m^3 m^{-2} s^{-1} Pa^{-1} and 98.5%, respectively [42].

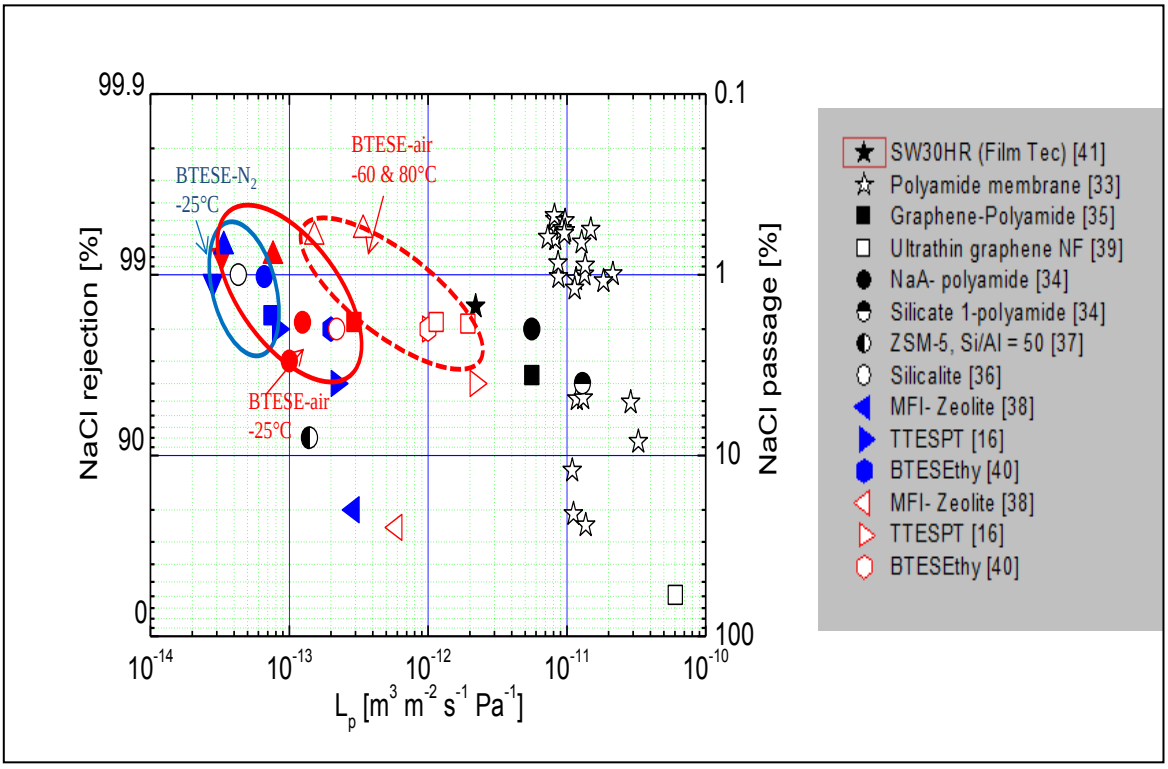

Figure 5-15 Trade-off between NaCl rejection and water permeability, L_p for different membrane materials. (Detail of operating conditions were listed in Table 2)

Table 5-2 Comparisons of the desalination performance of different types of membranes

Membranes	Operating condition for NaCl experiment	Water permeability [m^3m^{-2} s^{-1} Pa^{-1}]	R_{NaCl} [%]	Ref
Polyamide	1.0MPa; 25 °C; 2000 ppm	~$1x10^{-11}$	~99.5	[34]
NaA-TFC polyamide	1.6 MPa; 25 °C; 2000 ppm	~$5.6x10^{-12}$	~96	[35]
Silicate 1-TFC polyamide	1.6 MPa; 25 °C; 2000 ppm	~$1.3x10^{-11}$	~92	[35]
Graphene Oxide -TFC polyamide	1.5 Mpa; 25 °C; 2000 ppm	~$5.6x10^{-12}$	~96.4	[36]
Silicalite	2.7 MPa; 25 °C; 0.1 M	~$4.3x10^{-14}$	~99	[38]
ZSM-5, Si/Al = 50	2.7 MPa; 25 °C; 0.1 M	~$1.4x10^{-13}$	~92	[39]
MFI- Zeolite	7 MPa; 21 °C; 3000 ppm	~$2.9x10^{-13}$	~80	[40]
	7 MPa; 90 °C; 3000 ppm	~$5.9x10^{-13}$	~75	[40]
Ultrathin graphene Nano-filtration	0.5 MPa; 25 °C; 1168 ppm	~$6.1x10^{-11}$	~41	[41]
BTESEthy	1.15 MPa; 25 °C; 2000 ppm	~$2.0x10^{-13}$	~98	[37]
	1.15 MPa; 60 °C; 2000 ppm	~$1.0x10^{-12}$	~98	[37]
TTESPT-60	1 MPa; 25 °C; 2000 ppm	~$2.2x10^{-13}$	~96	[16]
	1 MPa; 60 °C; 2000 ppm	~$2.2x10^{-12}$	~96	[16]
TTESPT-240	1 MPa; 25 °C; 2000 ppm	~$8.3x10^{-14}$	~98	[16]
	1 MPa; 60 °C; 2000 ppm	~$1.0x10^{-12}$	~98	[16]
BTESE-3-air	1 MPa; 25 °C; 2000 ppm	~$2.9x10^{-13}$	~98.1	[This work]
	1 MPa; 80 °C; 2000 ppm	~$2.0x10^{-12}$	~98.1	[This work]
BTESE-240-air	1 MPa; 25 °C; 2000 ppm	~$3.3x10^{-14}$	~99.2	[This work]
	1 MPa; 80 °C; 2000 ppm	~$3.4x10^{-13}$	~99.4	[This work]

5.4. Conclusion

The aim of this work was to study the simultaneous effects of WR (3, 60, 120, 240) molar ratios and different in firing environments on the structural and performance properties of BTESE membranes. Samples were characterized by FTIR, contact angle, N_2 and H_2O adsorption. By characterization it was revealed that the ethoxides of BTESE were almost completely hydrolyzed and the silica networks became dense by increasing the WR from 3 to 240. Firing in N_2 environment seems to make the samples more hydrophobic compared with the sample fired in air environment. This is due to the firing in N_2 environment can induce the slow decomposition of organic bonds in the sample, thus making the structures more rigid structures within the networks. In addition,the correlation between gas and liquid permeances revealed that He can be a predictor of water permeance, N_2 and SF_6 as a predictor for IPA and NaCl permeance. Increasing in He and permeance ratio resulted in increasing in water permeance and rejection of solutes. From this result, it suggests that WR plays a primary factor in controlling the pore size and solutes rejections meanwhile firing environments play a main role in deciding the hydrophilicity and hydrophobicity of membrane surface and pore networks during BTESE membranes fabrication.

References

[1] B.C. Bonekamp, R. Kreiter and J.F. Vente, Sol-gel approaches in the synthesis of membrane materials for nanofiltration and pervaporation. Sol-Gel Methods for Materials Processing NATO Science for Peace and Security Series C: Environmental Security, (2008) 47-65

[2] M.A. Anderson, M.J. Gieselmann and Q. Xu, Titania and alumina ceramic membranes, J. Membr. Sci. 39 (1988) 243-258

[3] M. Kanezashi, M. Kawano, T. Yoshioka and T. Tsuru, Organic Inorganic Hybrid Silica Membranes with Controlled Silica Network Size for Propylene/Propane Separation, Ind. Eng. Chem. Res. 51 (2012) 944–953

[4] T. Niimi, H. Nagasawa, M. Kanezashi, T. Yoshioka, K. Ito, T. Tsuru, Preparation of BTESE-derived organosilica membranes for catalytic membrane reactors of methylcyclohexane dehydrogenation, J. Membr. Sci. 455 (2014) 375–383

[5] S.M. Ibrahim, R. Xu, H. Nagasawa, A. Naka, J. Ohshita, T. Yoshioka, M. Kanezashi and T. Tsuru, A closer look at the development and performance of organic–inorganic membranes using 2,4,6-tris-[3(triethoxysilyl)-1-propoxyl]-1,3,5-triazine (TTESPT), RSC Adv. 4 (2014) 12404-12407

[6] M. Nomura, H. Aida, S. Gopalakrishnan, T. Sugawara, S. Nakao, S. Yamazaki, T. Inada, Y. Iwamoto, Steam stability of a silica membrane prepared by counter-diffusion chemical vapor deposition, Desalination 193 (2006) 1–7

[7] Y. Gu and S.T. Oyama, High molecular permeance in a poreless ceramic membrane. Adv Mater. 19 (2007) 1636–1640

[8] C.J. Brinker, Hydrolysis and condensation of silicates: Effects on structure, J. Non-Crystal. Solids 100 (1988) 31-50

[9] D.R. Azolin, C.C. Moro, T.M.H. Costa, E.V. Benvenutti, Effects of organic content and H_2O/TEOS molar ratio on the porosity and pore size distribution of hybrid naphthaleneaminepropylsilica xerogel. J. Non-Crystal. Solids 337 (2004) 201–206

[10] Y. Ma, M. Kanezashi and T. Tsuru, Preparation of organic/inorganic hybrid silica using methyltriethoxysilane and tetraethoxysilane as co-precursors. J Sol-Gel Sci Technol 53 (2010) 93–99

[11] O. A. Shilova, Synthesis and structure features of composite silicate and hybrid TEOS-derived thin films doped by inorganic and organic additives, J. Sol-Gel Sci. and Tech. 68 (2013) 387-410

[12] B. Topuz and M. Çiftçioğlu, Sol–gel derived mesoporous and microporous alumina membranes, J Sol-Gel Sci Technol 56 (2010) 287–299

[13] G.C. Hoang, Pore-Size Control of Silica Gels in Acidic Water Conditions Using Sol-Gel Processing, J. Korean Phys. Society 31 (1997) 227-230

[14] M. Kanezashi, K. Yada, T. Yoshioka, and T. Tsuru, Design of Silica Networks for Development of Highly Permeable Hydrogen Separation Membranes with Hydrothermal Stability, J. Am. Chem. Soc. 131 (2009) 414–415

[15] R. Xu, J. Wang, M. Kanezashi, T. Yoshioka, T. Tsuru, Development of robust organosilica membranes for reverse osmosis, Langmuir 27 (2011) 13996–13999.

[16] S.M. Ibrahim, R. Xu, H. Nagasawa, A. Naka, J. Ohshita, T. Yoshioka, M. Kanezashi, T. Tsuru, Insight into the pore tuning of triazine-based nitrogen-rich organoalkoxysilane membranes for use in water desalination, RSC Adv. 4 (2014) 23759-23769.

[17] B. Zhu, J.H. Kim, Y.H. Na, I.S. Moon, G. Connor, S. Maeda, G. Morris, S. Gray and M. Duke, Temperature and Pressure Effects of Desalination Using a MFI-Type Zeolite Membrane, Membranes 3 (2013) 155-168.

[18] Osmosis equation: http://www.chemteam.info/Solutions/Osmosis-Equation.html

[19] T. Tsuru, K. Ogawa, M. Kanezashi, T. Yoshioka, Permeation characteristics of electrolytes and neutral solutes through titania nanofiltration membranes at high temperatures, Langmuir 26 (2010) 10897–10905.

[20] R. Xu, J. Wang, M. Kanezashi, T. Yoshioka, T. Tsuru, Reverse osmosis performance of organosilica membranes and comparison with the pervaporation and gas permeation properties, AIChE J. 59 (2013) 1298–1307.

[21] T. Tsuru, S. Izumi, T. Yoshioka, M. Asaeda, Temperature effect on transport performance by inorganic nanofiltration membranes. AIChE J. 46 (2000) 565–574.

[22] Y.H. Han, A. Taylor, M.D. Mantle, K.M. Knowles, Sol–gel-derived organic– inorganic hybrid materials, J. Non-Cryst. Solids 353 (2007) 313–320.

[23] S.K. Parida, S. Dash, S. Patel, B.K. Mishra, Adsorption of organic molecules on silica surface, Adv. in Colloid and Inter. Sci. 121 (2006) 77–110

[24] J.Coates, Interpretation of infrared spectra, a practical approach, Encyclopedia of Analytical Chemistry, doi:10.1002/9780470027318.a5606.

[25] B. Cao, Y. Tang and C. Zhu, Synthesis and Hydrolysis of Hybridized Silicon Alkoxide: $Si(OEt)_x(OBut)_{4-x}$. Part I: Synthesis and Identification of the $Si(OEt)_x(OBut)_{4-x}$, J. Sol-Gel Sci.Technol. 10 (1997) 247-253

[26] H.R. Lee, M. Kanezashi, Y. Shimomura, T. Yoshioka, and T. Tsuru, Evaluation and Fabrication of Pore-Size-Tuned Silica Membranes with Tetraethoxydimethyl Disiloxane for Gas Separation, AIChE J. 57 (2011) 2755-2765

[27] W.M. Deen, Hindered transport of large molecules in liquid-filled pores, AIChE J. 33 (1987) 1409–1425.

[28] P. Dechadilok and W.M. Deen, Hindrance Factors for Diffusion and Convection in Pores, Ind. Eng. Chem. Res. 45 (2006) 6953-6959.

[29] G.Z. Cao, J. Meijerink, H. W. Brinkman and A.J. Burggraaf, Permporometry study on the size distribution of active pores in porous ceramic membranes, J. Membr. Sci. 83

(1993) 221-235

[30] E.R. Nightingale Jr., Phenomenological theory of ion solvation. Effective radii of hydrated ions, J. Phys. Chem. 63 (1959) 1381–1387.

[31] J. Yang, T. Yoshioka, T. Tsuru, M. Asaeda, Pervaporation characteristics of aqueous-organic solutions with microporous SiO_2-ZrO_2 membranes: Experimental study on separation mechanism, J Membr. Sci. 284 (2006) 205-213.

[32] J. S. Louie, I. Pinnau, M. Reinhard, Gas and liquid permeation properties of modified interfacial composite reverse osmosis membranes, J Membr. Sci. 325 (2008) 793–800

[33][41] I.S. Joung, T.E. Cheatham, Determination of Alkali and Halide Monovalent Ion Parameters for Use in Explicitly Solvated Biomolecular Simulations, J. Phys. Chem. B 112 (2008) 9020–9041.

[34] T. Kamada, T. Ohara, T Shintani, T. Tsuru, Optimizing the preparation of multi-layered polyamide membrane via the addition of a co-solvent, J Membr. Sci. 453 (2014) 489–497.

[35] H. Huang, X. Qu, X. Ji, X. Gao, L. Zhang, H. Chen and L. Hou, Acid and multivalent ion resistance of thin film nanocomposite RO membranes loaded with silicalite-1 nanozeolites, J. Mater. Chem. A, 1 (2013) 11343–11349

[36] W. Choi, J. Choi, J. Bang, and J.H. Lee, Layer-by-Layer Assembly of Graphene Oxide Nanosheets on Polyamide Membranes for Durable Reverse-Osmosis Applications, ACS Appl. Mater. Interfaces. 5 (2013) 12510−12519

[37] R. Xu, M. Kanezashi, T. Yoshioka, O. Tetsuji, O. Joji, T. Tsuru, Tailoring the affinity of organosilica membranes by introducing polarizable ethenylene bridges and aqueous ozone modification, ACS Appl. Mater. Interfaces. 5 (2013) 6147-6154.

[38] N. Liu, L. Li, B. McPherson, and R. Lee, Removal of organics from produced water by reverse osmosis using MFI-type zeolite membranes, J Membr. Sci. 325 (2008) 357–361

[39] L. Li, N. Liu, B. McPherson, and R. Lee, Enhanced Water Permeation of Reverse Osmosis through MFI-Type Zeolite Membranes with High Aluminum Contents, Ind. Eng. Chem. Res. 2007, 46, 1584-1589

[40] B. Zhu, J.H. Kim, Y. H. Na, I.S. Moon, G. Connor, S. Maeda, G. Morris, S. Gray and M. Duke, Temperature and Pressure Effects of Desalination Using a MFI-Type Zeolite Membrane, Membranes 3 (2013) 155-168

[41] Y. Han, Z. Xu, and C. Gao, Ultrathin Graphene Nanofiltration Membrane for Water Purification, Adv. Funct. Mater. 23 (2013) 3693–3700

[42] E.S. Hatakeyama, C.J. Gabriel, B.R.Wiesenauer, J.L. Lohr, M.J. Zhou, R.D. Noble, D.L. Gin, Water filtration performance of a lyotropic liquid crystal polymer membrane with uniform, sub-1-nm pores, J. Membr. Sci. 366 (2011) 62–72.

Chapter 6

New insights on fouling and cleaning properties of reverse osmosis (RO) BTESE membrane

6.1. Introduction

RO membrane fouling is one of the pressing issue the industry need to solve. Potts et al. [1] provides a range of definitions for membrane fouling varying from a simple to complex definitions. The simplest of all definitions is "the phenomenon where foulants accumulate on RO membranes leading to performance deterioration [1]. In order to predict membrane permeate flux decline, a thorough understanding of all contributing fouling mechanisms is required. As mentioned earlier, membrane fouling occurs as a result of foulants being brought to and accumulating on the membrane surface. Mechanisms leading to flux decline for loose membranes, such as MF and UF, include pore blocking (when foulants cover membrane pore surfaces] and pore constriction (when foulants reduce pore size by clogging pores). Concentration polarization and cake/gel layer formation are fouling mechanisms of all types of membranes. Fouling during NF and RO is often assumed to occur only on the membrane surface or form cake layer due to the tightness of NF and RO membranes and relative size of the foulants compared to membrane pore size [2].

Fouling behavior is mainly influenced by three factors; hydrodynamic conditions at the membrane surface, membrane surface characteristics, and feed solution characteristics (including foulant characteristics and solution conditions). Generally, spiral wound, hollow fiber, plate and frame set-ups are all used in industrial applications incorporating with two configurations such as a "cross-flow" and "dead-end" configurations. The advantage of cross-flow filtration over dead-end filtration is that accumulation of particles on the membrane surface is reduced [3]. In term of RO membranes, they are usually characterized by hydrophobicity/hydrophilicity and surface charge of the thin outermost layer [2, 4, 5]. A large portion of fouling is thought to be caused by organic compounds that adsorb on the membrane surface via hydrophobic interactions. Meanwhile, hydrophilic non-interacting membranes are thought to decrease protein adsorption, even though hydrophobic interaction is not the only interaction involved in adsorption [6]. If the membrane surface is charged, electrostatic attraction or repulsion forces between charged foulant components and the membrane surface can also influence the degree of fouling [7].

Fouling behavior also depend on the type of foulants being filtered such as its surface charge, molecular weight, particle size, or hydrophobicity. In addition, solution conditions (i.e. pH, salt ion type, and ionic strength) can affect foulant characteristics, membrane surface properties, and how foulants interact with each other and the membrane surface. Generally, organic fouling experiments performed with bovine serum albumin [BSA] on reverse osmosis membranes show that fouling of solutions with a pH close to BSA's iso-electric point (IEP) created the greatest fouling flux decline due to aggregation caused by weakened electrostatic repulsion of the BSA molecules [8]. Calcium ions have been shown to significantly enhance fouling in the presence of natural organic matter (NOM) by forming complexes which result in highly compacted fouling layers and thus more severe flux decline [9-11].

Another type of foulants is surfactant. Surfactants are a class of industrially very important amphiphilic substances which consist of a hydrophilic head group to which a hydrocarbon chain is connected. One of the characteristic properties of amphiphilic substances is that they tend to assemble at interfaces. They are therefore often referred to as surface-active agents. Another characteristic property of amphiphilic substances is the formation of large aggregates (micelles). In these micelles, the hydrophilic heads are directed towards the aqueous solution, while the hydrophobic tails are turned inside. Surfactants are categorized into four groups depending on the charge on the head group: nonionic, anionic, cationic and zwitterionic surfactants [12].

With regard to the effect of fouling on membrane performance, vast efforts to reduce fouling have been undertaken by improved in membrane properties and pretreatment of feed waters [13]. However, fouling is still inevitable thus cleaning process is needed to avoid the drop in the membrane productivity. Several types of cleaning agents are used for cleaning of organic fouled membranes, including alkalines, acids, metal chelating agents, surfactants and enzymes [14-17]. Initially, our attention is restricted to BTESE membranes and to understand the fundamentals of fouling phenomenon on the membrane surface by using varieties of types of foulants such as protein, sodium alginate, anionic and cationic surfactants as well as its cleaning process. It is worthwhile to point out that inorganic membranes have inherently versatile characteristics; high thermal stability and chemical resistance. Thus, these advantages make them suitable candidates for possible cleaning with hot water. Our main concern is to avoid any types of chemical cleaning agents in order to clean BTESE membranes.

6.2.Experimental (Materials and Methods)

6.2.1Types of Foulants

Figure 6-1 shows structure of foulants such as; Bovine serum albumin (BSA) (Sigma-Aldrich, purity 99%) and sodium alginate (SA) (Sigma-Aldrich, purity 99%) were chosen to represent proteins and polysaccharides in effluent organic matter. The molecular weight (MW) of the BSA and sodium alginate is about 66 kDa and 80 kDa, respectively. On the other hand, sodium dodecyl sulfate (SDS) (MW: 288.38 g/mol, Sigma-Aldrich, purity 99%), an anionic surfactant and dodecyltrimethyl ammonium bromide (DTAB) (MW: 308.34 g/mol, Sigma-Aldrich, purity 99%), a cationic surfactant, were used to represent industrial waste. All the foulants were used as received without further purification. Each foulants were prepared at different concentrations of 100 ppm and 500 ppm by dissolving each foulants in deionized water. Mixing of these each foulant solutions was performed for over 24 hours to ensure complete dissolution of the foulant. Then, the foulants solutions were stored at 4 °C overnight.

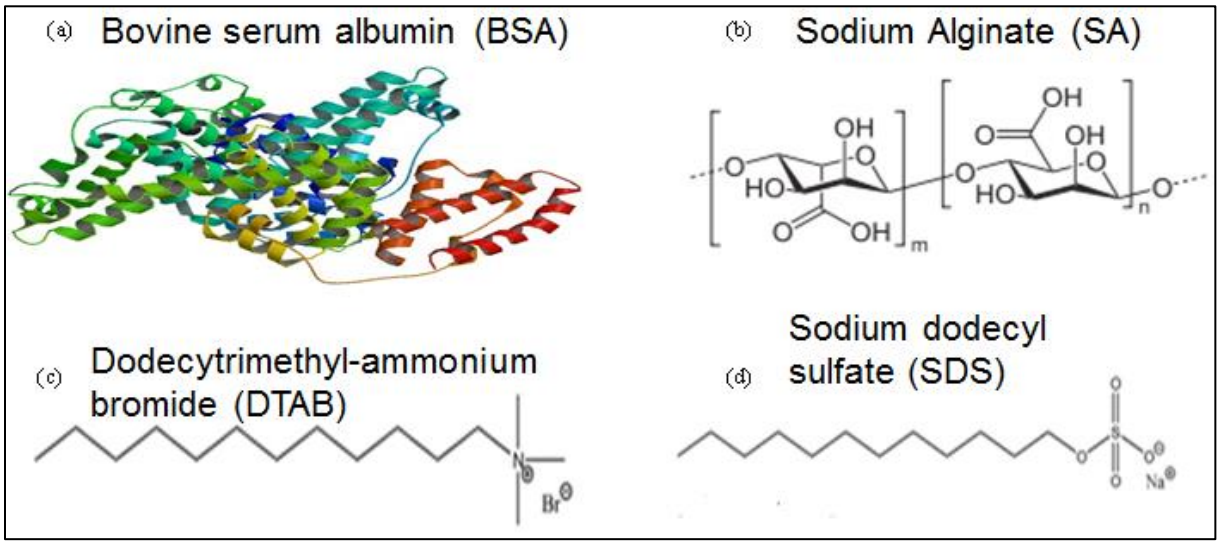

Figure 6-1 Structure of foulants (a) Bovine serum albumin (BSA), (b) Sodium Alginate (SA), (c) Dodecytrimethylammonium bromide (DTAB) and (d) Sodium dodecyl sulfate (SDS)

6.2.2. RO membrane

BTESE-derived silica membranes were used as the model RO membrane. Details on membrane preparation can be found elsewhere [18-20]. Fouling experiment was conducted using a number of BTESE-derived membranes with the same preparation method.

6.2.3. Membrane surface zeta potential and foulants zeta potential

Membrane surface zeta potential was determined by using Malvern instruments. The tracer used here is polystyrene latex pH =7. The foulants zeta potential was measured at pH ranging from 2 to 11.

6.2.4. Fouling and cleaning test units

The laboratory scale RO cross-flow test unit was used to carry out for in-situ fouling experiment. Meanwhile, immersion fouling experiment was conducted by using static beaker (for membrane immersion in the foulant solution) and the same RO cross-flow test unit used for in-situ fouling experiment for evaluation of pure water and NaCl sol via BTESE membrane.

6.2.5. Fouling and cleaning experiment flow

The experimental protocol developed for fouling/cleaning for in-situ and immersion fouling experiments were shown in Figure 6-2 (a) In-situ fouling and (b) Immersion fouling. For both fouling experiments, the membrane was first evaluated for its performance by using 2000 ppm NaCl and then followed by deionized water. All these measurements were run until the permeate flux became constant. After attaining a stable flux, fouling experiment was run.

The differences between in-situ and immersion fouling experiments as described below:

(a) In-situ-fouling experiment: The experiment was done in the cross-flow test unit. Fouling experiment was initiated by preparing different foulants (i.e. BSA, SA, SDS and DTAB) as a feed solution at desired concentrations. Fouling experiments were carried out for several hours.

(b) Immersion fouling experiment: The membrane was immersed in a flask containing foulants (i.e. BSA, SA, SDS and DTAB) at desired concentrations for 16 hours. Then, the membrane was take-out and rinsed witf pure water and followed by cross-flow experiment.

The operating condition for cross-flow test unit; the system was pressurized with a plunger pump at a pressure difference of 1 MPa. The water bath was maintained at a temperature of 25 °C unless otherwise specified. The retentate was recycled back to the feed container, and the permeate stream was maintained at an atmospheric pressure and collected using a peristaltic pump type. The permeate was then transported, at ambient pressure, toward the pump outlet by using silicone tubing. The feed solution was vigorously agitated using a magnetic stirrer at 600 rpm. At the end of each experiment run in the cross-flow test unit, the solution in the feed

reservoir and cross-flow unit were disposed and membrane cell were rinsed with deionized water.

The cleaning of the fouled membrane was run outside the cross-flow membrane test unit. The cleaning procedure will be mention later in the next section. The cleaned membrane was subjected to the second baseline performance with deionized water to determine the pure water flux again. The operating conditions (i.e., initial flux, and temperature) at this stage were identical to those applied during the initial baseline performance, so as to determine the cleaning efficiency by comparing the pure water fluxes determined before fouling and after cleaning. To confirm the reproducibility of determined cleaning efficiency, selected fouling/cleaning runs were duplicated. Results showed that fouling rate and cleaning efficiency obtained from the duplicate runs were always within less than 5% difference.

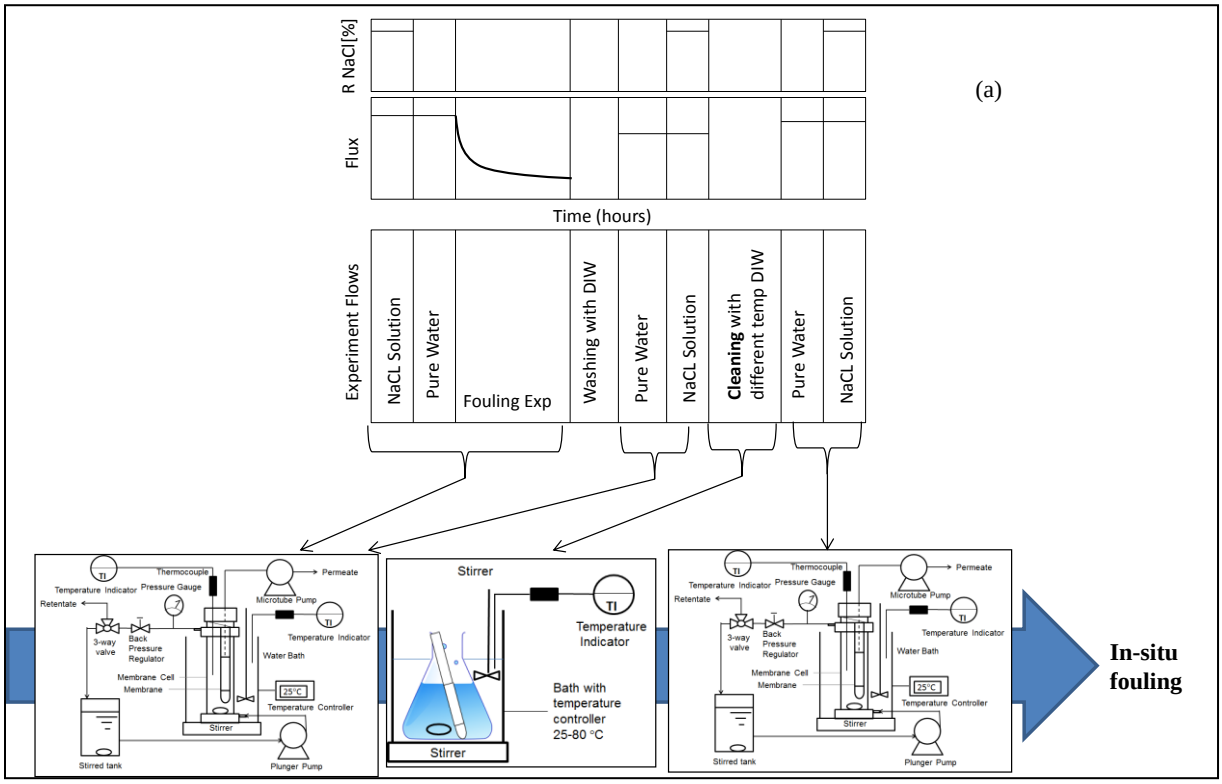

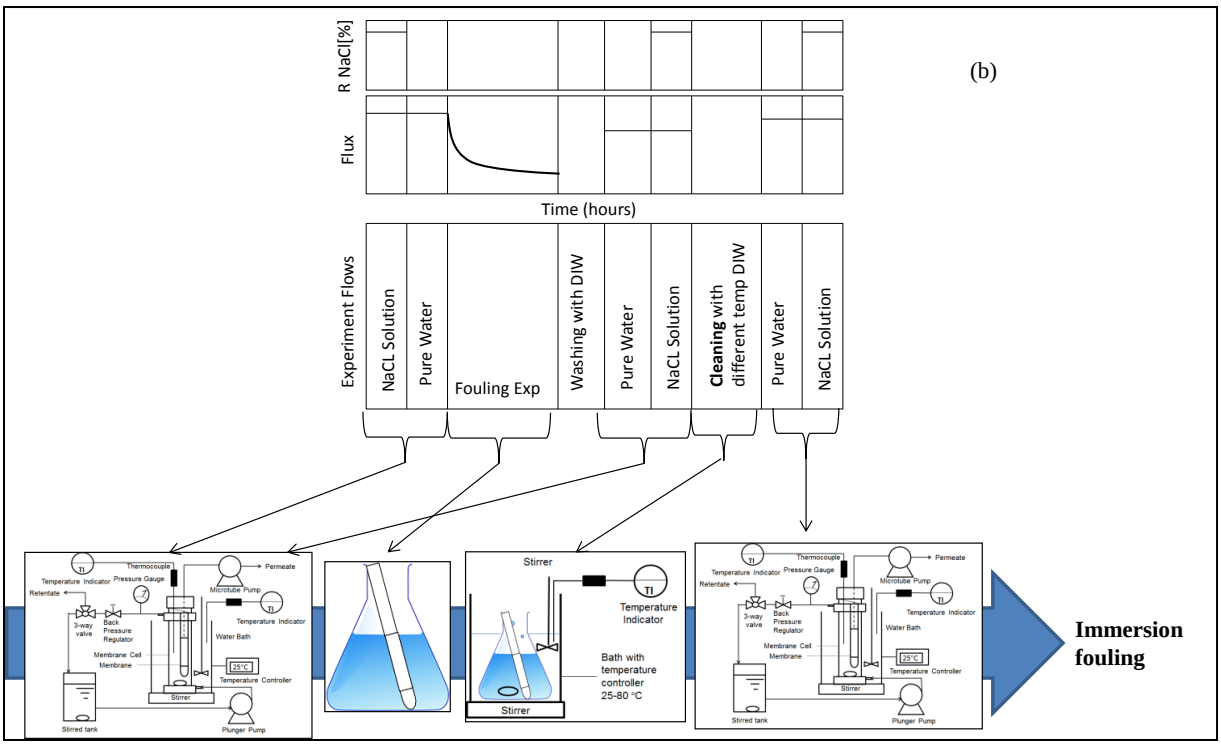

Figure 6-2 Experimental protocol for the fouling/cleaning runs (a) In-situ fouling and (b) Immersion fouling

6.3.Result and discussion

6.3.1. Surface zeta potential of membranes and zeta potential of foulant solutions

Table 6-1 shows the surface zeta potential for BTESE and PA (PA) membranes for comparison. All membranes exhibited negative charge at pH=7. Meanwhile, Figure 6-3 shows zeta potential of each solutes used in this study. Only BSA had IEP at pH=4.9 where pH> 4.9 BSA exhibits negative charge and pH<4.9 BSA exhibits positive charge. DTAB showed positive charge as cationic surfactant, while SDS exhibited negative charge as anionic surfactant. SA on the other hand, also exhibit negative charge due to alginate groups.

Table 6-1 Surface zeta potential of membranes

Membranes	Manufacturer	Zeta Potential (mV)	Ref
Polyamide LFC-1 (RO)	Hydranautics, Oceanside, CA	-13 at pH=6.8	[21]
Polyamide AG (RO)	GE Water & Process Technologies (Minnetonka,MN)	-40.6 at pH=7	[22]
BTESE fired at 300 °C in air	-	-96.6 at pH =7	[this work]
BTESE fired at 350 °C in air	-	-63.4 at pH= 7	[this work]

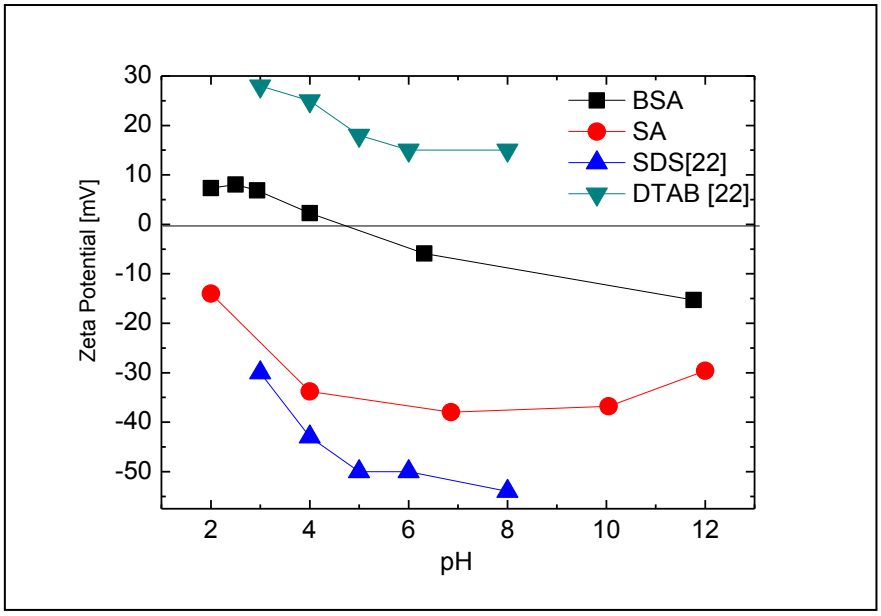

Figure 6-3 Zeta potential for foulants

6.3.2. In-situ fouling and cleaning experiment for organic foulants types-BSA and SA

6.3.2.1. Effect of different foulant solutions

Figure 6-4 shows the time course for the fouling/cleaning runs for BTESE membranes for pure foulant solutions (a) 500 ppm SA and (b) 500 ppm BSA. It shows by cleaning using deionized water (DIW) at 600 rpm for 3 hours was enough to clean both fouled BTESE membranes as the pure water flux and the NaCl rejection remains the same like initial value. The water flux value for BTESE membranes fired at 300 °C was lower than the BTESE membrane fired at 350 °C in air. This was due to the different pore network formed. BTESE membrane fired at 350 °C seemed to have large pore network due to the decomposition of some organic bonds via template method.

For better view on the fouling effect on BTESE and PA membranes, Figure 6-5 (a) and (b) show normalized water flux for different feed solutions containing; (a) pure 500 ppm SA for BTESE membranes and 20 ppm SA with addition of electrolytes 0.5mM Ca^{2+} contained 8.5mM NaCl for PA membrane (b) pure 500 ppm BSA for BTESE membranes and 20 ppm BSA with addition of electrolytes 0.5mM Ca^{2+} contained 8.5mM NaCl for PA membrane. Fouling occurs almost immediately for PA membrane compared to BTESE membranes. PA membrane experienced the largest flux decline, although the zeta potential values for BTESE membranes are the most negatively charge. BTESE membranes on the other hand, show just a slight decline in flux. Perhaps the largest flux decline for PA membrane was due to the addition of Ca^{2+} and NaCl into the feed solutions. Calcium ions have been shown to significantly enhance fouling in the presence of natural organic matter (NOM) by forming complexes which result in highly compacted fouling layers and thus more severe flux decline

[9-11]. In case of BTESE membrane, the smaller and tight pore sizes had able to completely reject both foulants. Moreover, the feed solution was vigorously agitated using a magnetic stirrer at 600 rpm to minimize the effect of concentration polarization [24-26]. Hence, the effect of concentration polarization was rationally ignored in this study due to the low permeate flux.

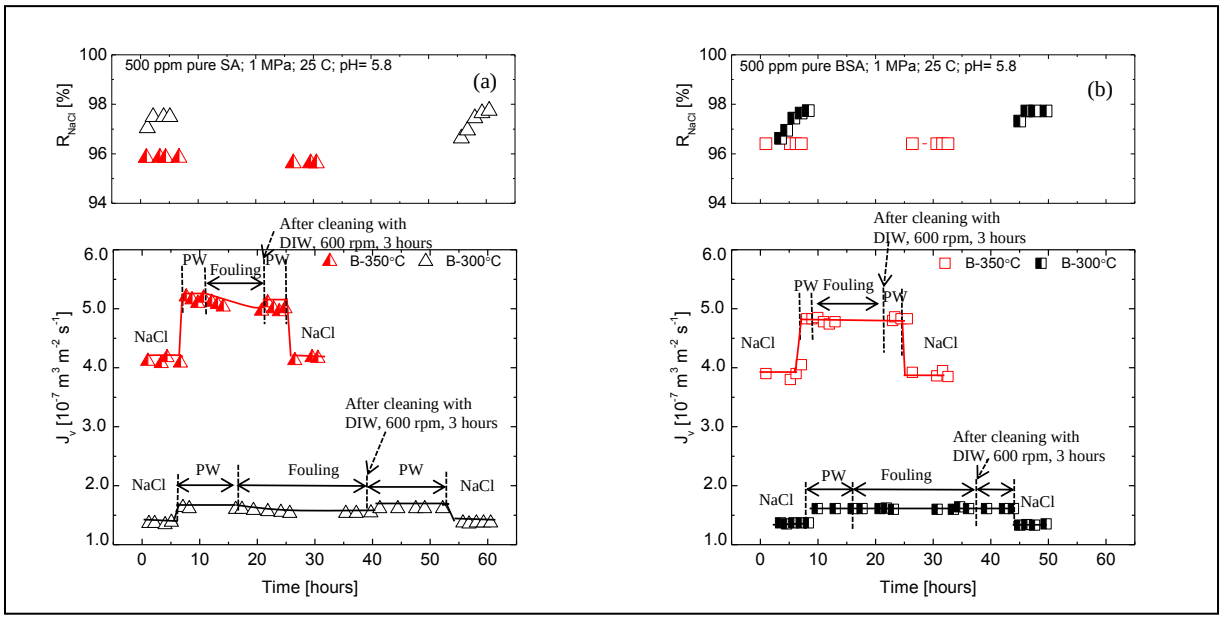

Figure 6-4 Experimental protocol for the fouling /cleaning runs for BTESE membranes. Effect of different foulant solutions on the different types of membranes (a) 500 ppm SA and (b) 500 ppm BSA sols

*Experimental conditions for BTESE membrane: Feed solution = Pure 500 ppm SA or BSA **without** 0.5mM Ca^{2+} and 8.5mM NaCl; pH 5.8±0.1; temperature = 21.0±0.5 °C

*Membrane cleaning properties: Deionized water (DIW) at 600 rpm for 3 hours

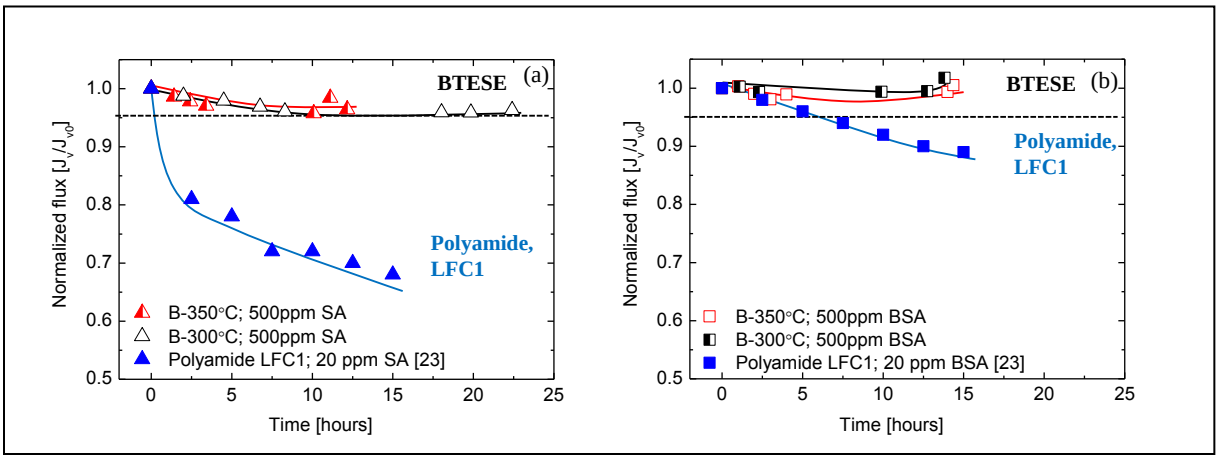

Figure 6-5 Fouling trend for PA and BTESE membranes. Effect of different foulant solutions on the different types of membranes (a) 500 ppm SA and (b) 500 ppm BSA sols

*Experimental conditions for BTESE membrane: Feed solution = Pure 500 ppm SA or BSA **without** 0.5mM Ca^{2+} and 8.5mM NaCl; pH 5.8±0.1; temperature = 21.0±0.5 °C

*Experimental conditions for PA LFC-1 (RO) membrane: Feed solution = 20 ppm SA or BSA **with** 0.5mM Ca^{2+} contained 8.5mM NaCl; pH 5.8±0.1; temperature = 21.0±0.5 °C [23]

6.3.2.2. Effect of different pH of BSA solution

Meanwhile, Figure 6-6 shows the experimental protocol for the fouling/cleaning runs for BTESE membranes for different pH value of BSA solution (a) pH=4.7 and (b) pH=5.8. The same result was seen as to clean the BTESE membrane.

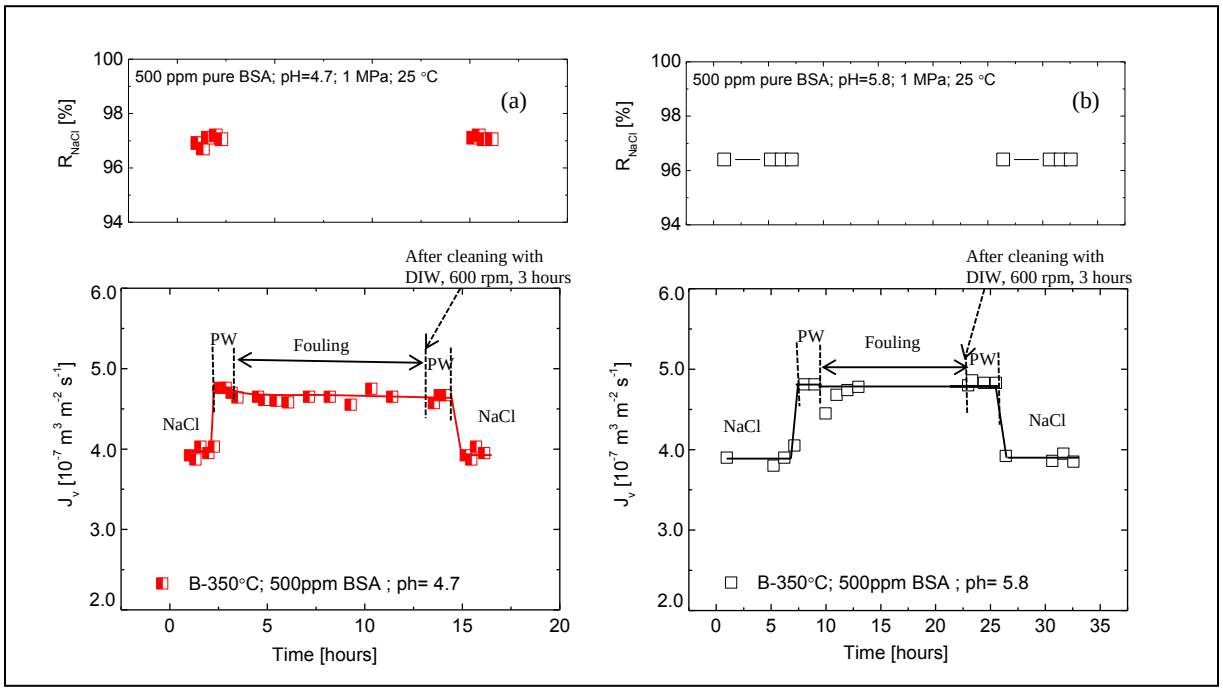

Figure 6-6 Experimental protocol for the fouling /cleaning runs for BTESE membranes. Effect of different pH of BSA solution (a) 4.7 and (b) 5.8

*Experimental conditions for BTESE membrane: Feed solution = Pure 500 ppm SA or BSA **without** 10 mM NaCl; pH 5.8±0.1; temperature = 21.0±0.5 °C

*Membrane cleaning properties: Deionized water (DIW) at 600 rpm for 3 hours

Figure 6-7 presents the normalized flux profiles under various feed solution pH (a) 4.7 and (b) 5.8. For PA membrane feed solution was set with 300 ppm BSA and addition of 10 mM NaCl, while feed solution for BTESE membranes consists of pure 500 ppm BSA solution. The flux-decline was seen for PA membrane for both feed solutions pH with the most severe at pH=4.7. It should be noted that, pH 4.7 is the isoelectric point (IEP) of the BSA molecules. Here BSA molecules are neutrally charged and have no electrostatic

repulsion among them hence they tend to deposit on the PA membrane surface [23]. On the other hand, BTESE membrane showed slight decline in flux at both pH conditions. This provides the idea that the resistance of BTESE membrane was much higher than the resistance of BSA due to the tighter pore network than PA membrane. However, it should be noted in the BTESE case, at pH=4.7 seems to decrease more than pH=5.8.

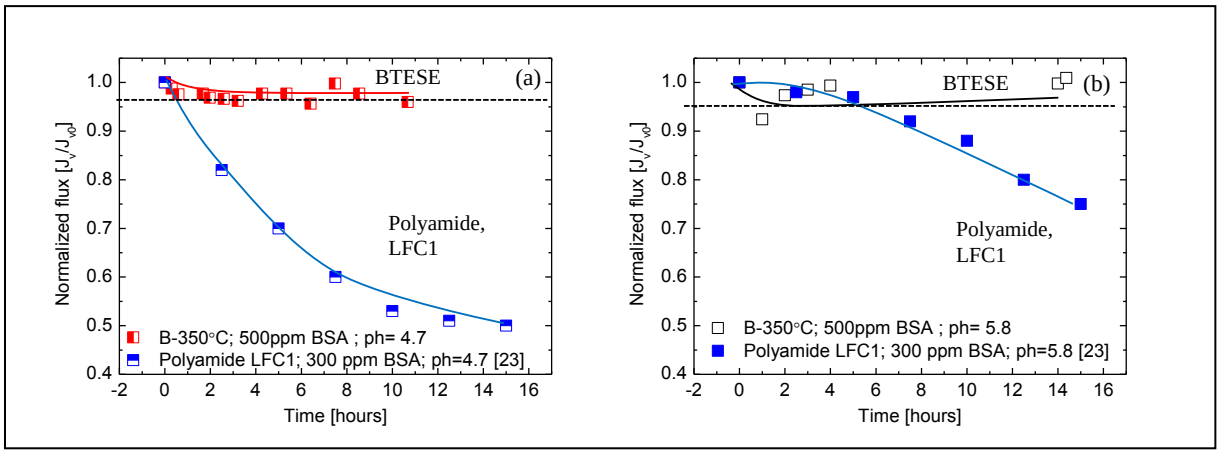

Figure 6-7 Fouling trend for PA and BTESE membranes. Effect of different pH of BSA solution (a) 4.7 and (b) 5.8

*Experimental conditions for BTESE membrane: Feed solution = Pure 500 ppm BSA **without** 10 mM NaCl; pH 5.8±0.1; temperature = 21.0±0.5 °C

*Experimental conditions for Polyamide LFC-1 (RO) membrane: Feed solution = 300 ppm BSA **with** 10 mM NaCl; pH 5.8±0.1; temperature = 21.0±0.5 °C [23]

6.3.2.3. Effect of different feed foulant compositions

Again, Figure 6-8 shows the experimental protocol for the fouling/cleaning runs for BTESE membranes for different different feed composition of foulants. The same result was seen as to clean the BTESE membrane that is by using deionized water. For comparison fouling study for BTESE and PA membranes, fouling experiment was carried out using pure and different feed composition of foulants (by varying proportion of SA and BSA with addition of electolytes sols 0.5mM Ca^{2+}, at an ionic strength of 10mM (adjusted with NaCl) with the total foulant concentration maintained at 500 ppm for BTESE membrane and total foulant of 20 ppm for PA membrane [23] as shown in Figure 6-9 (a) and (b).

As can be seen for BTESE membrane, the flux profiles for pure 500 ppm BSA and pure 500 ppm SA show the least flux decline. With the addition of electrolyte solution contained 0.5mM Ca^{2+}, at an ionic strength of 10mM (adjusted with NaCl) to both pure 500 ppm pure BSA and pure 500 ppm SA solutions exhibited a slightly decrease for 500 ppm BSA but more severe decline for 500 ppm SA solutions. More pronounced decline in flux for SA solution was due to the interaction of Ca^{2+} with SA molecules to form a gel-type fouling layer in the

presence of Ca^{2+}. Intermolecular bridging of the alginate molecules takes place in the presence of Ca^{2+}, resulting in the formation of a gel-like fouling layer which increases the hydraulic resistance significantly. The "egg-box" model has been used in the literature to explain alginate gel formation in the presence of Ca^{2+} [23, 27, 28]. Interestingly, for both membranes it can be seen that the flux profiles of the feed with both cofoulants (BSA and SA) are similar to the flux profile of the feed containing SA with addition of electrolytes. According to Elimelech et al. [23], the similar flux decline happened was due to the BSA molecules only play an enhanced role in the presence of SA as co-foulant, and the SA-calcium complex is crosslinked with BSA molecules in the fouling layer matrix, resulting in a fouling layer which has similar hydraulic resistance to that of a fouling layer of SA-calcium complexes. If the SA concentration of was increased the gel formation should be more pronounced.

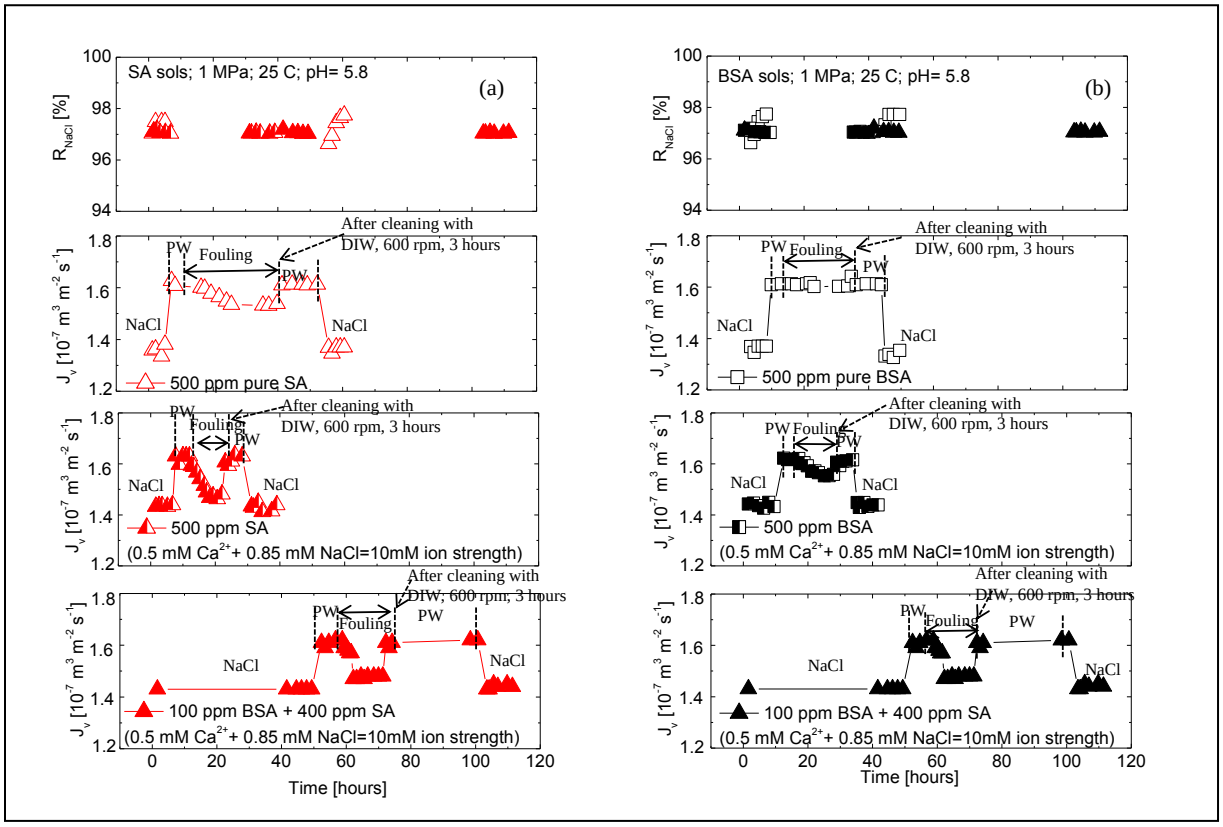

Figure 6-8 Experimental protocol for the fouling /cleaning runs for BTESE membranes. Effect of different feed foulant compositions (a) SA and (b) BSA.

*Experimental conditions for BTESE and PA membrane: pH 5.8±0.1; temperature = 21.0±0.5 °C

*Membrane cleaning properties: Deionized water (DIW) at 600 rpm for 3 hours

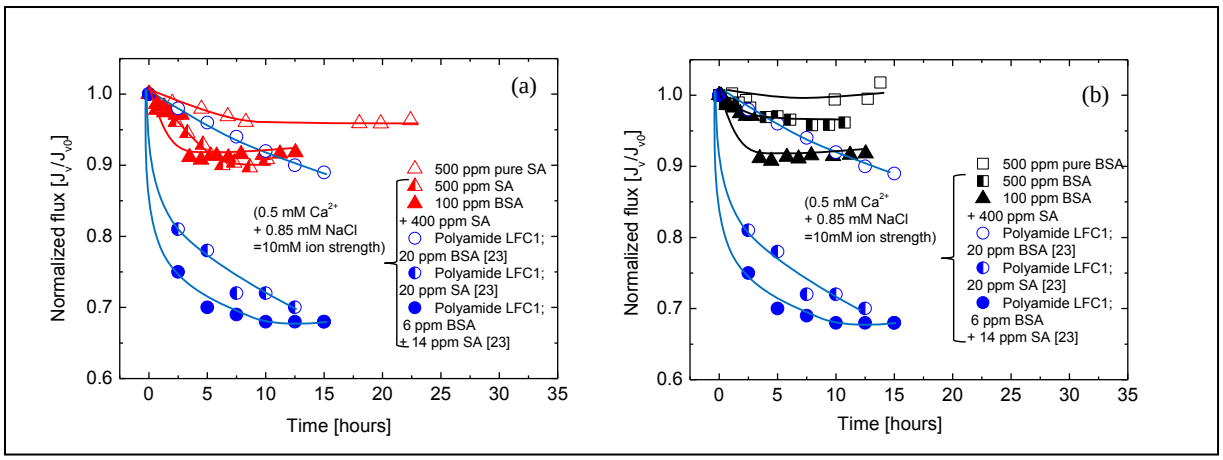

Figure 6-9 Fouling trend for PA and BTESE membranes. Effect of different feed foulant compositions (a) SA and (b) BSA.

*Experimental conditions for BTESE and PA membrane: pH 5.8±0.1; temperature = 21.0±0.5 °C

6.3.3. Fouling and cleaning experiment for surfactants-DTAB and SDS

6.3.3.1. Effect of different types of surfactants and feed composition (In-situ fouling experiment)

Figure 6-10 (a) shows the experimental protocol for the fouling experiment runs for BTESE membranes fired at 300 °C in air environment for different different feed composition of foulants. A series of cross-flow filtration experiments were conducted to evaluate the effect of surfactant charge on BTESE membrane. The feed of foulants were prepared with concentration for cationic (DTAB) and anionic (SDS) surfactants with 100 ppm and 500 ppm each without addition of electrolyte solution for several hours. It can be seen that more significant decreased in BTESE flux for DTAB compared to SDS as a foulants.

As to compare the fouling trend of BTESE membrane with polymer membrane hence we decided to choose AG RO membrane [22]. The feed composition for this PA membrane was set by adding 200 ppm of DTAB to a 2000 mg/L NaCl and likewise to the SDS feed composition as shown in Figure 6-10 (b) .

BTESE showed the same fouling trend for each surfactant which PA membrane leads the way due to the addition of NaCl. As can be seen, fouling occured almost immediately for DTAB sols case, and as time progressed, it did not decrease for AG RO membrane but show a significant flux decline for BTESE membrane as DTAB continue to deposit on the BTESE membrane surface. After 20 hours, the permeate flux of BTESE membrane became constant.

In case of anionic surfactant fouling, there is little or no fouling is detected. Generally, fouling is not expected in the presence of SDS based on electrostatic repulsion: the negatively charged surfactant should not be attracted to the negatively charged surface of the AG RO

membrane [12, 22, 29].

It is well known that, the surfactant concentration has an influence on membrane fouling, as it is known in the literature that adsorption on membrane surfaces increases with increasing concentration [12, 30]. However, in this study only a slight decreased in flux decline for 100 ppm and 500 ppm DTAB/SDS due to small different of concentration of foulants.

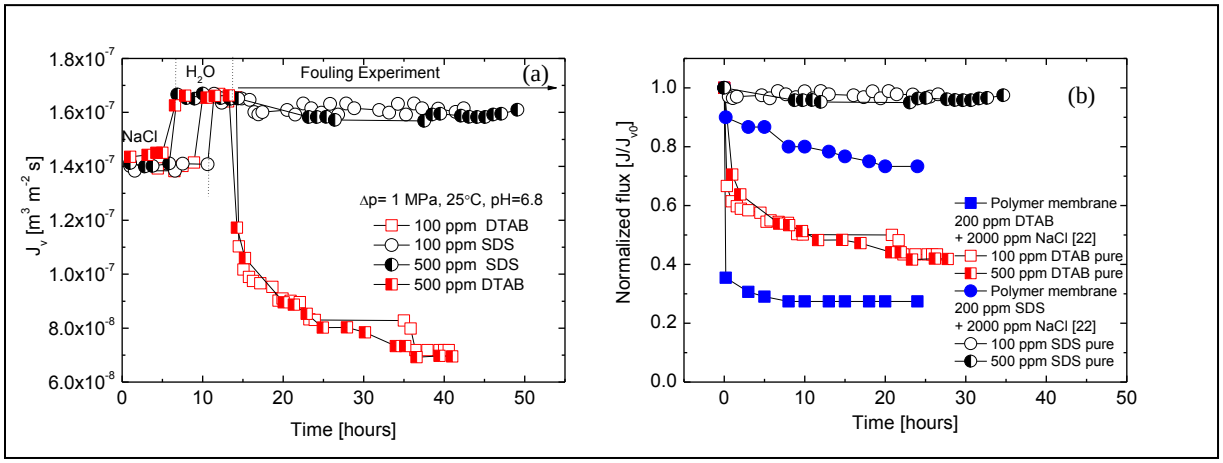

Figure 6-10 (a) Experimental protocol for the fouling runs for BTESE membranes and (b) Effect of different feed foulant compositions SDS and DTAB on the fouling trend for PA and BTESE membranes

Figure 6-11 shows the experimental protocol for the cleaning runs for BTESE membranes on the effect of different feed concentration of foulants (a) 100 ppm DTAB (b) 500 ppm DTAB (c) 100 ppm SDS (d) 500 ppm SDS. The cleaning process for fouled BTESE membrane in case of DTAB fouling experiment need more cleaning steps compared to SDS fouling experiment. As can be seen, cleaning efficiency increased with increasing cleaning agitation speed and temperature. It quite remarkable that by increased the DIW temperature by 60 °C for total 2 hours at 1000 rpm, is so effective in cleaning the 100 or 500 ppm DTAB layer formed on the membrane surface. In SDS fouling experiment case study, by applying 3 steps of cleaning using a room temperature (RT) (25 °C) DIW is enough to remove SDS molecules on the membrane surface.

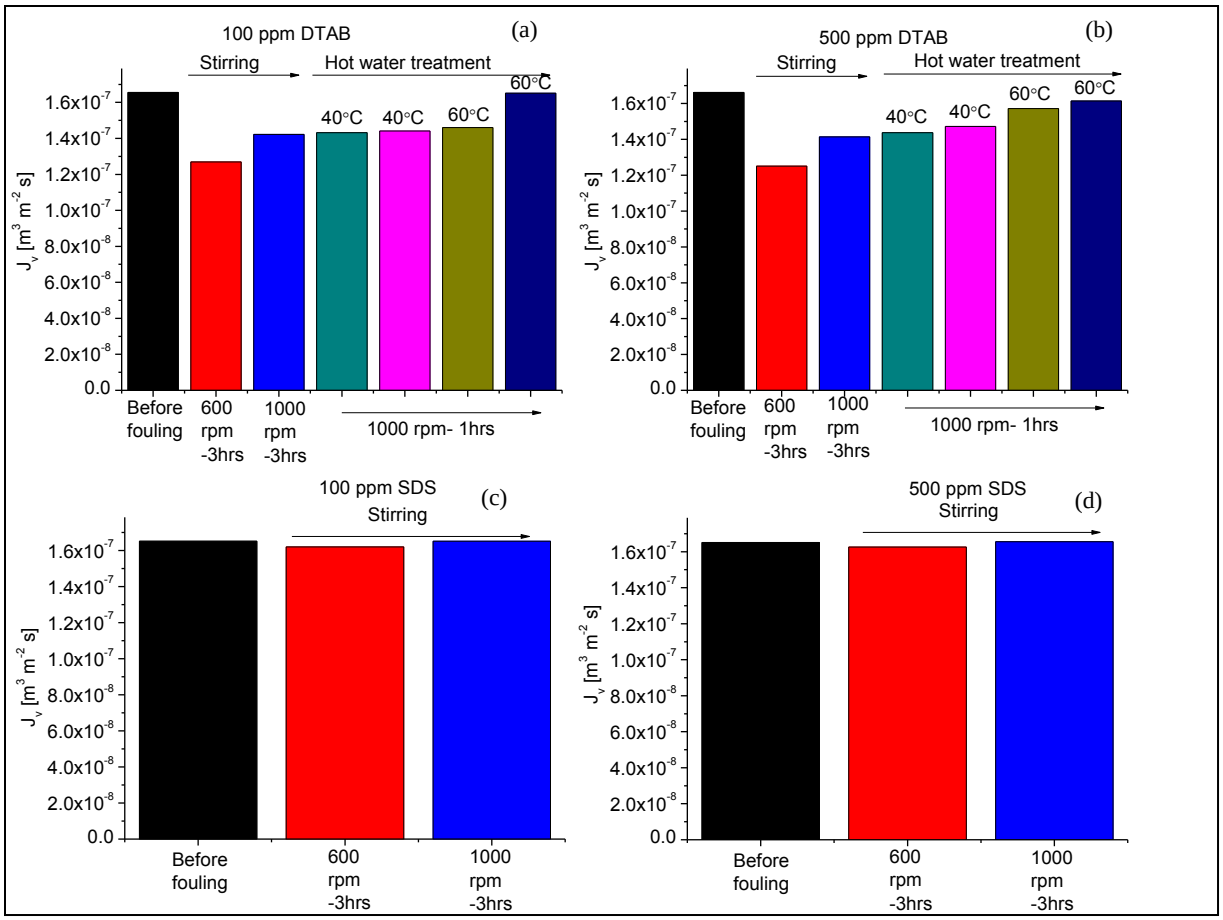

Figure 6-11 Experimental protocol for the cleaning runs for BTESE membranes. Effect of different feed concentration of foulants (a) 100 ppm DTAB (b) 500 ppm DTAB (c) 100 ppm SDS (d) 500 ppm SDS

6.3.3.2. Effect of different types of cleaning temperatures for DTAB fouling experiment (Immersion fouling experiment (16 hours))

Immersion fouling experiment using 500 ppm DTAB was conducted for 16 hours to evaluate the most appropriate cleaning steps using hot water to clean fouled BTESE membrane. As shown in Figure 6-12 (a) , three different temperatures (25, 60 and 80 °C) had been applied to clean the fouled BTESE membrane for 1 hour at agitation speed of 1000 rpm. As mentioned earlier, the cleaned membrane was subjected to the second baseline performance with deionized water to determine the pure water flux. In this study, it seems 80 °C is an appropriate temperature to remove the adsorbed DTAB from the membrane surface. Figure 6-12 (b) shows the detailed of the cleaning process using 80 °C hot water as well as NaCl rejection before and after cleaning process.

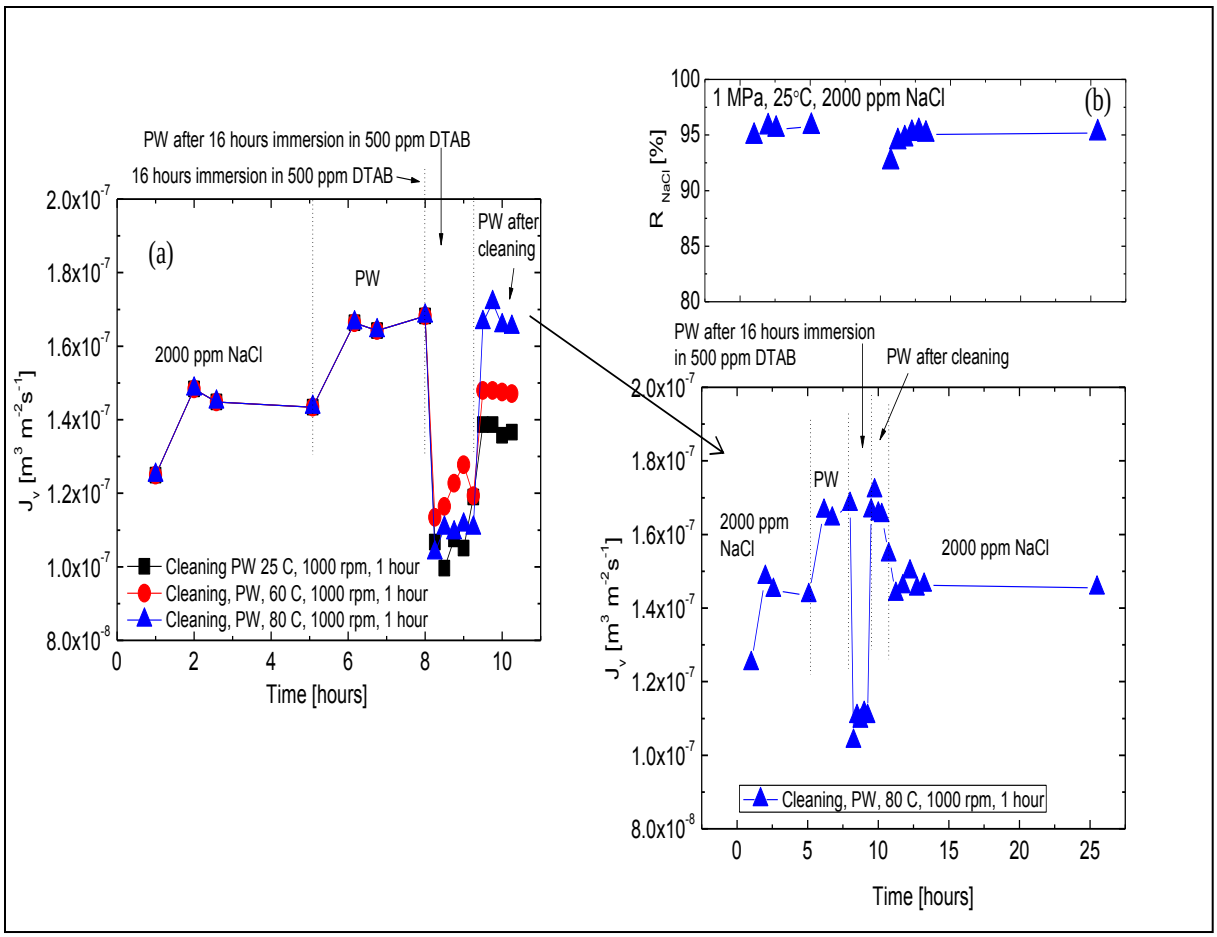

Figure 6-12 Experimental protocol for the cleaning runs for immersion fouling experiment study using (a) different temperatures (25, 60 and 80 °C) and (b) detailed cleaning process using 80 °C

In order to determine the optimum time required to totally remove the deposited DTAB on the BTESE membrane surface, we decided to conduct a cleaning experiment for each 10 minutes by using two temperatures 25 and 80 °C. Figure 6-13 shows that cleaning with water 25 °C, at 1000 rpm need more time to remove the deposited DTAB from the membrane surface. On the other hand, cleaning with hot water 80 °C, 1000 rpm is more efficient as it can save much time. The fouled membrane has been totally clean in 30 minutes as the water flux was recovered to its initial value in 30 minutes.

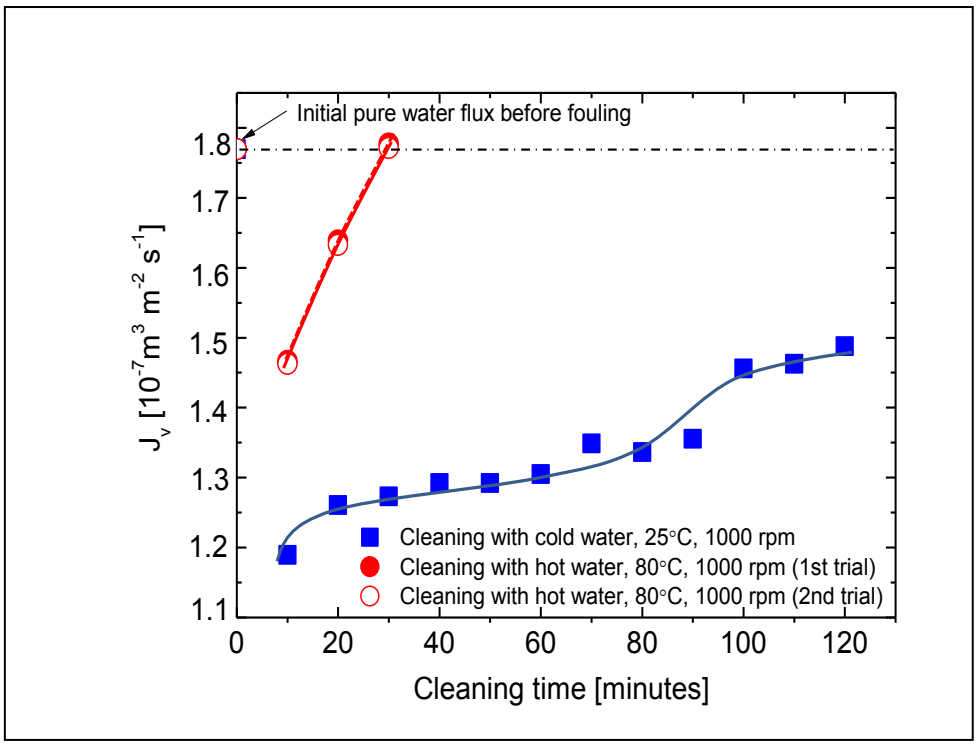

Figure 6-13 Optimization of cleaning time (Evaluation of flux pure water was conducted at 1 MPa, 25°C

6.4.Conclusion

The fouling experiment was conducted by using different types of foulants on BTESE membrane. Bovine serum albumin (BSA) and sodium alginate (SA) were chosen to represent proteins and polysaccharides in effluent organic matter. On the other hand, sodium dodecyl sulfate (SDS), an anionic surfactant and dodecyltrimethyl ammonium bromide (DTAB), a cationic surfactant, were used to represent industrial waste. In case of pure BSA and SA fouling experiment, it can be seen just a slight or little fouling occurred. This is due to the small pore network of BTESE membrane thus can completely rejected the pure BSA and SA molecules. However, by adding some electrolytes the fouling was occurred a little. This is due to the formation of gel like type deposited on the membrane surface. The BTESE membrane can easily clean by using DIW at room temperature at agiatation speed 600 rpm. The fouling experiment was more pronounced when using DTAB as a foulants solution as it is a cationic surfactant. From this fouling experiment, the optimum cleaning time required to clean the fouled BTESE membrane was determined by using hot water temperature 80°C agitation speed 1000 rpm for 30 minutes.

References:

[1] D.E. Potts, R.C. Ahlert, S.S. Wang. A critical review of fouling or reverse osmosis membranes, Desalination, 36, (1981) 235-264.

[2] K. Boussu, A. Belpaire, A. Volodin, C. Van Haesendonck, P. Van der Meeren, C. Vandecasteele, B. Van der Bruggen, Influence of membrane and colloid characteristics on fouling of nanofiltration membranes. J of Membr. Sci., 289 (2007) 220-230.

[3] S. Chellam and M.R. Wiesner, Evaluation of cross-flow filtration models based on shear-induced diffusion and particle adhesion: Complications induced by feed suspension polydispersivity. J of Membr. Sci., 138(1998) 83-97.

[4] W. Peng, I. C. Escobar, and D.B. White, Effects of water chemistries and properties of membrane on the performance and fouling--a model development study. J of Membr. Sci., 238 (1-2) (2004) 33-46.

[5] K. Boussu, C. Vandecasteele, and B. Van der Bruggen, Relation between membrane characteristics and performance in nanofiltration. J of Membr. Sci., 310 (1-2) (2008) 51-65.

[6] L. Gourley, M. Britten, S.F. Gauthier, Y. Pouliot, Characterization of adsorptive fouling on ultrafiltration membranes by peptides mixtures using contact angle measurements. J of Membr. Sci., 97 (1994) 283-289.

[7] M. Mänttäri, L. Puro, J. Nuortila-Jokinen, M. Nyström, Fouling effects of polysaccharides and humic acid in nanofiltration. J of Membr. Sci., 165 (2000) 1-17.

[8] H. Mo, K.G. Tay, and H.Y. Ng, Fouling of reverse osmosis membrane by protein (BSA): Effects of pH, calcium, magnesium, ionic strength and temperature. J. of Membr. Sci., 315 (2008) 28-35.

[9] C.Y. Tang, Y. N. Kwon, and J.O. Leckie, Fouling of reverse osmosis and nanofiltration membranes by humic acid—Effects of solution composition and hydrodynamic conditions. J of Membr. Sci., 290 (2007) 86-94.

[10] S. Hong and M. Elimelech, Chemical and physical aspects of natural organic matter (NOM) fouling of nano filtration membranes. J of Membr. Sci., 132 (1997) 159-181.

[11] S. Lee, J.W. Cho, and M. Elimelech, Combined influence of natural organic matter (NOM) and colloidal particles on nanofiltration membrane fouling. J of Membr. Sci., 262 (2005) 27-41.

[12] K. Boussu, C. Kindts, C. Vandecasteele, and B. Van der Bruggen, Surfactant Fouling of Nanofiltration Membranes: Measurements and Mechanisms, Chem. Phys. Chem 8 (2007) 1836 – 1845

[13] C. Y. Tang, T.H. Chong, A. G. Fane, Colloidal interactions and fouling of NF and RO membranes: A review, Advances in Colloid and Interface Science 164 (2011) 126–143

[14] S. Lee and M. Elimelech, Salt cleaning of organic-fouled reverse osmosis membranes,

Water research, 41 (2007) 1134 – 1142
[15] S. S. Madaeni, T. Mohammadi, M. K. Moghadam, Chemical cleaning of reverse osmosis membrane, Desalination, 134, (2001) 77–82.
[16] Z. Zhong, W. Xing, X. Liu, W. Jin, N. Xu, Fouling and regeneration of ceramic membranes used in recovering titanium silicalite-1 catalysts, J. of Membr. Sci. 301 (2007) 67–75
[17] W. S. Ang, A. Tiraferri, K. L. Chen, M. Elimelech, Fouling and cleaning of RO membranes fouled by mixtures of organic foulants simulating wastewater effluent, J. of Membr. Sci. 376 (2011) 196–206
[18] R. Xu, J. Wang, M. Kanezashi, T. Yoshioka and T. Tsuru, Development of Robust Organosilica Membranes for Reverse Osmosis, Langmuir, 27 (2011) 13996–13999.
[19] M. Kanezashi, K. Yada K, T. Yoshioka, T. Tsuru, Design of silica networks for development of highly permeable hydrogen separation membranes with hydrothermal stability. J Am Chem Soc. 131 (2009) 414–415.
[20] T. Niimi, H. Nagasawa, M. Kanezashi, T. Yoshioka, K. Ito, T. Tsuru, Preparation of BTESE-derived organosilica membranes for catalytic membrane reactors of methylcyclohexane dehydrogenation, J of Membr Sci 455 (2014) 375–383
[21] E. M. Vrijenhoek, S. Hong, M. Elimelech, Influence of membrane surface properties on initial rate of colloidal fouling of reverse osmosis and nanofiltration membranes, J. of Membr. Sci. 188 (2001) 115–128
[22] A. C. Sagle, E. M. VanWagner, H. Ju, B. D. McCloskey, B. D. Freeman, M. M. Sharma, PEG-coated reverse osmosis membranes: Desalination properties and fouling resistance, J. of Membr. Sci. 340 (2009) 92–108
[23] W. S. Ang, M. Elimelech, Protein (BSA) fouling of reverse osmosis membranes: Implications for wastewater reclamation, J of Membr. Sci. 296 (2007) 83–92
[24] T. Tsuru, K. Ogawa, M. Kanezashi, T. Yoshioka, Permeation characteristics of electrolytes and neutral solutes through titania nanofiltration membranes at high temperatures, Langmuir 26 (2010) 10897–10905.
[25] R. Xu, J. Wang, M. Kanezashi, T. Yoshioka, T. Tsuru, Reverse osmosis performance of organosilica membranes and comparison with the pervaporation and gas permeation properties, AIChE J. 59 (2013) 1298–1307.
[26] T. Tsuru, S. Izumi, T. Yoshioka, M. Asaeda, Temperature effect on transport performance by inorganic nanofiltration membranes. AIChE J. 46 (2000) 565–574.
[27] D.A. Rees, Polysaccharide shapes and their interactions—some recent advances, Pure Appl. Chem. 53 (1981) 1–14.
[28] G.T. Grant, E.R. Morris, D.A. Rees, J.C. Smith, D. Thom, Biological interactions between polysaccharides and divalent cations: the egg-box model, FEBS Lett. 32 (1973) 195–198.

[29] M. Elimelech, W.H. Chen, J.J. Waypa, Measuring the zeta (electrokinetic) potential of reverse osmosis membranes by a streaming potential analyzer, Desalination 95 (1994) 269–286.

[30] S. Paria, K. C. Khilar, A review on experimental studies of surfactant adsorption at the hydrophilic solid–water interface, Adv. Colloid Interface Sci. 110 (2004) 75–95.

Chapter 7

Conclusions and Recommendations

7.1. Conclusions

The overall of this dissertation research is focus on the preparation of organosilica membrane and application to use in gas separation (GS) and reverse osmosis (RO) applications. Two types of organosilica materials; TTESPT and BTESE were chosen for this study. Since, TTESPT is a new existence organosilica; hence we emphasized more extra study on its potential in gas and RO separation areas (Chapter 2 and 3). However, due to much coating times of top layer (6 times) needed to prepare a good separation performance of TTESPT membranes, thus we decided to study more detail on the optimization part of the BTESE membranes involving a more comparative study for the temperature dependency permeation properties of NaCl as well alcohols (ethanol and isopropanol) via different water ratio (WR) of BTESE membranes (Chapter 4). In Chapter 5, the morphology, structural properties and separation performance of BTESE membranes in gas and reverse osmosis (RO) applications were investigated with respect to WR and different firing environments. Furthermore, we tried to correlate the relationship between gas and water permeance as well permeance ratio of gases with the rejection of solute. Finally, in Chapter 6 we examined the technical capabilities of the BTESE membrane in term of fouling and cleaning processes.

The main conclusions in this thesis were summarized according to each chapter as follows:

1. 2,4,6-Tris[3(triethoxysilyl)-1-propoxy]-1,3,5-triazine (TTESPT) is a new precursor for preparing membranes. Since, TTESPT is a new existence organosilica; hence we emphasized more extra study on its potential in gas separation area. The TTESPT-derived silica membrane exhibits a significant degree of selectivity for C_3H_6–C_3H_8 ~37 at a permeation temperature of 50 °C, which greatly surpasses the upper-bounds of selectivity and permeance trade-off of carbon membranes. This indicates the potential for further development toward C_3H_6–C_3H_8 separation applications.

2. A promising new triazine-based nitrogen-rich organosilica (TTESPT) membrane has been developed for molecular separation processes in gas (gas separation) and liquid phases

(reverse osmosis (RO)). By adjusting the H_2O/TTESPT molar ratio, we found a promising technique for tuning the pore network of TTESPT membranes. An increase in the H_2O/TTESPT molar ratio from 60 to 240 fully hydrolyzed all the ethoxide groups in the TTESPT membrane, which reduced the size of the pores in the silica pore network. A TTESPT membrane with a high H_2O/TTESPT molar ratio exhibited a high degree of selectivity for H_2/SF_6 (greater than 4000) at a permeation temperature of 200 °C. This membrane also demonstrated high sodium chloride (NaCl) rejection (>98.5%) with water permeability of $>1 \times 10^{-12}$ m^3 m^{-2} s^{-1} Pa^{-1} under operating conditions of 1 MPa and 60 °C during a RO experiment. As the operating temperature was increased from 25 to 60 °C, the NaCl rejection was constant without displaying the characteristic flux deterioration. This showed that the membrane retained a stable hybrid network structure

3. In this study, a pore network of bis(triethoxysilyl)ethane (BTESE) organosilica membranes was controlled by adjusting the molar ratios of BTESE/H_2O/acid=1/*x*/0.2 (*x*=3 and 240). The mechanisms for solute transport in the BTESE RO membrane were investigated using three different aqueous solutions of sodium chloride (NaCl), ethanol (EtOH) and isopropanol (IPA). The pressure and temperature were varied from 0.4 to 1 MPa and from 25 to 80 °C, respectively. Water flux and rejection increased for both alcohols and electrolyte with an increase in the applied pressure. It was noteworthy that the rejection of alcohols decreased with an increase in the RO operating temperature, while the electrolyte rejection remained almost constant. The BTESE membranes exhibited high thermal robustness under the long-term testing conditions, delivering salt rejections >98% until the end of the testing period (50 h). The BTESE membranes could also be regenerated after use in the gas and RO experiments, thus demonstrating robust properties.

4. The aim of this work was to study the simultaneous effects of H_2O/BTESE molar ratio (WR) = (3, 60, 120, 240) in different firing environments on the structural and permeation properties of BTESE membranes. We found that most of organic peaks for sample fired in N_2 environment were more intense as compared with the samples fired in air environment. Thus, the samples fired in N_2 environment are more hydrophobic compared with the sample fired in air environment and can be proven by contact angle and H_2O adsorption results. In term of separation performance, the permeance of gases and H_2O were clearly dependent on WR. Increasing WR decreased the permeance of both gases and H_2O via the pore network of BTESE membrane. On the other hand, changing the firing environments also affected the permeance of gases and H_2O. Samples fired in air environment exhibited higher permeance of gases and H_2O due to more open pore networks. In addition, the relationship between gas and liquid permeances was correlated by assuming He gas as a

predictor of water permeance, N_2 gas as a predictor for IPA and SF_6 gas as a predictor for NaCl permeance. Increasing in He and permeance ratio resulted in increasing in water permeance and rejection of solutes. Hence, it also suggests that WR plays a primary factor in controlling the pore size and solutes rejections meanwhile firing environments play a main role in deciding the hydrophilicity and hydrophobicity of membrane surface and pore networks during BTESE membranes fabrication.

5. The fouling experiment was conducted by using different types of foulants on BTESE membrane. Bovine serum albumin (BSA) and sodium alginate (SA) were chosen to represent proteins and polysaccharides in effluent organic matter. On the other hand, sodium dodecyl sulfate (SDS), an anionic surfactant and dodecyltrimethyl ammonium bromide (DTAB), a cationic surfactant, were used to represent industrial waste. In case of pure BSA and SA fouling experiment, it can be seen just a slight or little fouling occurred. This is due to the small pore network of BTESE membrane thus can completely rejected the pure BSA and SA molecules. However, by adding some electrolytes the fouling was occurred a little. This is due to the formation of gel like type deposited on the membrane surface. The BTESE membrane can easily clean by using DIW at room temperature at agiatation speed 600 rpm. The fouling experiment was more pronounced when using DTAB as a foulants solution as it is a cationic surfactant. From this fouling experiment, the optimum cleaning time required to clean the fouled BTESE membrane was determined by using hot water temperature 80°C agitation speed 1000 rpm for 30 minutes.

7.2. Recommendations

This research has led to some interesting ideas on the capabilities of organosilica membranes; TTESPT and BTESE in the gas separation (GS) and reverse osmosis (RO) areas. In this study, the organosilica BTESE membranes also exhibit superior hydrothermal stability and a good resistance fouling membrane. As the major concern of this study is more on the RO areas, organosilica membranes still possess lower water permeabilities compared to the commercialized polyamide-based RO membranes.

Based on results and conclusions derive from this study, the following recommendations are given for future work:

1. More studies focus on the adjusting the structure of the organic bridging groups by direct incorporation of more hydrophilic bridging groups or post modification of the organosilica networks, to further improve the water and salt rejection while maintaining its robustness
2. Possibility to fabricate organosilica membrane in the hollow fibers by using spinning

technologies similar to those used to make hollow fiber organic membranes in order to enhance the surface area of the organosilica membranes.

List of Publications

Published Papers:

Suhaina M. Ibrahim, Rong Xu,Hiroki Nagasawa, Akinobu Naka, Joji Ohshita, Tomohisa Yoshioka, Masakoto Kanezashi and Toshinori Tsuru* A closer look at the development and performance of organic–inorganic membranes using 2,4,6-tris-[3(triethoxysilyl)-1-propoxyl]-1,3,5-triazine (TTESPT) RSC Adv., 2014, 4, 12404

Suhaina M. Ibrahim, Rong Xu,Hiroki Nagasawa, Akinobu Naka, Joji Ohshita, Tomohisa Yoshioka, Masakoto Kanezashi and Toshinori Tsuru* Insight into the pore tuning of triazine-based nitrogen-rich organoalkoxysilane membranes for use in water desalination RSC Adv., 2014, 4, 23759

Suhaina M. Ibrahim, Hiroki Nagasawa, Masakoto Kanezashi, and Toshinori Tsuru, Robust organosilica membranes for high temperature reverse osmosis (RO) application: Membrane preparation, separation characteristics of solutes and membrane regeneration, JMS-15-166R1 Accepted for publication

Rong Xu, **Suhaina Ibrahim**, Masakoto Kanezashi, Tomohisa,Yoshioka, Kenji Ito, Joji Ohshita, and Toshinori Tsuru, New insights into the microstructure-separation properties of organosilica membranes with ethane, ethylene and acetylene bridges, *ACS Appl. Mater. Interfaces*, **2014,** *6* (12), pp 9357–9364

Toshinori Tsuru, **Suhaina Mohd Ibrahim** and Waravut Puthai, Pore Size Control of Porous Ceramic Membranes and Application to ROBUST Nanofiltration and Reverse Osmosis Membranes, Bulletin of the Ceramic Society of Japan, 50（2015）No. 2,pp 121-125

Proceeding/ Papers presented

Suhaina M. Ibrahim, Hiroki Nagasawa, Joji Ohshita, Akinobu Naka,Tomohisa Yoshioka, Masakoto Kanezashi, Toshinori Tsuru, Tailoring the Pore Size and Gas Separation Properties of Organic/Inorganic Membranes Using 2,4,6-tris[3(triethoxysilyl)-1-propoxyl]
-1,3,5-triazine (Triazine) as a triple–Silicon Alkoxide and Comparison With mono and di-Silicon Alkoxides, 11th International Conference on Membrane Science and Technology 2013 (MST 2013) 27-29th Aug 2013 (Oral Presenter)

Suhaina M. Ibrahim, Hiroki Nagasawa, Akinobu Naka, Joji Ohshita, Tomohisa Yoshioka, Masakoto Kanezashi and Toshinori Tsuru, Preparation 1,3,5-Triazine derivatives as a new organo-silica membrane for gas and reverse osmosis:Effect of coating and firing temperatures, Poster presentation at 10th International Conference on Separation Science and Technology (ICSST14) Nara, Japan, 30 October -1 November, 2014 (Poster presenter)

Suhaina M. Ibrahim, Hiroki Nagasawa, Masakoto Kanezashi, Tomohisa Yoshioka, and Toshinori Tsuru Robust BTESE-derived reverse osmosis organosilica membranes: Effect of sols properties, firing temperatures and environments on the micro- structure and permeation properties 2nd International Conference on Desalination using Membrane Technology, 26-29 July 2015, Singapore (Elsevier) (Poster presenter)

ACKNOWLEDGEMENTS

First and foremost, I thank Allah the almighty for His grace, love, mercy and guidance throughout my life.

I would like to give my special thanks to my both dedicated supervisor, Prof. Toshinori Tsuru, for his guidance, inspiration and encouragement in every stage of my PhD study. I am very grateful to Prof. Tomohisa Yoshioka, Prof. Masakoto Kanezashi, and Dr. Hiroki Nagasawa for their kind assistant in my experiments and insightful discussion on my research work. I would also like to thank grateful to Prof. Joji Ohshita and Prof. Watara Nishijima in my dissertation committee for reading my thesis in their busy schedule.

Not forgetting my tutor Ms Takahashi, for her warm-hearted assistance in my research work and daily life, when I came to Japan. I would like to thank all other group members in the Separation Engineering Lab, for their sustained help and all the good moments we spent together.

I am also grateful to Japan Government for for granting me generous financial support under Monbukagakusho Scholarship, that enabling this work to be successfully completed.

Lastly, I would like to express my deepest gratitude to my beloved family, my son Niel, Farina, Laila, RSW, Man, Pablo, friends and those who have directly or indirectly gave me endless encouragements and support through the entire three-year journey